INFORMATION TO USERS

This manuscript has been reproduced from the microfilm master. UMI films the text directly from the original or copy submitted. Thus, some thesis and dissertation copies are in typewriter face, while others may be from any type of computer printer.

The quality of this reproduction is dependent upon the quality of the copy submitted. Broken or indistinct print, colored or poor quality illustrations and photographs, print bleedthrough, substandard margins, and improper alignment can adversely affect reproduction.

In the unlikely event that the author did not send UMI a complete manuscript and there are missing pages, these will be noted. Also, if unauthorized copyright material had to be removed, a note will indicate the deletion.

Oversize materials (e.g., maps, drawings, charts) are reproduced by sectioning the original, beginning at the upper left-hand corner and continuing from left to right in equal sections with small overlaps. Each original is also photographed in one exposure and is included in reduced form at the back of the book.

Photographs included in the original manuscript have been reproduced xerographically in this copy. Higher quality 6" x 9" black and white photographic prints are available for any photographs or illustrations appearing in this copy for an additional charge. Contact UMI directly to order.

UMI

A Bell & Howell Information Company
300 North Zeeb Road, Ann Arbor MI 48106-1346 USA
313/761-4700 800/521-0600

STUDIES ON ANTICOINCIDENCE GAMMA-RAY SPECTROMETRY IN NEUTRON ACTIVATION ANALYSIS

Weihua Zhang

Submitted in partial fulfilment of the requirements
for the degree of Doctor of Philosophy
at
Dalhousie University
Halifax, Nova Scotia
1997 July

DALHOUSIE UNIVERSITY

FACULTY OF GRADUATE STUDIES

The undersigned hereby certify that they have read and recommend to the Faculty of Graduate Studies for acceptance a thesis entitled "Studies on Anticoincidence Gamma-Ray Spectrometry in Neutron Activation Analysis"

by Weihua Zhang

in partial fulfillment of the requirements for the degree of Doctor of Philosophy.

Dated: September 11, 1997

External Examiner

Research Supervisor

Examining Committee

Dalhousie University

Author: **Weihua Zhang**

Title: **Studies on Anticoincidence Gamma-Ray Spectrometry in Neutron Activation Analysis**

Department: Chemistry
Degree: Ph.D.
Convocation: 1997 Fall

Permission is herewith granted to Dalhousie University to circulate and have copied for non-commercial purposes, at its discretion, the above title upon the request of individuals and institutions.

Signature of Author

TABLE OF CONTENTS

LIST OF TABLES

LIST OF FIGURES

ABSTRACT

Instrumental neutron activation analysis (INAA) is a well-established analytical technique for the simultaneous determination of multielement concentrations in a variety of sample matrices. One of the problems generally encountered in INAA is the high background activity arising from the scattering of photons, a phenomenon known as the Compton effect. In order to reduce the Compton background events and lower the detection limits, anticoincidence spectrometry can be employed. The spectrometer used here consists of a 25% relative efficiency HPGe detector surrounded by a 10" x 10" NaI(Tl) annulus and a 3" x 3" NaI(Tl) plug as well as timing electronics. This system has been characterized. A peak-to-background-plateau ratio of 590 has been obtained; an improvement factor of 7 has been achieved compared to a single HPGe detector. Several factors that can influence efficiency of the methodology have been evaluated. The distance of the sample from the HPGe detector surface and the relative position of the NaI(Tl) annulus with respect to the HPGe detector have been investigated to obtain the best efficiency.

A systematic investigation has been carried out on the merits and limitations of anticoincidence counting for the nuclides which are most commonly used in NAA. Short-lived nuclides (half-life < 120 s) have been studied using both conventional INAA procedure as well as by pseudo-cyclic INAA. The list of short-lived nuclides include: ^{108}Ag, ^{110}Ag, ^{165m}Dy, ^{20}F, ^{75m}Ge, ^{179m}Hf, ^{86m}Rb, ^{46m}Sc, ^{77m}Se, and ^{177m}Yb. Medium-lived nuclides (half-life < 3 h) which are commonly used in NAA, namely ^{28}Al, ^{139}Ba, ^{80}Br, ^{38}Cl, ^{66}Cu, ^{165}Dy, ^{128}I, ^{27}Mg, ^{56}Mn, ^{65}Ni, ^{233}Th, ^{51}Ti, and ^{52}V, have also been investigated using anticoincidence counting and conventional INAA. The long-lived nuclides (half-life > 12.5 h) of interest in the present study are: ^{76}As, ^{198}Au, ^{82}Br, ^{141}Ce, ^{51}Cr, ^{60}Co, ^{59}Fe, ^{197}Hg, ^{203}Hg, ^{42}K, ^{140}La, ^{24}Na, ^{147}Nd, ^{86}Rb, ^{122}Sb, ^{46}Sc, ^{182}Ta, ^{160}Tb, ^{187}W, ^{175}Yb, ^{69m}Zn, and ^{65}Zn.

The benefits of anticoincidence counting are frequently described by the peak efficiency reduction factor (PERF) of the nuclide of interest. Experiments were done in this work to calculate the PERF values of major gamma-rays of the above nuclides. The results showed that about 70% of the nuclides studied have no peak efficiency reduction in anticoincidence spectrometry. An attempt has been made to define an "analytical figure of merit (AFOM)" term for assessing the practical advantages of anticoincidence counting. This term includes parameters, such as resolution, peak area, background around the peak, dead time, counting time, and counting statistics which vary with changes in sample matrix activity. The effectiveness of the AFOM terms has been evaluated by analyzing a number of biological reference materials of diverse types of matrix and varying amounts of major and interfering elements. The variation of AFOM with dead time has also been investigated.

LIST OF ABBREVIATIONS AND SYMBOLS

a	Annum (year)
A_{corr}	Corrected peak area
ADC	Analog-to-digital converter
AF_{anti}	Advantage factor of anticoincidence counting
AF_{conv}	Advantage factor of conventional counting
AFOM	Analytical figure of merit
B	Background counts
BGO	Bismuth germanite (detector)
Bq	Becquerel, one disintegration per second
BSR	Background suppression ratio
C	Counts
CFD	Constant fraction discriminator
cps	Counts per second
CRM	Certified reference material
CsI(Tl)	Thallium activated cesium iodide (detector)
CSS	Compton suppression system
d	Day
MDA	Minimum detectable activity
dpm	Disintegrations per minute
EINAA	Epithermal instrumental neutron activation analysis

Ge(Li)	Lithium drifted germanium (detector)
h	Hour
HI	Heavy-ion
HPGe	High-purity germanium (detector)
HV	High voltage
i.d.	Inner diameter
INAA	Instrumental neutron activation analysis
L_C	Decision limit
L_D	Qualitative detection limit
L_Q	Quantitative determination limit
MCA	Multichannel analyzer
min	Minute
N	Avogadro's number
NAA	Neutron activation analysis
NaI(Tl)	Thallium activated sodium iodide (detector)
N_B	Number of background counts
N_T	Number of a peak area counts at the maximum of the peak
o.d.	outer diameter
PA_{anti}	Net peak area statistical accuracy in anticoincidence counting
PA_{conv}	Net peak statistical accuracy in conventional counting
PCA	Principal component analysis
PERF	Peak efficiency reduction factor

PGNAA	Prompt gamma-ray neutron activation analysis
PIXE	Proton induced X-ray emission
PMT	Photomultiplier tube
PNAA	Preconcentration neutron activation analysis
ppb	Parts per billion = ng/g
ppm	Parts per million = μg/g
P/C_p	Peak-to-Compton plateau
P/C_e	Peak-to-Compton edge
P/T_a	Peak-total area
REE	Rare earth elements
RM	Reference material
RNAA	Radiochemical neutron activation analysis
R_{anti}	Peak-to-background ratio in anticoincidence counting
R_{conv}	Peak-to-background ratio in conventional counting
R_{PA}	Net peak area statistical accuracy improvement
RSD	Relative standard deviation
s	Second
SCA	Single channel analyzer
Si(Li)	Lithium drifted silicon detector
MMA	Main matrix activity
SWA	Sum of weighted activity
SRM	Standard reference material

TAC	Time-to-amplitude converter
TFA	Timing filter amplifier
t_c	Counting time
t_d	Decay time
t_i	Irradiation time
$t_{1/2}$	Half-life of a nuclide
$W_{0.5}$	Full-width at half-maximum
% Overlap	Peak percentage overlap
γ	Gamma-ray
ϵ	Detector efficiency
Φ	Neutron flux
γ'	Gamma-ray branching ratio
Λ	Activation cross section
θ	Isotopic abundance
λ	Decay constant of a nuclide

ACKNOWLEDGEMENTS

The author wishes to thank Prof. Amares Chatt, my supervisor, for his guidance and helpful advice during the course of this thesis. Without his encouragement and wonderful experience, this thesis probably would not have been finished. Again I would like to express my deepest gratitude to him for all the academical help and moral support.

I gratefully acknowledge the SLOWPOKE-2 reactor staff, Dr. Jiri Holzbecher and Mr. Blaine Zwicker, for their help in sample irradiations and helpful advice as well as interesting discussions. The help of Mr. Brian Millier for numerous electronics maintenance work is also greatly appreciated.

I would like to thank the other members of the Nuclear Analytical Chemistry group for their friendly cooperation and pleasant help.

Special thanks to my wife Zhaoxia who was always willing to give me her encouragement and help throughout this work.

Finally I gratefully acknowledge the financial support from Natural Sciences and Engineering Research Council of Canada and Dalhousie University Faculty of Graduate Studies.

1. INTRODUCTION

Neutron activation analysis (NAA) was discovered by Hevesy and Levi in 1936 [1]. In NAA, a sample is bombarded in a flux of neutrons; target nuclei in the sample interact with the neutrons by capture reactions, most commonly by the (n,γ) reaction, whereby radionuclides (*i.e.* radioactive isotopes) may be formed. A radionuclide has a characteristic half-life and mode of decay. During the decay process, a nuclide may emit positrons, alpha-, beta- and/or gamma-rays, or be involved in electron capture or internal conversion. The majority (about 90%) of the nuclides formed by the (n,γ) process undergo beta decay which is most often associated with the emission of one or more gamma-rays as the product nuclide de-excites to a more stable state [2,3].

In general, the energy of a gamma-ray is characteristic of a nuclide. The gamma-ray energies ranging between 70 and 3100 keV are commonly used for multielement determination by NAA. This specificity coupled with the development of high-resolution and high-efficiency semiconductor detectors as well as the availability of high neutron fluxes in reactors, makes NAA-gamma spectrometry a powerful multielement analysis technique.

Methods based on NAA are continually being developed for the determination of elements with high sensitivity, precision, and accuracy. There are various types of NAA reported in the literature. In radiochemical NAA (RNAA), a

sample is first irradiated, followed by a chemical separation of the element(s) of interest from the sample. The most important advantages of RNAA include freedom from reagent blanks and excellent sensitivity. However, RNAA methods are generally time-consuming and thus cannot be easily applied to short-lived nuclides. On the other hand, preconcentration NAA (PNAA) can be used for studying short-lived nuclides because the element(s) of interest is chemically separated prior to irradiation. However, PNAA methods are not free from reagent blanks, and can also be time-consuming.

The most common form of NAA is called instrumental NAA (INAA) or nondestructive NAA where an irradiated sample is counted on a detector without any pre- or post-irradiation chemical treatment. There are many advantages of INAA over its sister techniques (*viz.* RNAA and PNAA) and other analytical techniques. These include nondestructive analysis, freedom from reagent blanks, and simultaneous multielement determination.

One of the problems generally encountered in INAA is high background activity arising from the scattering of photons; this phenomenon is called the Compton effect. Better detection limits could be obtained if the Compton continuum is suppressed. The main objective of this thesis is to develop INAA methods in conjunction with anticoincidence gamma-ray spectrometry which can be used for lowering the background activities.

Theories of NAA and anticoincidence gamma-ray spectrometry as well as a literature survey are presented in this chapter.

1.1 Neutron Activation Analysis

Several books and review papers have been published covering various aspects of NAA [2-5]. Many conference proceedings on fundamental development and applications of NAA are also available [6-13]. Only a brief description of the relevant equations on NAA will be given here. The number of counts detected in a specific gamma-ray peak by a detector is directly proportional to the amount of various elements present in the sample. The number of counts is a function of several parameters as shown in the following "activation equation" [2]:

$$C = N \Phi w \Delta \theta \varepsilon M^{-1} \gamma' \lambda^{-1} (1- \exp(- \lambda t_i)) (\exp(- \lambda t_d)) (1- \exp(- \lambda t_c)) \quad [1.1]$$

Where:

C = number of counts detected,

N = Avogadro's Number (6.023×10^{23} mol^{-1}),

w = mass of the element of interest in the sample (g),

Φ = flux of neutrons (cm^{-2} s^{-1}),

Δ = activation cross section of target isotope (cm^2),

θ = fractional isotopic abundance of the isotope of interest,

M = atomic weight of the element of interest (g mol^{-1}),

$\lambda = (\ln 2)/t_{1/2}$ is the decay constant of the product nuclide (s^{-1}),

ε = efficiency of the detector at the photopeak energy,

t_i = length of irradiation (s),

t_d = length of decay (s),

t_c = length of counting (s),

$t_{1/2}$ = half-life of the nuclide of interest (s), and

γ' = gamma branching ratio.

It is obvious that the number of counts detected is directly proportional to the detection sensitivity. The activity can be generally increased by increasing parameters such as the neutron flux, mass of a sample, irradiation time, and detector efficiency. The relative sensitivities for various elements are also dependent on their properties such as cross section, half-life, atomic weight, abundance of the parent isotope of the element, and the decay scheme of the nuclide.

The concentration of an element can be calculated directly using the "activation equation" 1.1 if the parameters Φ, λ, σ, θ, ε, and the decay scheme of the nuclide are known. However, NAA is most commonly done using comparator standards rather than this absolute method because uncertainty in any of the above parameters can easily affect the accuracy of the result. In the comparator method, a known amount of the element of interest (called the standard) is irradiated together with the sample, and both the sample and the standard are counted under exactly the same conditions. This way any uncertainties in the parameters σ, Φ, the decay scheme and the detection efficiency are eliminated.

Equation 1.1 can then be simplified for the comparator method as:

$$M_{sample} = C_{sample} \times \frac{M_{standard}}{C_{standard}} \qquad [1.2]$$

where M_{sample} and $M_{standard}$ are the masses of the element in the sample and in the standard, respectively, and C_{sample} and $C_{standard}$ are the number of counts due to the nuclide in the sample and the standard, respectively. M_{sample} can be calculated if the other three parameters are known. It may be necessary to correct C_{sample} and $C_{standard}$ to a given decay time.

Cyclic instrumental neutron activation analysis (CINAA) technique is used to enhance the sensitivity of short-lived nuclides by improving counting statistics. This is done by repeating the irradiation-transfer-counting process of a sample for a suitable number of cycles; the gamma-ray spectrum of each cycle is recorded to finally yield a cumulative spectrum. Using a pneumatic sample transfer system, this approach was first introduced to activation analysis by Anders [14] who used the $^{19}F(n,\alpha)^{16}N$ reaction to determine F via the ^{16}N (half-life = 7.4 s). Later Spyrou and coworkers [15], Grass and coworkers [16], and Chatt coworkers [17] applied CINAA technique for trace analysis using reactors as neutron sources.

The CINAA technique often requires rather expensive automated equipment which is not commonly available in most nuclear analytical laboratories. In addition, elaborate dead-time and pulse pile-up corrections are necessary to

account for the very high count rates in CINAA. Alternatively, a pseudo-cyclic instrumental neutron activation analysis (PCINAA) method can be developed based on the principles of CINAA but using the facilities available for conventional INAA. The PCINAA technique has been developed and successfully applied to biological materials for detecting nuclides with half-lives ranging between 10 s and 65 s by Chatt and coworkers [18]. One of the PCINAA methods involved manual transfer of samples from a receiver to a detector for the determination of up to 5 elements in several RM and SRM using short-lived nuclides [19]. In order to minimize sample activity due to ^{28}Al, ^{38}Cl, ^{56}Mn, and ^{24}Na, the delay between the end of counting time of one cycle to the start of irradiation of the next cycle was varied from 2 to 24 h depending on the composition of the sample matrix. After several hours delay, the irradiated sample becomes virtually inactive and the same sample can be re-irradiated and analyzed under identical conditions.

1.2 Interactions of Gamma-rays with Detector Material

The principles of gamma-ray detection are based on the interactions of gamma radiation with the detector material. The most relevant processes are photoelectric absorption, Compton scattering, and pair production [20].

Photoelectric absorption is an interaction in which an incident gamma photon transfers all of its energy to an atom causing an inner electron to be ejected. The kinetic energy of the electron is equal to the energy of the gamma

photon minus the binding energy of the electron to the nucleus. X-rays and Auger electrons are then released. The kinetic energy of Auger electrons is dissipated through a series of ionization collisions within the detector; therefore, the total energy is deposited in the detector. Generally, the whole process results in a monoenergetic peak in the energy spectrum collected by the detector, which is generally known as the full-energy peak. The energy of photon emitted from the nuclide equals the energy of the photopeak. A diagram illustrating the photoelectric interaction is shown in Fig. 1.1.

In the energy region between 150 keV and about 4 MeV, one of the most important interaction processes is Compton scattering where the incident gamma photon collides with a free electron and deflects away from its original direction. The photon transfers only part of its energy to the recoil electron depositing it in the detector. If the scattered photon is absorbed in the detector either immediately or after further scattering, the result is total photon absorption, and a corresponding count will be registered in the full-energy peak. If the scattered photon escapes from the detector, only the energy transferred to the recoil electron is deposited in the detector. The amount of energy deposited will depend on the scattering angle. In normal circumstances, all scattering angles are possible; therefore, a continuum of energies can be transferred to the detector through recoil electrons, ranging from the minimum at $\theta = 0^0$ to the maximum at $\theta = 180^0$. The escaping gamma-rays caused by the Compton effect give rise to the continuous Compton spectrum shown in Fig. 1.2.

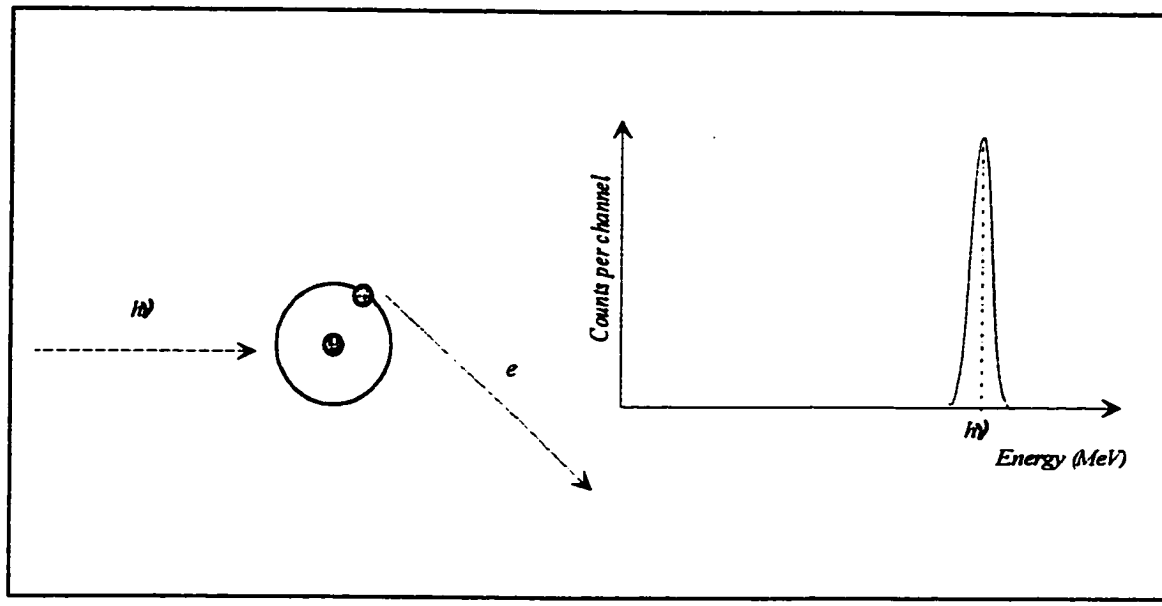

Fig. 1.1. Diagrams of photoelectric interaction and a single gamma-ray spectrum.

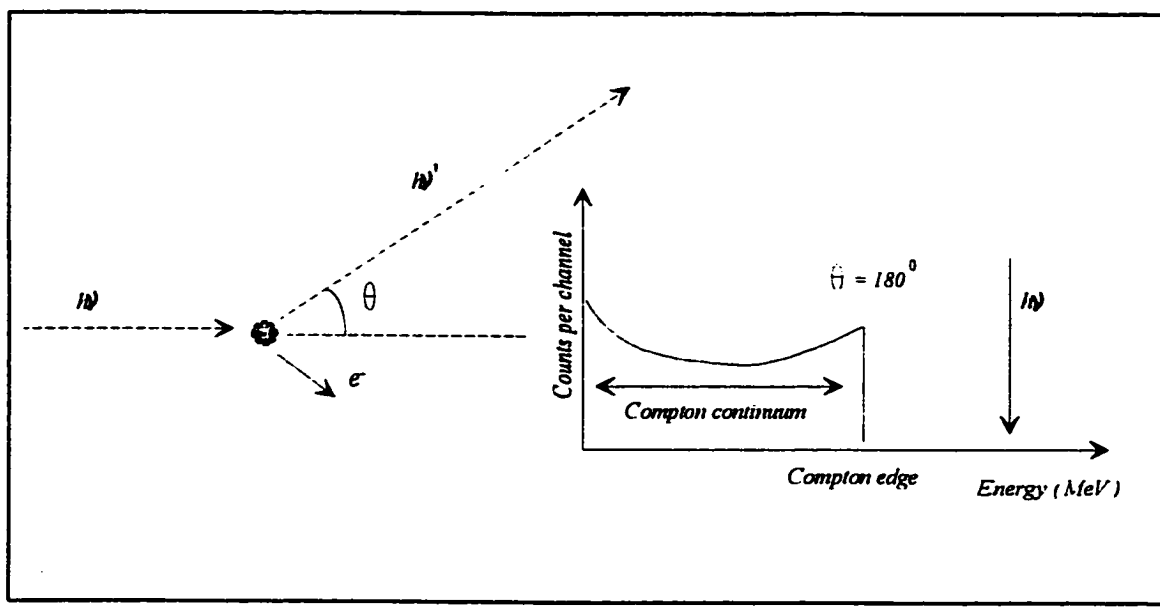

Fig. 1.2. A sketch of the Compton interaction and Compton continuum.

Pair production occurs with gamma-rays of energy greater than 1.022 MeV. The process involves converting the incident gamma photon into an electron and a positron. Virtually at the same time, the positron is annihilated with a normal electron; as a result two annihilation gamma photons with energies of 511 keV are emitted in opposite directions. One or both of these photons can escape from the detector which gives rise to two escape peaks as shown in Fig. 1.3.

If we have a detector of small size compared to the mean free path of the scattered gamma-ray, most of the incident gamma-rays will escape from the detector. Only charged particles such as photoelectrons, Compton electrons and pair electrons will be completely absorbed along with their energy within the detector volume. The energy spectrum under these conditions will be similar to the one shown in Fig. 1.4.

One can imagine the opposite case where the detector dimensions are sufficiently large so that all secondary radiations such as Compton scattered gamma-rays and annihilation photons all interact within the detector several times, and eventually photoelectric absorption occurs. Because nothing escapes from the detector, the detector response is the same as if the original gamma photon had undergone a simple photoelectric absorption in a single step. The resulting spectrum would contain a single well-resolved photopeak with no associated continuum as shown in Fig. 1.5.

Although it would be ideal to have such a gamma-ray detector, it is neither practical to construct such a large detector nor does it exist. Since there

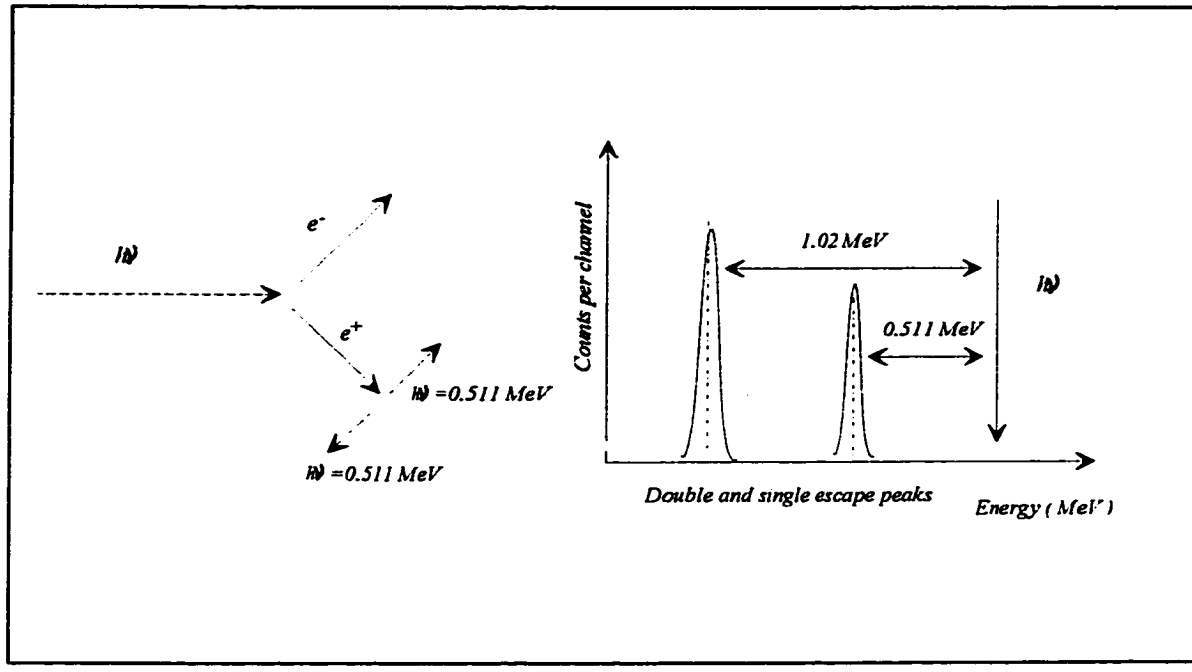

Fig. 1.3. Pair production and its escape peaks.

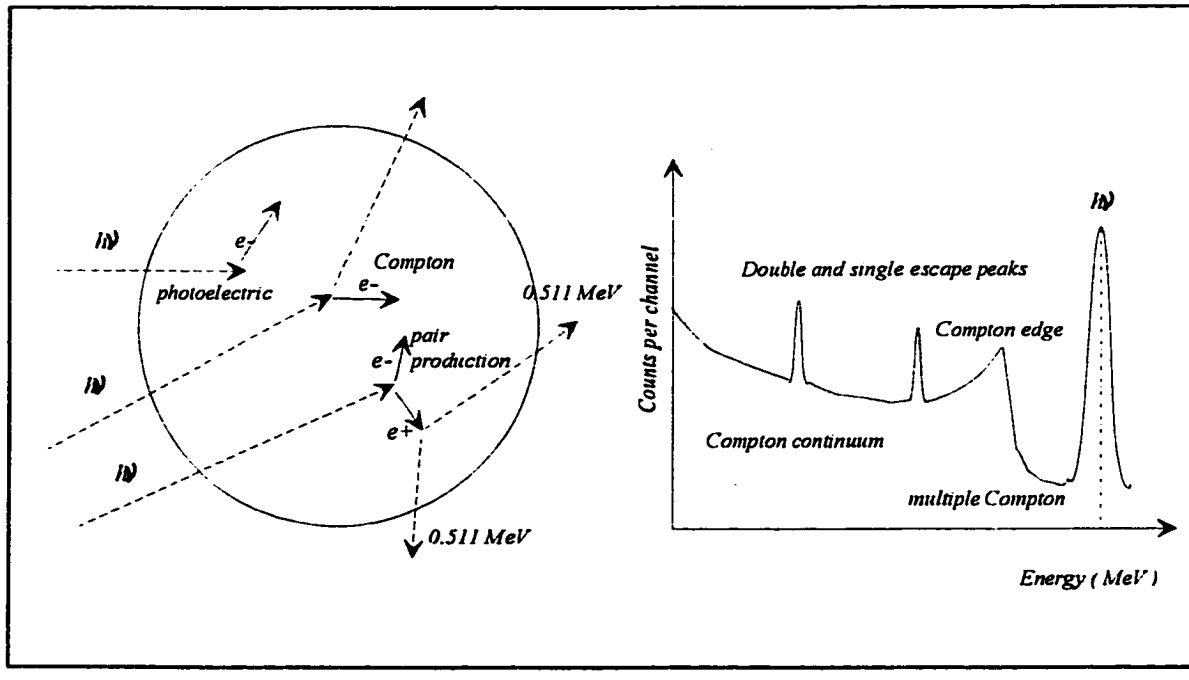

Fig. 1.4. Interaction of radiation with detector material.

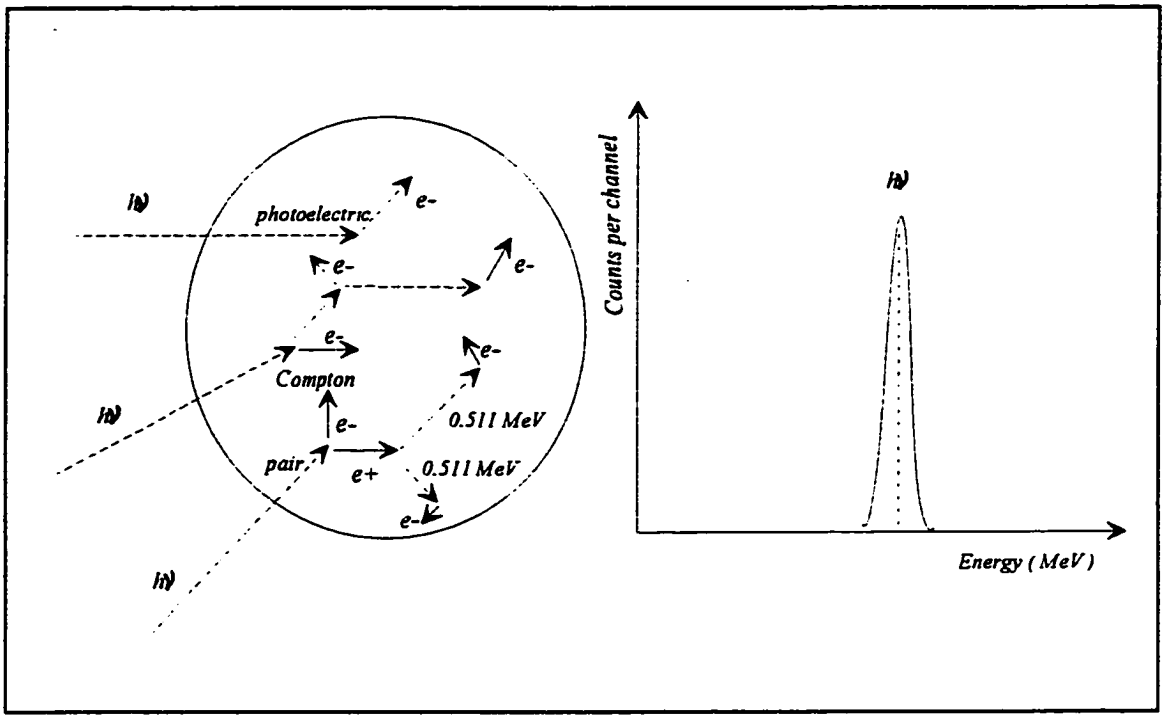

Fig. 1.5. An ideal detector and its single gamma-ray peak.

are always escaping Compton photons, the gamma-ray spectrum from the detector is always characterized by a very prominent background continuum. This continuum makes the analysis of a complex gamma-ray spectrum much more difficult. In addition, it gives a high background at the low-energy end of the spectrum due to the Compton scattering of all higher energy gamma-rays. This causes a poorer detection sensitivity for photopeaks in the lower energy region. It is desirable to suppress the Compton continuum in a gamma-ray spectrum to improve detection limits.

1.3 Compton Suppression

As mentioned above, the Compton continuum is caused by scattered photons escaping from the principal detector. Each count in the Compton continuum is accompanied by an escaping gamma-photon which can be used to differentiate this count from photoelectric events by employing anticoincidence and coincidence techniques. The result is the suppression of the Compton continuum in the gamma-ray spectrum.

The most common method of Compton suppression involves the use of an annular detector surrounding the principal crystal [21]. Compton scattering in the principal detector may produce scattered gamma-rays that interact with the surrounding annulus. If the two detectors are operated in anticoincidence mode, most of the Compton interactions in the principal detector can be rejected. Total

absorption events do not involve the escape of scattered radiation and thus are not affected by the use of anticoincidence counting.

One disadvantage of this approach is also apparent. Nuclides with complex decay schemes may emit many gamma rays in coincidence. There is a possibility of two gamma-rays from the same disintegration being detected by both detectors at the same time. These events will be considered as Compton events and rejected, leading to the undesired suppression of some full-energy peaks.

In order to solve this problem, another technique known as coincidence counting has been developed. The same equipment as that for the anticoincidence system is used except that it is in the "coincidence mode" and "an energy window setting" of the surrounding detector is set up [22]. When a specified energy is deposited in the surrounding detector, it triggers an output timing signal. The principal detector events which are in coincidence with such a signal, and hence a selected energy event in surrounding detector, will be recorded in the spectrum. The idea is that one of the cascading gamma-rays is used to gate the analog-to-digital converter (ADC) so that another peak in the spectrum is recorded with very low background. This technique is quite suitable for cases of coincident gamma-ray emitting nuclides because this additional energy requirement maintains a high peak efficiency while at the same time reduces the Compton background.

The sum coincidence mode is also used as a means of Compton suppression. This technique is based on the principle of multiple interaction [23-

25]. Most of the Compton continuum consists of a single Compton scattering followed by the escape of the scattered gamma-ray, whereas full-energy events at typical gamma-ray energies are mostly comprised of multiple scattering sequences finally ending with a photoelectric absorption. The detector can be subdivided into several segments and let the detector record only the events which involve interactions with more than one segment of the detector. The Compton continuum, usually caused by interactions within one segment, can be greatly suppressed. This reduces the full-energy peak efficiency because the events that correspond to full-energy absorption but are confined to a single detector segment are also inevitably lost. The major disadvantage of this technique is this large reduction in the full-energy peak intensity which explains why this technique can only be used for the measurement of a few nuclides.

There is another approach to reducing the Compton continuum of gamma-spectra, which attempts to select only the double escape peak [26]. If the gamma-ray energy is sufficiently high, a significant fraction of all interactions will involve pair production. The two 0.511 MeV photons produced by positron annihilation will escape from the principal detector almost always in opposite directions at the same time. On opposite sides of the principal detector, two additional detectors are placed and all three detectors are operated in coincidence mode. With this mode, only the double escape events in the principal detector can be recorded with high specificity, and most of the continuum as well as full-energy peaks will be suppressed. This procedure effectively isolates the double

escape peak and suppresses the background but at a considerable sacrifice of counting efficiency provided the gamma-ray energy is greater than 1.5 MeV.

In this thesis anticoincidence counting has been used to suppress the Compton continuum in the gamma-ray spectra of samples irradiated with neutrons. In order to quantitatively describe the benefits of anticoincidence counting several terms are frequently used. Two most commonly used terms are: peak counting statistics and peak efficiency reduction factor (PERF). These terms have been mathematically derived and explained in detail in sections 3.1 and 3.2.

In many cases, anticoincidence counting lowers not only the background under the peak but also the general background on both sides of the peak. Galloway [27] characterized peaks by peak height (N) and peak standard deviation (σ). He defined peak height as the difference between the number of counts at the maximum of the peak (N_T) and the background counts (N_B) without Compton suppression, and N_T' and N_B' with suppression, as shown in Fig. 1.6. Galloway used the term "statistical accuracy (A)" of the peak height as:

$$A=\frac{\sigma}{N} \qquad [1.3]$$

where N = (N_T - N_B) without suppression. Galloway compared the ratio of the measure of accuracy with background suppression (A) to that without background suppression (A') as:

$$\frac{A}{A'}=\left[\frac{er(R+2)}{rR+2}\right]^{\frac{1}{2}} \qquad [1.4]$$

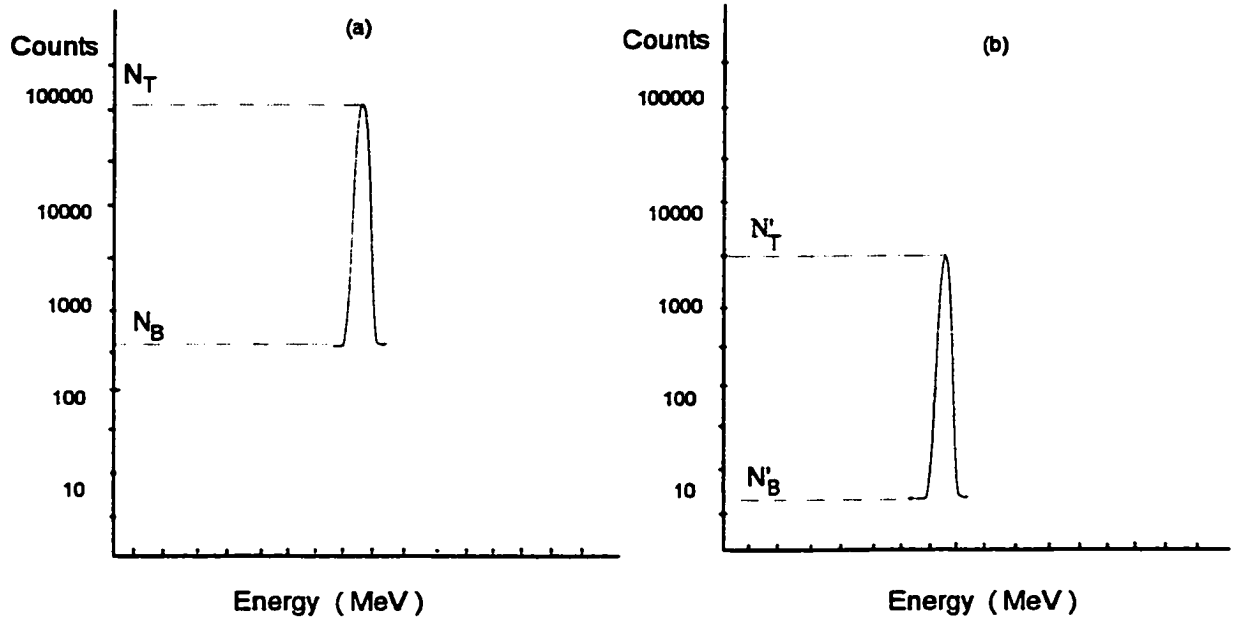

Fig. 1.6. (a) A gamma-ray spectrum of a peak superimposed on a normal background. (b) The result of applying a background suppression technique on (a).

where: R is peak-to-background ratio (N/N_B) without background suppression, r is peak-to-background ratio improvement, and e is peak efficiency reduction factor (N'/N, *i.e.* PERF). The ratio of A/A' can be used to indicate the extent of improvement in the peak height counting statistics. A value of (A/A') >1 means the peak height counting statistics is improved by anticoincidence counting. However, for cascading gamma-ray emitting nuclides, e is always less than 1. When a nuclide of interest decays with the emission of noncoincident or partially coincident gamma-rays, e could be slightly less than 1 due to random coincidence. However, the overall accuracy (A/A') may still be improved if r is sufficiently increased by Compton suppression, *i.e.* if $(e \times r) > 1$.

Therefore, the improvement in statistical accuracy depends not only on the extent of background suppression, but also on e, R, and r as shown in Fig. 1.7 [27]. For e = 1, if r is varied between 10 and 100, and R between 0.01 and 100, the improvement in overall accuracy will always be greater than 1 and to a maximum of 8. In the other case of e = 0.1 (*i.e.* the peak efficiency is reduced by a factor of 10), R <0.3, and $(e \times r) > 1$, there is a possibility of some improvement in A/A' only if r>10. Background must be reduced by 100 times or more before any improvement in A/A' could be achieved, which is hardly achievable by ordinary anticoincidence spectrometers. Thus, before applying anticoincidence counting technique to NAA, one of the most important factors to be considered is the PERF (*i.e.* e) of the nuclides of interest. One of the objectives of the present work is to calculate the PERF of short-, medium-, and long-lived nuclides and their gamma-

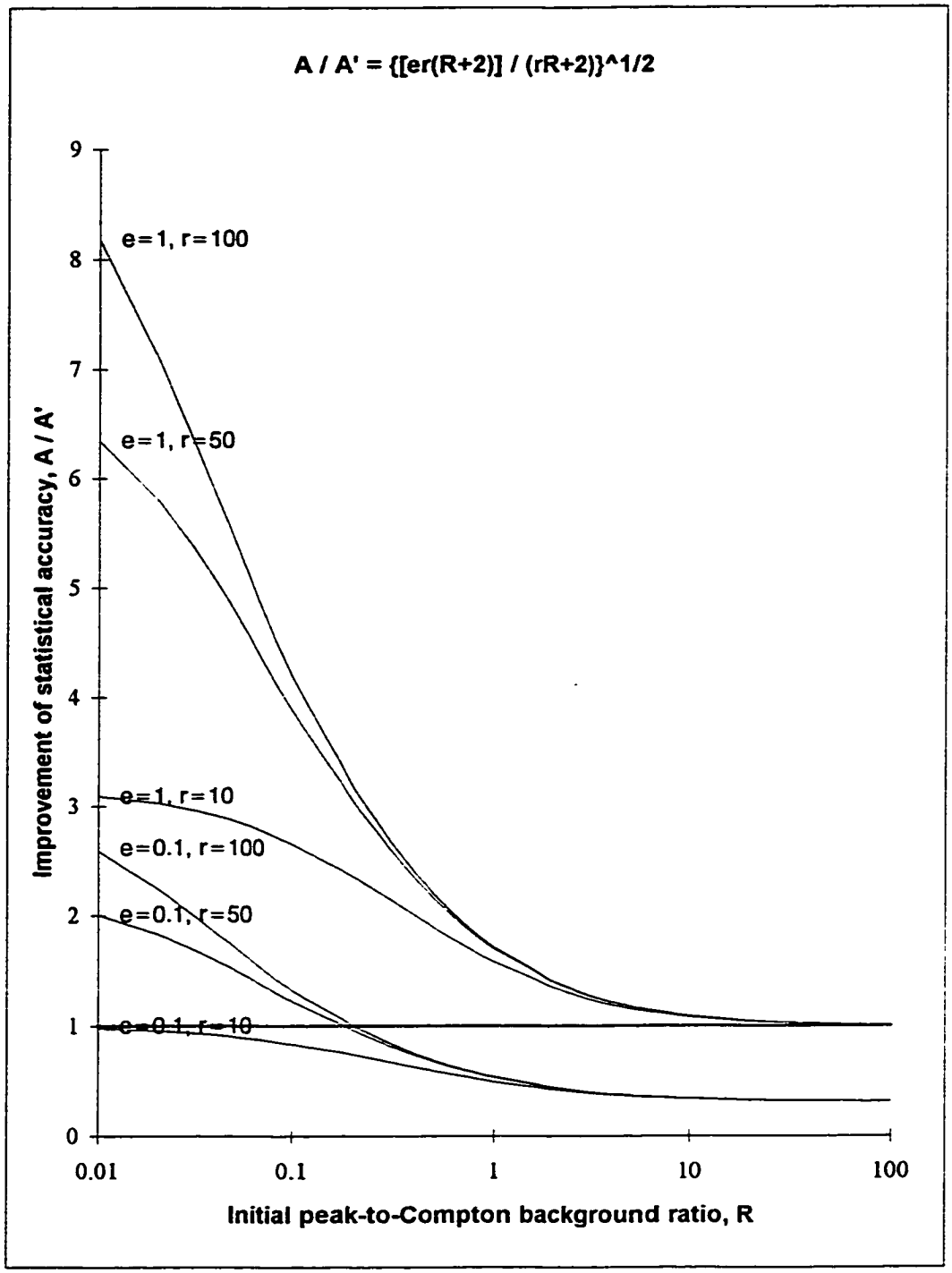

Fig. 1.7. The dependence of the improvement in sensitivity on the initial peak-to-background ratio R, peak efficiency reduction factor e, and peak-to-background improvement ratio r.

rays from experimental measurements. Our interest lies in the application of anticoincidence counting to most commonly used gamma-rays which could also have a PERF of 1.

The PERF value depends on the decay scheme of the particular nuclide and the total detection efficiency of the coincident radiation in the surrounding NaI(Tl) annulus. If one neglects the losses due to random coincident events (usually less than 1%), for a nuclide such as ^{137}Cs which has only one peak, as shown in Fig. 1.8(a), the PERF will be equal to 1 because there is no coincidence loss. In such a case, any reduction in background will improve the sensitivity of measurement.

In another case, a nuclide such as ^{60}Co decays primarily by the emission of two coincident gamma rays (Fig. 1.8(b)) with a mean life time of only 8×10^{-13} s for the 1332.5 keV gamma-ray excited state. This time is so short that the events detected by the main detector and the annulus detector will be seen as taking place at the same time and be rejected as a Compton event. For nuclides with more than two cascade gamma-rays, there is a possibility of both of them being detected in coincidence with more than one additional gamma-ray. However, this does not mean that a nuclide with multiple gamma-rays will have a very high reduction in peak efficiency. One such nuclide of interest in the present work is ^{59}Fe which has photopeaks at 143.1, 192.3, 335.4, 1099.3, and 1291.6 keV as shown in Fig. 1.8(c). The degree of peak efficiency reduction depends on the extent to which a gamma-ray is involved in the cascade. For positron emitting

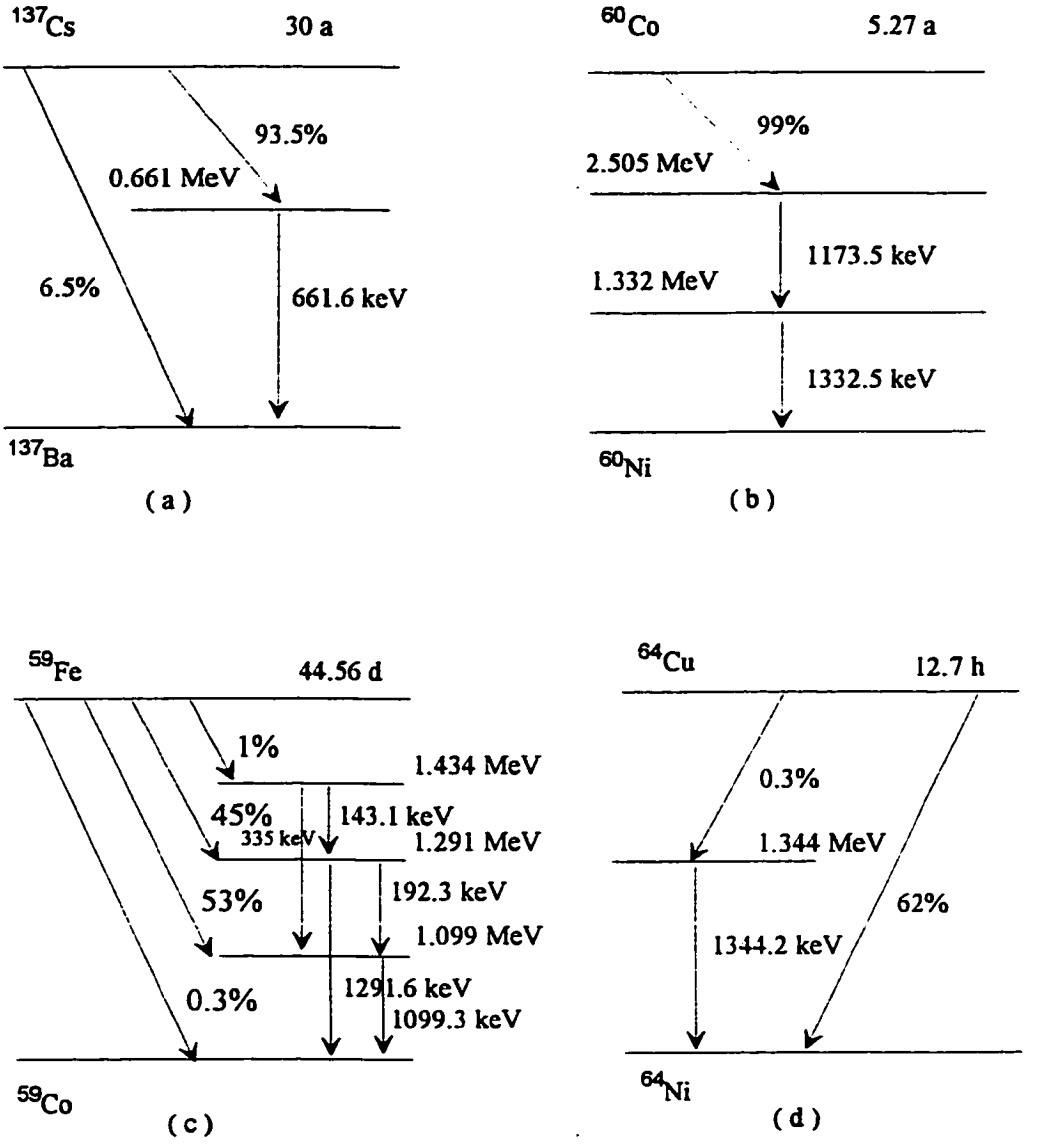

Fig. 1.8. Decay schemes of (a) ^{137}Cs, (b) ^{60}Co, (c) ^{59}Fe, and (d) ^{64}Cu illustrating cascade and independent gamma-rays.

nuclides, such as ^{64}Cu shown in Fig. 1.8(d), peak intensities will also be reduced by anticoincidence counting because of the annihilation quanta (0.511 MeV) accompanying the positron.

The improvement in A/A' for a photopeak with an e between 1 and 0.1 will depend on the extent of background suppression and the original peak-to-background ratio. Both of these factors depend on the concentrations of the element of interest and of the major or interfering elements in the sample matrix.

1.4 Sample Matrix and Background Reduction

Several of the major elements present in biological and environmental materials have stable nuclides which have high thermal neutron cross-sections; they can induce high background activities (*i.e.* Compton plateau and Bremsstrahlung) on irradiation, and can pose a serious problem in INAA. These activities can mask the photopeaks of interest, worsen the detection limits, and lead to poorer precision and accuracy. For example, the gamma-ray spectrum of a zoological material is generally dominated by Compton and Bremsstrahlung background activities from nuclides ^{24}Na, ^{38}Cl, ^{82}Br, ^{42}K, and ^{32}P, while in geological and botanical samples ^{28}Al, ^{54}Mn, ^{46}Sc, and ^{32}P can be the major interfering nuclides. Since the Compton background under a given peak results from gamma-rays with energies higher than that peak, the detection limit for the same element, even at the same concentration, will vary depending on the major

and minor elements present in the sample matrix.

It has been shown in Fig. 1.7 that the maximum improvement in statistical accuracy by anticoincidence spectrometry is obtained when the initial peak-to-background ratio (R) is small. This means that when the peak of interest is difficult or impossible to detect because of high Compton background and/or low concentration, anticoincidence counting can offer a great improvement for its measurement. For peaks with high R values (*e.g.* R>10), the improvement in A/A' is not that significant. Consequently, the improvement in the peak statistical accuracy will depend on the sample activity including background and matrix activity.

The advantages of anticoincidence counting relative to conventional counting cannot be evaluated using the peak statistical accuracy improvement factor alone. For a well-defined peak, with a high initial peak-to-background ratio, the percent improvement will be small. The peak-to-background ratio improvement factor (r) and A/A' vary with the concentrations of the element of interest and that of interfering elements in a sample. An estimate of r and A/A' can be obtained by measuring both conventional and anticoincidence gamma-ray spectra of the sample. One of the objectives of the present work is to develop a term for the prediction and evaluation of the practical advantages of anticoincidence counting. Such a term called "Analytical Figure of Merit (AFOM)" has been developed here and is described in Section 3.2. It has been applied for a number of elements using their short-, medium-, and long-lived nuclides to 16

different biological reference materials representing various types of sample matrices and interfering elements.

1.5 Development of Compton Suppression Spectrometers

Although the principles of Compton suppression have been well known for many years, but were not put into practical use until the 1950's. Hofstadar and McIntyre [28] in 1950 used two detectors, one at a specific angle with respect to the other, and recorded pulses from both detectors in coincidence to accurately measure the energies of gamma-rays. The technique was then introduced for the measurement of photopeak areas in gamma-ray spectra with the aims of suppressing Compton background and improving detection limits. The development of this technique has occurred in roughly three stages.

The first stage involves the use of NaI(Tl) detectors as main (principal or primary) detectors. A number of procedures were put forward for eliminating the Compton continuum that appears in scintillation spectra. One system was developed by Albert [29] in 1952. This system consisted of a cluster of NaI(Tl) crystals which surrounded the main NaI(Tl) detector as completely as possible, *i.e.*, the cluster covered the main detector in almost 4π geometry, and they were connected to the main detector in anticoincidence with each other. The spectra showed that Compton backgrounds from ^{137}Cs and ^{24}Na were substantially suppressed. Several improved scintillation spectrometers were then constructed.

Instead of a cluster of NaI(Tl) crystals for which the light collection properties were relatively poor, phosphor solutions [21] and plastic phosphors [30] were used as guard detectors in order to increase the efficiency of the shielding. At that time, the reduction in the Compton background was good but scientists still aimed at greater Compton reduction to permit observations of very low intensity gamma-rays.

A combination of various sizes and shapes of primary NaI(Tl) crystals surrounded by a large liquid phosphor shield was studied by Davis and Bell [31]. The results showed that a 4.75" diameter NaI(Tl) crystal, with a 0.25" hole which extended approximately to the centre of the crystal, surrounded by a 28" liquid phosphor shield gave best Compton suppression; the peak-to-Compton ratio was 90:1 in a ^{137}Cs spectrum. Trail and Raboy [32], in order to reduce the size of the spectrometer and to increase the efficiency of shielding, designed a system consisting of a 2.4" diameter x 6" long NaI(Tl) crystal placed inside a 12" i.d. x 8" o.d. NaI(Tl) annulus which was "optically cemented" by three hollow NaI(Tl) cylindrical detectors.

Perkins *et al.* [33] designed two Compton suppression spectrometry systems. In one system, the principal detector was a 5" x 5" NaI(Tl) crystal surrounded by a large plastic phosphor shield. In the other, a 3" x 3" NaI(Tl) principal detector was placed in a NaI(Tl) well-type guard detector. The Compton suppression ability of the two systems was compared. They found that although the plastic phosphor is not effective at high counting rates and has a low

efficiency, it can be used to build large shields which can hold large principal detectors.

Busuoli *et al.* [34] in 1962 constructed an anticoincidence spectrometer consisting of a 1.75" x 2" NaI(Tl) detector placed in a plastic scintillator shielding of 29.8 cm x 26.4 cm. The ratio of peak-to-total area for this system is 0.610 for ^{137}Cs compared favourably to that of a 4" x 4" Na(Tl) detector without anticoincidence shielding.

Along with the development of instruments, some new applications were also investigated. Bostrom and Draper [35] in 1961 used an anticoincidence system in a neutron capture study for measurements in the 0-10 MeV energy region. Beech *et al.* [36] in 1964 placed a high-resolution solid state detector into an anticoincidence system with an annular plastic scintillator. This successfully reduced the Compton background and made it possible to examine complex spectra, such as those from fission product sources.

In 1964 Perkins [37] designed a multidimensional gamma-ray spectrometer based on his old system [33]. The new system consisted of two NaI(Tl) principal detectors and a well-type NaI(Tl) anticoincidence annulus of 11.5" diameter x 12" thickness for simultaneous anticoincidence and coincidence countings. Nuclides which emit two or more gamma-rays can often be measured with much better precision and sensitivity by the coincidence counting technique. The shielding annulus could be used in conjunction with the other two for triple coincidence gamma-ray spectrometry or anticoincidence shielded gamma-gamma

coincidence studies. This system provided selectivity and sensitivity for the measurement of many nuclides, and was orders of magnitude better than those with a single crystal gamma-ray spectrometer.

In order to efficiently use this multidimensional spectrometer, Kantele and Kohonen [38] developed a versatile routing system for the multichannel analyzer (MCA) by which four independent spectra can be simultaneously stored. These would include conventional, coincidence and anticoincidence gamma-ray spectra. With certain modes of operation, it is also possible to store the sum of the amplitudes of two coincident pulses. Kantele *et al.* [39] developed an anti-Compton annulus in conjunction with different coincidence spectrometer configurations. This approach provided a great versatility in gamma-ray spectrometry. With this system, the annulus can function as the principal detector or it can be employed for coincidence or anticoincidence gating using different electronic configurations. It can be used as a total absorption spectrometer, an anti-Compton spectrometer, a summing Compton spectrometer, a multiple coincidence spectrometer, and a pair spectrometer. Maximum and average reduction factors of 11.7 and 5.4, respectively, were obtained for the 1332.5 keV peak of ^{60}Co by the anti-Compton spectrometer.

In 1966, Evans *et al.* [40] followed up by enlarging the size of the central crystal and the anticoincidence shielding, and obtained a higher peak-to-total area ratio than that by using detectors of smaller size. Their experiment made it clear that larger the annulus and the principal detector, the better is the

suppression.

Several researchers suggested various configurations for Compton suppression spectrometers (CSS) with an aim to reduce the Compton continuum. At the same time, the applications of CSS to such fields as nuclear reaction studies, neutron capture spectroscopy, and low-level counting for environmental studies appeared in the literature.

The poor resolution of the NaI(Tl) detector greatly restricted its use in gamma-ray spectrometry. The second stage of development started in the late 1960's when lithium-drifted germanium, Ge(Li), detectors became available. The Ge(Li) detectors made it possible to record gamma-ray spectra over almost the entire range of nuclide or capture gamma-ray energies (*viz.* 50 keV to 4 MeV) with much better resolution and satisfactory efficiency. Due to the disadvantage of the inferior peak-to-background ratio resulting from the Compton background, anticoincidence counting techniques were used in combination with the Ge(Li) detectors as soon as they were available.

Sever and Lippert [41] were among the first researchers to place a Ge detector into a NaI(Tl) well in anticoincidence counting mode. With this system, the Compton edge of a ^{137}Cs spectrum was lowered by a factor of about 9, but the system had the disadvantage of being unable to completely remove the backscattered peaks which resulted from the p-layer of the counter and the metal support. Kantele and Suominen [42] built a system in which the sample was placed outside the guard detector, and found to be more suitable for highly active

sources. In this system, the maximum reduction of the Compton background was 16 (near the Compton edge) and the average suppression of the tail above 0.3 MeV was 9.8. They concluded that in order to obtain the most effective overall Compton suppression, one must find the optimum relative positions of the Ge detector and the NaI(Tl) annulus. Since both ends of the annulus were open, gamma-rays scattered through small and large angles could freely escape the system. The high-energy gamma-rays escaping through the small angle give rise to a smooth increase in the Compton tail, and those escaping through the large angle give rise to the Compton edge. Consideration must be given to both of these phenomena to obtain better Compton suppression.

Several different systems were developed at this stage. In 1966, Orphan and Rasmussen [26] built a system for use in a neutron capture study that can work in two ways. They positioned a 30 cm^3 coaxial Ge(Li) detector between two NaI(Tl) detectors and pulses from these three detectors were put through a triple coincidence circuitry to gate an MCA. This configuration was capable of being used as a pair spectrometer at high energies and in the Compton suppression mode at low energies to study double-escape peaks, single escape peaks, and full-energy peaks. The ratio of the double-escape peak-to-background was improved by a factor of 70. The average Compton background was reduced by a factor of 2.2.

Wogman *et al.* [43] developed a multidimensional detector system in which four detectors were used. Two of them were main detectors that could

work in conventional and coincidence modes; the third served as an anticoincidence annulus; and the fourth detector was in the form of an annulus disc for further reduction of the backscatter response. The advantage of this system was that two coincidence photons each interacting with a different main detector were stored in the MCA, and the gamma-rays which were scattered from the two principal detectors had a high probability of being detected by the plastic phosphor annulus or by the backscatter detector causing a cancellation of that particular photon event. This type of system can solve the problem of detecting cascading gamma-rays using anticoincidence spectrometer, and can enhance the sensitivity of their detection.

In 1969, Wogman *et al.* [44] made an improvement of the above system by exchanging plastic annuli with NaI(Tl) shields. This all-NaI(Tl) multidimensional gamma-ray spectrometer was carefully evaluated. The major advantage of the NaI(Tl) anticoincidence shield over the plastic phosphor shield was that the former provided better discrimination at low energies because the NaI(Tl) has a much higher detection efficiency for the scattered radiation from low-energy photons.

Auble *et al.* [45], in 1966, developed a versatile system which was characterized by a split annulus NaI(Tl) detector. In this system, the split annulus detector could be used as an anticoincidence spectrometer if the optically isolated halves are operated separately. One can also do triple coincidence experiments using this spectrometer. This system solved the problem of an anticoincidence

system that cannot distinguish between scattered events and true coincidences from gamma-ray cascades.

Progress on the development of anticoincidence systems continued. Cooper and Brownell [46] designed a system consisting of a 35 cm^3 Ge(Li) detector surrounded by a large plastic scintillator which was operated in anticoincidence mode. This system had two counting positions: an upper position and a lower position in which the plastic scintillator could not "see" the sample directly. In the upper position, counting could be done in anticoincidence and free mode. Thus very weak samples requiring high counting efficiency could be measured in the upper position with the free mode, while samples requiring Compton suppression could be measured in the lower position.

Gruhn *et al.* [47] used one Ge detector to construct a Compton suppression system. They placed two Ge segments to make one detector. Whenever a recoil Compton electron in one segment was detected simultaneously with a scattered photon in the other segment, the resulting summed pulse corresponded to the full-energy of the incident gamma-ray. Instead of eliminating the detection of Compton events, in this system the Compton events were emphasized by demanding a coincidence between the two Ge segments. This device showed considerable promise in detecting gamma-rays in the presence of strong Compton and neutron backgrounds.

Michaelis and Kupfer [48] made an improvement of the above system for the purpose of lowering the cost. A hole in the front of plastic annular

scintillation shielding detector was made and a NaI(Tl) section was inserted. Because of the higher density of NaI(Tl), this device could effectively absorb gamma-rays scattered in the forward direction (*i.e.* higher energy gamma-rays). For this system, the peak-to-background ratio at the Compton edge was 40:1 and 100:1 for smaller scattering angles.

Since the detection of weak gamma-rays masked by the prominent Compton tail of other peaks was more important, it appeared that a spectrometer providing suppression in the low-energy region would be welcome. For this reason, Kantele and Suominen [49] in 1967 built a system consisting of two Ge(Li) detectors, one at a specific angle with respect to the other. The gamma-rays from samples were collimated and the coincident pulses from two detectors were added and the sum analyzed. Then they designed a total absorption Ge(Li) gamma-ray spectrometer. Their idea was that since many Compton scattered gamma-rays were further scattered many times in the detector's sensitive volume but were still totally absorbed, these events would appear in the energy peak together with the photoelectric events. In fact, at energies greater than 600 keV, these events comprise 80% of the full-energy peak. If a detector were divided so that each event could be identified for its local characteristics, single position events could be distinguished from others. Using this property, they could reject single position events and discard that portion of the Compton continuum. The disadvantage of this approach was that up to 20% of the peak due to photoelectric interaction was sacrificed.

The third stage of development started with Sayres and Baicker [23] and Palms *et al.* [24] who developed diode Ge(Li) detectors which consisted of two planar or concentric coaxial detectors within a single crystal of Ge. Coincidence techniques were used to record a gamma-ray which interacted by multiple processes (*i.e.*, one or more Compton events followed by a photoelectric event) in each portion of the diode Ge(Li) detector. In this case, an event in the full-energy peak was recorded only if the total energy deposition occurred as a result of multiple events. The resulting spectrum was made up of full-energy peaks above a low background without Compton edges.

In 1968, Alexander *et al.* [50] built a system for an accelerator experiment. In this system, three detectors were operated in triple coincidence and anticoincidence modes, simultaneously yielding pair and escape suppressed spectra. Hick and Pepelnik [25], in the same year, developed a Ge(Li)-Ge(Li) coincidence summing technique. The idea was that if two detectors were used, one for the backscattered ($\theta > 135^{0}$) Compton quanta and another for its Compton electrons, then the summing coincidence pulses from these two detectors would be recorded under the full-energy peak. For this device, good peak-to-tail ratios of 400 at 662 keV and 360 at 1120 keV were obtained. From the consideration of different behaviour of high-energy and low-energy gamma-rays, White and Birkett [51] developed a system which combined pair spectrometry and anticoincidence spectrometry together to work in different energy regions. In the 0.06-2.5 MeV low-energy region, a Ge(Li) detector worked in anticoincidence mode with a NaI(Tl)

annulus, and in the 2-12 MeV high-energy region a Ge(Li) detector flanked by two NaI(Tl) counters operated in coincidence mode (*i.e.* a three-crystal pair spectrometer).

In 1971, a spectrometer was designed by Cooper and Perkins [22,52] to maximize the solid angle by utilizing two high-efficiency Ge(Li) detectors located opposite to each other. Both Ge(Li) detectors were operated in anticoincidence with the entire plastic phosphor shield as well as in anticoincidence with one other. This design provided greater sensitivity and versatility for measuring low levels of nuclides. In addition, it could be used in the modes of gamma-gamma coincidence with and without anticoincidence shielding. Later on Cooper and Perkins changed the plastic phosphor shielding to NaI(Tl) in order to further improve sensitivity for both coincident and noncoincident gamma-ray emitting nuclides.

For the purpose of comparing several spectrometers and evaluating their performances, a series of standard experiments and calculation procedures were set up. These included peak-to-Compton ratios, resolution, efficiency, as well as background and Compton reduction factors. One system developed by Cooper and Perkins [52] with a peak-to-Compton edge ratio of 790:1 was the highest one reported so far.

In general, the CSS developed during this third stage can be divided into two basic categories: all Ge(Li) coincidence summing spectrometers and

anticoincidence shielded Ge systems. The latter spectrometers can be further subdivided into two groups: those with the source inside the shield, and those with the source outside. A number of sophisticated Ge(Li) Compton suppression spectrometers were developed.

1.6 Compton Suppression Spectrometry in Fields other than NAA

Along with the development of instruments, several studies on applications of these systems were done. In 1970, Lewis and Shafrir [53] built a Ge(Li)-NaI(Tl) anticoincidence system which gave good sensitivity for the detection of many radionuclides in environmental samples without any chemical separation. Levels of ^{137}Cs in biota, sediments and seawater were measured and found to have a range of 0.02-0.15 pCi/μg, with a relative standard deviation of 10-20%. A decrease in the ^{137}Cs activity with increasing depth was observed for seawater samples.

In 1980, Wogman and Laul [54] investigated radionuclides in construction materials used for building detection systems by a low-level gamma-ray spectrometer. Results showed that, in general, aluminum contained high quantities of ^{232}Th and ^{238}U and minimal amounts of ^{40}K, and stainless steels contained ^{60}Co. The radioactive contents of foams, cements and light reflective materials were quite variable, and the molecular sieve materials used in Ge detectors contained 4-9 dpm g^{-1} of total activity.

A HPGe/NaI(Tl) system with an optimum Compton suppression factor of 52 at 662 keV [55] was used for environmental monitoring of rainwater collected after the Chernobyl accident in 1987. The minimum detectable concentration of ^{137}Cs in the precipitation was 0.03 Bq L^{-1}.

Yuan *et al.* [56] used a Compton suppression gamma-ray spectrometer to routinely monitor radionuclides in the gaseous effluent and in the water coolant from a research reactor facility. The system had a HPGe detector and NaI(Tl) annulus, and it greatly improved the detection limits of ^{131}I and ^{41}Ar activities. More recently, Sanchez *et al.* [57], using Monte Carlo calculations simulated Compton suppression of NaI(Tl), plastic, and BGO, along with a HPGe primary detector, that could be encountered in counting of large environmental samples in Marinelli beaker and petri vial geometries.

The next series of advances occurred in the late 1970's. At this time, several anti-Compton and anticoincidence shielded gamma-gamma coincidence spectrometers were built for the purpose of studying (HI,xn) reactions [58, 59]. Since the gamma-ray spectra produced in heavy ion (HI) induced reactions were rather complex, there was a demand for spectrometers with high resolution and low background. For this purpose, various configurations and materials were used, and many new designs were attempted. These included asymmetrical design (in order to obtain effective suppression in the low-energy part of the spectrum), fast slow coincidence electronic circuits (to reduce the accidental coincidence rate between the Ge(Li) and the annular detector), and bismuth

germanate (BGO) scintillation materials used for suppression shields.

A study on the effect of the dead-layer thickness of the Ge(Li) detector on Compton suppression showed that the thinner the dead layer, the better was the suppression [60]. The geometry and dimensions of NaI(Tl) anticoincidence shields were optimized by means of Monte Carlo calculations [61]. It was shown that a high solid angle gave excellent Compton suppression and that an asymmetrical arrangement gave superior suppression, particularly for high-energy gamma-rays which preferentially scatter in the forward direction.

Herges and Klapdor [62] put two Compton suppression spectrometers together by using one integrated anticoincidence shield consisting of a NaI(Tl) detector optically divided into four parts for both Ge(Li) detectors in order to increase solid angle. As a result, an extraordinarily large solid angle of 100 msr was obtained for each of the two spectrometers at the same time. The total solid angle of the NaI(Tl) shield was minimized eliminating the key problem for measuring gamma cascades.

In order to increase the efficiency of detection for scattered gamma-rays, BGO was used by Lieder *et al.* [63], Nolan *et al.* [64] as well as by Byrne and Dracoulis [65]. Due to the high density of BGO, it has a total gamma-ray absorption coefficient that is about 2.2 times larger than that of NaI(Tl). As a result, the size of the anticoincidence shield can be reduced; this allows for an increase in the solid angle. However, NaI(Tl) was still used in the front of the guard detector because of its better light transport properties. Monte Carlo

calculations were also used to calculate the degree of suppression as a function of various parameters.

The idea of using anticoincidence counting has been applied to X-ray spectroscopy by Gloystein *et al.* [66]. A Si(Li)/CsI(Tl) anticoincidence system was set up, in which the Compton background mainly caused by the scattering of gamma-rays in the Si(Li) detector, could be reduced. Their results showed that such a system could be used to improve the sensitivity of PIXE analysis for trace elements of high atomic number such as Mo, Cd and I. Peelle and Spencer [67] used the anticoincidence technique for efficiency calibration of a multiplicity detector to reduce statistical uncertainty. A HPGe/NaI(Tl) [68,69] anticoincidence and coincidence system was used for investigating the β^--decay of ^{180m}Ta and ^{48}Ca.

1.7 Compton Suppression Spectrometry in NAA

The Compton suppression spectrometer has been around since the 1950's. The electronic instrumentation and spectrometry systems have been periodically developed over the last 40 years or so. Recently, much more attention has been paid to this technique by nuclear analytical chemists. Anticoincidence spectrometry has lately been used in INAA, EINAA and RNAA for the suppression of the Compton background and to improve detection limits for several nuclides.

Wogman *et al.* [70] used a ^{252}Cf irradiation facility with a neutron flux

of 1×10^{10} cm^{-2} s^{-1} and a Ge/NaI(Tl) multidimensional gamma-ray spectrometer to detect over 65 elements, and over 40 of them were measurable at the 1 ppm level with a precision $\pm$10%. They concluded that the method could be used for the routine multielement analysis of a wide variety of solid and liquid samples.

In 1976, Murata *et al.* [71] developed an automated NAA system for medium-lived nuclides and reported that the detection limits for nuclides such as ^{28}Al, ^{66}Cu, ^{56}Mn, ^{51}Ti, and ^{52}V in aerosol samples could be improved using an anticoincidence system.

In the same year, Rosick and Bratter [72] designed a system which could work in both anticoincidence and coincidence modes. The operation of the spectrometer in the coincidence mode resulted in a significant suppression of the Bremsstrahlung background, which was highly advantageous for the analysis of phosphorous-rich biological materials. In the analysis of blood serum, the ^{32}P background was reduced greatly, making it possible to improve the detection limit by a factor of 5 for the determination of selenium via the 136.0-keV gamma-ray of ^{75}Se.

Laul *et al.* [73] applied anticoincidence spectrometry to the preconcentration NAA (PNAA) and radiochemical NAA (RNAA) of rare earth elements (REE) at ppb to ppt levels. Their experiments showed that an anticoincidence system was favoured for the following nuclides: ^{141}Ce, ^{143}Ce, ^{142}Pr, ^{153}Sm, ^{171}Er and ^{175}Yb. In 1988, Laul *et al.* [74] again used this technique to measure REE in briny ground waters. They noted that ^{140}La, ^{153}Sm, ^{152}Eu and ^{160}Tb were better measured using

a conventional system, while ^{141}Ce, ^{143}Ce, ^{142}Pr, ^{147}Nd, ^{170}Tm and ^{175}Tb were measured best using an anticoincidence system; for ^{153}Gd, ^{166}Ho, ^{169}Yb and ^{177}Lu, either counting system was equally effective.

Since count rates can vary greatly in NAA, Millard [75] investigated the effect of count rate on the ratio of the photopeak counts in the anticoincidence and coincidence spectra (called A/C ratio) for different nuclides. He found that a calibration curve is necessary in order to obtain quantitative data in anticoincidence counting, especially at high count rates.

As soon as instrumental photon activation analysis (IPAA) was recognized as a technique complementary to NAA, the Compton suppression technique was used by Ledingham *et al.* [76] for the determination of trace elements in NIST (U.S. National Institute of Standards and Technology) Coal and Fly Ash standard reference materials (SRMs). When an asymmetric NaI(Tl) annulus was used in anticoincidence mode, the sensitivities for ^{67}Cu, ^{99}Mo, ^{237}U, and ^{65}Zn were increased by as much as a factor of 3. When operated in coincidence mode, the detection of ^{47}Ca, ^{60}Co, ^{42}K, ^{24}Na, and ^{46}Sc was enhanced.

Zeisler and Becker [77] used a Compton suppression spectrometer to measure zinc in a Monel alloy. They achieved a Compton suppression factor of greater than 20, a relative uncertainty of 18% at the 95% confidence level, and an accuracy of better than 94% for the determination of zinc.

Das and Zonderhuis [78] and Das [79,80] proposed an advantage factor as a parameter to estimate the inherent advantage of anticoincidence

counting over conventional counting. They showed that the influence of anticoincidence counting on the limits of decision, detection, and determination could be calculated from the reduction factors of peak and Compton background. They investigated peak area and Compton continuum reduction factors as well as advantage factors for many nuclides in several matrices. They reported that interferences due to ^{24}Na and ^{82}Br in biological samples could be eliminated for detecting nuclides with half-lives greater than 50 h. In silicate matrices, detection limits were lowered by up to a factor of 4, ^{82}Br interference was reduced, and the scope of INAA was extended.

In the 1990's, nuclear analytical chemists became more interested in the application of Compton suppression systems to NAA primarily because of its ability to reduce background activities. Landsberger *et al.* [81] used the Compton suppression technique combined with epithermal NAA to determine arsenic in artificially doped urine samples and in biological and geological reference materials. They obtained a detection limit of 10 ppb, relative standard deviation (RSD) of $\pm$2-12%, and accuracies of 80-99%.

Later on, iodine and other halogens in bioenvironmental samples were determined by the same group [82] using thermal and epithermal neutrons in conjunction with Compton suppression spectrometry. For the measurement of iodine, they concluded that the use of epithermal neutrons dramatically increased the sensitivity while the Compton suppression method lowered the detection limit even further.

Another study by Landsberger [83] applied the same system to the determination of nanogram levels of cadmium in seven biological reference materials with epithermal NAA. Detection limits between 10-20 ppb were obtained with an overall RSD of $\pm$4%-15%. Landsberger *et al.* [84] reported the measurement of cadmium in air filter samples in which the detection limit for this element was lowered to a few ng per filter. Results showed that cadmium concentrations were significantly higher in a room with tobacco smoke compared to the background levels. An anticoincidence spectrometer was utilized to increase the sensitivity for nuclides which emit gamma-rays between 200 and 800 keV in a research project on the elemental characterization of size-fractionated municipal solid waste incinerator ash [85].

Carlson [86] measured cadmium in biological certified reference materials using a Compton suppression system and stated that the method could provide an improved detection limit of 50 ppb needed for the INAA determination of cadmium in biological specimens.

Khrbish and Spyrou [87] used a Compton suppression spectrometer to investigate the applicability of the absolute method in prompt gamma-ray NAA (PGNAA), and experimentally determined the advantage factor for a number of elements.

Masse *et al.* [88] used a system in both anticoincidence and gamma-gamma coincidence modes. Using the anticoincidence mode, the activity of ^{189}Ir was determined while the coincidence mode was used for ^{101}Rh. The detection

limits of ^{189}Ir and ^{101}Rh were lowered by factors of 4 and 15, respectively.

A new method for the determination of iridium was proposed by Cumming *et al.* [89]. Since the long-lived nuclide ^{192}Ir, the most commonly used nuclide for iridium determination, has a cascade decay scheme, its counting efficiency will be suppressed along with the background in anticoincidence spectrometry. They used a well-type HPGe detector/NaI(Tl) annulus anticoincidence spectrometer for the enhancement of the 784.6 (316.5 + 468.1) keV and 920.9 (296.0 + 308.5 + 316.4) keV sumpeaks of ^{192}Ir and the reduction of the Compton background for iridium determination. This is the first reported example of the usage of a sumpeak in conjunction with anticoincidence spectrometry. By this method, iridium can be determined instrumentally with a detection limit around 5 ppb in peridotite.

In 1990, this work was further developed by Murali *et al.* [90]. They designed a well-type HPGe detector and annulus NaI(Tl) crystal system so that it can be operated both in coincidence and anticoincidence modes. It was well suited for the nondestructive measurement of Ir in diverse types of small geological samples (less than 20 mg). Detection limits ranging from 0.1 ng to 0.004 ng, depending on the sample matrix, were obtained. This method could also be applied to microsamples of about 1 μg for the measurement of Ir.

Most recently, Lin *et al.* [91] have designed an innovative Compton suppression spectrometer. The main detector of the system is a low energy HPGe detector (LO-AX), which is shielded by 50% n-type HPGe and two Na(Tl) detectors.

The Compton suppression cut-off energy is 15 keV. The capability of applying this system to INAA has been evaluated for 13 elements in biological and environmental samples. The advantages and problems of using this system are discussed for each element.

Deibel *et al.* [92] reported the use of coincidence and anticoincidence techniques for non-destructive analysis of Cu in human brain tissues. In this method, the tissue samples were irradiated in an epithermal neutron flux of 2×10^{11} cm^{-2} s^{-1} for 5 min, allowed to decay for 3 min, and the 1039.2 keV peak of ^{66}Cu counted in an anticoincidence spectrometer for 10 min. The minimum detectable amount of Cu is about 6 ppm dry weight, which is comparable to the value obtained by coincidence spectrometry of annihilation photons from the positron emitting nuclide of ^{64}Cu after long irradiations.

Landsberger and Peshev [93] recently published a review paper on Compton suppression in NAA, for low-level counting and in-beam experiments. The application of Compton suppression counting in INAA reduces the detection limits and improves the accuracy for several elements by substantial reduction of the background activities. They concluded that future applications of coincidence spectrometry in activation analysis should include better enclosures of the primary detector, utilization of X-ray and well-type detectors, as well as gamma-gamma, beta-gamma, and beta-gamma-gamma coincidence techniques.

Mauerhoger *et al.* [94] developed a Compton suppression spectrometer using three main Ge detectors and an anticoincident shield

consisting of a BGO annulus and a CsI(Tl) active collimator. The sample was counted outside the anti-Compton shield. The performance of the system with respect to Compton suppression was evaluated by calculating Compton suppression factors of ^{28}Al, ^{198}Au, ^{60}Co, ^{137}Cs, ^{51}Ti, and ^{52}V in the energy range of 300 to 1800 keV.

1.8 Objectives

An anticoincidence gamma-ray spectrometer has been set up by ORTEC at the Dalhousie University SLOWPOKE-2 Reactor (DUSR) facility. The spectrometer consists of a high-resolution HPGe detector surrounded by a 10" x 10" NaI(Tl) annulus and a 3" x 3" NaI(Tl) plug. One of the first objectives of this research project was to evaluate the performance of this spectrometer. Various ratios such as the peak-to-Compton plateau, peak-to-Compton edge, and peak-to-total area were calculated using ^{60}Co and ^{137}Cs standard sources. Background suppression ratios (BSR), which is the ratio of background counts by conventional gamma-ray spectrometry to that by anticoincidence spectrometry, were measured for gamma-ray energies between 80 and 2000 keV using a mixed source of ^{152}Eu and ^{154}Eu. The effectiveness of this Compton suppression system was examined using an advantage factor, defined by the ratio of the peak-to-background in the anticoincidence spectrum to the corresponding value in the conventional spectrum, with the aid of a mixed source of ^{152}Eu, ^{59}Fe, and ^{95}Zr. The effects of annulus

position and the sample distance were examined in order to obtain the best anticoincidence counting efficiency.

It is evident from the literature survey in the preceding section that most of the studies on anticoincidence gamma-ray spectrometry have been concerned with either a few elements or a particular application. Very few researchers have systematically investigated the merits and limitations of anticoincidence counting for the nuclides which are most commonly used in NAA. One of the objectives of this thesis was to experimentally determine PERF values and sensitivities of short-, medium-, and long-lived neutron activation products.

Much of the past research in anticoincidence spectrometry was focused on long-lived neutron activation products. A recent trend in NAA, however, has been to utilize short- and medium-lived nuclides which have many advantages over their long-lived counterparts. A technique called pseudo-cyclic INAA (PCINAA) is particularly beneficial for the detection of short-lived nuclides (half-life < 120 s). One of the purposes of this research was to investigate the following short-lived nuclides by PCINAA in conjunction with anticoincidence spectrometry: ^{108}Ag, ^{110}Ag, ^{165m}Dy, ^{20}F, ^{75m}Ge, ^{179m}Hf, ^{86m}Rb, ^{46m}Sc, ^{77m}Se, and ^{177m}Yb. Medium-lived nuclides (half-life < 3 h) which are commonly used in NAA, namely ^{28}Al, ^{139}Ba, ^{80}Br, ^{38}Cl, ^{66}Cu, ^{165}Dy, ^{128}I, ^{27}Mg, ^{56}Mn, ^{65}Ni, ^{233}Th, ^{51}Ti, and ^{52}V, were also investigated using anticoincidence counting but conventional INAA. The long-lived nuclides (half-life > 12.5 h) of interest in the present study are: ^{76}As, ^{198}Au, ^{82}Br, ^{141}Ce, ^{51}Cr, ^{60}Co, ^{59}Fe, ^{197}Hg, ^{203}Hg, ^{42}K, ^{140}La, ^{24}Na, ^{147}Nd, ^{86}Rb, ^{122}Sb, ^{46}Sc,

^{182}Ta, ^{160}Tb, ^{187}W, ^{175}Yb, ^{69m}Zn, and ^{65}Zn.

Perhaps the most important advantage of anticoincidence counting is the considerable decrease of the background activity with no reduction of the peak area for non-coincident gamma-rays. The quantification of this advantage is rather difficult. An attempt was made in this work to define an "analytical figure of merit (AFOM)" term for assessing the practical advantages of anticoincidence counting. This term should: (i) include parameters, such as resolution, peak area, background around the peak, dead time, counting time, and counting statistics, which are related to the sensitivity of the peak; (ii) reflect changes in sample matrix activity; and (iii) provide parameters that can be easily measured. The effectiveness of the AFOM terms was evaluated by analyzing a number of biological reference materials of diverse types of matrix and varying amounts of major and interfering elements. This AFOM term was compared with other such terms reported in the literature.

Several of the short-, medium-, and long-lived neutron activation products were studied in detail using both conventional and anticoincidence gamma-ray spectrometry. The precision, accuracy, and detection limits were compared in many cases. The advantages of anticoincidence counting for the determination of magnesium and selenium were extensively investigated.

2. EXPERIMENTAL

A general description of the experiments done is given in this chapter. The elemental standard solutions, various types of reference materials, and chemicals used are also described. The facilities available for the irradiation and counting of samples are illustrated as well. A detailed description of the anticoincidence gamma-ray spectrometer is given here.

2.1 Elemental Comparator Standards

All elemental comparator standards used in this work were made from the plasma emission spectroscopy standard solutions supplied by the Seigniory Chemical Products (SCP) Canada Ltd. These standards had a certified purity of >99.999% and most of them had a concentration of 1000 ppm. For the measurement of PERF of nuclides and the determination of elemental levels in reference materials using short irradiations, the comparator standard solutions were prepared by pipetting 1 mL of the diluted plasma emission standard solutions into 1.2-mL (small) polyethylene vials, capping and heat-sealing the vials.

For long irradiations, 500 μL of the diluted standard solutions were pipetted on to finely ground sucrose (obtained from the Koch Light Laboratories in the U.S.A.) in small polyethylene vials and a few drops of distilled deionized water (DDW) were added to form a homogeneous mixture, which were then dried

under an IR lamp. The amount of sucrose used was such that it would take up half of the vial after drying. If, due to its viscosity, the sucrose support solution stuck to the walls of the vials on drying, the vial was briefly centrifuged to achieve a reproducible geometry.

The iodine comparator standard solutions, used for measuring iodine levels in reference materials and for constructing quality control charts, were prepared by diluting 1000 ppm KI stock solution (supplied by the Mallinckrodt Chemical Works) to obtain different concentrations and pipetting them into the small vials. An identical geometry among various comparator standards and samples, and similar count rates are needed to achieve good precision and accuracy; these were obtained by pipetting 500 μL and 1 mL of the standards for half-vial and full-vial sample geometries, respectively.

The water used was first distilled in a quartz apparatus and then deionized using an ultrapure deionization column purchased from the Fisher Scientific Company. This distilled deionized water (DDW) was used for making solutions, diluting solutions and washing all apparatus.

2.2 Reference Materials

A number of reference materials (RMs), certified reference materials (CRMs), and standard reference materials (SRMs) were obtained from the U.S. National Institute of Standards and Technology (NIST) and the International Atomic

Energy Agency (IAEA). These were used for evaluating the accuracy of the methods developed and for studying matrix interferences.

The following materials were obtained from the NIST: Apple Leaves (SRM 1515), Peach Leaves (SRM 1547), Non-Fat Milk Powder (SRM 1549), Wheat Flour (SRM 1567a), Rice Flour (SRM 1568a), Spinach (SRM 1570 & 1570a), Pine Needles (SRM 1575), Bovine Liver (SRM 1577b), Whole Egg Powder (RM 8415), Wheat Gluten (RM 8418), Corn Starch (RM 8432), Corn Bran (RM 8433), Durum Wheat Flour (RM 8436), Hard Red Spring Wheat Flour (RM 8437), and Soft Winter Wheat Flour (RM 8438). The materials obtained from the IAEA were: Animal Blood (RM A-13), Animal Muscle (RM H-4), and Horse Kidney (RM H-8).

The mass of these materials used varied between 100 and 700 mg depending on the minimum mass recommended, sample matrix, and dead time of the principal detector. Several samples of the materials were weighed directly into small polyethylene vials, capped and then heat-sealed. If the vial was half full with the sample then a trimmed vial cap was pushed down the vial to maintain a constant geometry before heat-sealing. This small sample vial was then placed inside a medium-size (2.8 cm diameter, 5.2 cm height) polyethylene irradiation vial and heat-sealed. A second empty small vial (called a spacer) was put on the top of the small vial containing the sample inside the medium-size vial to hold the sample vial in place. This double sealing was a safety precaution in case one of the seals were to break open, it would prevent the contamination of the pneumatic tube when the sample was being transferred out of the irradiation site of the

reactor.

All vials used were obtained from the Olympic Plastic Company (USA) and were precleaned prior to use by the following procedure. The vials were first washed with distilled water to remove dust particles before soaking them in 1:4 analytical grade HCl acid for 24 h, then rinsed with DDW to get rid of the remaining HCl from the vials. These vials were further soaked in 1:4 ultrapure HNO_3 for another 24 h. The vials were then rinsed thoroughly with DDW and dried in air.

2.3 Irradiations

All samples and standards were irradiated in the inner pneumatic irradiation sites of the Dalhousie University SLOWPOKE-2 reactor (DUSR) facility. At these sites, the thermal flux is 5×10^{11} n cm^{-2} s^{-1} and the epithermal flux is 2×10^{11} n cm^{-2} s^{-1} when the DUSR is operated at half power, *i.e.* 8 kW. The stability, homogeneity, and reproducibility of the DUSR neutron flux have previously been described [95,96].

The selection of timing parameters, namely the irradiation time (t_i), decay time (t_d), and counting time (t_c), depends on many factors including the half-life of the nuclide of interest. For short-lived nuclides (half-lives < 120 s), the values for t_i varied from 20 to 30 s depending on the sample matrix, and those for t_d and t_c were 10 s and 40 s, respectively. For medium-lived nuclides (half-lives

between 2.3 min and 2.6 h), the values for t_i, t_d and t_c were 1 min, 1 min, and 10 min, respectively. For long-lived nuclides (half-lives > 13 h), the values for t_i, t_d and t_c ranged from 7-16 h, 1-14 d, and 0.5-8 h, respectively.

2.4 Conventional and Anticoincidence Gamma-ray Spectrometers

The principal detector used in this work, in both conventional and anticoincidence gamma-ray spectrometry, consisted of an EG&G Ortec HPGe p-type coaxial detector with a crystal diameter of 51.2 mm and a length of 65.2 mm. This detector had a peak-to-Compton ratio of 93:1, a relative efficiency of 25% with respect to a standard NaI(Tl) detector, and a resolution (FWHM) of 1.72 keV at the 1332.5-keV photopeak of ^{60}Co.

The guard detector used in the anticoincidence gamma-ray spectrometry consisted of a 10" × 10" NaI(Tl) annulus with 5 photomultiplier tubes (PMTs) supplied by Harshaw and a 3" × 3" NaI(Tl) plug with one PMT supplied by Teledyne. The peak-to-Compton plateau ratio of this system was 582:1 at the 662-keV photopeak of ^{137}Cs, using the IEEE convention of the number of counts per channel in the Compton plateau (358 to 382 keV).

A block diagram of the anticoincidence gamma-ray spectrometry system used in this work is shown in Fig. 2.1. The HPGe (principal) detector was inserted into one end of the annular guard detector and the NaI(Tl) plug was placed at the other end. In order to get nearly equal gains from the two guard

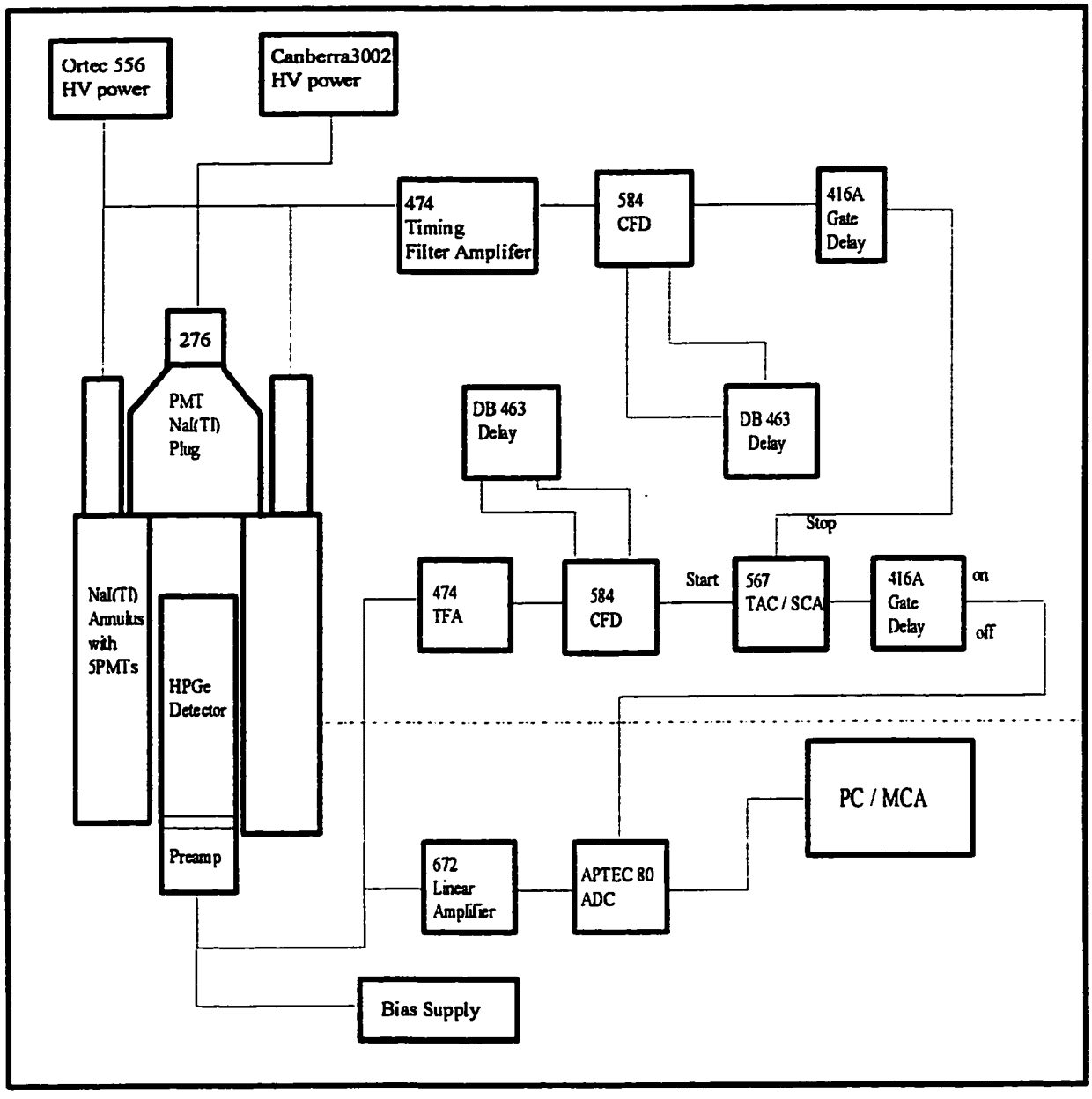

Fig. 2.1. The block diagram of the conventional and anticoincidence gamma-ray spectrometer.

detectors, two separate power supplies were used. One of the high voltage (HV) power supplies (Canberra model 3002) was connected to the photomultiplier tube (PMT) of the plug detector and the voltage was set at +954 V. Each of the five PMT on the annulus was connected through a junction box to the other HV power supply (Ortec model 556) and the voltage was set at +1240 V. The outputs from all six PMTs were collected using T-connection into one cable which was connected to a timing filter amplifier [97].

The major difference between the anticoincidence and conventional spectrometer was that the former had two sets of electronics. One set was sensitive to the timing relationship between signals from the principal and guard detectors. The HPGe timing electronics consisted of a timing filter amplifier (TFA, Ortec model 474) and a constant fraction discriminator (CFD, Ortec model 584). The NaI(Tl) timing chain input signal was obtained by summing all PMT signals into a single TFA followed by a CFD [97]. The TFA functioned as an amplifier and for shaping the pulses from the detector which always gave a negative output signal. The choice of the TFA compared to other types of amplifiers lies in its pulse shaping function and in its ability to maintain the important timing information of the anticoincidence system.

The negative analog outputs from each TFA were changed into timing logic pulses in the CFD. The CFD was chosen for the purpose of time pick-off. This is a technique which can produce an output signal at a fixed time after the leading edge of the input pulse has reached a constant fraction of the peak

pulse amplitude. This method gives the best leading edge timing characteristic and is generally independent of pulse amplitude so that a large timing certainty can be obtained. The two delay boxes attached to each CFD were used to delay the input pulse by a time fraction which is greater than its rise time so that the difference between them corresponded to the time at which the pulses reached the fraction f of its final amplitude [98]. The HPGe CFD is delayed by 35 ns and the NaI(Tl) CFD is delayed by 96 ns. Both CFDs threshold were adjusted down to 90 keV, which is lower than the most interesting energy range, reducing the random coincidence events.

The time logic pulses provided by the primary detector and the guard detector were supplied to the start and stop inputs of the TAC/SCA (time to amplitude converter / single channel analyzer), respectively. A fixed time delay between the input and output signal was provided in the guard detector branch by an Ortec model 416A gate and delay box. The function of the TAC is that when the timing logic pulses from the primary detector branch reached the TAC, it was used to initiate a timing event; if a logic pulse from the guard detector arrived at the stop input within a certain timing window (1 μs in our system), the time difference between these two pulses was measured and a pulse with an amplitude proportional to the time was produced. A typical timing spectrum is shown in Fig. 2.2(a). The major peak resulted from the coincidence events between the NaI(Tl) annulus and the HPGe primary detector. The small right shoulder of that peak represents the coincidence events between the NaI(Tl) plug and HPGe primary

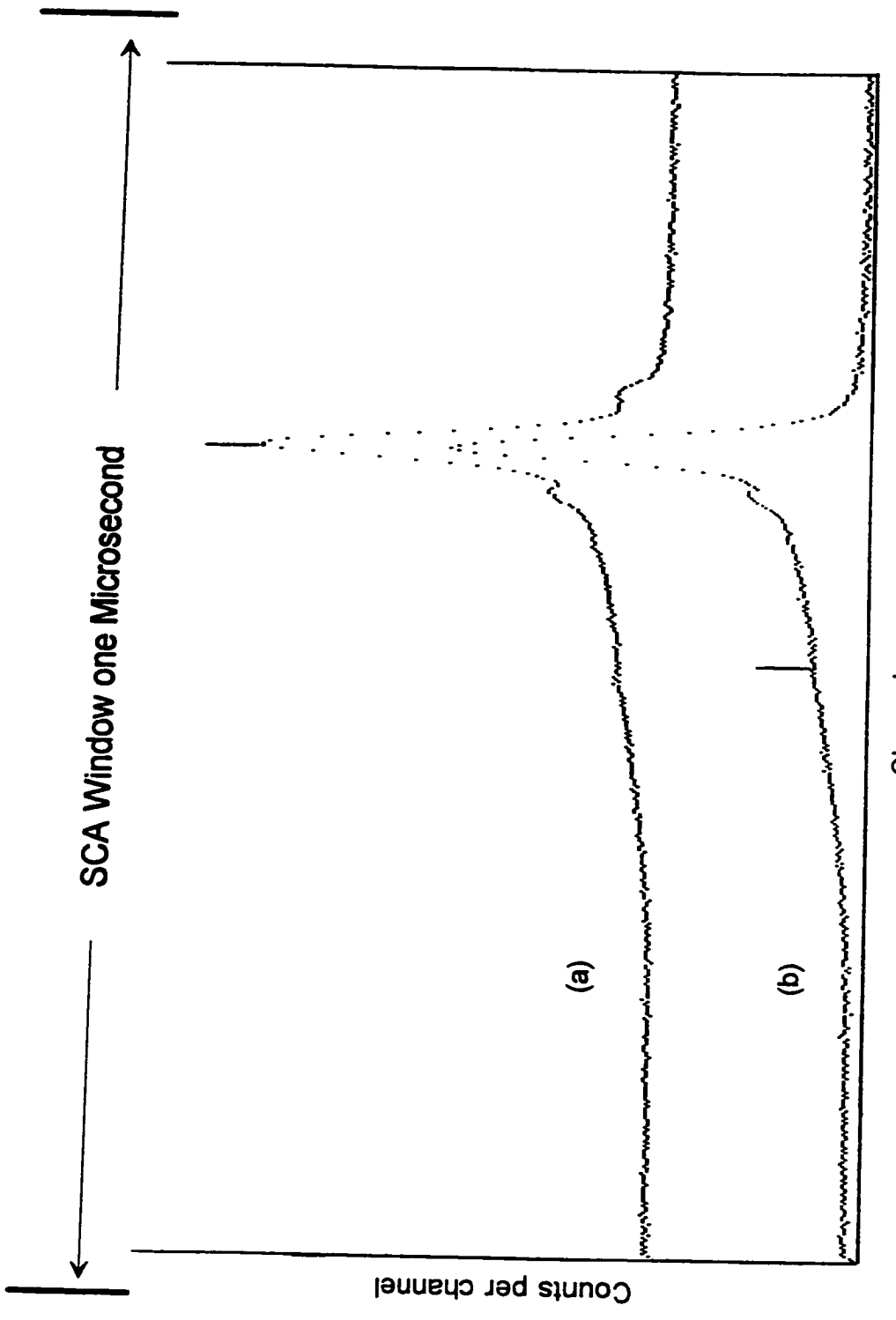

Fig. 2.2. (a) Typical time spectrum using the anticoincidence Compton suppression spectrometer with a NaI(Tl) plug; (b) time spectrum using same system but without NaI(Tl) plug.

detector. This was demonstrated when disconnecting the NaI(Tl) plug, this shoulder disappeared, as shown in Fig. 2.2(b). The leading edge of the spectrum is due to the slow rise time and real coincidence events. The function of the SCA was to generate a coincidence output signal whenever the stop pulse arrived within 1 μs of a start pulse. As a result, the SCA window should cover the entire time spectrum as shown in Fig. 2.2, which ranged from 0 to 10 V.

Therefore, the combined function of a TAC/SCA is to determine coincidence events. Whenever a coincidence event is detected, the logic signal from SCA is used to control the ADC. The sequence of events was as follows. First, the TAC output was tested by the SCA under the requirements of the SCA window. As a result, only TAC outputs within this window produced the SCA logic pulse. These pulses were +5 V square wave and went to the other 416A gate and delay box where they were converted into 50 μs gate pulses to control the ADC gate on or gate off. The energy chain started at the output of the principal HPGe detector *via* a preamplifier and an Ortec model 672 linear amplifier which was set to run approximately between 0 to 2 MeV. The amplitude of the pulse from the linear amplifier was proportional to the gamma-ray energy. These pulses were put into the ADC which were gated by SCA logic pulses [99,100].

For pulses to be gated off, the gating pulse must be ahead of the ADC-triggering pulse by 100 ns. It usually happens when both the principal and guard detectors sense a gamma-ray at the same time. During the time ADC is gated off, no signal from the principal detector can be registered in the MCA,

causing the Compton continuum to be suppressed. If the conventional gamma-ray spectrum was to be acquired, a simple switch was used to change it from the anticoincidence setting.

In order to achieve the maximum improvement of the anticoincidence counting efficiency, it was necessary to optimize factors such as sample to detector distance as well as the relative distance of the NaI(Tl) annulus to the primary HPGe detector. A platform was designed to hold the NaI(Tl) detector, and it was attached to a vertical rod with adjustable grooves. This platform, built in our Department of Chemistry, can be moved using a simple handle. It was built in our Department. The entire set-up is shown in Fig. 2.3.

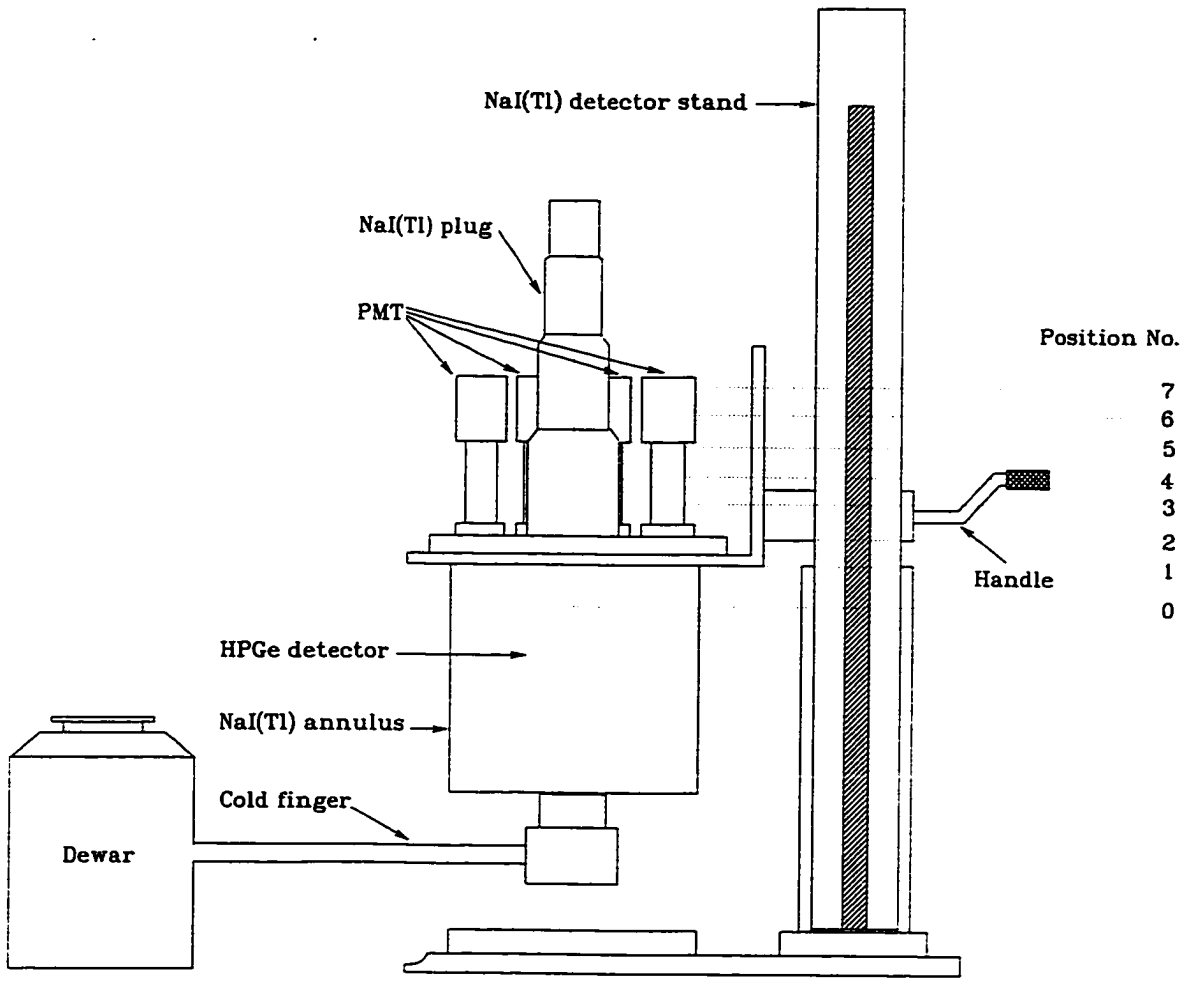

Fig. 2.3. A diagram of the NaI(Tl) guard detector stand assembly.

3. RESULTS AND DISCUSSION

3.1 Performance of the Anticoincidence System

3.1.1 Improvement of Peak-to-Compton ratios

The performance of the anticoincidence counting system was evaluated by collecting, analyzing and comparing several conventional and anticoincidence gamma-ray spectra. The 661.6 keV photopeak of a ^{137}Cs standard source was commonly used for this purpose. The conventional and anticoincidence gamma-ray spectra of this standard source are shown in Fig. 3.1. Three parameters were calculated in these two spectra, namely peak-to-Compton plateau, peak-to-Compton edge, and peak-to-total area. According to the ANSI/IEEE standard 325-1986 procedure [101], the Compton plateau value is the average number of counts per channel for the energy range 358-382 keV, the Compton edge is the average number of counts per channel for the energy range 475-481 keV, and the total area is the number of counts in the entire spectrum. These 3 parameters for conventional and anticoincidence systems are summarized in Table 3.1 together with the improvement ratios. These parameters provide important information on the system's basic performance and form a basis for comparison with other systems.

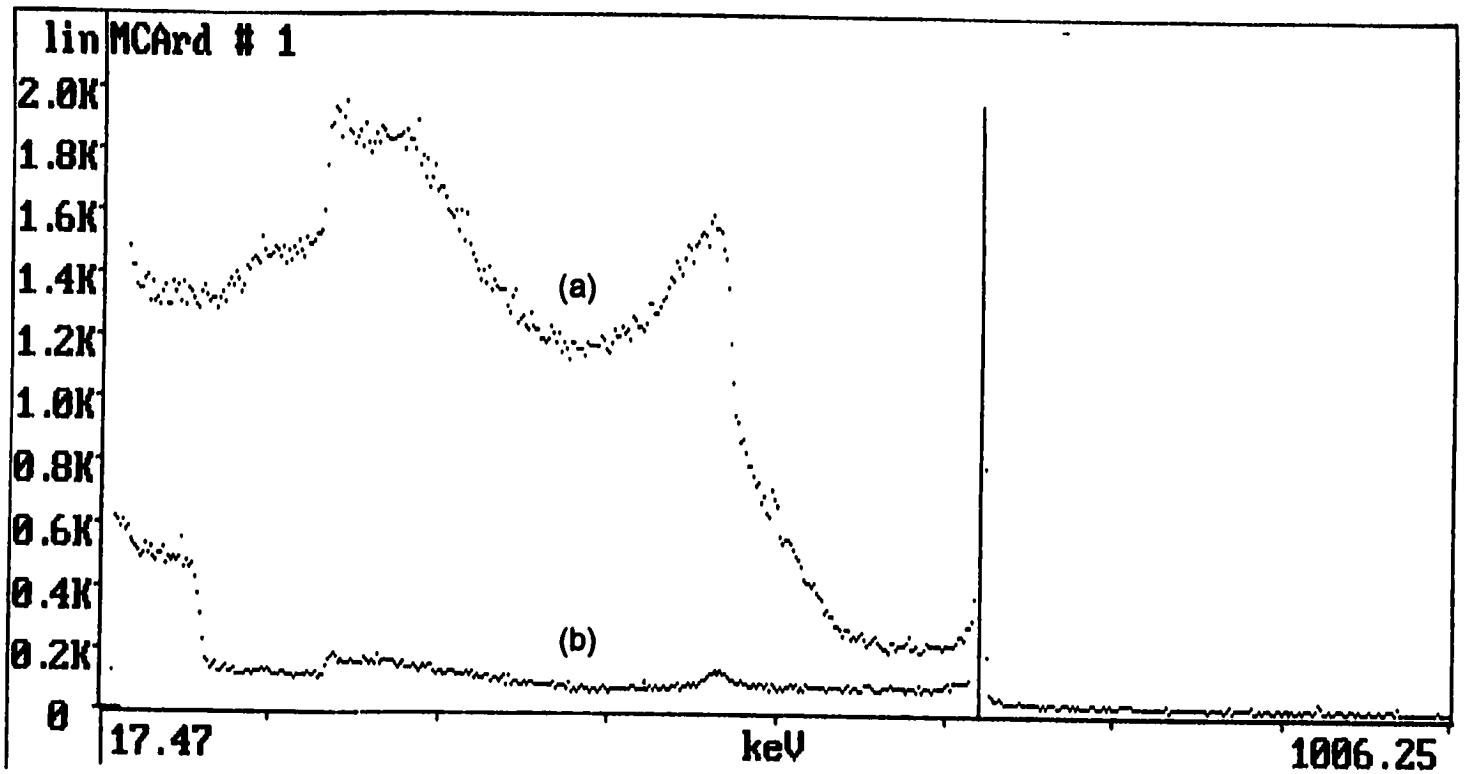

Fig. 3.1. (a) Conventional and (b) anticoincidence gamma-ray spectra of a ^{137}Cs standard source.

Table 3.1. Comparison of conventional and anticoincidence counting systems using a ^{137}Cs standard source.

System	P/C_p	P/C_e	P/T_a
Conventional	93.4	89.5	0.07
Anticoincidence	582	410	0.17
Improvement ratio	6.26	4.58	2.43

Where: P/C_p is the peak-to-Compton plateau;
P/C_e is the peak-to-Compton edge;
P/T_a is the peak-to-total area.

As shown in Fig. 3.1, the anticoincidence mode of operation can greatly enhance the peak-to-background ratio of a photopeak. For example, the Compton edge (469-471 keV) of ^{137}Cs was reduced by a factor of 12 on the average in the anticoincidence spectrum compared to that in the conventional spectrum, and the P/C_e (662/(475-481) keV) was improved by a factor of 4.6 (Table 3.1).

Another region of interest is the Compton plateau as shown in Fig. 3.1. A reduction factor of 8 on the average was obtained for Compton plateau (358-382 keV) using the anticoincidence system compared to the conventional system, and the P/C_p (662/(358-382) keV) had an improved ratio of about 6.3 as shown in Table 3.1. The peak-to-total area (P/T_a) measurements also showed significant improvement with the anticoincidence system.

In the case of nuclides emitting coincident gamma-rays, there are two or more gamma-rays that can be detected by the anticoincidence shield. For example, a Compton interaction in the germanium detector from the 1332.5-keV gamma-ray of ^{60}Co will be removed from the anticoincidence spectrum, either by the 1173.5-keV coincidence gamma-ray or by its Compton scattered gamma-ray being detected by the NaI(Tl) well. In the conventional mode, this Compton interaction will be recorded. The high probability of cancelling the Compton interference due to coincident gamma-ray emitting nuclides is illustrated by the ^{60}Co spectra shown in Fig. 3.2. The Compton edge reduction factor using the anticoincidence system was 29 times greater than that obtained using coincidence counting.

Although the anticoincidence mode of counting can rarely improve the sensitivity of measurement for ^{60}Co, it can significantly improve the sensitivity of measurement for other nuclides whose gamma-ray peaks may be interfered with by the ^{60}Co gamma-rays or other coincident gamma-ray emitting nuclides such as ^{24}Na and ^{38}Cl.

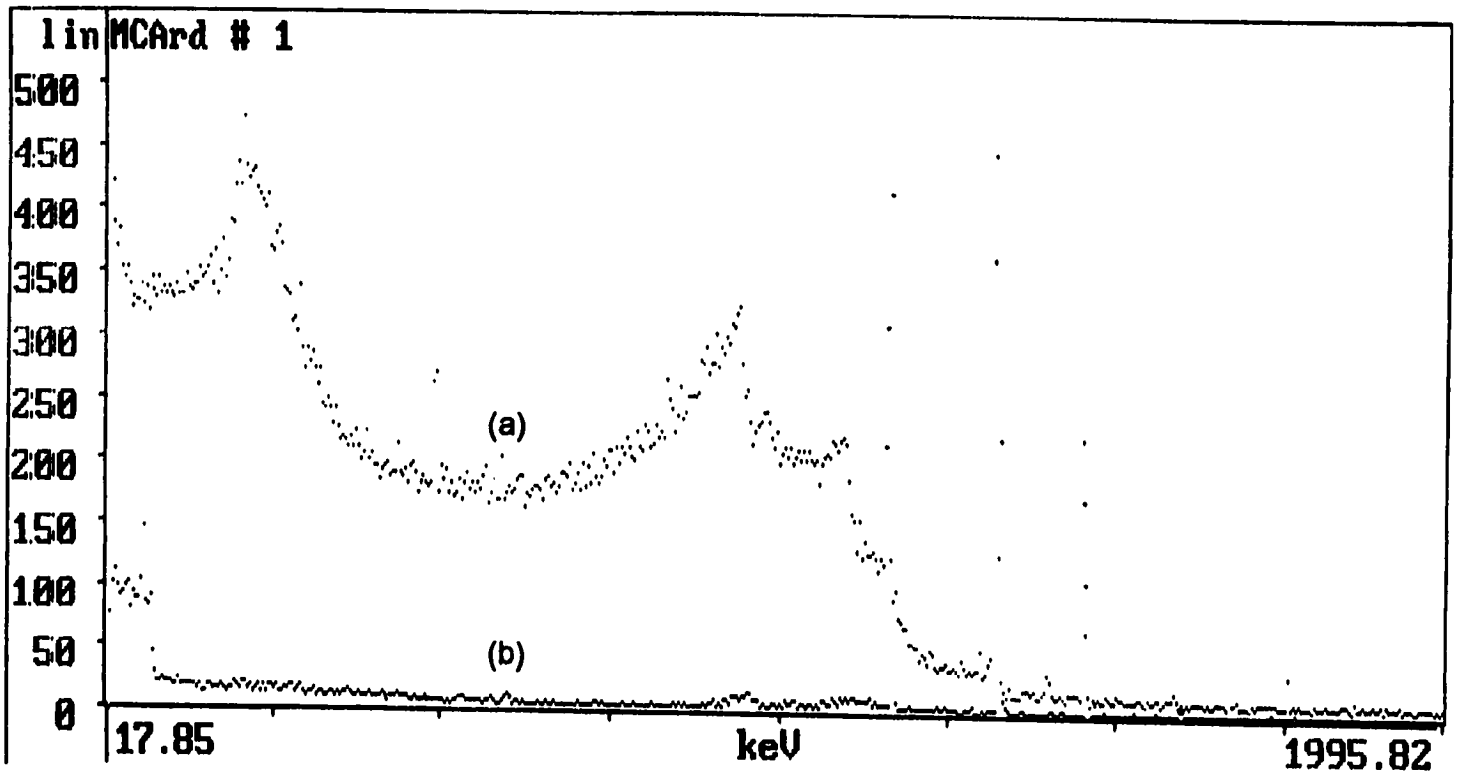

Fig. 3.2. (a) Conventional and (b) anticoincidence gamma-ray spectra of a ^{60}Co standard source.

The ability of the anticoincidence system to reduce the number of Compton background counts over most of the gamma-ray energy spectrum in presence of many photopeaks is another of its important functions. In order to evaluate the performance of this system, a mixed source of ^{152}Eu and ^{154}Eu was used here since these two nuclides have a number of gamma-rays between 80 and 2000 keV. The anticoincidence and conventional gamma-ray spectra of the mixed source are shown in Fig. 3.3. Twenty three regions were analyzed and the background counts per channel were measured. The ratio of background counts in conventional to anticoincidence spectra, called background suppression ratio (BSR), as a function of gamma-ray energy is shown in Fig. 3.4. It is clear that the maximum values for BSR of about 6 could be obtained in the middle energy region (*i.e.* 300 to 1100 keV). It can then be concluded that the use of an anticoincidence system should be more beneficial in this region.

At relatively low and high gamma-ray energies (below 300 and above 1100 keV), the effectiveness of background reduction was not that significant and the ratio was about 4. The reason for this reduction of effectiveness can perhaps be explained as follows. In the high-energy region of a gamma-ray spectrum, the background is generally low to start with and therefore Compton suppression is not as effective. Gamma-rays, especially those at high energy, will deposit only small amounts of energy in a Ge detector and deflect little from their original path. Some of them will escape from the hole in the NaI(Tl) annulus and cannot be

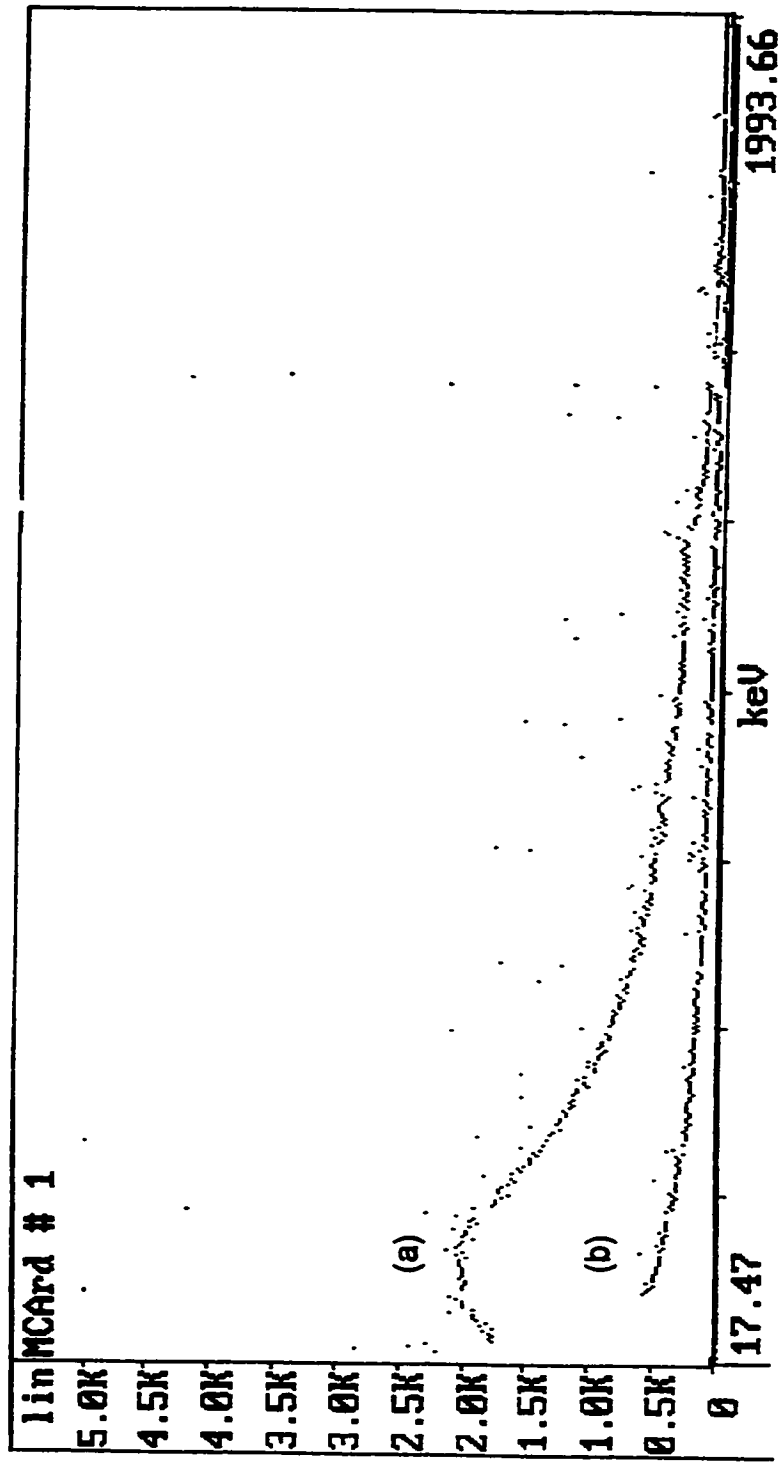

Fig. 3.3. (a) Conventional and (b) anticoincidence gamma-ray spectra of a mixed source of ^{152}Eu and ^{154}Eu.

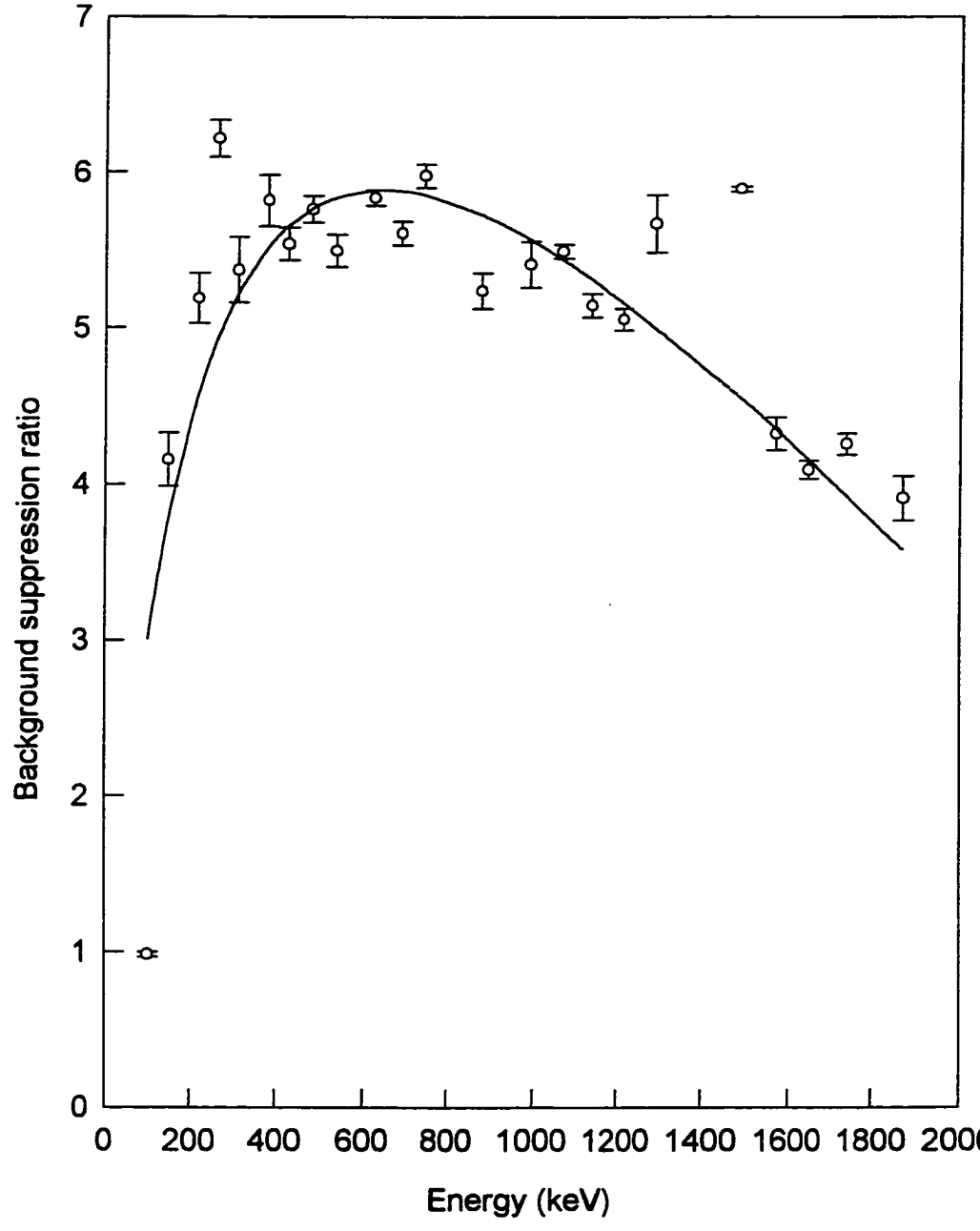

Fig. 3.4. Background suppression ratio as a function of gamma-ray energy.

detected. Thus, these scattered events will contribute to the low-energy portion of the spectrum. The rather low effectiveness of the anticoincidence shield at the low-energy end of the spectrum is due to the large hole in the bottom of the NaI(Tl) annulus. The Compton background in the middle-energy region is usually higher because it is influenced by all gamma-rays of higher energies. Thus the background improvement is most apparent. Therefore, if the full-energy peak intensity is not reduced at all; sensitivity will be most improved for peaks located in the middle area of the spectrum.

An advantage factor is used to measure the effectiveness of a Compton suppression system and it is essentially a net peak-to-background ratio improvement factor. The net peak counts, in turn, are obtained by subtracting the background counts from the gross counts under the peak. The advantage factors were measured in this work using a mixed source of ^{152}Eu, ^{59}Fe and ^{95}Zr. The nuclear data of these sources are given in Table 3.2. The advantage factor for each peak, *i.e.,* the ratio of the peak-to-background in the anticoincidence spectrum to the corresponding value in the conventional spectrum, is plotted in Fig. 3.5.

Apparently there were three distinct types of data as shown in Fig. 3.5. The advantage factors for ^{152}Eu ranged from less than 1 to about 2, meaning that there is not much to be gained by using the anticoincidence system. The improvement factors for ^{95}Zr are all around 4. This dramatic difference between ^{152}Eu and ^{95}Zr is somewhat expected since the Eu lines are often in coincidence

Table 3.2. Nuclear data for a mixed standard radioactive source of ^{152}Eu, ^{59}Fe, and ^{95}Zr.

Element	Isotope (% abund.)	Cross section (b)	Nuclides	Half-life	γ-ray energy, keV (% int.)
Eu	^{151}Eu(47.8)	5900±200	^{152}Eu	13.5 a	121.8 (28.4)
					344.3 (26.6)
					444.0 (2.8)
					778.9 (13.0)
					1112.1 (13.3)
					1408.0 (20.9)
Fe	^{58}Fe(0.31)	1.15±0.02	^{59}Fe	44.5 d	192.3 (1.02)
					1099.3 (56.5)
					1291.6 (43.2)
Zr	^{94}Zr(17.4)	0.056±0.004	^{95}Zr	64.0 d	724.1 (44.2)
					756.8 (99.81)
			^{95}Nb	35.0 d	765.8 (99.8)

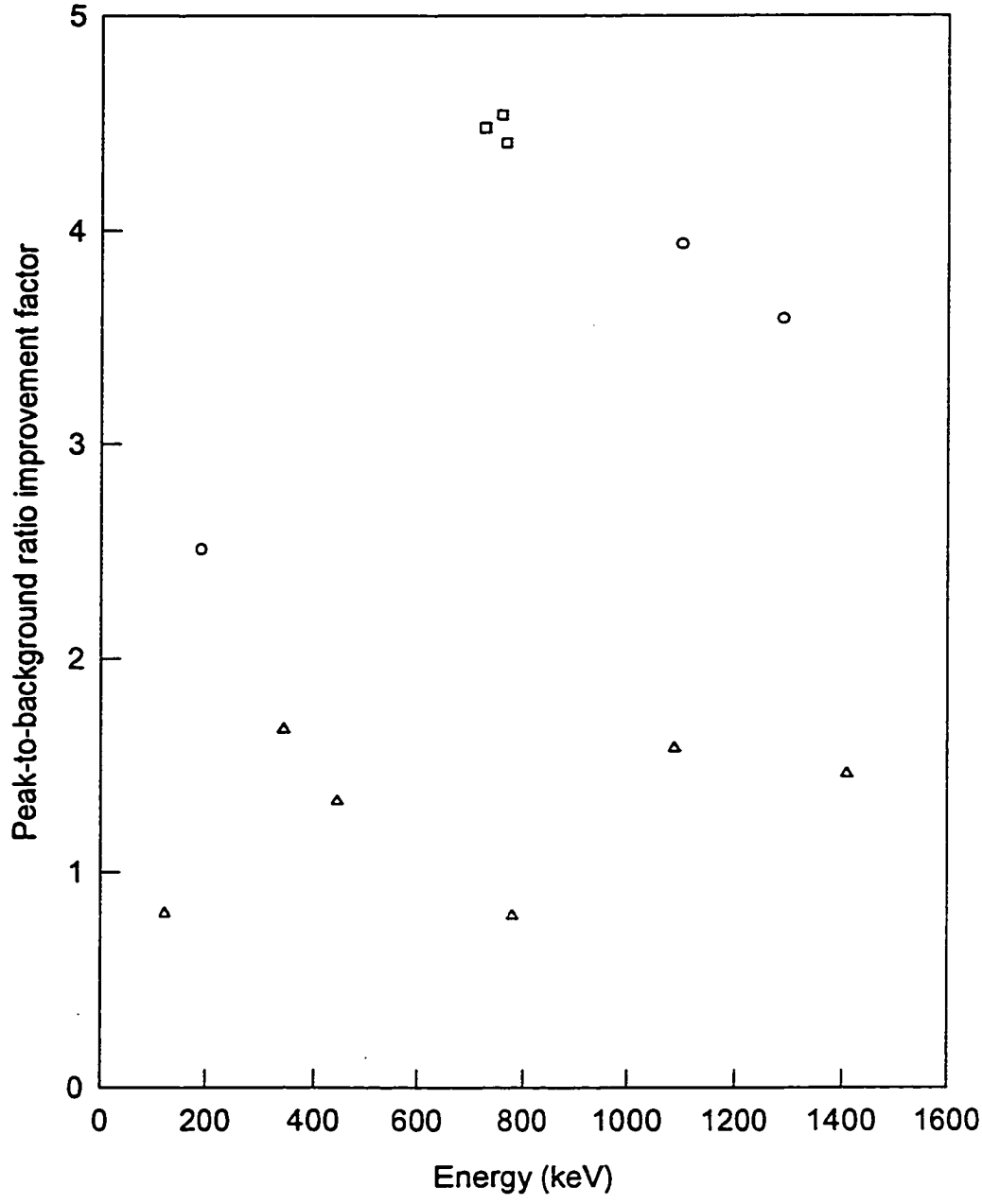

Fig. 3.5. Improvement factor for peak-to-background ratios of various nuclides as a function of gamma-ray energy.

legends : □ ^{95}Zr ○ ^{59}Fe △ ^{152}Eu

and therefore suppressed by the anticoincidence system. The three middle gamma-ray energy lines (*i.e.* those between 724.1 and 765.8 keV) of ^{95}Zr are not coincident and they show very good improvement factors. The three ^{59}Fe peaks are distributed among the low, middle and high energy regions. The middle-energy 1099.3 keV peak of ^{59}Fe may be partially cascaded by the 192.3 keV peak of the same nuclide, and therefore it does not show an improvement factor as good as to that of ^{95}Zr. The low- and high-energy lines of ^{59}Fe, where the background reduction is small, have lower improvement factors.

3.1.2 Effects of Annulus Position and Sample Distance

The geometry factors, namely the distance of the sample from the HPGe detector surface and the relative position of the NaI(Tl) annulus with respect to the HPGe detector, affecting the anticoincidence counting efficiency were investigated. A standard source of ^{137}Cs was used for this purpose. The source was counted at 0 to 8 cm from the surface of the HPGe detector keeping the NaI(Tl) annulus at the fixed position #1 (Fig. 2.2). The variation of the peak-to-Compton-plateau ratio (P/C_p) and that of the number of counts in the highest channel of the 661.6-keV photopeak of ^{137}Cs with sample distance are shown in Fig. 3.6. The rate of increase of the P/C_p ratio was rapid at the beginning (up to 3 cm), then it became slower for increasing sample distances. At the same time the peak height decreased significantly. It is evident from Fig. 3.6 that the

optimum sample distance should be 1 cm from the surface of the HPGe detector, where these two curves intersect.

It is well known that the angular distribution of the scattered photons depends on the energy of primary photons and on the interactions of primary photons with the detector material. In general, the scattering angle decreases with increasing energy of primary photons, and *vice versa*. Therefore, the relative position of the NaI(Tl) annulus with respect to the HPGe detector will have some influence on the extent of suppressing background due to scattering. Experiments have been carried out to find the optimum position of the NaI(Tl) annulus with respect to the HPGe detector. Again, a standard source of ^{137}Cs was used for this purpose. The source was counted at a fixed sample distance of 1 cm from surface of the HPGe detector. The NaI(Tl) annulus position was varied from position #0 through 7 (Fig. 2.3). The variations of the P/C_p and the peak-to-Compton edge (P/C_e) ratios of ^{137}Cs with the NaI(Tl) annulus distance are shown in Fig. 3.7. The Compton edge and Compton plateau were measured as the average count per channel over the energy range of 475-481 keV and 358-382 keV, respectively; the conversion gain was kept at 0.48 keV per channel. It is evident from Fig. 3.7 that the best P/C_p was obtained over a range of 9.5-12.5 cm annulus distance, which means that about 1/3rd. of the annulus is above the HPGe detector surface. The effectiveness of the Compton plateau background suppression was reduced above 12.5 cm. On the other hand, the P/C_e ratio continuously improved with the increasing annulus distance (Fig. 3.7) from the

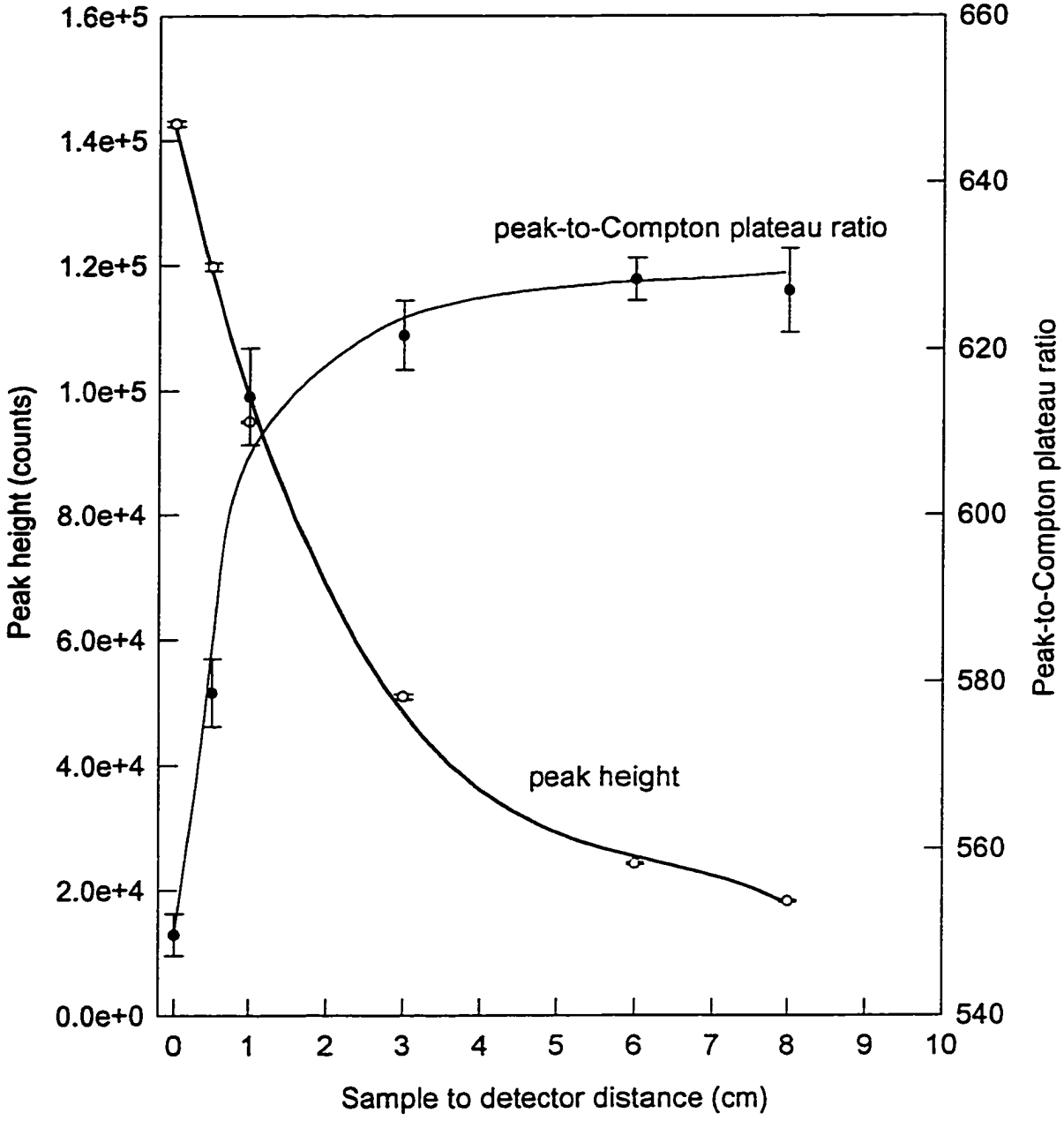

Fig. 3.6. Effect of sample distance from detector on peak height and peak-to-Compton plateau ratio using ^{137}Cs at a fixed annulus position #1.

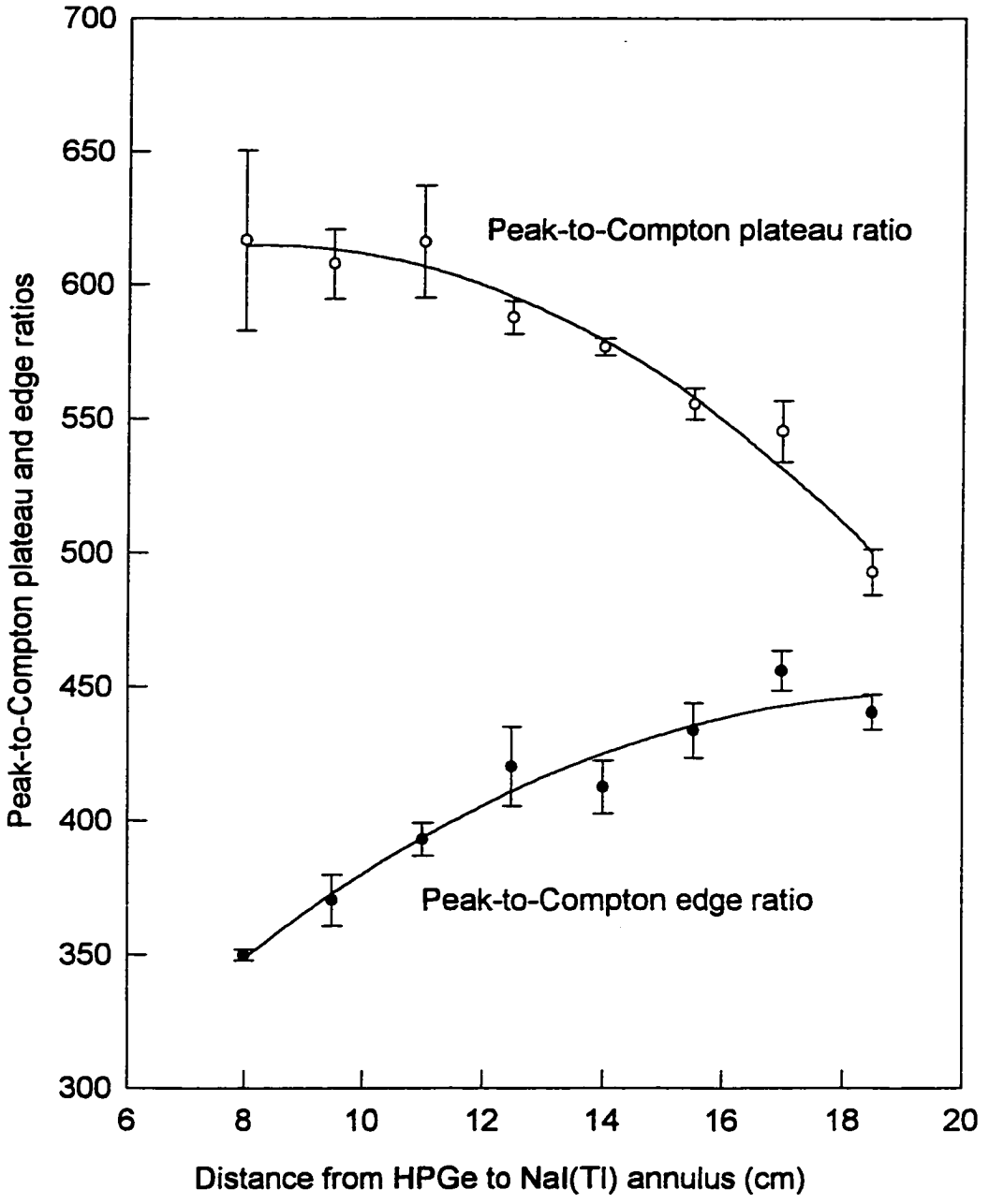

Fig. 3.7. Effect of annulus position on the peak-to-Compton plateau and edge ratios using a ^{137}Cs source at a fixed sample to detector distance of 1 cm.

HPGe detector surface because of the increased suppression of the Compton edge arising from the backward scattering.

In order to evaluate the effects of annulus position for nuclides emitting cascading gamma-rays, ^{116m1}In (half-life = 54.1 min) was selected. The peak efficiency reduction factors and sensitivities of the four gamma-rays of ^{116m1}In are shown in Table 3.3. It is evident that the gamma-rays were significantly suppressed because of their cascading transitions, and did not give improved sensitivities in the anticoincidence counting mode. The peak efficiency reduction factors (PERF) listed together with standard deviation in Table 3.3 were the average of eight independent determinations at different annulus positions (*i.e.* one determination at each of the eight positions). The relatively high standard deviations attached to these average values suggest that the peak efficiency of each peak for ^{116m1}In in anticoincidence counting can be affected by the position of the annulus with respect to the HPGe detector. A plot of the observed PERF values *vs.* the annulus distance is shown in Fig. 3.8. It is clear that PERF depends not only on the annulus position but also on the energy of the gamma-ray. The minimum and maximum reductions were obtained for the 1097.3 and 818.7 keV gamma-rays, respectively.

The characteristics and performance of the anticoincidence spectrometer used in this work are comparable to similar systems in other laboratories [91,93]. There are not that many anticoincidence spectrometers available in university laboratories due to their fairly high cost.

Table 3.3. Peak efficiency reduction factors and sensitivities for ^{116m1}In (half-life = 54.1 min) using anticoincidence spectrometry (t_i = 30 s, t_d = 10 s, t_c = 40 s).

γ-ray energy, keV (% pop.)	Peak efficiency reduction factor ± 1 σ	Sensitivity counts/μg ± 1 σ
138.3 (3.33)	0.10 ± 0.04	16.3 ± 0.9
416.8 (32.4)	0.15 ± 0.02	158 ± 17
818.7 (11.6)	0.041 ± 0.014	12.3 ± 0.8
1097.3 (55.7)	0.19 ± 0.03	182 ± 13

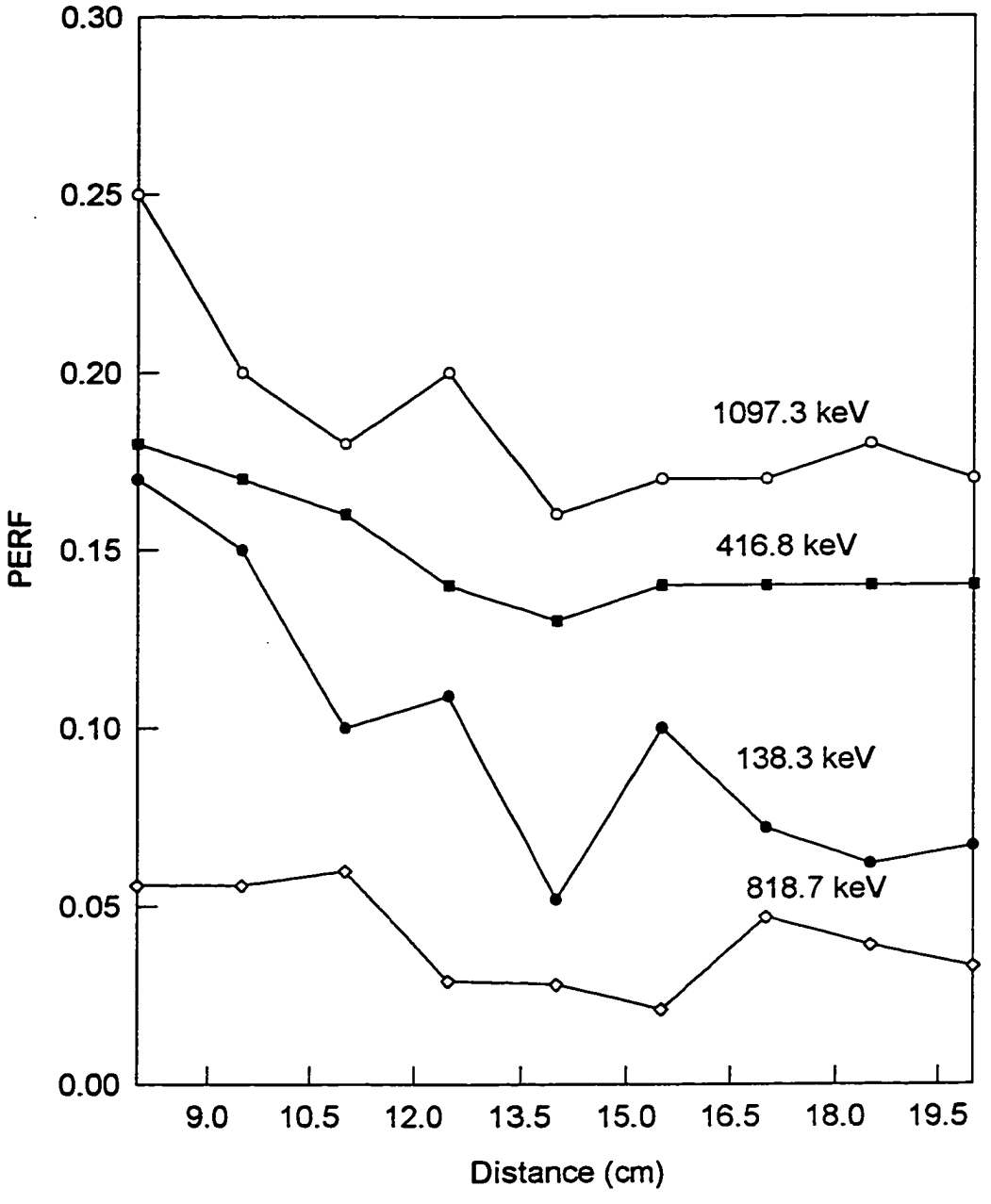

Fig. 3.8. Effect of annulus position on the peak efficiency reduction factor (PERF) for various photopeaks of ^{116m1}In.

3.2 Analytical Figure of Merit (AFOM) Factor

One of the most important advantages of anticoincidence counting is the substantial decrease of background activity leading to improved detection limits for photopeaks with no reduction in the peak area under ideal conditions. In practice, however, this technique will cause some reduction of the peak areas for nuclides with cascading gamma-rays and due to accidental coincident events. The quantification of the advantage of using anticoincidence counting is therefore not an easy problem.

Several attempts have been made to derive a general equation for assessing the advantage of using anticoincidence counting for different nuclides and sample matrices. For example, the following formula has been derived by Galloway [27] to describe the extent of improvement of precision, which he called "statistical accuracy (A)", by anticoincidence counting technique:

$$A=\frac{\sigma}{N}=\frac{(N+2N_B)^{\frac{1}{2}}}{N}=[\frac{(1+2R^{-1})}{N}]^{\frac{1}{2}} \qquad [3.1]$$

Where: N_T is the number of counts at the maximum of the peak,

N_B is the number of background counts,

$N = N_T - N_B$, *i.e.* the peak height,

$\sigma = (N_T + N_B)^{1/2}$, *i.e.* the standard deviation in N, and

$R = N/N_B$, *i.e.* the peak to background ratio.

The ratio of statistical accuracy between conventional and anticoincidence counting has been used to show the advantage of anticoincidence counting.

Cooper and coworkers [102,103] defined a term called "figure-of-merit" (FOM)" which is a measure of a detector's ability to detect a gamma-ray (#1) of energy E_1 in the presence of a higher energy gamma-ray (#2) of energy E_2. The FOM term, $F_2(E_1)$, under this condition is given by:

$$F_2(E_1)=\frac{\varepsilon_p(E_1)}{[R(E_1)\varepsilon_c(E_1)]^{\frac{1}{2}}} \qquad [3.2]$$

where: $\varepsilon_p(E_1)$ is peak efficiency of γ-ray #1,

$R(E_1)$ is the resolution of the detector at energy E_1, and

$\varepsilon_c(E_1)$ is Compton efficiency at energy E_1 due to γ-ray #2.

Cooper used the gamma-rays of a standard ^{88}Y source to demonstrate the usefulness of his FOM. It should be noted here that the Compton efficiency at one energy due to many other gamma-rays in a real sample is not easily determined.

Rossbach *et al.* [104] proposed a time gain factor to express the advantage of anticoincidence counting. It involved a comparison between the collection time necessary for equal peak counting error of anticoincidence and conventional systems. The counting error of a given peak in percent (f) is a function of the inverse square root of the collection time (t_c):

$$f = c \times t_c^{-\frac{1}{2}} \qquad [3.3]$$

where c is a constant.

Many of these approaches appear not to be practical for real samples. For this reason, Das and coworkers [78-80] defined a semiempirical advantage factor (F) as:

$$F = \frac{R_c}{R_p} \qquad [3.4]$$

Where: R_p is the reduction in the net peak area, and

R_c is the reduction in the accompanying Compton background.

According to this formula, for single gamma-ray emitting nuclides the F term is actually represented by the extent of background suppression. Equation 3.4 considers the improvement in peak-to-background ratio, but does not take into account the improvement of counting statistics in the net peak area.

Recently, Mauerhoger [105] described the advantages of anticoincidence counting in terms of an improvement factor for the counting statistics (f_{stat}) and that for the limit of detection (f_L). The application of these factors to two cases are given here. In one case, $P_0 << B_0$,

$$f_{stat} = \frac{C^{\frac{1}{2}}}{R_p} \qquad [3.5]$$

where R_p is the ratio of the net peak areas of unsuppressed and suppressed spectra (P_0/P), C is the ratio of the areas of the Compton background lying under the full-energy peak of interest in unsuppressed and suppressed spectra (B_0/B). In another case, $B_0/R_p^2 >> (a_m^2/8)$,

$$f_L = \frac{C}{R_P} \qquad [3.6]$$

where a_m, depending on the required accuracy of results, can take values between 1 and 10. The author claimed that the results are only applicable for a Compton suppression system of BGO/CsI/Ge detectors with the source positioned outside the shield. The influence of sample matrix on f_{stat} and f_L was not considered in this case.

In the present work we attempted to define a factor for assessing the advantages of anticoincidence counting, which would satisfy the following requirements. This factor should (i) take into account most of the parameters related to sensitivity of a peak, such as resolution, peak area, background around the peak, dead time, counting time, and counting statistics; (ii) be general and should represent changes in the sample matrix composition; and (iii) provide parameters that can be easily measured.

From the point of view of analytical usefulness, good counting statistics and sensitivity of a peak are very important. Both net peak area (P) and peak-to-background ratio (P/B) should be maximized for this purpose. One way

to do this is to make P^2/B as large as possible. An advantage factor (AF) can then be defined as:

$$AF=\frac{P^2}{B} \qquad [3.7]$$

For a given type of sample matrix and a given counting system, the term AF can be used to describe the peak to background ratio, sensitivity, and the standard deviation of the net peak area (σ). A value for σ can be approximately calculated using the following equation:

$$\sigma=(P+2B)^{\frac{1}{2}} \qquad [3.8]$$

The net peak area statistical accuracy (PA) using conventional gamma-ray spectrometry can then be defined as:

$$PA=\frac{(P+2B)^{\frac{1}{2}}}{P} \qquad [3.9]$$

It should be noted here that this "PA" is different from Galloway's [27] "statistical accuracy (A)" which applies to the net peak height rather than the net peak area. Equation 3.9 can be rewritten for conventional and anticoincidence gamma-ray spectrometry as:

$$PA_{conv}=\frac{(P_{conv}+2B_{conv})^{\frac{1}{2}}}{P_{conv}} \qquad [3.10]$$

$$PA_{anti}=\frac{(P_{anti}+2B_{anti})^{\frac{1}{2}}}{P_{anti}} \qquad [3.11]$$

Where, the subscripts "conv" and "anti" refer to the conventional and anticoincidence counting modes, respectively. The AF term for conventional gamma-ray spectrometry (AF_{conv}) can then be defined by combining equations 3.7 and 3.10:

$$AF_{conv}=\frac{P_{conv}}{PA^2_{conv}B_{conv}}+\frac{2}{PA^2_{conv}} \qquad [3.12]$$

Similarly, the AF term for the anticoincidence system (AF_{anti}) can be expressed as:

$$AF_{anti}=\frac{P_{anti}}{PA^2_{anti}B_{anti}}+\frac{2}{PA^2_{anti}} \qquad [3.13]$$

Finally, the ratio of AF terms of anticoincidence and conventional systems can be called analytical figure of merit (AFOM) to indicate the practical advantages of

anticoincidence counting:

$$AFOM=\frac{AF_{anti}}{AF_{conv}} \qquad [3.14]$$

Insertion of values from equations 3.12 and 3.13 to 3.14, and simplification of it gives:

$$AFOM=R^{2}_{PA}\frac{(R_{anti}+2)}{(R_{conv}+2)} \qquad [3.15]$$

Where: $R_{PA} = PA_{conv} / PA_{anti}$ is the net peak area statistical accuracy improvement factor,

$R_{anti} = P_{anti} / B_{anti}$ is the peak-to-background ratio in anticoincidence counting, and

$R_{conv} = P_{conv} / B_{conv}$ is the peak-to-background ratio in conventional counting.

Equation 3.15 describes the advantages of anticoincidence counting in terms of not only background suppression and peak efficiency reduction but also the improvement of standard deviation of the net peak area.

In order to demonstrate the effectiveness of the AFOM term developed in this work, 15 biological reference materials (RM) and standard

reference materials (SRM) supplied by NIST and one RM by IAEA were analyzed for Mg by INAA. Between 200 and 700 mg of these materials, depending upon the levels of major and interfering elements present, were weighed. The materials were irradiated at a flux of 5×10^{11} n cm^{-2} s^{-1} for 1 min, allowed to decay for 1 min, and the 1014.4 keV gamma-ray of ^{27}Mg counted for 10 min. The sensitivity for magnesium standard solutions under these conditions was 2.24 counts/μg using anticoincidence gamma-ray spectrometry. The sensitivity by conventional gamma-ray spectrometry is similar since the PERF is 0.98 (described in section 3.4.1). The reference materials were analyzed in triplicate and the results are presented in Table 3.4 in order of increasing magnesium concentrations. It is obvious from this table that both precision and accuracy of the method developed here are very good.

The RMs and SRMs used here consisted of diverse types of matrix and varying amounts of major and interfering elements. The improvement in detection limits achieved by the anticoincidence counting technique is reflected in the AFOM terms (Table 3.4) which ranged from 3.21 to 16.6. The detection limits of magnesium in both counting modes are also reported in Table 3.4. It is clear that the magnesium levels measured in almost all reference materials are significantly higher than the corresponding detection limits by both counting modes. The net effect of anticoincidence counting is further improvement of the detection limits. For Animal Blood and Whole Egg Powder, the detection limits calculated using conventional counting mode are very close to the magnesium

Table 3.4. Concentrations, detection limits, and AFOM terms of magnesium in reference materials by anticoincidence gamma-ray spectrometry.

Reference material (*IAEA, all others NIST)	This work, ppm	Certified, [literature] values, ppm	Detection limits, ppm		AFOM factor
			anti.	conv.	
Corn Starch (RM 8432)	30 ± 2	31 ± 4.9	2.3	8.7	7.03
Animal Blood (RM A-13)*	98 ± 11	99 ± 29	38	94	3.21
Soft Wheat Flour (RM 8438)	210 ± 14	219 ± 15	3.9	15	10.8
Whole Egg Powder (RM 8415)	365 ± 40	305 ± 27	47	1.4×10^2	3.52
Hard Wheat Flour (RM 8437)	375 ± 26	365 ± 29	3.5	8.5	9.65
Wheat Flour (SRM 1567a)	410 ± 16	400 ± 20	3.9	12	7.86
Wheat Gluten (SRM 8418)	485 ± 9	510 ± 46	10	23	3.77
Rice Flour (SRM 1568a)	555 ± 28	560 ± 22	3.9	13	6.09
Bovine Liver (SRM 1577b)	605 ± 23	601 ± 30	14	38	6.47
Corn Bran (RM 8433)	815 ± 16	818 ± 57	3.1	14	16.6
Durum Wheat Flour (RM 8436)	1040 ± 38	1070 ± 75	6.8	19	7.21
Non-Fat Milk Powder (SRM 1549)	1200 ± 90	1300 ± 39	41	93	4.15
Pine Needles (SRM 1575)	1260 ± 27	[1250 ± 170]	33	86	4.27
Apple Leaves (SRM 1515)	2655 ± 99	2710 ± 81	33	77	4.65
Peach leaves (SRM 1547)	4300 ± 300	4320 ± 86	31	1.1×10^2	9.54
Spinach (SRM 1570)	8030 ± 600	[8700 ± 600]	88	2.1×10^2	4.65

levels in these two materials making its determination very difficult. However, in the anticoincidence counting mode, the detection limits were reduced by about 3 times so that magnesium could be reliably determined.

The net peak area, background counts, statistical accuracy of the net peak area, FWHM, and dead time can change in the anticoincidence gamma-ray spectra compared to the conventional spectra. The data presented in Table 3.5 show that the dead times of the principal detector recorded by the two counting modes were not very different, and the dead time ratio of conventional to anticoincidence counting for each material varied only to a small extent, *e.g.* between 1.03 for Corn Bran (RM 8433) and 1.29 for Durum Wheat Flour (RM 8436).

The effects of magnesium concentration and sample activity on the net peak area statistical accuracy improvement factor ($R_{PA} = PA_{conv} / PA_{anti}$) and BSR are quite significant as shown in Table 3.5. For example, Corn Bran (RM 8433) had medium levels of Mg (about 815 ppm, Table 3.4) and very low levels of other elements such as Al, Cl, Na, *etc.* leading to low sample activity and low dead time (1.90%). The 1014.4 keV photopeak was well defined, and the R_{PA} term improved by a factor of 1.12 only. However, the background counts were suppressed by a factor of 20, which lead to a low RSD of 2% in the measured Mg content and a high AFOM of 16.6 (Table 3.4). On the other hand, a RSD of about 7.5% and an AFOM of only 4.15 (Table 3.4) were obtained for Non-Fat Milk Powder (SRM 1549) with a Mg level of about 1200 ppm, and a high dead time of

Table 3.5. Comparison of parameters related to the sensitivity of 1014.4 keV peak of ^{27}Mg in various reference materials by anticoincidence and conventional spectrometry.

Reference material (*IAEA, all others NIST)	Background counts		Background suppression factor	Peak statistics accuracy (%)		Improvement factor, R_{PA}	FWHM keV		Dead Time%	
	conv.	anti.		conv.	anti.		conv.	anti.	conv.	anti.
Corn Starch (RM 8432)	91	7	13	49.9	33.3	1.50	1.17	1.68	1.62	1.56
Animal Blood (RM A-13)*	1620	233	6.95	102	60.6	1.68	0.89	1.13	7.81	6.72
Soft Wheat Flour (RM 8438)	484	32	15.1	19.9	12.0	1.66	1.76	1.76	2.54	2.24
Whole Egg Powder(RM8415)	1045	147	7.11	63.5	38.3	1.66	0.93	0.88	5.17	4.29
Hard Wheat Flour (RM 8437)	333	57	5.84	11.6	7.5	1.54	1.73	1.86	2.59	2.35
Wheat Flour (SRM 1567a)	429	52	8.25	11.7	8.3	1.34	2.09	1.62	2.82	2.55
Wheat Gluten (RM 8418)	1853	336	5.5	17.2	11.3	1.52	1.60	1.46	7.01	6.09
Rice Flour (SRM 1568a)	480	70	6.86	8.7	7.1	1.22	1.64	1.74	3.01	2.68
Bovine Liver (SRM 1577b)	1476	207	7.13	22.3	12.1	1.84	1.74	1.81	4.65	4.12
Corn Bran (RM 8433)	262	13	20	7.8	6.9	1.12	1.88	1.55	1.90	1.84
Durum Wheat Flour(RM8436)	594	77	7.71	6.8	5.5	1.23	1.57	1.84	2.94	2.39
Non-Fat Milk Powder(SRM1549)	2094	433	4.84	21.5	12.7	1.69	1.76	1.72	7.63	6.40
Pine Needles (SRM 1575)	1336	209	6.39	21.8	13.8	1.58	1.71	1.82	8.24	7.32
Apple Leaves (SRM 1515)	603	112	5.38	9.4	7.3	1.28	1.71	1.61	3.45	3.11
Peach Leaves (RM 1547)	897	95	9.44	8.6	5.9	1.47	1.77	1.61	3.43	3.11
Spinach (RM 1570)	3938	690	5.71	9.6	6.1	1.58	1.73	1.77	8.65	7.50

7.63% due to high activities of ^{28}Al (from ^{31}P) and ^{24}Na. In this case, the R_{PA} term improved by a factor of 1.69 but the background was suppressed by a factor of 4.84 only. In another case, Corn Starch (RM 8432) had a low Mg level (30 ppm) and a low dead time of 1.62% (Table 3.5), the R_{PA} term improved by a factor of 1.50 only but the background was suppressed by a factor of 13. The AFOM for this sample was about 7.03 and a RSD of 6.67% (Table 3.4). It is clear from these discussions that the effects of sample matrix, major elements in the sample, levels of the element of interest, and dead times on the efficacy of anticoincidence counting can be conveniently expressed by the AFOM term developed here. It should also be noted that equation 3.15 defining AFOM does not contain any term related to FWHM of a peak. The values of the ratios of FWHM for conventional and anticoincidence systems for the RMs and SRMs listed in Table 3.5 do not exhibit any distinguishable trends.

The two advantage factors of anticoincidence counting reported by Galloway [27] and Das *et al.* [78-80] are compared with the AFOM term developed in this work for the determination of Mg in NIST and IAEA reference materials of diverse composition. The results are presented in Table 3.6. The 1014.4 keV peak of ^{27}Mg is not cascaded with other gamma-rays and has a peak efficiency reduction factor of 0.98 ± 0.02 (Table 3.16). The advantage terms calculated through the statistical accuracy improvement factors defined by Galloway [27] vary within a narrow range of 1.22 to 1.96, and are not very sensitive to the changes in sample matrix composition. The advantage terms "F" of Das *et al.* [78-80] and

AFOM of the present work give similar values, as shown in Table 3.6, for sample matrices with high Mg levels and low background activity such as Peach Leaves (SRM 1547) and Spinach (SRM 1570). However, for the samples which have low levels of Mg and comparatively high background counts under the 1014.4 keV peak, such as Animal Blood (RM A-13) and Whole Egg Power (RM 8415), the difference between these two advantage terms can be as high as 40%. Under these conditions, the AFOM term is generally lower and reflects more realistic advantages of anticoincidence counting. Since the AFOM term not only considers the peak-to-background ratio improvement but also the peak statistical accuracy improvement, it better represents the variation of advantage terms with the changes in sample matrix.

Since the Compton background around the 1014.4 keV peak of ^{27}Mg is influenced by all gamma-rays of higher energy, the AFOM value also varied with the change in the gamma-ray emitting nuclides arising from different major element composition of the sample. Thus, It would be of interest to further explore the relationship between AFOM and the type of sample matrix, which could be very useful in designing optimized INAA procedures. In the case of biological samples, the major interference to the 1014.4 keV peak of ^{27}Mg was caused by Compton scattering of the gamma-ray emissions from the activated elements, such as sodium, chlorine, aluminum and manganese, which either have high cross-sections for thermal neutrons or are present in large amounts. Therefore, the background around the 1014.4 keV peak is mainly due to 1778.9 keV of ^{28}Al, 1368.6 keV of

Table 3.6. Comparison of three advantage factor evaluation methods for the determination of Mg in various reference materials

Reference material (*IAEA, all others NIST)	Statistical accuracy improvement, Galloway [27]	Advantage factor, Das [78-80]	AFOM Factor, This work	Remarks
Corn Starch (SRM 8432)	1.45	8.50	7.03	(Low Mg with
Hard Wheat Flour (RM 8437)	1.37	7.20	9.65	low background)
Soft Wheat Flour (RM 8438)	1.53	8.96	10.8	
Animal Blood (RM A-13)*	1.96	4.41	3.21	(Low Mg with
Whole Egg Powder (RM 8415)	1.56	5.94	3.52	high background)
Bovine Liver (SRM 1577b)	1.78	7.87	6.47	(High Mg with
Non-Fat Milk Powder(SRM 1549)	1.47	4.16	4.15	high background)
Pine Needles (SRM 1575)	1.34	5.84	4.27	
Apple Leaves (SRM 1515)	1.35	5.10	4.65	
Peach Leaves (SRM 1547)	1.46	8.57	9.54	
Spinach (SRM 1570)	1.45	5.15	4.65	
Wheat Gluten (RM 8418)	1.43	4.87	3.77	
Wheat Flour (SRM 1567a)	1.31	9.26	7.86	(High Mg with
Rice Flour (SRM 1568a)	1.32	7.71	6.09	low background)
Corn Bran (RM 8433)	1.22	21.0	16.6	
Durum Wheat Flour (RM 8436)	1.47	7.96	7.21	

^{24}Na, 1642.7 keV of ^{38}Cl, and 1810.7 keV of ^{56}Mn. The net areas of these four peaks in conventional gamma-ray spectra were measured for all 16 reference materials listed in Table 3.4. For each material, the counts per second (cps) were also calculated for each peak. The sum of these four cps is called main matrix activity (MMA) in this thesis.

For each reference material, the MMA terms together with the contributions from each of the four nuclides, and several parameters such as the peak-to-background ratio in conventional mode (R_{conv}), peak-to-background ratio in anticoincidence mode (R_{anti}), net peak area statistical accuracy improvement factor (R_{PA}) of the 1014.4 keV peak of ^{27}Mg are summarized in Table 3.7. The AFOM values of this peak (Table 3.4) are plotted against the corresponding MMA values (Table 3.7) for 13 of the reference materials, and shown in Fig. 3.9. It is evident that AFOM is highly dependent on MMA. Corn Bran had the maximum AFOM value of 16.6 and the lowest MMA value of 2.54. For reference materials with high MMA (*e.g.* above 35 cps), the AFOM values were between 3.2 and 4.7; but they increased exponentially with lower MMA. This trend suggests that the AFOM term is a better indicator of sample activity at lower MMA values. Much of the high MMA values in the reference materials analyzed can be attributed to the high activities of ^{24}Na and ^{38}Cl in them.

The curve in Fig. 3.9 was obtained by fitting a non-linear regression equation [AFOM = 11.55 × exp(-0.1 × MMA) + 4.57] to the data. To evaluate the usefulness of AFOM *vs.* MMA plots, this equation was used to calculate the AFOM

Table 3.7. Main matrix activity and peak parameters for the 1014.4 keV peak of ^{27}Mg in various reference materials using anticoincidence and conventional spectrometry.

Reference material (*IAEA, all others NIST)	R_{anti}	R_{conv}	R_{PA}	Activity (cps)				
				^{28}Al	^{38}Cl	^{56}Mn	^{24}Na	MMA
Corn Starch (RM 8432)	6.71	0.79	1.50	0.39	0.20	0.35	4.70	5.61
Soft Wheat Flour (RM 8438)	10.4	1.16	1.66	1.49	6.51	0.96	0.99	9.91
Animal Blood (RM A-13)*	0.33	0.07	1.69	0.39	36.5	0.10	44.0	81.0
Whole Egg Powder (RM 8415)	0.71	0.12	1.66	0.43	12.4	0.14	10.6	66.4
Bovine Liver (SRM 1577b)	2.41	0.31	1.84	3.43	16.0	0.30	17.7	37.4
Non-Fat Milk Powder (SRM 1549)	1.39	0.33	1.69	4.34	38.6	2.18	18.3	63.5
Apple Leaves (SRM 1515)	8.30	1.63	1.28	22.9	1.57	2.19	0.17	26.8
Peach Leaves (SRM 1547)	14.1	1.56	1.47	18.0	0.85	3.72	0.10	22.7
Spinach (SRM 1570)	2.71	0.53	1.58	48.3	13.7	5.13	36.7	104
Wheat Flour (SRM 1567a)	12.8	1.38	1.34	3.33	7.19	1.98	0.10	12.6
Rice Flour (SRM 1568a)	13.2	1.71	1.22	3.13	4.21	4.40	0.18	11.9
Corn Bran (RM 8433)	65.8	3.13	1.12	0.66	0.43	0.04	1.41	2.54
Durum Wheat Flour (RM 8436)	18.8	2.36	1.23	6.14	7.07	2.58	0.31	16.1

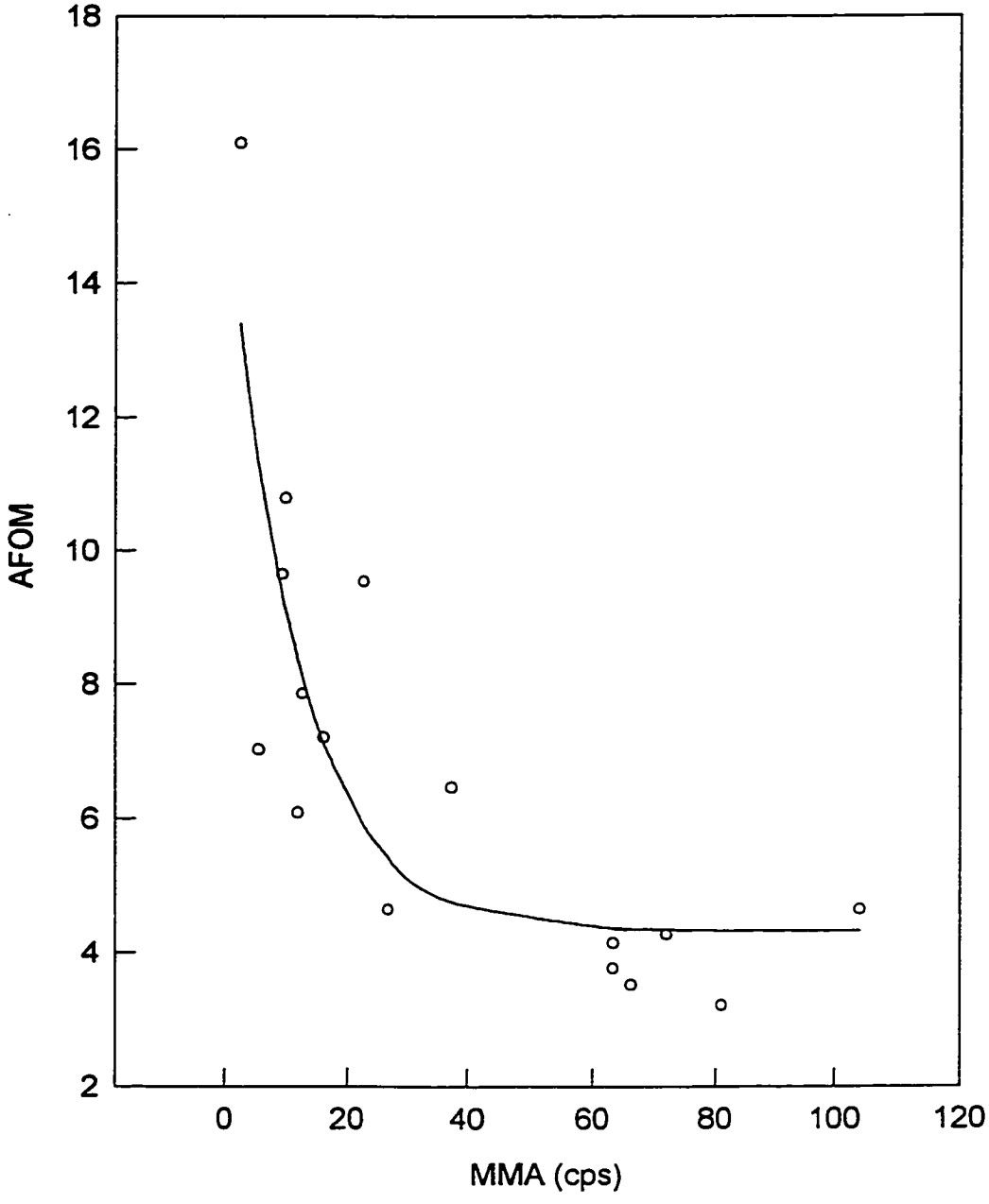

Fig. 3.9. The plot of analytical figure of merit (AFOM) against the corresponding main matrix activity (MMA) for 1014.4 keV peak of ^{27}Mg.

Table 3.8. Comparison of calculated and experimental AFOM values for the 1014.4 keV peak of ^{27}Mg in three reference materials using anticoincidence and conventional spectrometry.

Reference material (all NIST)	R_{anti}	R_{conv}	R_{PA}	MMA (cps)	AFOM values	
					Calculated	Experimental
Hard Wheat Flour (RM 8437)	14.1	1.96	1.54	9.34	9.11	9.65
Wheat Gluten (RM 8418)	1.9	0.39	1.52	63.4	4.59	3.77
Pine Needles (SRM 1575)	2.01	0.34	1.58	72.2	4.58	4.27

values of the remaining three reference materials. The calculated AFOM values are compared with the experimentally determined values (from Table 3.4) in Table 3.8. The deviation between these two values were 5.6% for Hard Wheat Flour, 22% for Wheat Gluten, and 7.2% for Pine Needles. These deviations may be explained in the light of assumptions made in calculating MMA. It was assumed that the Compton scattering from 1778.9 keV of ^{28}Al, 1368.6 keV of ^{24}Na, 1642.7 keV of ^{38}Cl, and 1810.7 keV of ^{56}Mn contribute equally to the background of 1014.4 keV of ^{27}Mg. In practice, the extent of this contribution will depend on the levels of the interfering elements. Moreover, the half-lives and decay schemes (cascading or single gamma-ray emitting) of the nuclides, and the concentration of magnesium should also be taken into account if more reliable estimate of MMA is required. In general, the calculated AFOM differed from the experimental value for materials with high magnesium and high levels of background elements.

In order to evaluate the practical benefits of the AFOM term to nuclides emitting cascading gamma-rays, the 1642.7 keV peak of ^{38}Cl was selected. The same 16 biological RMs and SRMs used for Mg determination were also analyzed here for Cl by INAA. The samples were irradiated at a flux of 5 x 10^{11} n cm^{-2} s^{-1} for 1 min, allowed to decay for 1 min, and the 1642.7 keV gamma-ray of ^{38}Cl counted for 10 min. The three advantage terms for Cl in these materials are given in Table 3.9. The advantage factor "F" developed by Das *et al.* [78-80] is always greater than one. Since the 1642.7 keV peak of ^{38}Cl is a cascade gamma-ray with a peak efficiency reduction factor of 0.38 ± 0.05 (Table 3.16), the

values of greater than one cannot be explained. The "F" values do not appear to vary much with matrix composition. On the other hand the statistical accuracy improvement factor of Galloway [27] is calculated to be less than one, but the values are remarkably constant around 0.6, which means that it cannot reflect the change in sample matrix. The values of the AFOM terms for the 1642.7-keV peak in various matrices are generally less than one, as expected; but unlike Galloway's factor, most of our values have been found to vary between 0.18 and 0.81 reflecting the change in background matrix activity. However, there are a few exceptions, such as Corn Starch (RM 8432), Hard Wheat Flour (RM 8437), Soft Wheat Flour (RM 8438), Rice Flour (SRM 1568a), and Durum Wheat Flour (RM 8436). The AFOM values for these samples range from 0.92 to 1.51. It should be noted that the peak-to-background ratios were also high for the 1642.7-keV peak in conventional gamma-ray spectrometry, as shown in Table 3.9.

3.3 Anticoincidence Counting in Short-Lived Nuclides

3.3.1 Analytical Potential of Short-Lived Nuclides

The combination of generally high isotopic abundances, large cross sections, short times to reach saturation activities, and interference-free gamma-rays indicate that the short-lived nuclides can be produced in high yields and can be advantageously used for trace element determination within a relatively short total experimental time. For the purpose of the work reported here, the short-lived

Table 3.9. Comparison of three advantage factor evaluation methods for the determination of ^{36}Cl using the 1642.7 keV peak in various reference materials.

Reference material (*IAEA, all others by NIST)	Statistical accuracy improvement, Galloway [27]	Advantage factor, Das [78-80]	AFOM, This work	Peak-to-background ratio by conventional spectrometry
Hard Wheat Flour (RM 8437)	0.67	3.54	1.45	16.4
Soft Wheat Flour (RM 8438)	0.65	2.62	1.03	14.3
Corn Starch (RM 8432)	0.69	2.11	0.92	12.2
Durum Wheat Flour (RM 8436)	0.67	3.73	1.51	11.8
Rice Flour (SRM 1568a)	0.66	2.79	1.06	7.71
Bovine Liver (SRM 1577b)	0.66	1.64	0.65	7.69
Animal Blood (RM A-13)*	0.65	1.24	0.50	6.52
Wheat Gluten (RM 8418)	0.65	1.05	0.44	6.06
Non-Fat Milk Powder (SRM 1549)	0.65	1.01	0.43	6.06
Whole Egg Powder (RM 8415)	0.60	1.10	0.39	5.46
Wheat Flour (SRM 1567a)	0.62	1.54	0.56	4.71
Spinach (SRM 1570)	0.64	1.74	0.18	3.62
Apple Leaves (SRM 1515)	0.64	1.16	0.45	3.13
Corn Bran (RM 8433)	0.64	2.60	0.76	2.24
Peach Leaves (SRM 1547)	0.62	1.15	0.41	1.89
Pine Needles (SRM 1575)	0.84	1.79	0.81	0.48

nuclides are defined as those with half-lives of less than 120 s. The elements which have a sensitivity ratio of about 1 or less than 1 for long-to-short-lived nuclides [106] for experimental conditions used here are chosen for the present study. The elements of interest include Ag, Dy, F, Ge, Hf, Rb, Sc, Se, and Yb. The nuclear data [107-109] for these elements are given in Table 3.10.

One of the problems associated with the usage of short-lived nuclides lies in the fact that the counting time is usually limited by the half-life of the nuclide due to its rapid radioactive decay. Moreover, the total count rate should not be very high because of pulse pile-up effects, dead time losses, and other distortions such as those caused by pile-ups from tail or undershoot of a preceding pulse.

In order to improve the counting statistics, methods based on cyclic activation analysis can be used. A pseudo-cyclic INAA (PCIAA) method has been developed for this purpose, and has been described in Section 1.1. In the PCINAA method, the irradiation-decay-counting times and the delay time before the repetition of the irradiation-decay-counting for an optimum number of cycles are adjusted. Alternatively, an improvement in counting statistics of the photopeak of interest can be achieved by suppressing the background activities under that photopeak, instead of increasing the number of counts under the photopeak area by increasing the number of cycles as done in PCINAA using conventional gamma-ray spectrometry. The reduction of background activities has the quantitative effect of reducing the statistical uncertainties associated with the net

Table 3.10. Nuclear data for short-lived nuclides studied using anticoincidence spectrometry.

Element	Isotope (% abund.)	Cross section	Nuclides	Half-life, s	γ-ray energy, keV (% int.)
Ag	^{109}Ag (48.2)	4.5 ± 0.2 b	^{110}Ag	24.6	657.7 (4.5)
					815.5 (0.035)
	^{107}Ag (51.8)	35 b	^{108}Ag	120 s	632.9 (1.7)
Dy	^{164}Dy (28.2)	1700 ±250 b	^{165m}Dy	75.4	108.2 (21.2)
					515.5 (11.7)
F	^{19}F (100)	9.5 ± 0.7 mb	^{20}F	11.0	1633.6 (100)
					3334
Ge	^{74}Ge (36.4)	143 ± 14 mb	^{75m}Ge	48.9	139.8 (40)
Hf	^{178}Hf (27.2)	53 ± 6 b	^{179m}Hf	18.7	215.5 (82)
					161 (2.8)
Rb	^{85}Rb (72.2)	50 ± 5 mb	^{86m}Rb	61.0	555.4 (98.2)
Sc	^{45}Sc (100)	9.6 ± 1 b	^{46m}Sc	18.7	142.5 (100)
Se	^{76}Se (9.0)	21 ± 1 b	^{77m}Se	17.4	161.9 (52.5)
Yb	^{176}Yb (12.7)	2.4 ± 0.2 b	^{177m}Yb	6.41	104 (65)
					228 (13)

peak area.

In the past, the application of anticoincidence gamma-ray spectrometry in INAA has been mainly restricted to long-lived nuclides. One of the reasons is the lack of facilities for studying short-lived nuclides, another being the location of an anticoincidence spectrometer which is not close to the irradiation source. Long-lived nuclides are generally assayed after a long cooling time during which short- and medium-lived nuclides have completely decayed resulting in a low dead-time and a gamma-ray spectrum with only a few photopeaks. However, analysis through long-lived nuclides could be time-consuming because of the requirements of long irradiation, decay and counting times. Alternatively, the short-lived counterparts of the long-lived nuclides can be used in some cases.

The present study deals with the scope and application of the anticoincidence counting technique in INAA using short-lived nuclides. The PERF values for the short-lived nuclides of interest in anticoincidence counting mode, and their sensitivities have been measured. The effects of the NaI(Tl) annulus position on PERF for the short-lived nuclides are discussed below.

The intensities of the analytically useful gamma-rays of the short-lived nuclides (Table 3.10) were measured by both conventional and anticoincidence spectrometry. The sensitivities and PERF of these nuclides were determined and are given in Table 3.11. It is evident that the behaviour of short-lived nuclides in anticoincidence counting mode will depend on a given nuclide as well as its photopeaks.

Table 3.11. Peak efficiency reduction factors and sensitivities for short-lived nuclides using anticoincidence spectrometry (t_i = 30 s, t_d = 10 s, t_c = 40 s).

Nuclide	γ-ray energy, keV (%pop.)	Peak efficiency reduction factor ± 1 σ	Sensitivity counts/μg ± 1 σ
^{110}Ag	657.7 (4.5)	0.96 ± 0.04	1 540 ± 30
	815.5 (0.035)	---	---
^{108}Ag	632.9 (1.7)	0.92 ± 0.03	74 ± 6
^{165m}Dy	108.2 (21.2)	0.97 ± 0.04	9 044 ± 440
	515.5 (11.7)	0.82 ± 0.05	1 800 ± 95
^{20}F	1633.6 (100)	0.85 ± 0.08	5.61 ± 0.3
	3334	---	---
^{75m}Ge	139.8 (40)	1.01 ± 0.04	47.3 ± 1.2
^{179m}Hf	215.5 (82)	0.76 ± 0.06	25300 ± 500
	161 (2.8)	---	---
^{86m}Rb	555.4 (98.2)	0.97 ± 0.03	39.6 ± 1.2
^{46m}Sc	142.5 (100)	0.99 ± 0.03	20400 ± 600
^{77m}Se	161.9 (52.5)	0.98 ± 0.02	2200 ± 110
^{177m}Yb	104 (65)	1.05 ± 0.04	68.5 ± 4.3
	228 (13)	0.31 ± 0.05	2.3 ± 0.3

For the nuclides such as ^{110}Ag, ^{165m}Dy, ^{20}F, ^{179m}Hf, and ^{177m}Yb, which emit two or more gamma-rays per disintegration, their peak efficiency in anticoincidence counting depends significantly on the individual peak. This means that for the same nuclide, one peak is reduced whereas the other stays virtually the same or suffers only a small reduction, such as in ^{165m}Dy where the gamma-rays are not in coincidence with each other. In the case of ^{20}F and ^{110}Ag, even though two gamma-rays are in coincidence with each other, and one of them is very weak, the more intense peak's efficiency in anticoincidence counting is only slightly reduced. The explanation for nuclides ^{177m}Yb and ^{179m}Hf is not clear but it could be due to an internal conversion. The PERF values for ^{20}F and ^{179m}Hf are shown in Fig. 3.10 as a function of the distance from the top of the HPGe to the edge of the NaI(Tl) annulus. A maximum of peak efficiency in the anticoincidence counting was obtained over the range of 10-12 cm; above and below this distance the efficiency was smaller.

The peak efficiency of single gamma-ray emitting nuclides, such as ^{75m}Ge, ^{86m}Rb, ^{46m}Sc, and ^{77m}Se, did not suffer any reduction in anticoincidence counting, so they can be advantageously measured in an anticoincidence system. Fig. 3.11 shows the variation of PERF of these nuclides as a function of distance from the HPGe endcap to the edge of the NaI(Tl). Similar variations for ^{108}Ag, ^{110}Ag, and ^{177m}Yb are given in Fig. 3.12. These very flat curves together with the very small relative standard deviations of average PERF suggest that single energy peaks are not affected by geometric position of NaI(Tl) annulus detector.

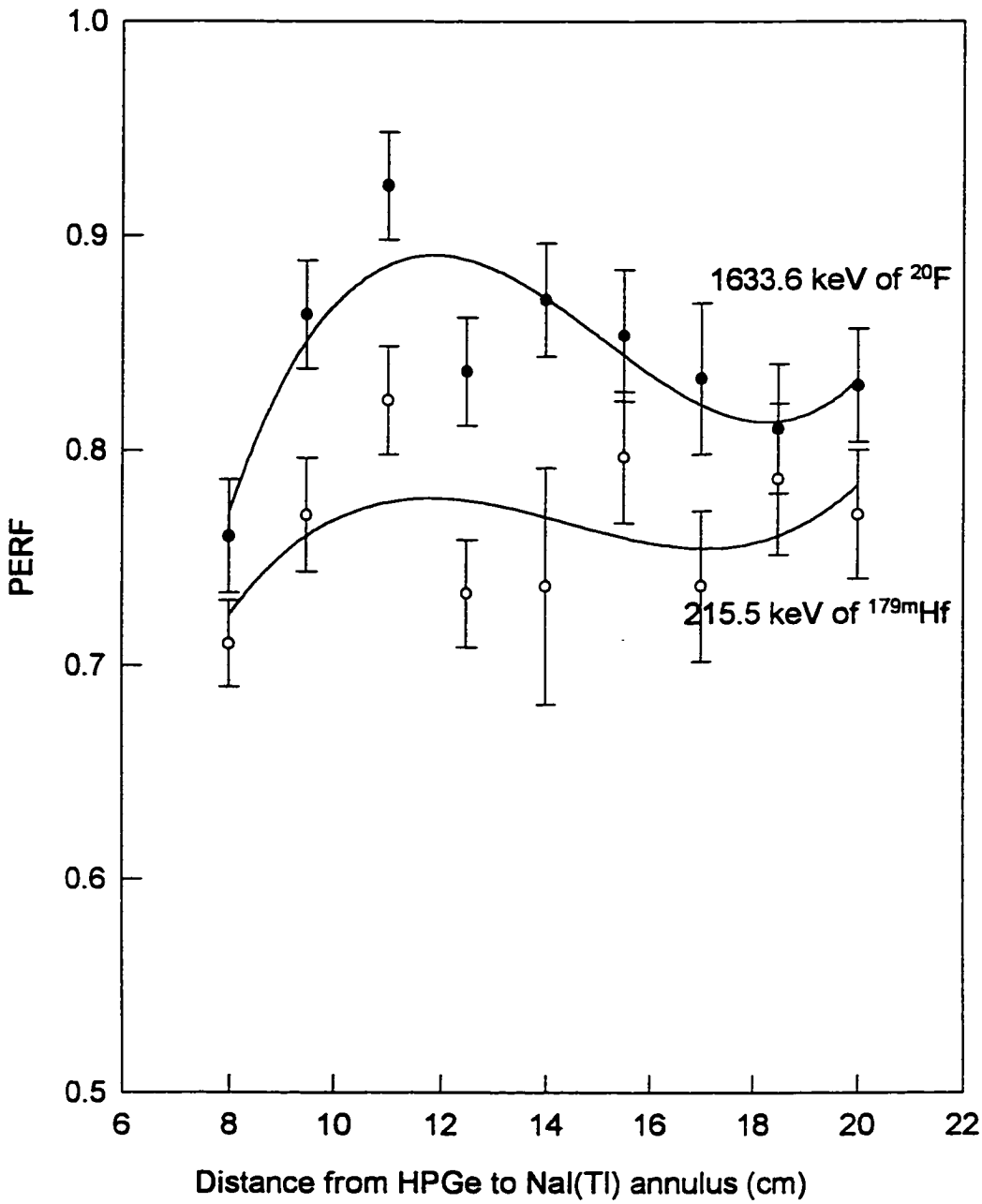

Fig. 3.10. Effect of annulus position on the peak efficiency reduction factor (PERF) of ^{20}F and ^{179m}Hf.

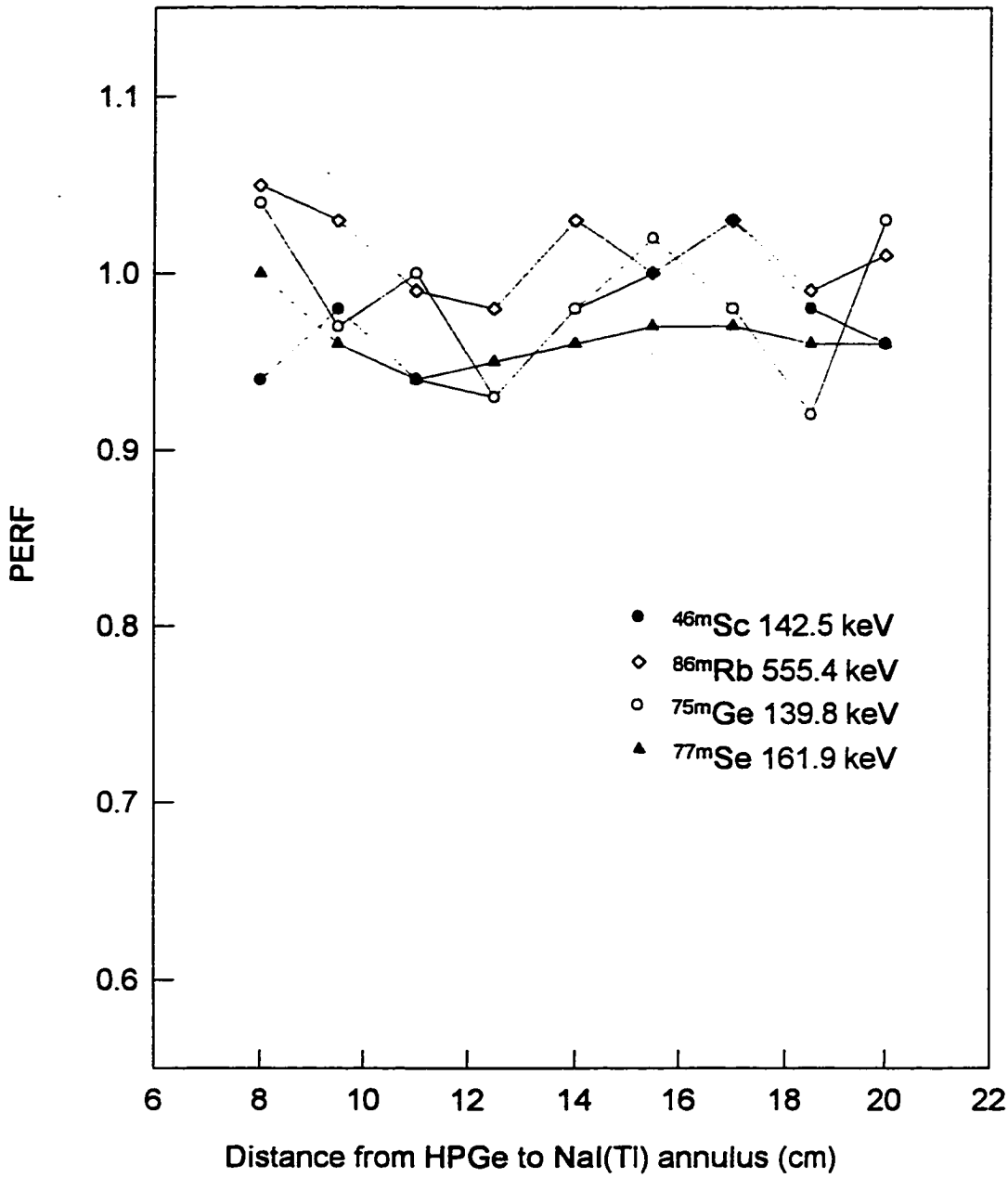

Fig. 3.11. Effect of annulus position on the peak efficiency reduction factor (PERF) of gamma-ray emitting nuclides of ^{46m}Sc, ^{86m}Rb, ^{75m}Ge, and ^{77m}Se.

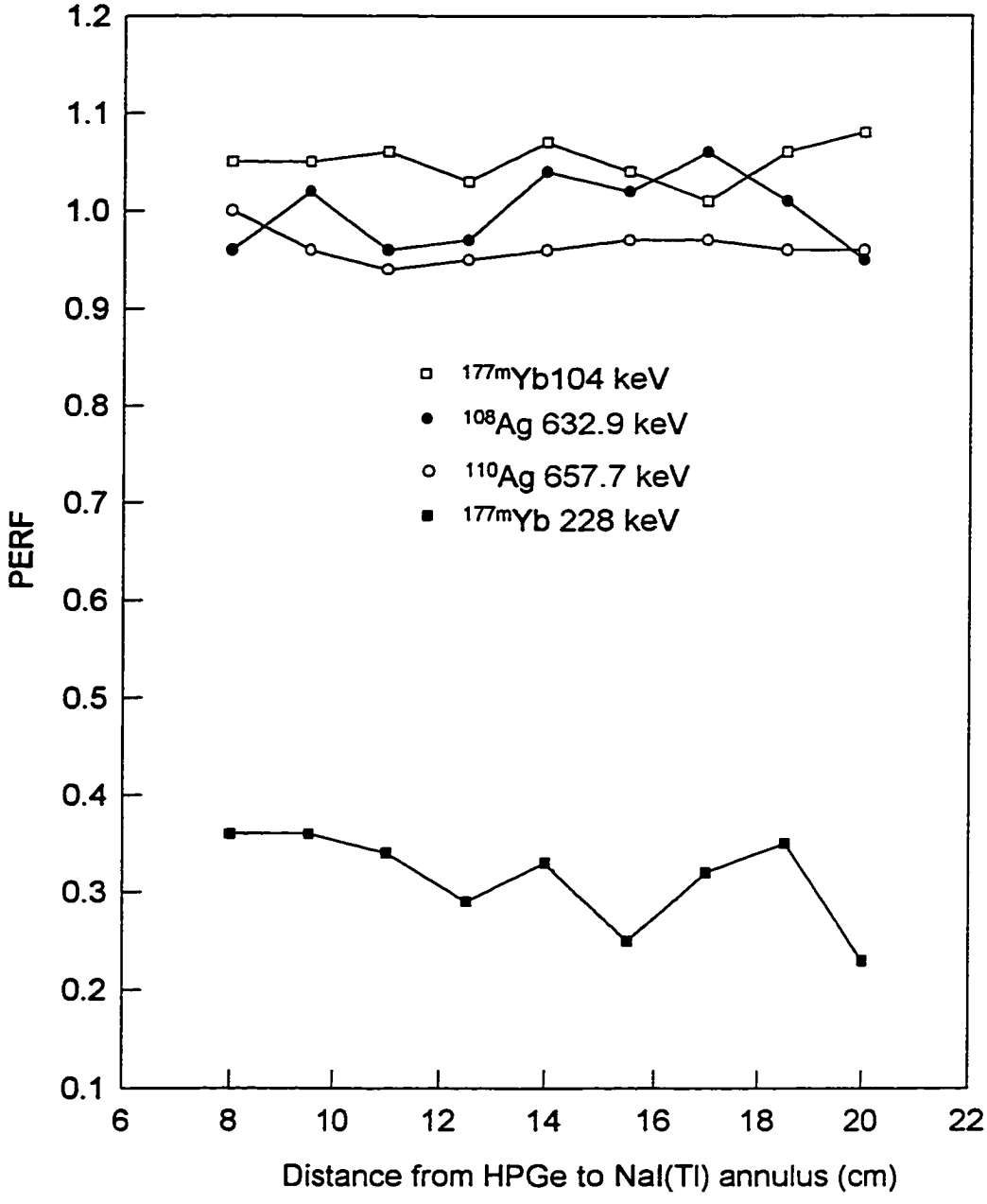

Fig. 3.12. Effect of the annulus position on the peak efficiency reduction factor (PERF) of ^{117m}Yb, ^{110}Ag, and ^{108}Ag.

3.3.2 Pseudo-cyclic INAA with Anticoincidence Counting

A pseudo-cyclic INAA (PCINAA) method was developed for the detection of the short-lived nuclides listed in Table 3.11. The method has been applied to the determination of Dy, Hf, Rb, Sc, and Se in botanical and zoological SRMs. The precision and detection limits of these trace elements can be significantly improved by increasing the number of cycles up to four [110]. However, as the long-lived nuclides such as ^{38}Cl build up and create significant undesirable Compton background activities, the number of cycles a sample can be irradiated becomes limited. If a long delay period, *e.g.* several days, is allowed between the repetition of cycles, the sensitivity of measurement can be improved. Obviously, the total analysis time then could become undesirably long. Alternatively, anticoincidence counting could be coupled to PCINAA to achieve similar or better results within a shorter analysis time.

In this work, an irradiation time of 30 s was used for producing the short-lived nuclides of interest. A decay time of 10 s was employed; within this time an irradiated sample could be manually transferred with good reproducibility from the sample receiver to the detector. Moreover, this 10 s decay was sufficient for detecting short-lived nuclides of interest with good sensitivity. In order to minimize error caused by possibly high dead time, the distance between the detector and the sample was set to 1 cm for maintaining dead times of less than 10%. This distance of 1 cm also happens to be the optimal counting distance as

described in Section 3.1.2. The delay between the end of counting of one cycle and the start of irradiation of the next cycle was 24 hours, which is long enough to eliminate the background counts caused by ^{38}Cl and ^{56}Mn. The number of cycles (n) was selected as 5, which is short enough to keep the total experimental time short but is long enough to give good peak counting statistics and to show the advantages of anticoincidence counting. The same experimental conditions were used in both anticoincidence and conventional counting schemes.

The term minimum detectable activity (MDA) is defined here as:

$$MDA = \frac{B^{\frac{1}{2}}}{P} \qquad [3.16]$$

where P is the peak area counts, B is the background under that peak. The value of MDA was calculated by conducting experiments for both counting modes in each cycle. The term MDA_{conv} is used in conjunction with conventional gamma-ray spectrometry, and MDA_{anti} for anticoincidence gamma-ray spectrometry. The AFOM factor of each cycle was also calculated according to the method described earlier. These factors and detection limits for both conventional and anticoincidence counting modes are listed in Table 3.12 for Dy in NIST Apple Leaves (SRM 1515), Hf and Rb in NIST Peach Leaves (SRM 1547), and Sc in NIST Whole Egg Powder (RM 8415).

The variation of detection limits and AFOM factors with the number of cycles are graphically presented in Fig. 3.13. In the case of 142.5 keV gamma-

Table 3.12. Comparison of MDA and AFOM terms for selected nuclides in reference materials by PCINAA using conventional and anticoincidence counting.

No. of cyc-les	Sc in Whole egg powder			Rb in Peach leaves			Hf in Peach leaves			Dy in Apple leaves					
	MDA			MDA			MDA			MDA (107-keV)			MDA (515-keV)		
	anti.	conv.	AFOM	anti.	conv.	AFOM	anti.	conv.	AFOM	anti.	conv.	AFOM	anti.	conv.	AFOM
1	0.15	0.21	1.79	0.032	0.068	4.63	0.044	0.084	3.64	0.0071	0.011	2.52	0.018	0.036	4.14
2	0.096	0.18	3.61	0.028	0.062	5.05	0.030	0.063	4.49	0.0053	0.0078	2.10	0.011	0.026	5.59
3	0.075	0.15	3.97	0.021	0.058	7.73	0.029	0.063	5.10	0.0045	0.0065	2.13	0.0097	0.027	7.59
4	0.061	0.12	3.92	0.017	0.053	9.34	0.027	0.048	3.23	0.0040	0.0054	1.95	0.0076	0.018	5.66
5	0.057	0.099	3.04	0.019	0.049	7.82	0.027	0.049	3.24	0.0037	0.0055	2.16	0.0074	0.016	4.76

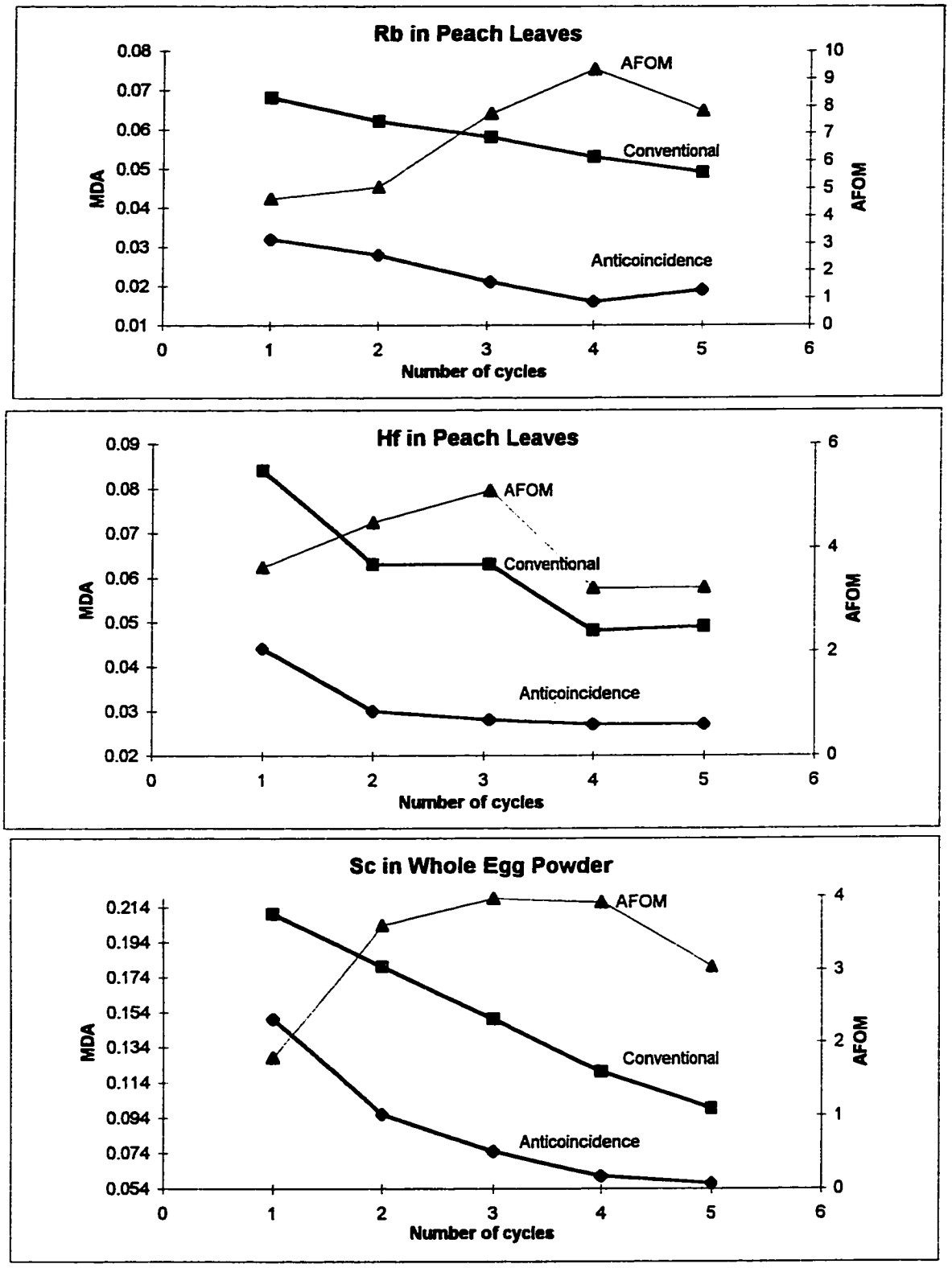

Fig. 3.13. The optimization of the numbers of the cycles with MDA (arbitrary unit) and AFOM for selected nuclides in reference materials PCINAA using conventional and anticoincidence counting.

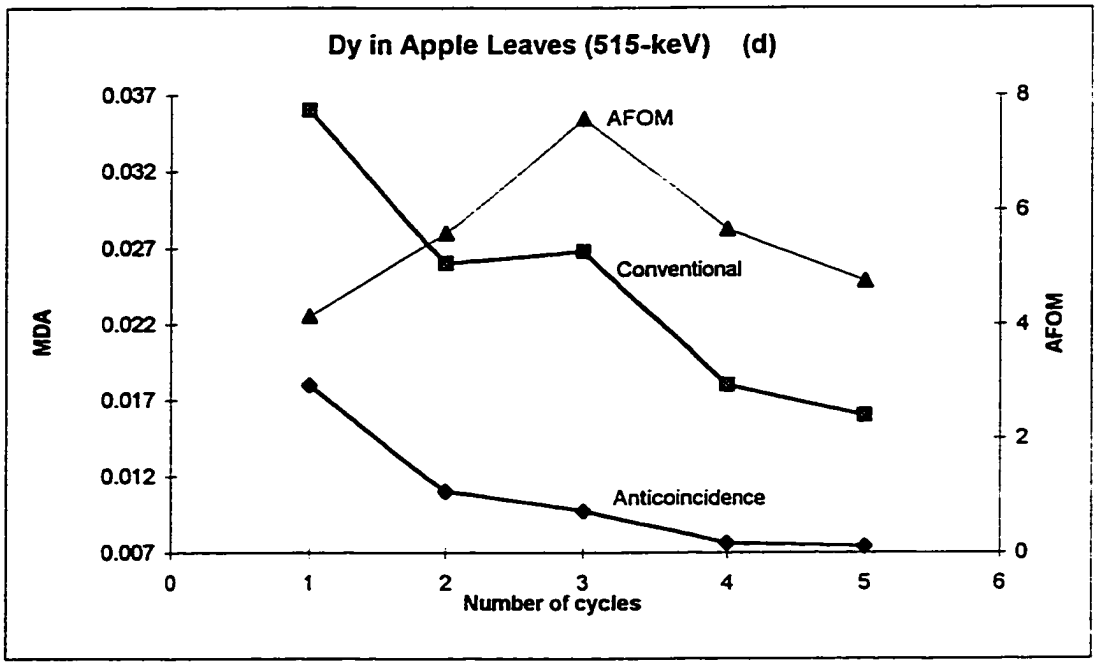

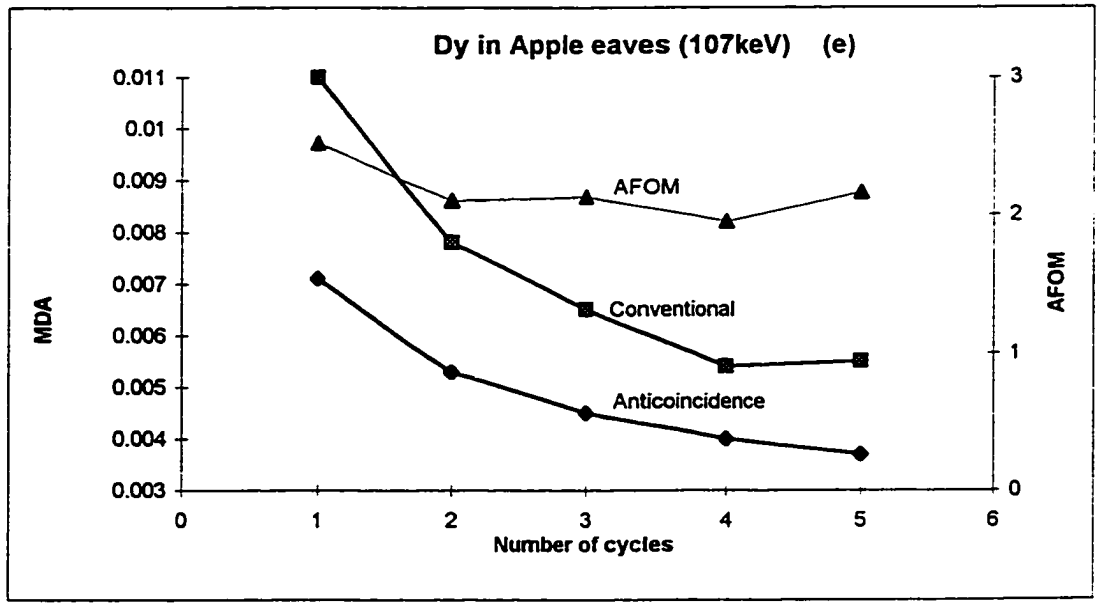

Fig. 3.13 (continued).

ray of ^{46m}Sc, the detection limit improved rapidly in the first three cycles. A further increase in the number of cycles did not improve this parameter significantly. The MDA_{conv} values followed the same trend as the MDA_{anti} ones, but the MDA_{conv} was always worse than MDA_{anti} for each cycle. These results suggest that the background counts in the anticoincidence counting mode increase more slowly than the peak area counts.

The 555.4-keV and 215.5-keV gamma-rays of ^{86m}Rb and ^{179m}Hf, respectively, were assayed in NIST SRM Peach Leaves. The detection limits at each cycle in both counting modes were calculated and are shown in Fig. 3.13 as a function of the number of cycles. These curves are similar to those of ^{46m}Sc: the lower detection limits are obtained by anticoincidence counting at each cycle, but they show a much milder dependence on the increasing number of cycles. The detection limits improved by about 30% for ^{86m}Rb and by about 40% for ^{179m}Hf from the first to the fifth cycle in anticoincidence counting mode.

Two full energy peaks, namely 108.2 and 515.5 keV, of ^{165m}Dy were assayed in NIST SRM Apple Leaves. It is evident from Fig. 3.13 that the 515.5 keV peak benefited more from anticoincidence counting due to the suppression of the 511 keV annihilation peak. The detection limit, using the 515.5 keV peak, improved about 60% from the first to the fifth cycle. At the same time, the detection limit improved by only 40% over the entire five cycles for the 108.2 keV peak. Since the cut-off energy of our anticoincidence system is around 94 keV, not much advantage is gained at the low energy region near 108.2 keV of ^{165m}Dy.

The AFOM terms at each cycle were calculated from anticoincidence and conventional spectra as shown in Fig. 3.13. Except the 108.2-keV of ^{165m}Dy, these curves usually started at a lower value at the first cycle, increased with the increasing number of cycles, passed through a maximum near third or fourth cycle, then decreased. This trend can be explained by re-examining the definition of the AFOM terms. Insertions of equations 3.12 and 3.13 to 3.14 give:

$$AFOM=\frac{AF_{anti}}{AF_{conv}} \qquad [3.14]$$

$$AFOM=\frac{\frac{P_{anti}}{PA^2_{anti}B_{anti}}+\frac{2}{PA^2_{anti}}}{\frac{P_{conv}}{PA^2_{conv}B_{conv}}+\frac{2}{PA^2_{conv}}} \qquad [3.17]$$

Insertion of PA_{anti} and PA_{conv} from equations 3.10 and 3.11 into equation 3.17 yields:

$$AFOM=\frac{\frac{P_{anti}P^2_{anti}}{B_{anti}(P_{anti}+2B_{anti})}+\frac{2P^2_{anti}}{P_{anti}+2B_{anti}}}{\frac{P_{conv}P^2_{conv}}{B_{conv}(P_{conv}+2B_{conv})}+\frac{2P^2_{conv}}{P_{conv}+2B_{conv}}} \qquad [3.18]$$

Simplification of equation 3.18 gives:

$$AFOM=\frac{\frac{P^2_{anti}}{B_{anti}}}{\frac{P^2_{conv}}{B_{conv}}} \qquad [3.19]$$

Equation 3.19 can be rewritten as:

$$AFOM=\left(\frac{\frac{B^{\frac{1}{2}}_{conv}}{P_{conv}}}{\frac{B^{\frac{1}{2}}_{anti}}{P_{anti}}}\right)^2 \qquad [3.20]$$

By putting the definition of minimum detectable activity (MDA) from equation 3.16 in 3.20 gives:

$$AFOM=\left(\frac{MDA_{conv}}{MDA_{anti}}\right)^2 \qquad [3.21]$$

Thus, AFOM is essentially a term for predicting the improvement that can be achieved in the MDA of a given nuclide for a given type of sample matrix using anticoincidence gamma-ray spectrometry.

It is evident from the curves in Fig. 3.13 that there is a rapid reduction in the MDA_{anti} values compared to the MDA_{conv} values, for a given nuclide, with increasing number of cycles for first through third or fourth cycle. However, the improvement in MDA_{anti} decreases beyond 3 or 4 cycles due to the build-up of background activities from nuclides such as ^{38}Cl and ^{56}Mn present in the irradiated samples. As a result, the difference between the MDA_{conv} and MDA_{anti} values becomes smaller with increasing number of cycles. The ratio (MDA_{conv} / MDA_{anti}) and thereby AFOM, starts with a low value in the first cycle then increases with increasing number of cycles, and passes through a maximum before starting to decrease. For a given nuclide in a given matrix, the maximum improvement in the detection limit will therefore be obtained at the highest AFOM. It is evident from Table 3.12 that the AFOM of ^{46m}Sc in Whole Egg Powder (NIST RM 8415) and that of ^{86m}Rb in Peach Leaves (NIST SRM 1547) reached maximum values of 3.9 and 9.34, respectively, at the fourth cycle; while the maximum AFOM of ^{179m}Hf in the same Peach Leaves and ^{165m}Dy in Apple Leaves (NIST SRM 1515) were 5.1 and 7.6, respectively, at the third cycle.

It is obvious from the above discussions that the AFOM terms can be conveniently used for the optimization of number of cycles in PCINAA using

anticoincidence counting, and that this number of cycle varies from element to element in a given matrix. For simultaneous multielement analysis, the number of cycles needs to be optimized appropriately. For example, in Peach Leaves the AFOM of Rb reached its maximum value of 9.34 in the fourth cycle while that of Hf in the same sample decreased to 3.23 in the fourth cycle from its maximum value of 5.10 in the third cycle (Table 3.12). By increasing the number of cycles to four, about 20% of the detection limit improvement (*i.e.* AFOM) for Hf could be lost. If the Hf level of the sample is not very low, such as in Peach Leaves, both Hf and Rb can be simultaneously determined with good precision. For example, the percent RSD of Hf and Rb concentrations (Table 3.13) determined by PCINAA using four cycles are 6% and 3.3%, respectively.

The concentrations of Dy, Hf, Rb, and Sc were measured in six NIST SRMs and RMs by PCINAA using four cycles and anticoincidence counting. The results are shown in Table 3.13. Our values for Rb and Sc are in excellent agreement with the NIST certified or information values, where such comparisons can be made. The RSDs of most of our values are less than 10% with only a few exceptions. No comparisons can be made for Dy and Hf levels because of the lack of certified, information, and literature values. The RSD for Dy and Hf varied between 4 and 17% at ppb levels.

Samples of NIST SRM Citrus Leaves were analyzed using PCINAA in conjunction with conventional and anticoincidence counting modes. The gamma-ray spectra of the first and fifth cycles using anticoincidence spectrometry

Table 3.13. The concentration of Hf, Dy, Sc, and Rb determined by anticoincidence PCINAA methods.

Reference material	Concentration in ppm			
	Rb	Dy	Sc	Hf
Apple Leaves SRM 1515	11.3 ± 0.9	2.32 ± 0.11	0.034 ± 0.004	0.007 ± 0.001
NIST value	10.2 ± 1.5			
Peach Leaves SRM 1547	21.3 ± 0.7	0.69 ± 0.05	0.046 ± 0.004	0.050 ± 0.003
NIST value	(19.7)		(0.04)	
Citrus Leaves SRM 1572	4.47 ± 0.42	0.060 ± 0.007	0.008 ± 0.002	0.010 ± 0.001
NIST value	4.84 ± 0.06		(0.01)	
Pine Needles SRM 1575	10.9 ± 1.1	0.031 ± 0.005	0.028 ± 0.006	0.072 ± 0.004
NIST value	11.7 ± 0.1		(0.03)	
Bovine Liver SRM 1577b	13.3 ± 0.7	0.0021± 0.0009	0.003 ± 0.001	0.0019 ± 0.0007
NIST value	13.7 ± 1.1			
Whole Egg Powder RM 8415	2.2 ± 0.3	0.017 ± 0.003	0.041 ± 0.003	0.008 ± 0.001

NIST information values are given in parentheses.

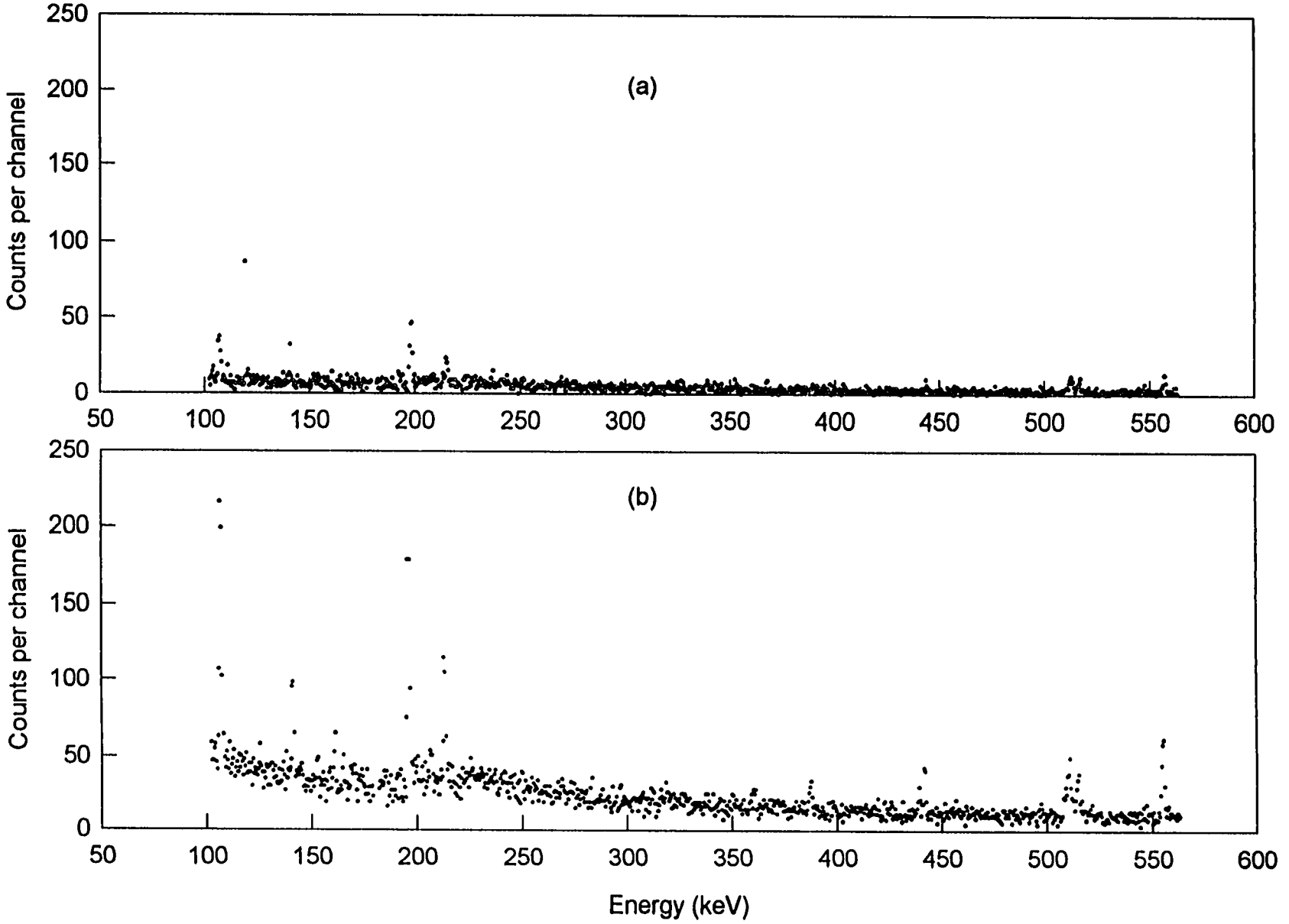

Fig. 3.14. Partial gamma-ray spectra of Citrus Leaves (NIST SRM 1572) by anticoincidence PCINAA : (a) one cycle (b) five cycles.

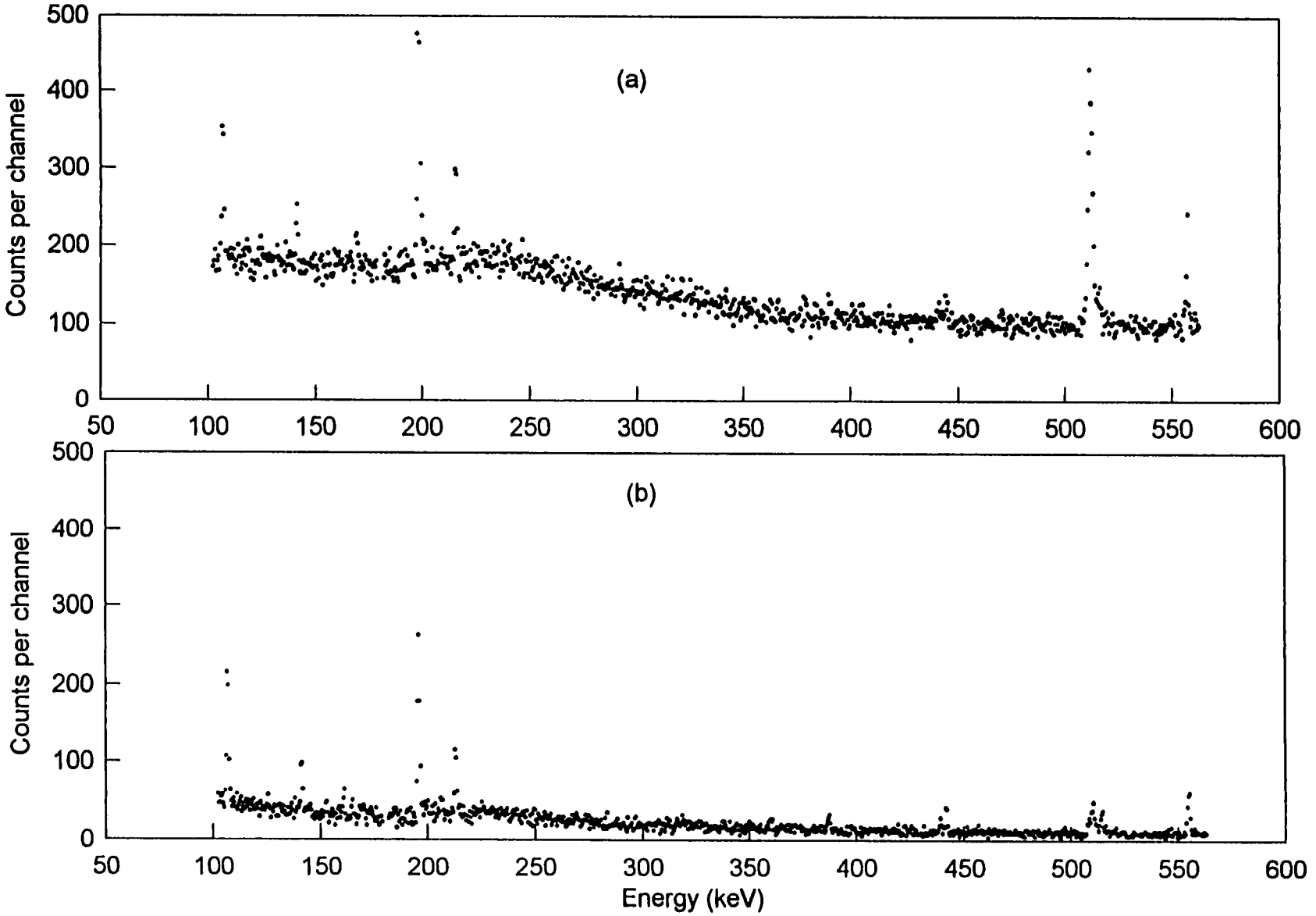

Fig. 3.15. Partial gamma-ray spectra of Citrus Leaves (NIST SRM 1572) by PCINAA (5 cycles) : (a) conventional and (b) anticoincidence.

are shown in Fig. 3.14. The peak-to-background ratios of the photopeaks of interest considerably improved from the first to the fifth cycle. Moreover, a larger number of peaks could be detected in the fifth cycle compared to those in the first cycle.

The conventional and anticoincidence gamma-ray spectra of the Citrus Leaves at the fifth cycle are shown in Fig. 3.15. The advantage of using PCINAA with anticoincidence counting is evident from this figure. The peak areas of interest generally improved by a factor of about 5 while the background was still kept at low levels even after five cycles in the anticoincidence counting mode. The improvement in detection limits varied with nuclides and peak energy involved. The background activities increased considerably in the conventional gamma-ray spectrometry leading to poorer detection limits. It is also evident from Fig. 3.15 that the 511 keV positron annihilation peak was significantly suppressed in the anticoincidence mode compared to the conventional mode. It has already been noted above that this reduction of the 511 keV peak allowed reliable measurement of the 515.5 keV peak of ^{165m}Dy.

Concentrations of Ag, F, Ge, and Yb in these reference materials were very low and could not be determined. The detection limits of these four elements obtained by anticoincidence PCINAA and 4 cycles were calculated [134] and are given in Table 3.14. As can be seen, these limits are generally low.

The detection limits of Ag, F, Ge, and Yb in NIST SRM Citrus Leaves from 1 through 5 cycles are also presented Table 3.14. By increasing the

Table 3.14. Detection limits of Ag, F, Ge, and Yb by anticoincidence PCINAA.

Reference material (NIST)		Detection limits in μg			
		Ag	F	Ge	Yb
Apple Leaves (SRM 1515)		1.4×10^{-3}	0.41	0.093	0.13
Peach Leaves (SRM 1547)		1.4×10^{-3}	0.47	0.065	0.092
Pine Needles (SRM 1575)		2.4×10^{-3}	0.55	0.13	0.097
Bovine Liver (SRM 1577b)		1.3×10^{-3}	0.89	0.11	0.084
Whole Egg Powder (RM 8415)		1.7×10^{-3}	0.95	0.13	0.091
Citrus Leaves	1st cycle	3.1×10^{-3}	0.99	0.24	0.27
(SRM 1572)	2nd cycle	2.2×10^{-3}	0.57	0.16	0.14
	3rd cycle	1.8×10^{-3}	0.46	0.12	0.11
	4th cycle	1.3×10^{-3}	0.36	0.09	0.07
	5th cycle	1.2×10^{-3}	0.34	0.09	0.07

number of cycles from 1 to 4, the detection limits of these elements could be improved by about 60%, while the improvement from 4th to 5th cycle is almost non-existent.

It can therefore be concluded that the anticoincidence counting technique in combination with pseudo-cyclic neutron activation provides a more reliable measurement in terms of improved precision and detection limits for short-lived nuclides compared to both one-shot and pseudo-cyclic INAA coupled to conventional counting. A lower detection limit was always obtained in anticoincidence counting for the same number of cycles compared to conventional counting. The maximum value for AFOM is generally obtained in the third or fourth cycle. This factor can be used for optimizing the number of cycles in PCINAA with anticoincidence counting mode.

3.4 Anticoincidence Counting in Medium-lived Nuclides

3.4.1 Analytical Potential of Medium-lived Nuclides

For the purpose of this work, the medium-lived nuclides are defined as those with half-lives between 2 min and 3 h. The use of medium-lived nuclides in INAA of biological and environmental materials is sometimes limited by spectral interference from high activities of other nuclides present in the sample. The major background interference is generally caused by medium- to long-lived nuclides such as ^{28}Al (half-life = 2.31 min), ^{38}Cl (37.3 min), ^{56}Mn (2.58h) and ^{24}Na (15.0 h)

depending on the nature of the material analyzed. Since some of the nuclides have relatively long half-lives, the background activity is almost always constant throughout the counting period while the medium-lived nuclides of interest decay rapidly. One of the objectives of this work is to investigate the behaviour of medium-lived nuclides and their interferences using anticoincidence gamma-ray spectrometry with a view to improve detection limits of some nuclides.

The nuclear data [107-109] for medium-lived nuclides of interest and those for commonly encountered interfering nuclides are given in Table 3.15. Standards of these elements were irradiated at the DUSR facility for 10 min, allowed to decay for 1 min, and then counted for 10 min using both conventional and anticoincidence spectrometry. The sensitivities and PERF of these nuclides were measured and the average of three values are presented in Table 3.16.

It has been stated before that anticoincidence counting can be advantageously used for nuclides with PERF of about one. If PERF is less than one, the improvement in detection limit will depend on sample matrix activity. It is evident from Table 3.16 that the measurement of nuclides such as ^{28}Al, ^{139}Ba, ^{66}Cu, ^{165}Dy, ^{128}I, ^{27}Mg, and ^{52}V will be improved in anticoincidence counting because their PERF is close to one. The application of this technique for the determination of Cu, I, Mg, and V in a number of SRMs and RMs of varied composition are discussed below in detail in separate subsections. The advantages over conventional counting, as given by the AFOM terms, for these elements are also described here.

Table 3.15. Nuclear data for medium-lived nuclides studied by anticoincidence spectrometry.

Element	Isotope (% abund.)	Cross section	Nuclides	Half-life,	γ-ray energy, keV (% int.)
Al	^{27}Al (100)	232 mb	^{28}Al	2.24 min	1778.9 (100)
Ba	^{138}Ba (71.7)	350 ± 150 mb	^{139}Ba	82.9 min	166.4 (23.7)
Br	^{79}Br (50.7)	8.5 ± 0.3 b	^{80}Br	17.7 min	616.8 (8.7)
					704.6 (1.1)
					1256.6 (0.19)
Cl	^{37}Cl (24.2)	428 ± 5 mb	^{38}Cl	37.2 min	1642.7 (31.9)
Cu	^{65}Cu (30.9)	2.17 ± 0.03 b	^{66}Cu	5.09 min	1039.2 (7.14)
Dy	^{164}Dy (28.2)	1000 ± 150 b	^{165}Dy	2.33 h	94.7 (3.6)
					279.7 (0.48)
					361.7 (0.85)
I	^{127}I (100)	6.2 ± 0.2 b	^{128}I	25.0 min	442.9 (17)
Mg	^{26}Mg (11.0)	38.2 ± 0.8 mb	^{27}Mg	9.46 min	843.8 (71.8)
					1014.4 (28.0)
Mn	^{55}Mn (100)	13.3 ± 0.2 b	^{56}Mn	2.58 h	846.8 (93.9)
					1810.7 (27.2)
Na	^{23}Na (100)	400 ± 30 mb	^{24}Na	15 h	1368.6 (99.99)
Ni	^{64}Ni (1.08)	1.49 ± 0.03 b	^{65}Ni	2.52 h	366.3 (4.81)
					1115.5 (15.4)
					1481.8 (23.6)
Th	^{232}Th(100)	7.40 ±0.08 b	^{233}Th	22.2 min	86.5 (1.6)
					162.5 (0.17)
					169.1 (0.28)
					459.2 (0.8)
					669.8 (0.38)
Ti	^{50}Ti (5.3)	179 ± 3 mb	^{51}Ti	5.76 min	320.1 (93.1)
V	^{51}V (99.75)	4.88 ± 0.04 b	^{52}V	3.74 min	1434.2 (100)

Table 3.16. Peak efficiency reduction factors and sensitivities for medium-lived nuclides using anticoincidence spectrometry (t_i = 10 min, t_d = 1 min, t_c = 10 min).

Nuclide	γ-ray energy, keV (% pop.)	Peak efficiency reduction factor ± 1 σ	Sensitivity counts/μg ± 1 σ
^{28}Al	1778.9 (100)	1.05 ± 0.04	(4.14 ± 0.12) × 10^3
^{139}Ba	166.4 (23.7)	0.94 ± 0.02	511 ± 13
^{80}Br	616.8 (8.7)	0.91 ± 0.02	(3.65 ± 0.09) x 10^3
	704.6 (1.1)	0.04 ± 0.02	186 ± 10
	1256.6 (0.19)	0.87 ± 0.03	68 ± 8
^{38}Cl	1642.7 (31.9)	0.38 ± 0.05	102 ± 2
^{66}Cu	1039.2 (7.14)	1.03 ± 0.03	944 ± 30
^{165}Dy	94.7 (3.6)	0.98 ± 0.04	(9.92 ± 0.40) ×10^4
	279.7 (0.48)	0.16 ± 0.01	(1.28 ± 0.07) ×10^3
	361.7 (0.85)	0.93 ± 0.03	(1.68 ± 0.08) ×10^4
^{128}I	442.9 (17)	0.92 ± 0.04	(1.37 ± 0.07) ×10^4
^{27}Mg	843.8 (71.8)	0.98 ± 0.02	148 ± 9
	1014.4 (28.0)	1.00 ± 0.04	47 ± 3
^{56}Mn	846.8 (93.9)	0.71 ± 0.04	(2.14 ± 0.04) ×10^4
	1810.7 (27.2)	0.22 ± 0.02	811 ± 57
^{24}Na	1368.6 (99.99)	0.38 ± 0.03	119 ± 7
^{65}Ni	366.3 (4.81)	0.29 ± 0.02	0.89 ± 0.11
	1115.5 (15.4)	0.68 ± 0.04	3.21 ± 0.35
	1481.8 (23.6)	0.82 ± 0.04	5.78 ± 0.54
^{233}Th	86.5 (1.6)	0.97 ± 0.03	(3.10 ± 0.06) ×10^3
	162.5 (0.17)	0.51 ± 0.02	134 ± 12
	169.1 (0.28)	0.61 ± 0.05	292 ± 26
	459.2 (0.8)	0.78 ± 0.03	533 ± 44
	669.8 (0.38)	0.80 ± 0.03	195 ± 7
^{51}Ti	320.1 (93.1)	1.08 ± 0.02	526 ± 39
^{52}V	1434.2 (100)	0.99 ± 0.01	(6.48 ± 0.04) ×10^4

The full-energy peaks of ^{38}Cl, ^{56}Mn, and ^{24}Na were reduced significantly in anticoincidence counting due to cascading transitions (Table 3.16). It is obvious that the sensitivities of these nuclides cannot be improved by the anticoincidence counting mode. However, since these three nuclides are major contributors to the Compton background interference observed in INAA using medium-lived nuclides, their effects can be greatly reduced by anticoincidence counting.

It should be noted that among the three gamma-rays of ^{65}Ni (Table 3.15), the 366.3 keV gamma-ray which cascades with the 1115.5 keV gamma-ray, has the highest PERF. The partially cascading 1481.8 keV gamma-ray has undergone only a small reduction. These results suggest that even for the same nuclide, care should be taken in selecting appropriate photopeaks for anticoincidence counting.

The nuclide ^{28}Al (half-life = 2.24 min) decays by a non-coincident gamma-ray of 1778.9 keV; its PERF is 1.05 ± 0.04 (Table 3.16). The application of anticoincidence spectrometry reduces the Compton background under the 1778.9 keV peak and lowers the detection limit. As shown in the Fig. 3.16, the background under the 1778.9 keV peak in Wheat Gluten (RM 8418) is reduced by a factor of about 10 using anticoincidence counting spectrometry. However, the concentration of Al in this material could not be reliably measured due to its high levels in the irradiation vials and in the laboratory atmosphere.

The nuclide ^{80}Br (half-life = 17.7 min) decays by β-emission followed

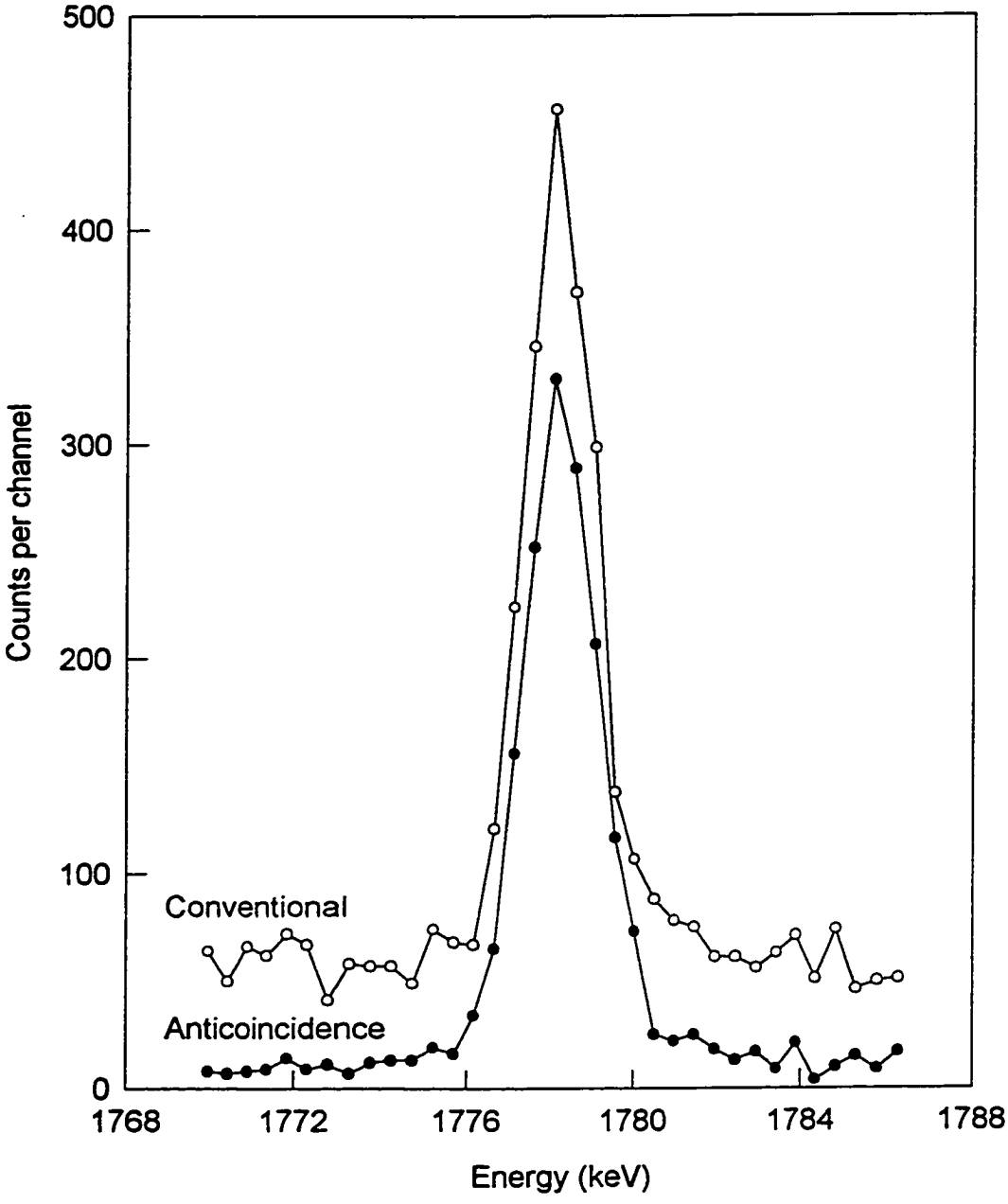

Fig. 3.16. Gamma-ray spectra near the 1778.9 keV peak of ^{28}Al in Wheat Gluten (NIST RM 8418) using conventional and anticoincidence spectrometry.

by three major gamma-rays, namely 616.8, 704.6 and 1256.6 keV. The 704.6-keV peak is cascaded with the 616.8 keV peak; due to the low population of the 704.6-keV peak, the PERF of the 616.8-keV peak is 0.91. The application of anticoincidence counting spectrometry not only reduces the background under the 616.8-keV peak but also eliminates the interference from the 620.7-keV double escape peak of ^{38}Cl. These improvements are evident from the partial gamma-ray spectra of NIST Not-Fat Milk Powder (SRM 1549) using both conventional and anticoincidence counting modes as shown in Fig. 3.17. The double escape peak of ^{38}Cl was virtually eliminated in the anticoincidence spectrum, and the overall background of the region of interest was reduced by a factor of 6 in Not-Fat Milk Powder. Bromine was not one of the elements of interest to the present work, and thus its levels were not measured. It should be noted here that the irradiation vials contained varied amounts of Br, which will require correction for reagent blank in any reliable measurement.

3.4.2 Determination of Magnesium

Magnesium is eighth most abundant element in the earth's crust. Magnesium is considered to be an essential element at moderate concentrations. The effects of Mg deficiency and toxicity in human body, and its roles in photosynthesis and in oxidative photosphorylation have been reported in the literature [111,112].

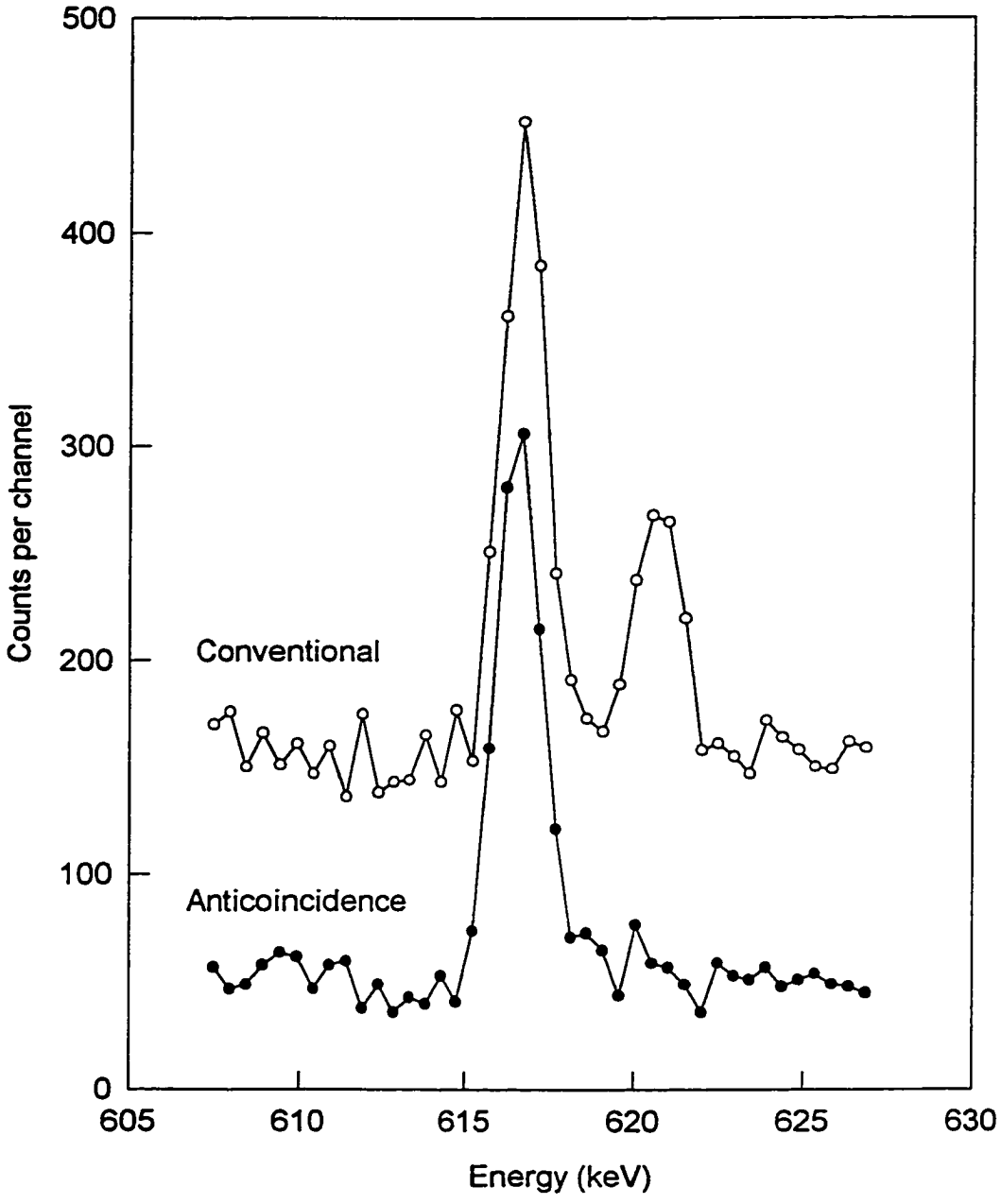

Fig. 3.17. Gamma-ray spectra near the 616.8 keV peak of ^{82}Br in Non-Fat Milk Powder (NIST SRM 1549) using conventional and anticoincidence spectrometry.

The most common techniques for Mg determination are titrimetry, spectrophotometry, and atomic absorption spectrometry [113]. Instrumental NAA has also been proven to be a promising and attractive tool for the rapid, simple and reliable determination of Mg, and is routinely used in many laboratories. However, because of the high activity produced by major nuclides such as ^{28}Al, ^{38}Cl, ^{56}Mn, and ^{24}Na in biological samples, the measurement of the shorter-lived nuclide ^{27}Mg is generally difficult at low Mg levels.

As shown in Fig. 3.18 [107], ^{27}Mg has a half-life of 9.46 min and it decays by β-emission and then two major gamma-rays, namely 843.8 and 1014.4 keV, which are not coincident. Therefore, the use of anticoincidence counting will not cause any reduction in peak efficiency of either of the gamma-rays. However, the Compton continuum from ^{28}Al, ^{38}Cl, ^{56}Mn, and ^{24}Na can be reduced by this counting mode.

The 1014.4-keV gamma-ray is free from interference and it has been used for the determination of Mg in biological and environmental samples. Due to the low intensity of 28.0% of this gamma-ray, the detection limit for Mg using conventional gamma-ray spectrometry could be rather high depending on the neutron flux and experimental conditions used. The application of anticoincidence counting can reduce the background under the 1014.4 keV peak, improve accuracy of the peak, and lower the detection limit. These improvements are evident from the partial gamma-ray spectra of NIST Pine Needles (SRM 1575) and Whole Egg Powder (RM 8415) using both conventional and anticoincidence

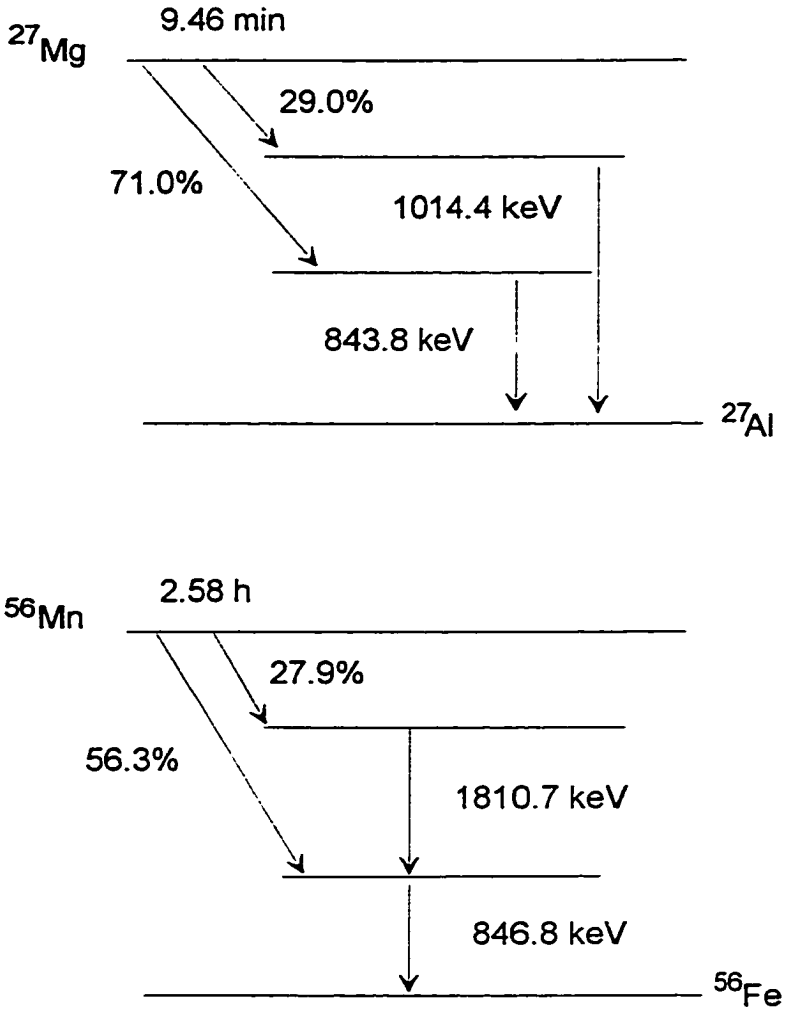

Fig. 3.18. Decay schemes (major transitions only) of ^{27}Mg and ^{56}Mn.

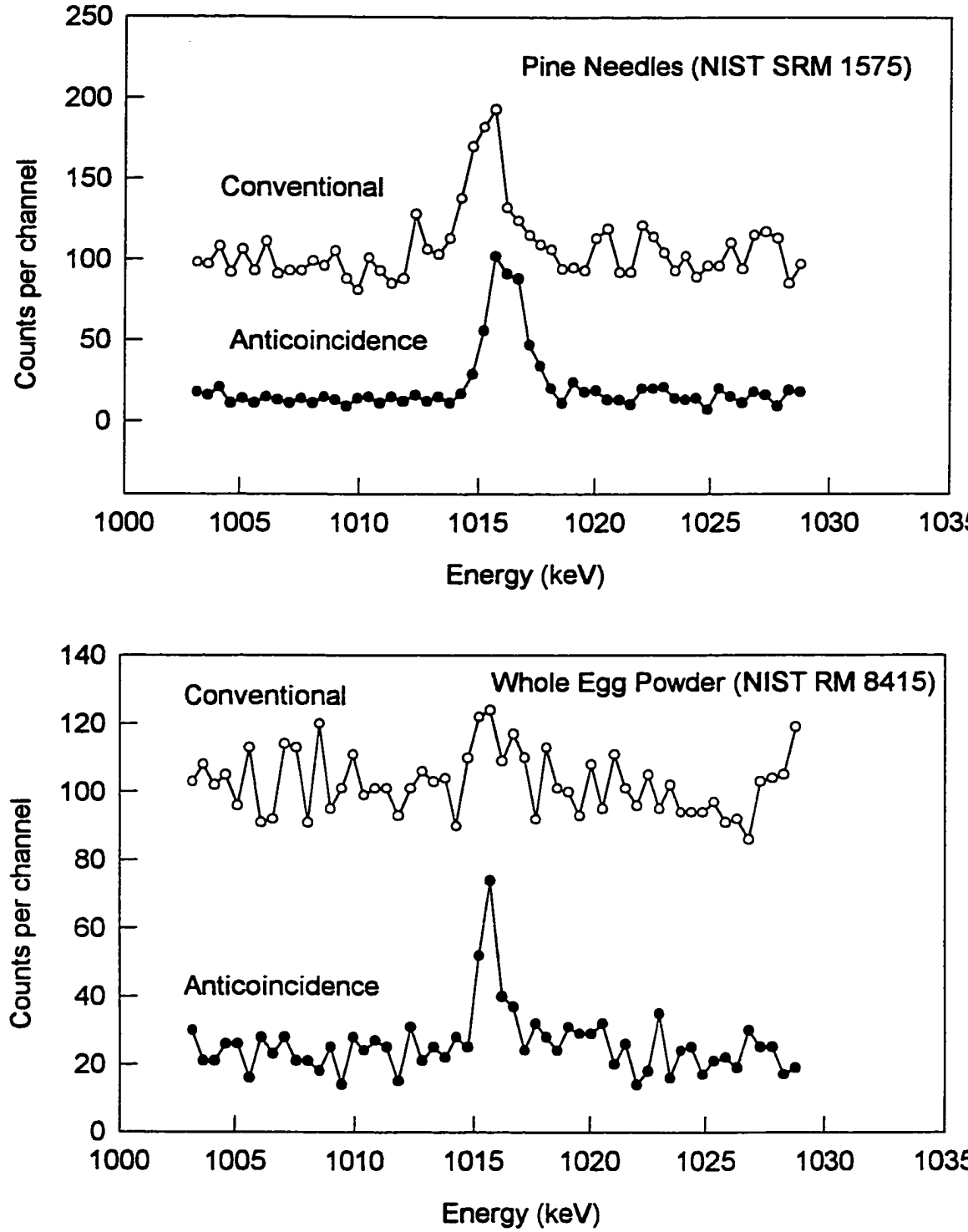

Fig. 3.19. Gamma-ray spectra near the 1014.4 keV peak of ^{27}Mg in Pine Needles (NIST SRM 1575) and in Whole Egg Powder (NIST RM 8415) using conventional and anticoincidence spectrometry.

counting modes as shown in Fig. 3.19. The overall background of the region of interest for Pine Needles was reduced by a factor of greater than 8. In Whole Egg Powder, the 1014.4-keV peak of ^{27}Mg was masked in the conventional counting mode, because of a high Compton continuum from ^{28}Al and ^{56}Mn which were also present in the irradiated sample. The 1014.4-keV peak became a well-defined narrow peak in anticoincidence counting, and it could then be measured with higher reliability.

Magnesium concentrations in samples can be measured using either 843.8 or 1014.4 keV peak of ^{27}Mg. The sensitivity of the 843.8-keV peak is 3.53 times higher than that of the 1014.4-keV peak as shown in Table 3.16. However, the 843.8-keV peak suffers from interference by the 846.8-keV peak of ^{56}Mn which has a longer half-life of 2.58 h. Consequently, the 1014.4-keV peak is mostly used for Mg determination in INAA despite its relatively lower sensitivity.

The tailing edge of the 843.8-keV peak of ^{27}Mg overlaps with the leading edge of the 846.8-keV peak of ^{56}Mn. Due to this overlap, the total peak area (TPA) method for the 843.8-keV peak area gives significant errors. The TPA method is very simple, fast and accurate for single-peaks, but cannot be applied easily to peaks overlapping in energy. The influence of the 846.8-keV peak of ^{56}Mn on the 843.8-keV peak of ^{27}Mg was investigated in this work by irradiating a series of standard solutions containing varying Mg/Mn ratios and studying the degree of overlap using both anticoincidence and conventional counting modes. The results, shown in Table 3.17, indicate that the interference is highly dependent

Table 3.17. Correction of interference of 843.8 keV peak of ^{27}Mg by 846.8 keV peak of ^{56}Mn using conventional and anticoincidence gamma-ray spectrometry.

Mg/Mn ratio	Ratio of 843.8/846.8 keV peak area		Overlap %		Sensitivity by A_{TPA}, counts/μg		Sensitivity by A_{corr}, counts/μg	
	conv.	anti.	conv.	anti.	conv.	anti.	conv.	anti.
3.3	0.0053	0.02	98	48	1.60	4.20	-	6.86
4.1	0.0068	0.04	76	45	2.55	4.70	-	7.11
8.2	0.025	0.05	66	46	3.73	4.91	5.93	8.34
16.4	0.05	0.09	64	43	3.68	4.03	7.73	6.87
81.9	0.4	0.82	38	15	5.70	6.98	8.25	8.15
131	0.72	1.17	28	13	6.13	7.53	7.80	8.62
328	2.34	3.84	23	13	7.13	6.43	7.67	7.17
410	3.32	5.56	9.3	5.1	6.77	7.07	7.67	7.73
546	4.56	6.26	11	7.7	7.29	6.45	7.86	6.95
655	4.92	16.2	8.8	8.5	7.83	6.96	8.34	7.55
1093	11.1	22.7	7.6	7.4	7.30	6.99	7.79	7.52
2186	26.8	58.5	5.4	3.9	7.33	7.17	7.65	7.43

on the Mg/Mn ratio for both anticoincidence and conventional counting modes.

An empirical parameter, called the percentage overlap, is defined here as the ratio of the counts at the overlapping point, C_o, to the peak height counts of the 843.8 keV peak, C_p, and reported as a percentage:

$$\%Overlap=\frac{C_o}{C_p}\times 100\% \qquad [3.22]$$

It is graphically shown in Fig. 3.20. The results presented in Table 3.17 show that the higher the Mg/Mn ratio in the sample, the greater is the ratio of two peak areas (*i.e.* 843.8/846.8 keV peaks), and less is the percent overlap. Both conventional and anticoincidence counting modes show the same trend. However, at the same Mg/Mn ratio, the percentage overlap in anticoincidence counting mode is less than that in conventional counting mode, as shown in Table 3.17.

For the quantification of this type of overlap, complex methods are used to separate the individual contributions of each peak. The most common procedure is called the Gaussian function fitting (GFF) method. This approach involves a nonlinear least-square fitting of the primary Gaussian function to the leading edge of the peak which can be clearly resolved, and assumes that the remainder of the peak is described by the Gaussian function [114]. The peak area can be calculated using the parameters (peak heights and widths) derived from the fitted shape. If the leading edge of the first peak is not distorted by the second peak, this method yields satisfactory results for overlapping peaks. There

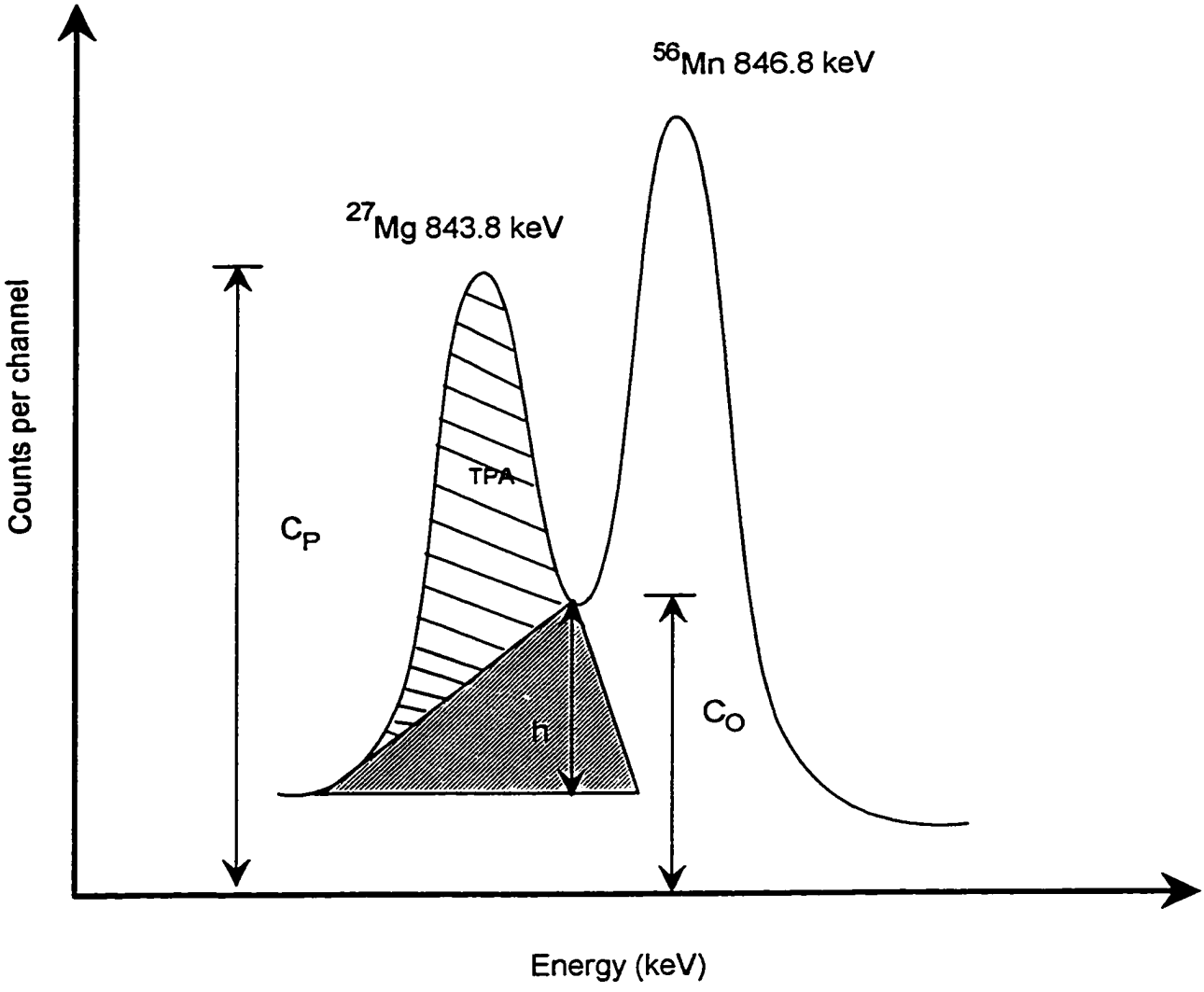

Fig. 3.20. An illustration of the region of overlap of 843.8 keV peak of ^{27}Mg by 846.8 keV peak of ^{56}Mn.

exists a maximum peak overlap that can be tolerated. However, in cases where peak shape does not follow Gaussian function, as shown in Fig. 3.21, the leading and tailing edges cannot both be fitted well at the same time by the Gaussian function only. Errors in peak area calculated by the GFF method can also be expected. The data used to plot the gamma-ray spectrum were obtained by irradiating a food (spinach) sample for 1 min, allowing it to decay 1 min, and counting for 10 min using anticoincidence spectrometry.

As shown in Fig. 3.20, the peak area calculated by the TPA method (APTEC software) is only the lined area, while a triangular shaped area (hatched) was missed by the software. As a general treatment, one of the edges of this triangle is the baseline of the peak with the length of $W_{0.1}$ (*i.e.*, full-width at tenth-maximum), and its vertex is at the lowest point of overlap. Therefore, its area can be simply calculated by the following equation:

$$A = 2.22\, W_{0.5}\, (C_o - C_L) \qquad [3.23]$$

Where A is the area of triangle, and C_L is the difference between the baseline and background counts ($C_L = C_0 - h$, as shown in Fig. 3.20), and $W_{0.5}$ is the full-width at half-maximum. Therefore, the corrected TPA (A_{corr}) can be calculated using the equation:

$$A_{corr} = A + A_{TPA} \qquad [3.24]$$

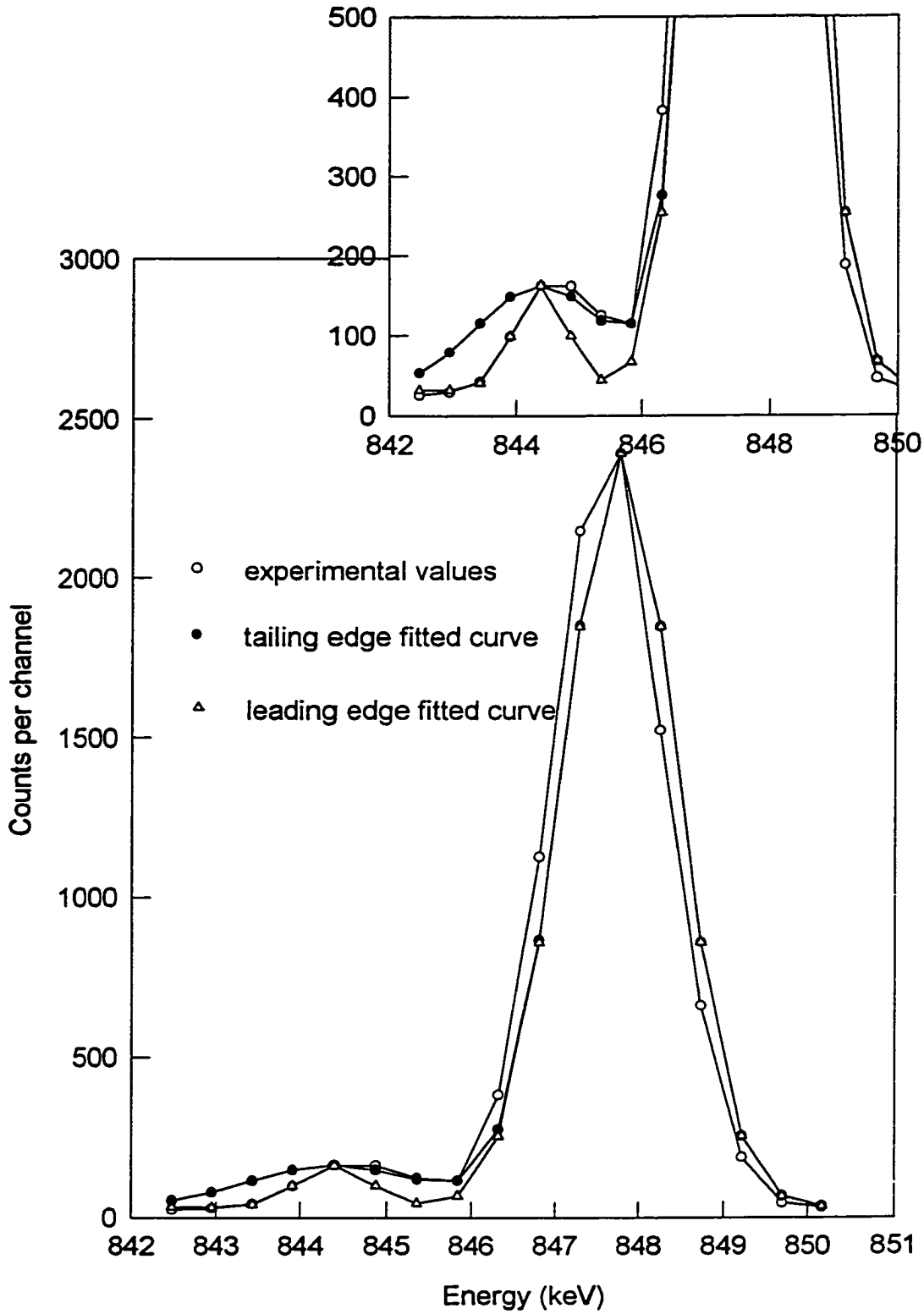

Fig. 3.21. Gamma-ray spectrum near the 843.8 keV peak of ^{27}Mg in a food sample and its Gaussian function fitted curves.

Where A is the area of triangle calculated by equation 3.23 and A_{TPA} is the peak area calculated using the TPA method by computer.

A pure Mg comparator standard (*i.e.*, without any detectable Mn) and a series of standard solutions containing varying ratios (*viz.* 3.3 to 2186) of Mg/Mn were irradiated at a flux of 5×10^{11} n cm^{-2} s^{-1} for 1 min, allowed to decay for 1 min, and counted for 10 min. Under these experimental conditions, the sensitivity of the 843.8-keV peak of ^{27}Mg (free from any interference of 846.8 keV peak of ^{56}Mn) were 7.43 and 7.62 counts per μg using anticoincidence and conventional counting modes, respectively. However, due to the overlap of these two gamma-rays, the sensitivities of the 843.8-keV peak in solutions containing both Mg and Mn calculated using A_{TPA} were lower than the values for the Mg standard alone. These sensitivities were found to decrease with decreasing Mg/Mn ratio in both counting modes, as shown in Table 3.17.

The sensitivities of the 843.8-keV peak of ^{27}Mg can be corrected for the interference by the 846.8-keV peak of ^{56}Mn using equation 3.24. This correction can be applied up to an overlap of 64% in the conventional counting mode (Table 3.17). In the anticoincidence counting mode, the percentage overlap of the 843.8-keV peak is less because of the suppression of the 846.8-keV peak. Consequently, the corrected sensitivity values are closer to that of the pure Mg standard. The results are graphically presented in Fig. 3.22 where the sensitivities based on A_{TPA} and A_{corr} by anticoincidence and conventional gamma-ray spectrometry are plotted against various Mg/Mn ratios.

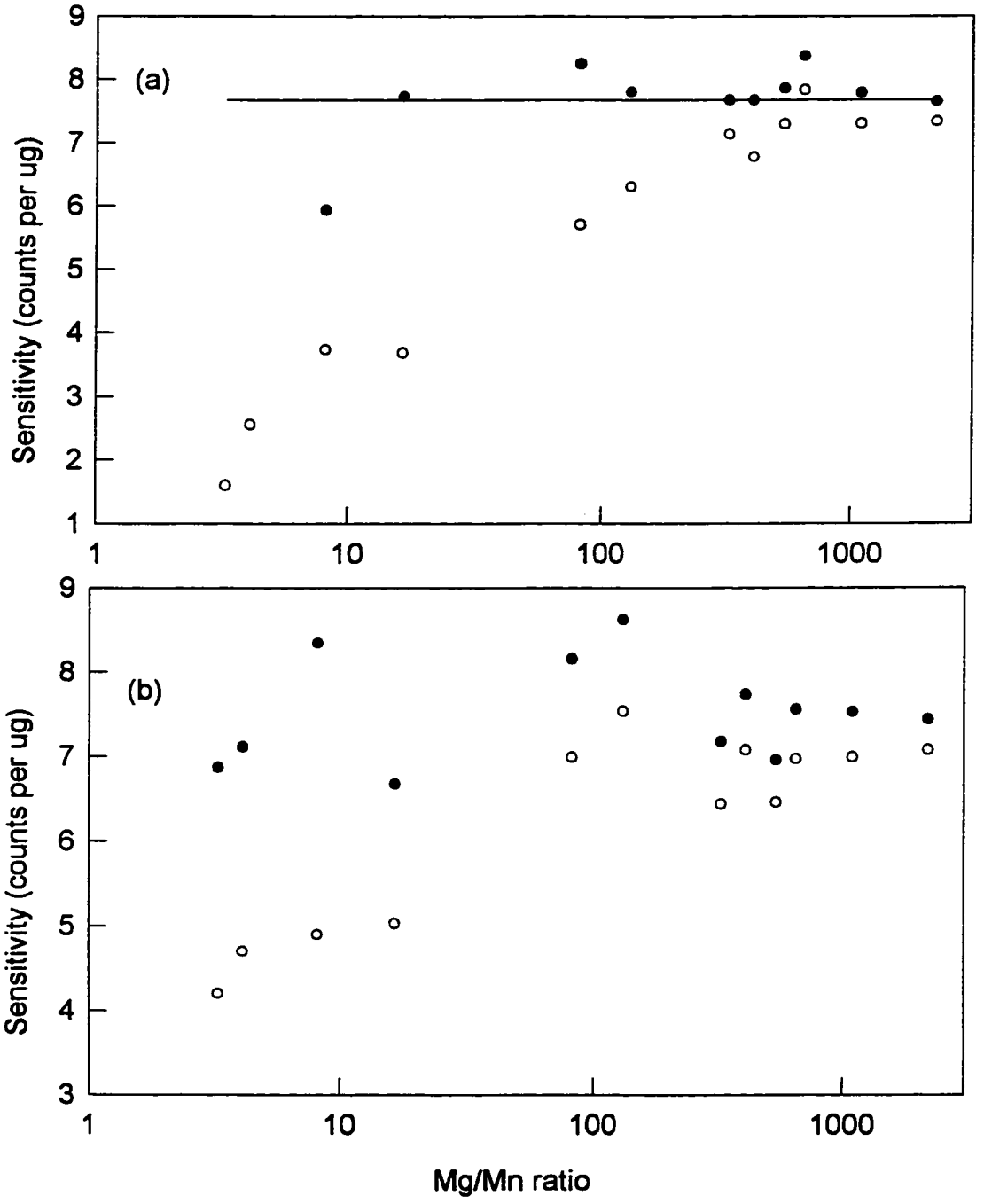

Fig. 3.22. The corrected and uncorrected sensitivity of 843.8 keV peak of ^{27}Mg at various Mg/Mn ratios by (a) conventional (b) anticoincidence spectrometry.

• corrected values ○ uncorrected values

The correction method described above was used for the determination of Mg in 15 NIST RM and SRM using the 843.8-keV gamma-ray of ^{27}Mg and both conventional and anticoincidence gamma-ray spectrometry. The results are presented in Table 3.18. It is evident that anticoincidence counting can provide a more reliable measurement of ^{27}Mg through the 843.8-keV peak by minimizing the interference from the 846.8-keV peak of ^{56}Mn. Examinations of the decay scheme (Fig. 3.18) of ^{56}Mn reveals that the 846.8 and 1810.7 peaks are partially cascading, and therefore an enhanced suppression of the 846.8-keV peak will occur in anticoincidence counting. The net effect is less overlapping of the two peaks; in some cases the interference from the 846.8-keV peak of ^{56}Mn can be completely eliminated and more reliable data can be obtained using the 846.8-keV peak of ^{27}Mg. The agreement between the values obtained by the correction method using the 846.8-keV peak and that by the interference-free peak of 1014.4 keV is generally good as shown in Table 3.18. The real advantage of the correction method in conjunction with anticoincidence counting is that an improved sensitivity can be obtained for the 846.8-keV peak compared to the 1014.4 keV peak.

It should be noted here that there are several computer programs available in the market for deconvoluting overlapping peaks. Some of them are already incorporated in the software delivered with the MCA. The software provided by APTEC was found not to be entirely satisfactory. No other software was available in our laboratory for this purpose. For this reason, a manual

Table 3.18. Concentration of magnesium (ppm) in NIST reference materials by anticoincidence and conventional gamma-ray spectrometry using the correction method.

Reference materials	Using 843.6 keV γ-ray				Using 1014.4 keV γ-ray
	Conventional		Anticoincidence		
	uncorrected	corrected	uncorrected	corrected	
Corn Starch (RM 8432)	27 ± 7.1	37 ± 6.4	30 ± 3.7	39 ± 2.1	30 ± 2
Soft Wheat Flour (RM 8438)	136 ± 18	171 ± 9.4	127 ± 4.2	188 ± 8.5	210 ± 14
Whole Egg Powder (RM 8415)	267 ± 15	301 ± 25	311 ± 45	365 ± 38	365 ± 40
Hard Wheat Flour (RM 8437)	254 ± 6.4	336 ± 14	261 ± 7.8	340 ± 16	375 ± 26
Wheat Flour (SRM 1567a)	220 ± 18	351 ± 38	376 ± 21	404 ± 11	410 ± 16
Wheat Gluten (RM 8418)	248 ± 44	383 ± 31	260 ± 7	473 ± 16	485 ± 9
Rice Flour (SRM 1568a)	275 ± 21	448 ± 16	471 ± 32	497 ± 14	556 ± 28
Bovine Liver (SRM 1577b)	336 ± 11	477 ± 17	366 ± 34	594 ± 31	605 ± 23
Corn Bran (RM 8433)	640 ± 26	746 ± 29	713 ± 49	801 ± 41	815 ± 16
Durum Wheat Flour (RM 8436)	652 ± 14	927 ± 35	846 ± 38	1170 ± 80	1040 ± 38
Non-Fat Milk Powder (SRM 1549)	1010 ± 7.1	1053 ± 14	913 ± 62	1130 ± 45	1200 ± 90
Pine Needles (SRM 1575)	64 ± 32	843 ± 352	210 ± 96	1150 ± 105	1260 ± 27
Apple Leaves (SRM 1515)	1536 ± 160	2155 ± 190	1170 ± 30	2680 ± 125	2655 ± 99
Peach leaves (SRM 1547)	2427 ± 109	3930 ± 285	3650 ± 540	4315 ± 245	4300 ± 300
Spinach (SRM 1570)	4138 ± 562	6950 ± 470	5990 ± 390	7740 ± 520	8030 ± 600

calculation approach was developed in this work. Although this method is simple, it still gives reliable results.

One of the approximations made in this correction method was the arbitrary assignment of peak baseline at $W_{0.1}$. In order to ascertain more accurate peak areas, the width of the baseline should be calculated based on the channel number on the left where the peak starts to rise. The other approximation was made by assuming that the peak's overlapping part could be simplified by a straight line rather than a Gaussian fit. For most of RMs, as shown in Table 3.19, the percentage overlap of the 843.8-keV peak by the 846.8-keV is less than 40% and the ratio of 843.8/846.8 keV peak area is relatively high. In such cases, the approximations made generally do not impart much error in Mg concentrations as evident from Tables 3.18 and 3.4. However, in cases where the percentage overlap is relatively high (*i.e.* >40%) and the ratio of 843.8/846.8 keV peak area is very low, such as in NIST SRM 1568a, 1575, and 1570 (Table 3.19), Mg levels calculated by the correction method are lower than those obtained by the 1014.4-keV peak and than the certified value (Table 3.4). It is evident from Table 3.19 that the percentage overlap is reduced and the ratio of 843.8/846.8 keV peak area is increased in the anticoincidence counting mode compared to the conventional counting mode. The above correction method for Mg can therefore be more reliably applied to anticoincidence spectra.

Table 3.19. Percentage overlap of 843.8 keV peak of ^{27}Mg by 846.8 keV peak of ^{56}Mn in various NIST reference materials.

Reference materials	Percentage overlap		Ratio of 843.8/846.8 peak areas	
	conv.	anti.	conv.	anti.
Corn Starch (RM 8432)	35.3	15.3	1.18	1.71
Soft Wheat Flour (RM 8438)	34.6	19.2	0.14	0.24
Whole Egg Powder (RM 8415)	14.1	8.3	1.38	2.06
Hard Wheat Flour (RM 8437)	23.7	12.8	0.37	0.57
Wheat Flour (SRM 1567a)	42.1	26.5	0.15	0.26
Wheat Gluten (RM 8418)	48.2	36.2	0.11	0.19
Rice Flour (SRM 1568a)	40.2	30.7	0.083	0.041
Bovine Liver (SRM 1577b)	30.6	19.2	0.22	0.40
Corn Bran (RM 8433)	14.5	8.53	1.96	3.92
Durum Wheat Flour (RM 8436)	30.5	16.9	0.28	0.52
Non-Fat Milk Powder (SRM 1549)	4.58	3.27	30.5	36.6
Pine Needles (SRM 1575)	98.2	65.5	0.00072	0.0029
Apple Leaves (SRM 1515)	35.9	22.4	0.18	0.36
Peach leaves (SRM 1547)	38.2	21.6	0.14	0.26
Spinach (SRM 1570)	63.5	57.6	0.17	0.25

3.4.3 Determination of Copper

Copper is considered to be an essential element [115,116]. Its accurate determination in tissues, body fluids, foods and other biological materials is needed for the purpose of studying the effect of Cu on human nutrition and health. In biological materials, Cu can be measured by NAA *via* $^{63}Cu(n,\gamma)^{64}Cu$ and $^{65}Cu(n,\gamma)^{66}Cu$ reactions. The positron-emitting nuclide ^{64}Cu (half-life = 12.7 h) is not commonly used for assaying copper since its 1345.8-keV gamma-ray has a low population and the 511-keV annihilation radiation may be interfered with by a number of positron emitters. Radiochemical NAA (RNAA) methods can be employed. In one such method sub-ppm levels of copper were separated by extraction chromatography [117]. Using an Advance Prediction Computer Program (APCP), it has been shown that short-lived ^{66}Cu (half-life = 5.09 min) can possibly be used for Cu determination in biological materials by INAA [118]. However, it is seldom done in practice, in particular for low copper content in high-salt biological materials, due to the Compton background interference from nuclides such as ^{28}Al, ^{38}Cl, and ^{24}Na. In order to eliminate Compton interference, a PNAA method has been developed using selective ion-exchange separation of Cu followed by short irradiation and gamma-spectrometric counting of ^{66}Cu; the detection limit, for the sample weight of 500 mg, was about 0.34 ppm [119].

The ^{66}Cu nuclide decays by a non-coincident 1039.2 keV photon. The application of anticoincidence spectrometry can reduce the Compton

background under the 1039.2-keV peak, improve the statistical accuracy of the peak and lower the detection limit. These improvements are evident from the partial gamma-ray spectra (*viz.* around 1039 keV) of NIST Rice Flour (SRM 1568a) and Peach Leaves (SRM 1547) using both conventional and anticoincidence counting modes shown in Fig. 3.23. The overall background around this region was reduced by a factor of 9 for the SRM Rice Flour. In Peach Leaves, the 1039.2-keV peak of ^{66}Cu was masked in the conventional counting mode due to its low copper content and a high Compton continuum from ^{28}Al and ^{56}Mn, while the 1039.2-keV peak became a well-defined peak using anticoincidence counting.

In order to evaluate the extent of improvement that can be achieved by anticoincidence counting, diverse types of biological RMs and SRMs were analyzed for Cu by INAA. Between 200 and 700 mg of these materials, depending on the levels of major and interfering elements present, were weighed. The materials were irradiated at a flux of 5×10^{11} n cm^{-2} s^{-1} for 1 min, allowed to decay for 1 min, and the 1039.2-keV gamma-ray of ^{66}Cu counted for 10 min. The sensitivity for Cu standard solutions under these conditions was 69 counts/μg in the anticoincidence counting mode. The RMs were analyzed in triplicate and their Cu concentrations are presented in Table 3.20 along with the certified values. The agreement between the certified and the measured values is generally good with the exception of a few values.

The detection limits of copper in both counting modes are also reported in Table 3.20. The copper concentrations are quite low in most of the

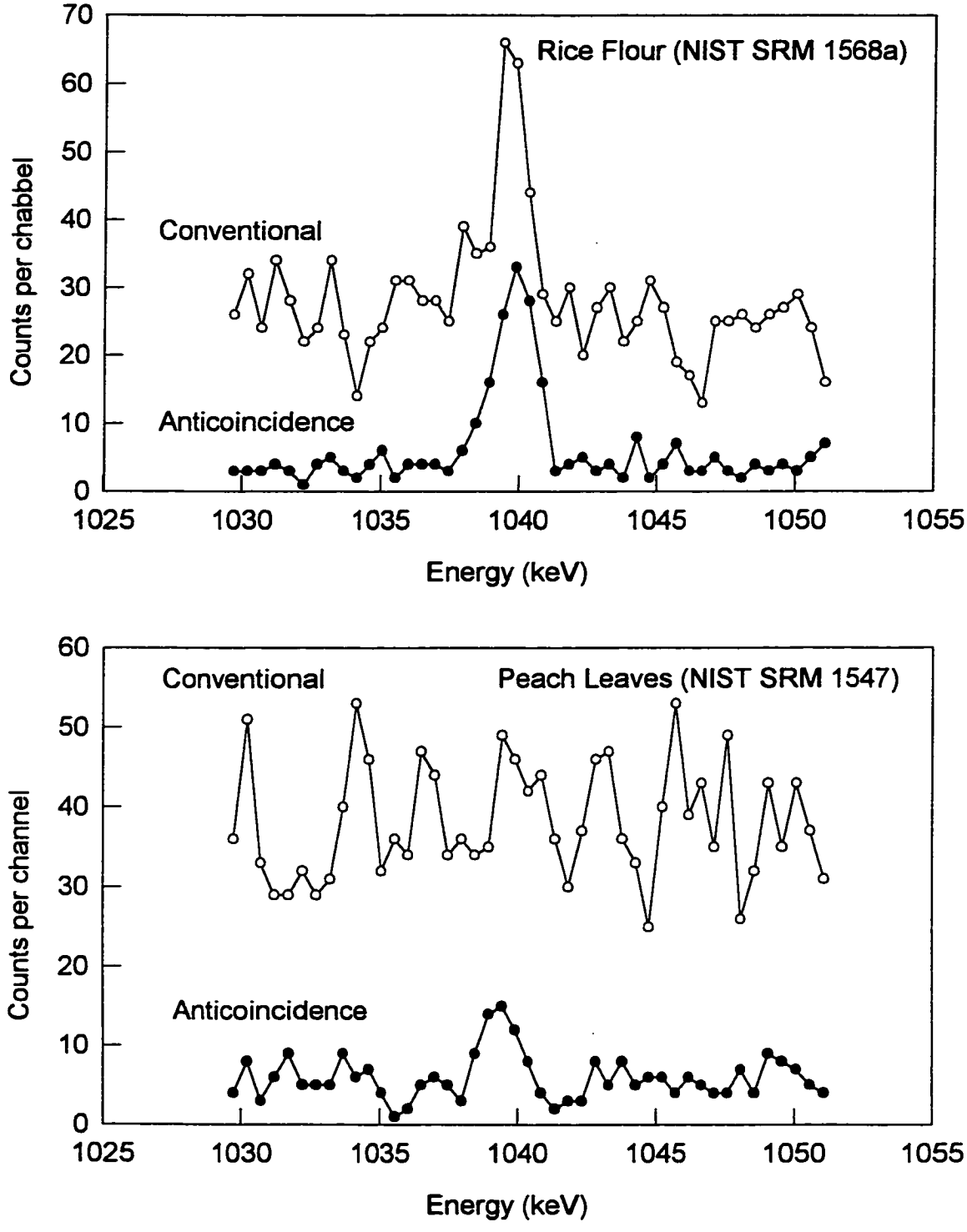

Fig. 3.23. Gamma-ray spectra near the 1039.2 keV peak of ^{66}Cu in Rice Flour (NIST SRM 1568a) and Peach Leaves (NIST SRM 1547) using conventional and anticoincidence spectrometry.

Table 3.20. Concentrations and detection limits of copper in reference materials by anticoincidence gamma-ray spectrometry.

Reference material (*IAEA, all others NIST)	This work, ppm	Certified values, ppm	Detection limits, ppm anti.	conv.
Corn Starch (RM 8432)	<0.08	0.06 ± 0.04		0.25
Non-Fat Milk Powder (SRM 1549)	0.72 ± 0.18	0.7 ± 0.1	0.41	1.2
Soft Wheat Flour (RM 8438)	1.25 ± 0.03	1.2 ± 0.4	0.12	0.36
Hard Wheat Flour (RM 8437)	1.96 ± 0.29	2.01 ± 0.48	0.092	0.22
Wheat Flour (SRM 1567a)	2.1 ± 0.2	2.1 ± 0.2	0.11	0.40
Corn Bran (RM 8433)	2.2 ± 0.2	2.47 ± 0.40	0.11	0.51
Rice Flour (SRM 1568a)	2.16 ± 0.13	2.4 ± 0.3	0.10	0.32
Pine Needles (SRM 1575)	2.7 ± 0.9	3.0 ± 0.3	1.1	2.4
Whole Egg Powder (RM 8415)	2.9 ± 0.1	2.70 ± 0.35	0.40	0.74
Durum Wheat Flour (RM 8436)	4.25 ± 0.22	4.30 ± 0.69	0.18	0.51
Peach leaves (SRM 1547)	4.5 ± 1.1	3.7 ± 0.4	0.69	4.2
Animal Blood (RM A-13)*	4.9 ± 1.4	4.3 ± 0.6	1.5	4.4
Wheat Gluten (RM 8418)	5.36 ± 0.29	5.94 ± 0.72	0.40	1.4
Apple Leaves (SRM 1515)	5.5 ± 0.6	5.64 ± 0.23	0.84	1.9
Spinach (SRM 1570)	13.7 ± 1.3	12 ± 2	2.0	4.8
Bovine Liver (SRM 1577b)	155 ± 7	160 ± 8	0.75	1.9

materials except Spinach and Bovine Liver. For materials such as Not-Fat Milk Powder, Pine Needles, Peach Leaves, and Animal Blood, the Cu concentrations are either very close to or higher than the detection limits calculated from the conventional counting data. However, in the anticoincidence counting mode, the detection limits were lowered by about 2 to 4 times making reliable Cu determinations possible.

The Compton background around the 1039.2-keV peak of ^{66}Cu is influenced by all gamma-rays of higher energy. The effect of sample matrix on the AFOM term cannot be simply estimated by using background interference from only one nuclide. The AFOM term varies with the change in the number of gamma-ray emitting nuclides and their intensities in the irradiated sample. Unlike Mg where its concentration varied considerably in the reference materials analyzed (Table 3.4), the Cu levels in these materials are all low (*viz.* a few ppm) with the exceptions of Bovine Liver (SRM 1577b) and Spinach (SRM 1570).

In many of these materials, the background around the 1039.2-keV peak of ^{66}Cu is mainly due to the 1778.9-keV peak of ^{28}Al, 1368.6-keV peak of ^{24}Na, 1642.7-keV peak of ^{38}Cl, and 1810.7-keV peak of ^{56}Mn. The sum of the peak intensities of these four peaks (MMA) was measured using conventional gamma-ray spectrometry. For each RM, the values for MMA, R_{conv}, R_{anti}, and R_{PA} of the 1039.2-keV peak are presented in Table 3.21. Using these parameters and equation 3.15, the AFOM terms were calculated for each sample, and also given in the same table. It is evident that for most of the materials, the AFOM terms are

Table 3.21. Main matrix activities and peak parameters for the 1039.2-keV peak of ^{66}Cu in various reference materials using anticoincidence and conventional gamma-ray spectrometry.

Reference materials (*IAEA, all others NIST)	R_{anti}	R_{conv}	R_{anti} / R_{conv}	R_{PA}	MMA	AFOM
Apple Leaves (SRM 1515)	0.83	0.13	6.4	1.77	26.8	4.12
Peach leaves (SRM 1547)	1.38	0.13	10.6	1.93	22.7	5.92
Non-Fat Milk Powder (SRM 1549)	0.19	0.070	2.7	1.77	63.5	3.32
Wheat Flour (SRM 1567a)	4.44	0.57	7.9	1.51	12.6	5.67
Rice Flour (SRM 1568a)	3.93	0.42	9.4	2.03	11.9	10.2
Spinach (SRM 1570)	0.59	0.091	6.5	1.89	104	4.43
Pine Needles (SRM 1575)	0.14	0.063	2.2	1.41	72.2	2.08
Bovine Liver (SRM 1577b)	8.61	1.59	5.4	1.17	37.4	4.08
Whole Egg Powder (RM 8415)	0.23	0.091	2.5	1.23	66.4	1.60
Wheat Gluten (RM 8418)	0.75	0.18	4.1	2.19	63.4	6.09
Corn Starch (RM 8432)	1.86	0.14	13.3	3.03	2.54	16.6
Corn Bran (RM 8433)	7.40	0.43	17.2	1.74	5.61	11.7
Durum Wheat Flour (RM 8436)	2.73	0.34	8.2	1.87	16.1	7.93
Hard Wheat Flour (RM 8437)	5.29	0.71	7.5	1.58	9.34	6.70
Soft Wheat Flour (RM 8438)	1.73	0.30	5.8	1.86	9.91	5.62
Animal Blood (RM A-13)*	1.22	0.063	19.3	1.58	81.0	3.96

positively correlated (correlation coefficient of 0.84 at 95% confidence level) with the improvement factors (R_{anti}/R_{conv}); there is only one exception of IAEA Animal Blood which has very high activities of ^{24}Na and ^{38}Cl leading to a low AFOM value. It can be concluded from Table 3.21 that the detection limit for Cu can be improved by anticoincidence counting.

Principal Component Analysis (PCA) is a useful approach for multivariate data analysis [120]. It can be applied to several variables or combinations of variables to reveal some inherent information and characteristics of individual sample matrices. The relationship between AFOM terms and their PCA groupings has been investigated using the Einsight software [121].

It was pointed out above that the major activities in the reference materials analyzed for Cu were due to ^{56}Mn, ^{28}Al, ^{24}Na, and ^{38}Cl in the matrix. The numerical values of these activities are individually shown in Table 3.22 along with their AFOM terms (Table 3.21) for each material. These values form the data matrix for PCA.

The correlation matrix of the data in Table 3.22 is shown in Table 3.23. It shows positive associations of Al with Mn, Na with Cl, and negative association of the AFOM term with all variables. These linear relationships between the activities of ^{28}Al and ^{56}Mn, and between ^{24}Na and ^{38}Cl are graphically presented in Fig. 3.24.

The data in Table 3.22 were analyzed by PCA. Three major principal component scores of all 16 RMs were obtained and are given in Table 3.24. A

Table 3.22. Data matrix for PCA of various reference materials for copper analysis.

Reference materials (*IAEA, all others NIST)	AFOM term	Activity (cps) ^{56}Mn	^{28}Al	^{24}Na	^{38}Cl
Whole Egg Powder (RM 8415)	1.60	20	43.3	10.6	12.4
Spinach (SRM 1570)	4.43	32	48.3	36.7	13.7
Pine Needles (SRM 1575)	2.08	28.3	43.0	0.20	0.74
Bovine Liver (SRM 1577b)	4.08	0.30	3.43	17.7	16.0
Wheat Gluten (RM 8418)	6.09	0.10	2.07	21.7	39.5
Non-Fat Milk Powder (SRM 1549)	3.32	2.18	4.34	18.3	38.6
Animal Blood (RM A-8)*	3.96	0.10	0.39	44.0	36.5
Corn Starch (RM 8432)	16.6	0.35	0.39	4.67	0.20
Durum Wheat Flour (RM 8436)	7.93	2.58	6.14	0.31	7.07
Corn Bran (RM 8433)	11.7	0.04	0.66	1.41	0.43
Apple Leaves (SRM 1515)	4.12	2.19	22.9	0.17	1.57
Soft Wheat Flour (RM 8438)	5.62	0.96	1.45	0.99	6.51
Hard Wheat Flour (RM 8437)	6.70	0.94	1.60	0.29	6.51
Rice Flour (SRM 1568a)	10.2	4.40	3.13	0.18	4.21
Peach leaves (SRM 1547)	5.92	3.72	18.0	0.10	0.85
Wheat Flour (SRM 1567a)	5.67	1.98	3.33	0.10	7.19

Table 3.23. Correlation matrix between variables given in Table 4.21.

	Al	Mn	Na	Cl
Al	1			
Mn	0.544	1		
Na	-0.188	0.127	1	
Cl	-0.267	-0.203	0.753	1

The matrix is symmetrical for the diagonal and values lie in the range -1 to +1.

Table 3.24. The PC scores for copper in various reference materials.

Reference materials (*IAEA, all others NIST)	PC1	PC2	PC3
Whole Egg Powder (RM 8415)	45.4	-21.1	-5.77
Spinach (SRM 1570)	66.6	-16.7	13.3
Pine Needles (SRM 1575)	37.2	-34.9	-5.22
Bovine Liver (SRM 1577b)	18.9	14.6	2.53
Wheat Gluten (RM 8418)	31.3	31.3	-9.10
Non-Fat Milk Powder (SRM 1549)	31.2	27.3	-11.2
Animal Blood (RM A-8)*	40.1	39.5	9.79
Corn Starch (RM 8432)	2.84	1.66	3.32
Durum Wheat Flour (RM 8436)	8.28	-0.191	-5.08
Corn Bran (RM 8433)	1.35	0.419	0.663
Apple Leaves (SRM 1515)	15.9	-13.5	-4.89
Soft Wheat Flour (RM 8438)	4.86	3.12	-3.52
Hard Wheat Flour (RM 8437)	4.59	2.75	-4.08
Rice Flour (SRM 1568a)	5.60	-0.761	-2.62
Peach leaves (SRM 1547)	13.0	-11.5	-3.41
Wheat Flour (SRM 1567a)	6.26	1.69	-4.85

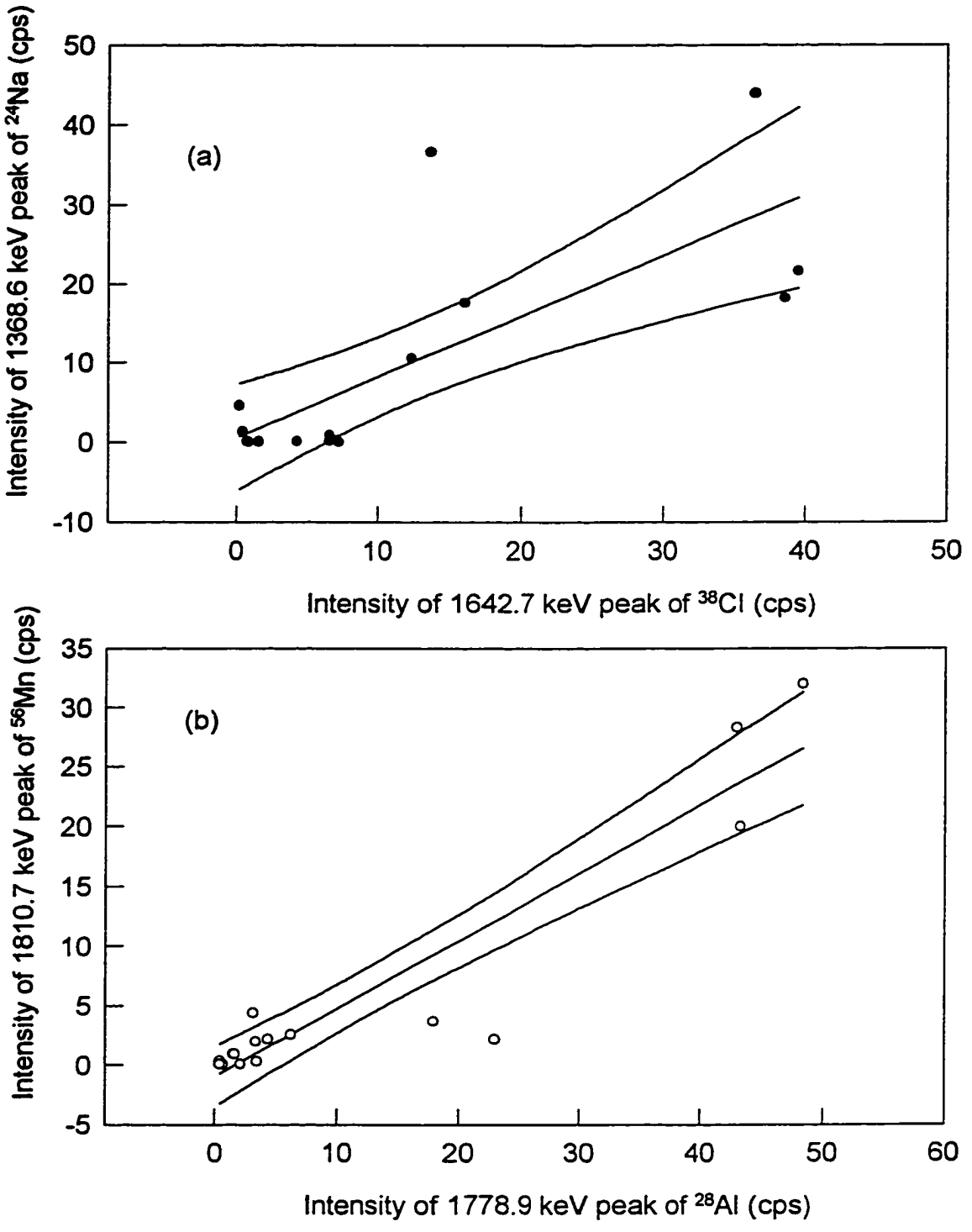

Fig. 3.24. Relationships between the activities of (a) ^{24}Na and ^{38}Cl, and (b) ^{28}Al and ^{56}Mn.

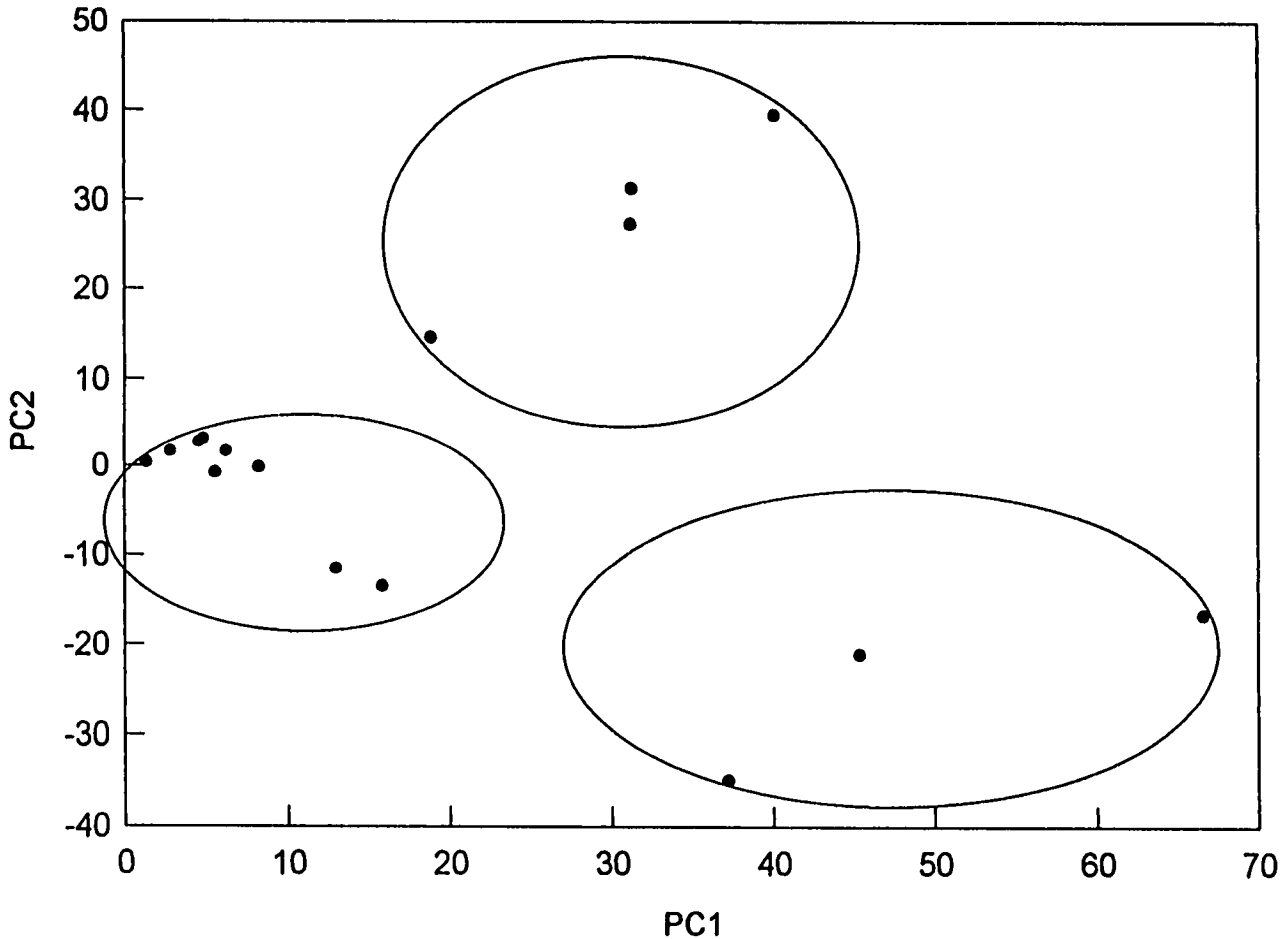

Fig. 3.25. Scatter plot of the 16 SRMs and RMs on first two principal components (Table 3.24).

scatter plot of the first two principal components scores, which explained 95% of the total variance, is shown in Fig. 3.25. It is evident from the scatter plot that these RMs can be grouped into three types of matrix. The Compton background of Pine Needles, Whole Egg Powder, and Spinach were mainly dominated by ^{28}Al and ^{56}Mn activities and constituted a group with an AFOM value of 2.70 ± 1.5. This group is distinguishable from the other two. The Compton background originated mainly from ^{24}Na and ^{38}Cl for Bovine Liver, Wheat Gluten, Non-Fat Milk Powder, and Animal Blood RMs, and constituted a second group with an AFOM value of 4.36 ± 1.2. Finally, the remaining 9 RMs with lower background interference formed a third group with an AFOM value 8.27 ± 2.9.

It can be concluded from the above discussions that samples with high Al and Mn levels give lowest AFOM values for Cu, followed by samples of high Cl and Na content. Highest AFOM values for Cu in anticoincidence counting can be achieved for samples with lower background.

3.4.4 Determination of Vanadium

The toxicity of V has been well known for a long time; but in 1971, it was recognized as an essential trace element which is required for growth and functions of many organisms [122]. The levels of V in biological materials have become increasingly important for understanding its physiological role. Several techniques such as spectrophotometry, atomic absorption, X-ray fluorescence, and

NAA can be used for its determination [123].

Vanadium can be determined in NAA through its short-lived nuclide ^{52}V, which has a 1434.2 keV gamma-ray and half-life of 3.74 min (Table 3.15). It has been reported that ^{52}V has sufficient sensitivity for measuring V down to nanogram levels [124]. However, the most serious problem associated with INAA of V in biological and environmental materials arises from the observation that many samples contain large quantities of Cl, Na, Al, and Mn. Upon thermal neutron activation, these elements will lead to the production of ^{38}Cl, ^{24}Na, ^{28}Al, and ^{56}Mn, respectively; all of them have half-lives longer than ^{52}V except ^{28}Al, and have higher energy gamma-rays except the 1368.6-keV gamma-ray of ^{24}Na (Table 3.15). The 1434.2-keV peak of ^{52}V will be superimposed on the Compton edge produced by the gamma-rays of ^{28}Al and ^{56}Mn. Therefore, the concentration of V in biological and environmental samples could not be reliably determined at low levels using INAA in conjunction with conventional gamma-ray spectrometry. Alternatively, RNAA or PNAA methods are used to separate V from major and interfering elements [125].

Two types of RMs were analyzed for V. One type was a botanical sample matrix, such as NIST SRM Pine Needles, which is characterized by high ^{28}Al and ^{56}Mn activities. The conventional and anticoincidence gamma-ray spectra of Pine Needles is shown in Fig. 3.26. The other RMs analyzed were of zoological/biomedical sample matrix type, in which the major induced activity was due to ^{24}Na and ^{38}Cl. The most extreme case of such activities was detected in

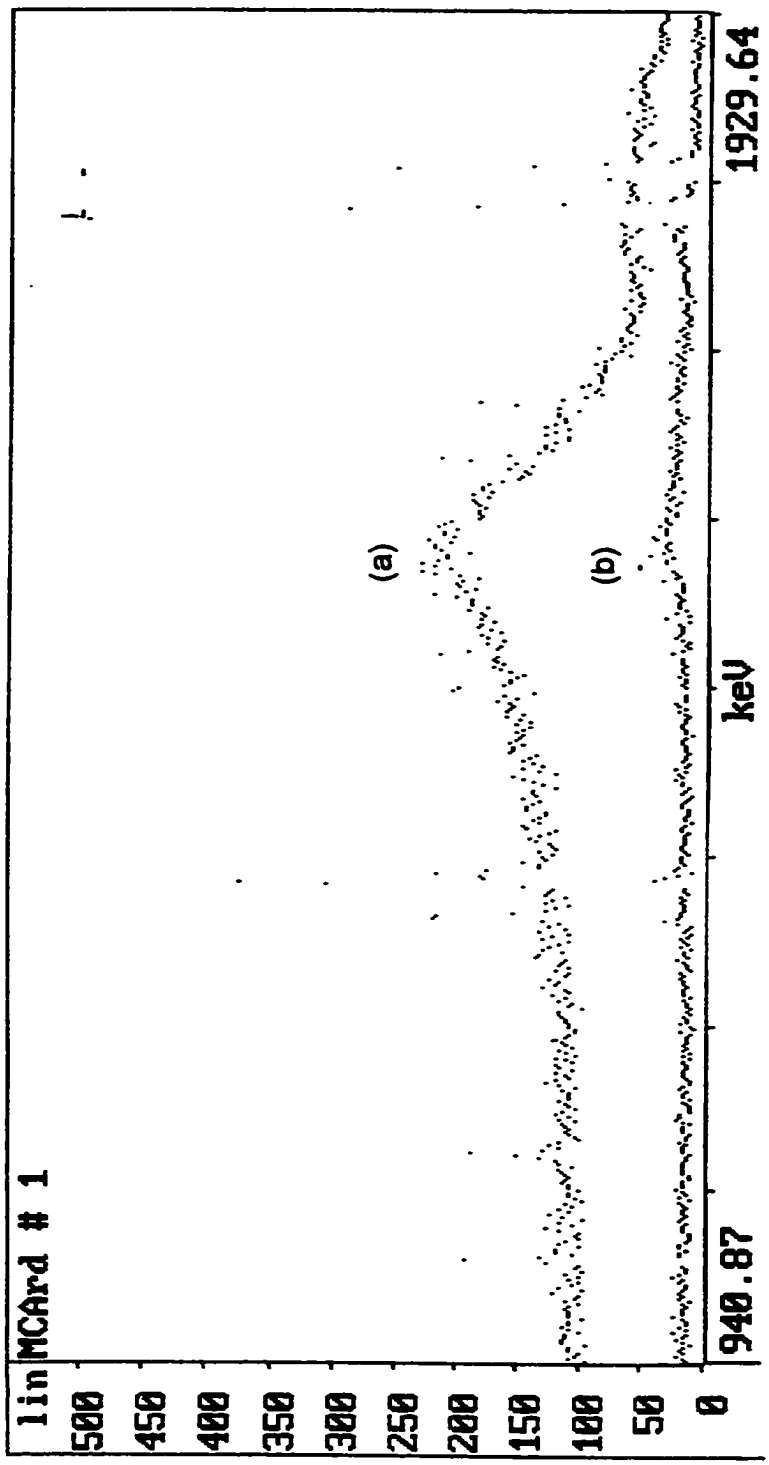

Fig. 3.26. Partial gamma-ray spectra of Pine Needles (NIST SRM 1575) in (a) conventional counting mode (b) anticoincidence counting mode.

IAEA RM Animal Blood. The conventional andanticoincidence gamma-ray spectra of Animal Blood are presented in Fig. 3.27.

In order to investigate the effectiveness of usage of the AFOM terms for V, the ratios of major activities, namely the 1778.9-keV peak of ^{28}Al, 1642.7-keV peak of ^{38}Cl, 1810.7-keV peak of ^{56}Mn, and 1368.6-keV peak of ^{24}Na, to that of the 1434.4-keV peak of ^{52}V for various RMs were calculated using the conventional counting mode. Other relevant parameters, such as R_{conv}, R_{anti}, R_{PA}, and AFOM values for ^{52}V are also listed in Table 3.25.

The Na/V and Cl/V ratios were plotted as a function of AFOM in Fig. 3.28(a) and Fig. 3.28(b), respectively. It is evident that there are three groups of sample matrix. Group I consists of materials of high Na/V as well as Cl/V ratios, and low AFOM (<1, Table 3.25), such as Not-Fat Milk Powder and Animal Blood samples. Group II includes SRMs such as Apple Leaves, Peach Leaves and Pine Needles which have low Na/V as well as Cl/V ratios, but high AFOM values (between 10 and 20, Table 3.25). Group III consists of several RMs with moderate Na/V as well as Cl/V ratios, and moderate AFOM values (between 1 and 6).

In anticoincidence counting, the peak statistical accuracy generally improves when the background under the peak is suppressed and PERF is about one. The two RMs in Group I have low V content and high Na/V as well as Cl/V ratios. Their peak statistical accuracy was not improved by anticoincidence counting (Table 3.25) because the background activity was still very high, making the measurement of the weak 1434.2-keV peak of ^{52}V difficult. As shown in Fig.

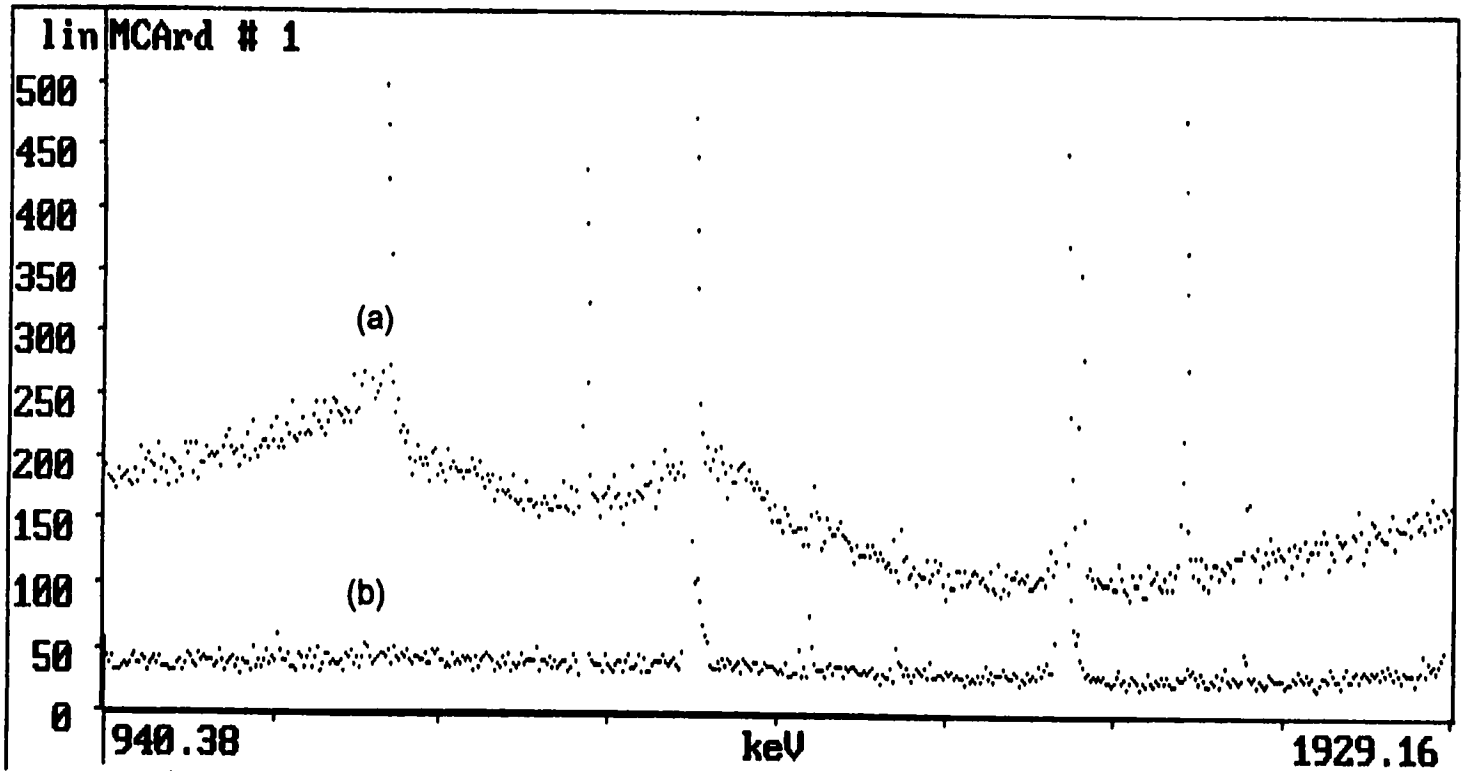

Fig. 3.27. Partial gamma-ray spectra of Animal Blood (IAEA RM A-13) in (a) conventional counting mode (b) anticoincidence counting mode.

Table 3.25. Peak parameters for the 1434.2-keV peak of ^{52}V and major activities in various reference materials using anticoincidence and conventional spectrometry.

Reference material (*IAEA, all others NIST)	R_{PA}	R_{anti}	R_{conv}	AFOM	Peak area ratio of vanadium with the matrices			
					Na / V	Cl / V	Al / V	Mn / V
Apple Leaves (SRM 1515)	2.43	4.64	0.28	17.2	0.65	5.97	87	8.3
Peach leaves (SRM 1547)	2.29	3.30	0.27	12.2	0.24	2.07	44.1	9.1
Non-Fat Milk Powder (SRM 1549)	0.55	0.11	0.08	0.31	1000	1827	95.5	4.38
Wheat Flour (SRM 1567a)	1.23	0.60	0.35	1.68	1.14	74.4	63.9	11.9
Rice Flour (SRM 1568a)	1.47	2.13	0.37	3.74	2.06	48.6	36.1	50.8
Spinach (SRM 1570)	1.86	1.08	0.22	4.81	42	15.7	55.3	5.9
Pine Needles (SRM 1575)	3.34	2.19	0.13	21.9	0.50	1.74	101	66.9
Bovine Liver (SRM 1577b)	1.22	1.16	0.38	1.97	39.4	62.8	13.4	4.02
Whole Egg Powder (RM 8415)	1.97	1.27	0.23	5.70	21	25	87	4.2
Wheat Gluten (RM 8418)	1.07	0.34	0.11	1.26	42	89	19.4	13.3
Corn Starch (RM 8432)	1.77	2.75	0.67	5.58	106	32	50	2.6
Corn Bran (RM 8433)					255	0.12	21.3	19.1
Durum Wheat Flour (RM 8436)	1.73	0.44	0.12	3.43	5.88	133	115	48
Hard Wheat Flour (RM 8437)	1.87	1.72	0.32	5.59	2.90	66.2	16.3	9.53
Soft Wheat Flour (RM 8438)	1.30	2.70	0.52	3.15	1.16	52.6	10.2	6.76
Animal Blood (RM A-13)*	0.78	0.17	0.092	0.63	851	707	7.45	1.84

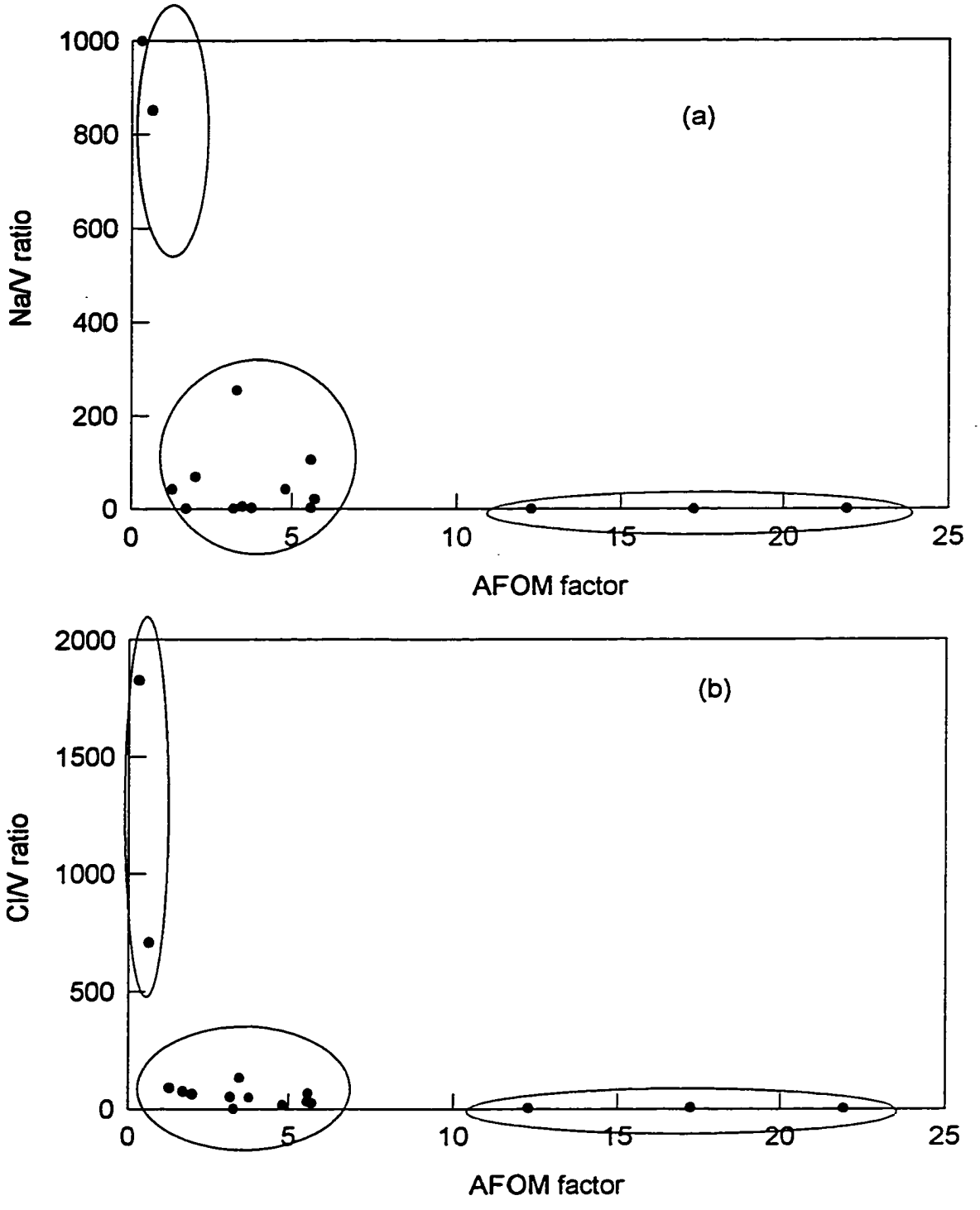

Fig. 3.28. Scatter plot of the 16 SRMs and RMs: (a) AFOM factor vs. Na/V ratios and (b) AFOM factor vs. Cl/V ratios.

3.28(a) and Fig. 3.28(b), the AFOM terms of V for these samples are dramatically reduced to less than 1 when the Cl/V and Na/V ratios increased to as high as 1000. Thus the improvement for V by anticoincidence counting is limited by Na/V and Cl/V ratios. The background counts from the Compton edge events of the 1642.7-keV peak of ^{38}Cl and the tail of the 1368.6-keV peak of ^{24}Na are less efficiently removed by the NaI(Tl) annulus. This behaviour might be related to the angular distribution of back-scattered gamma-rays that can be detected by the NaI(Tl) annulus of cylindrical geometry.

The variations of Al/V and Mn/V ratios as a function of AFOM are shown in Fig. 3.29(a) and Fig. 3.29(b), respectively. No particular trend is evident in either of these plots. One of the reasons for this observation could be the greater contribution of the tail of ^{24}Na and front edge of ^{38}Cl compared to the Compton edge of ^{28}Al and ^{56}Mn to the overall Compton edge on which the 1434.2-keV peak of ^{52}V is located. The improvement in V determination by anticoincidence counting is mainly dependent on the Cl and Na content of the sample.

The application of anticoincidence spectrometry can reduce the Compton background under the 1434.2-keV peak of ^{52}V, improve the peak statistical accuracy and lower the detection limit, if Cl and Na levels are not too high. These improvements can be demonstrated using Peach Leaves (NIST SRM 1547) which have low levels of Cl and Na, moderate level of Mn, and high level of Al, and Wheat Flour (NIST SRM 1567a) which has low levels of all of these four

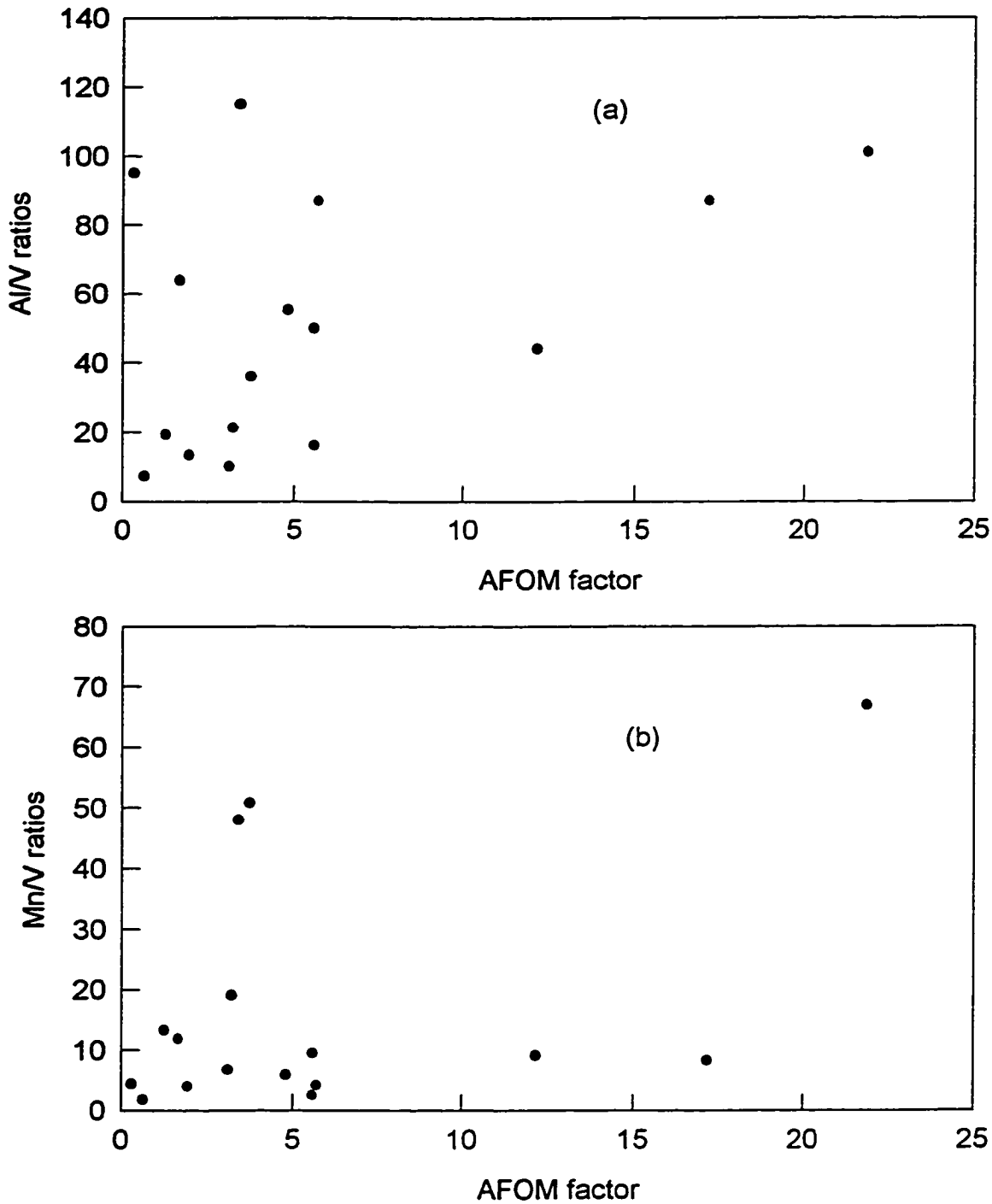

Fig. 3.29. The scatter plot of the 16 SRMs and RMs: (a) AFOM factor *vs.* Al/V ratios, and (b) AFOM factor *vs.* Mn/V ratios.

elements (Table 3.7).

The partial gamma-ray spectra of Peach Leaves and Wheat Flour SRMs using both conventional and anticoincidence counting modes are presented in Fig. 3.30. For Peach Leaves, the background around the 1434.2-keV peak of ^{52}V was reduced by a factor of about 10 in the anticoincidence counting mode. Compared to conventional counting, a better-shaped 1434.2-keV peak was detected (Fig. 3.30(a)), its peak area statistical accuracy was improved by a factor of 2.3, and it had a high AFOM of 12.2 in anticoincidence counting.

In the case of Wheat Flour, the 1434.2-keV peak was hardly distinguishable from the background in the conventional counting mode as shown in Fig. 3.30(b). The background in the anticoincidence spectrum was reduced by a factor of at least 10, leading to the detection of this peak. Analytically speaking, it is considered a great improvement. However, the AFOM value is only 1.68. The reason for this low value is that anticoincidence counting is only a technique for background suppression, and it cannot be used to increase the net peak area counts. The 1434.2-keV peak of Wheat Flour in anticoincidence counting still did not have enough net peak area counts to give a satisfactory peak statistical accuracy; consequently, R_{PA} improved only by a factor of 1.23.

In order to investigate the extent of improvement that can possibly be obtained by anticoincidence counting, 16 biological RMs and SRMs were analyzed for V by INAA. Between 200 and 700 mg of these materials, depending on the levels of major and interfering elements present, were weighed into

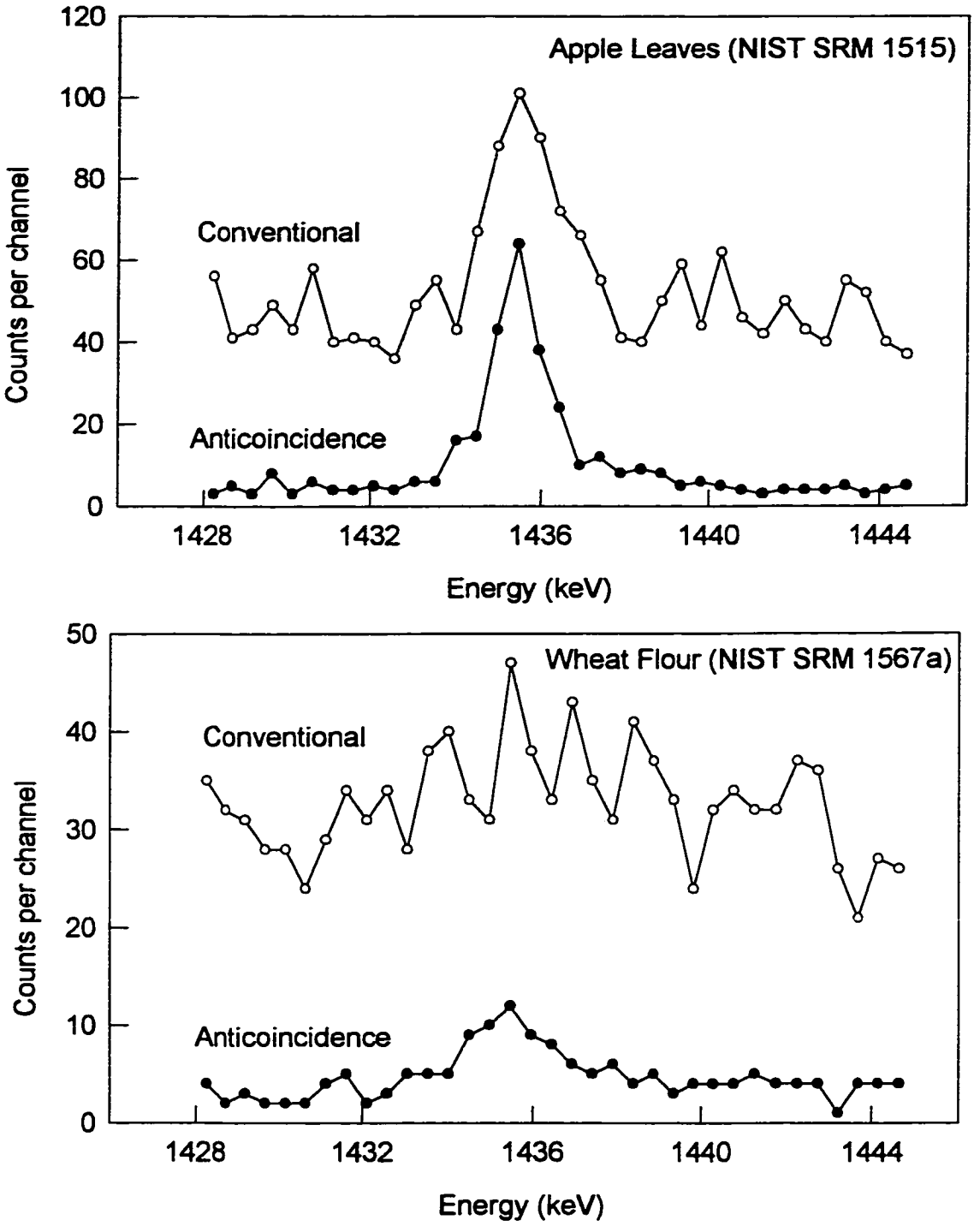

Fig. 3.30. Gamma-ray spectra near the 1434.2 keV peak of ^{52}V using conventional and anticoincidence spectrometry.

precleaned polyethylene irradiation vials. These materials were irradiated at a neutron flux of 5×10^{11} cm^{-2} s^{-1} for 1 min, allowed to decay for 1 min, and the 1434.2-keV gamma-ray of ^{52}V counted for 10 min. The sensitivity for V standard solutions under these conditions was 5025 counts/μg in the anticoincidence counting mode.

Since V can be determined with very high sensitivity by NAA, a trace amount of contamination can also yield detectable counts of ^{52}V. Precautions were taken in this study to minimize reagent blanks. For example, all polyethylene irradiation vials were thoroughly cleaned by soaking them in 4M NHO_3 for 24 h and rinsing them with DDW. These cleaned empty vials were subjected to the same experimental conditions, and no V was detected.

The 16 RMs and SRMs were analyzed in triplicate and their V concentrations are presented in Table 3.26 along with the certified values. Only 7 of the 16 materials have certified values. Values measured in this work agree well with the certified values, wherever such comparisons can be made.

The precision of measurement can be improved by improving the statistical accuracy of net peak area (R_{PA}) of the 1434.2-keV peak using anticoincidence counting. The R_{PA} values for NIST SRM Apple Leaves, Peach Leaves, and Pine Needles ranged between 2.29 and 3.34 (Table 3.25); the RSD of the V content of these three materials is less than 6% as shown in Table 3.26. On the other hand, the RSD varied between 23 and 28% for Non-Fat Milk Powder, Wheat Gluten, and Animal Blood for which R_{PA} varied from 0.55 to 1.07.

Table 3.26. Vanadium content and detection limits of reference materials by anticoincidence gamma-ray spectrometry.

Reference materials (*IAEA, all other NIST)	This work (ppb)	Certified, (information) value (ppb)	Detection limits (ppb) anti.	conv.
Corn Starch (RM 8432)	1.4 ± 0.3		0.61	1.9
Corn Bran (RM 8433)	6.5 ± 1.5	5 ± 2	0.91	3.0
Wheat Flour (SRM 1567a)	9.0 ± 2.9	(11)	1.8	8.6
Rice Flour (SRM 1568a)	9.6 ± 1.2	(7)	1.0	2.7
Non-Fat Milk Powder (SRM 1549)	14.1 ± 5.3		9.4	16
Animal Blood (RM A-8)*	15 ± 6		14	37
Hard Wheat Flour (RM 8437)	18.3 ± 1.3	20 ± 10	1.1	3.2
Durum Wheat Flour (RM 8436)	21.6 ± 0.9	21 ± 6	1.5	6.9
Wheat Gluten (RM 8418)	21.8 ± 4.5	(40)	4.1	7.7
Soft Wheat Flour (RM 8438)	31.0 ± 0.4	(30)	1.1	3.1
Bovine Liver (SRM 1577b)	99.3 ± 7.6	(123)	6.6	14
Apple Leaves (SRM 1515)	257 ± 13	(260 ± 31)	9.0	37
Pine Needle (SRM 1575)	330 ± 22	400 ± 50	18	74
Peach leaves (SRM 1547)	355 ± 17	370 ± 30	13	34
Whole Egg Powder (RM 8415)	449 ± 54	459 ± 81	4.1	9.8
Spinach (SRM 1570)	1058 ± 178	1180 ± 110	35	79

The detection limits of V in both counting modes are also reported in Table 3.26. For low-V containing RMs, such as Corn Starch, Corn Bran, Wheat Flour, Rice Flour, Not-Fat Milk Powder, and Animal Blood, the V levels are either very close to or higher than the detection limits calculated by the conventional counting mode. The application of anticoincidence spectrometry improves the detection limits by 2 to 4 times so that the V levels could be reliably measured.

3.4.5 Determination of Iodine

Neutron activation analysis (NAA) has excellent intrinsic sensitivity for the measurement of iodine. Iodine has been determined by INAA in many biological materials. Compared to some other medium-lived nuclides such as ^{52}V, ^{27}Mg and ^{66}Cu, ^{128}I has a slightly longer half-life of 25.0 min (Table 3.15), and thus the stable isotope ^{127}I needs a longer irradiation time to reach saturation activity. However, the irradiation time is limited because of interferences from the high activities of thermal neutron activation products of the major elements in the sample. Low levels of iodine cannot be easily measured by thermal INAA.

In order to circumvent this problem, epithermal INAA (EINAA) has been used by a few researchers with some success [126-131]. The EINAA methods are based on the fact that the resonance integral cross section for iodine is much larger (147 b) than that for some of the interfering elements such as Na, Cl, Al, and Mn (0.31, 0.21, 0.17, 14 b, respectively). Background activities can be

reduced to some extent by EINAA. The use of cadmium and/or boron shields to absorb thermal neutrons in EINAA allows for increased irradiation time. But the residual activity produced in the cadmium shield, for example, may cause a radiation safety and heating problem. These factors can limit the irradiation time, the removal of the sample from the shield within a reasonably short time, and the reuse of the shield for subsequent irradiations. Much of this problem can be eliminated by irradiating samples in a cadmium- or boron-lined pneumatic site. Although a cadmium-lined site is available at the DUSR facility, not many reactors are fitted with this type of site. The EINAA detection limit for iodine can be as low as 200 ppb [131], depending on the neutron flux used. Detection limits can be further improved by increasing the sample mass, irradiating for a longer period, and by counting the samples in a more sensitive detector. However, the background in the region of the 443 keV photopeak of ^{128}I is often dominated by Compton scattering from the gamma-rays of ^{24}Na, ^{56}Mn, ^{82}Br, and ^{38}Cl, so the detection limits are often not that greatly improved.

Radiochemical NAA (RNAA) and preconcentration NAA (PNAA) methods have been used to eliminate interfering elements as well as to further suppress background and improve the sensitivity of measurement [132,133]. Both PNAA and RNAA are destructive methods, involve complicated operations, and are time consuming compared to INAA. Moreover, in PNAA precautions must be taken to ensure minimal contamination from reagents and handling.

Anticoincidence counting as a background suppression technique

can be used in conjunction with EINAA to further reduce background. This approach can have the advantage of simplicity; it can be less time consuming and free from reagent blanks, and lower the detection limit even further. For this reason, an EINAA method using anticoincidence counting has been developed in the present study for the determination of low levels of iodine. In this method, typically 200-700 mg of a sample were irradiated for 10 to 20 min, followed by 1 min decay and then counting for 30 min. The 442.9 keV gamma-ray of ^{128}I was used.

A sensitivity of 4536 counts per μg of iodine was obtained using 20 min irradiations. An internal quality assessment chart was constructed by irradiating iodine comparator standards with every batch of samples, and it is shown in Fig. 3.31. All results were found to be within $\pm 2\sigma$.

In order to evaluate the applicability of the EINAA method in conjunction with anticoincidence gamma-ray spectrometry to a wide variety of biological materials, 17 RMs containing various levels of iodine and background interfering elements were chosen (Table 3.27). Materials such as NIST Corn Bran, Corn Starch, Wheat Gluten, Soft Wheat Flour, Hard Wheat Flour, Durum Wheat Flour, Rice Flour, and Peach Leaves contained low levels of interfering elements such as Cl and Na, and gave low induced activities on neutron irradiation. They were irradiated for 20 min, allowed to decay for 1 min, and counted for 20 min.

Reference materials such as NIST Whole Egg Powder, Non-Fat Milk Powder, Bovine Liver, Spinach, and Pine Needles, and IAEA Horse Kidney, Animal

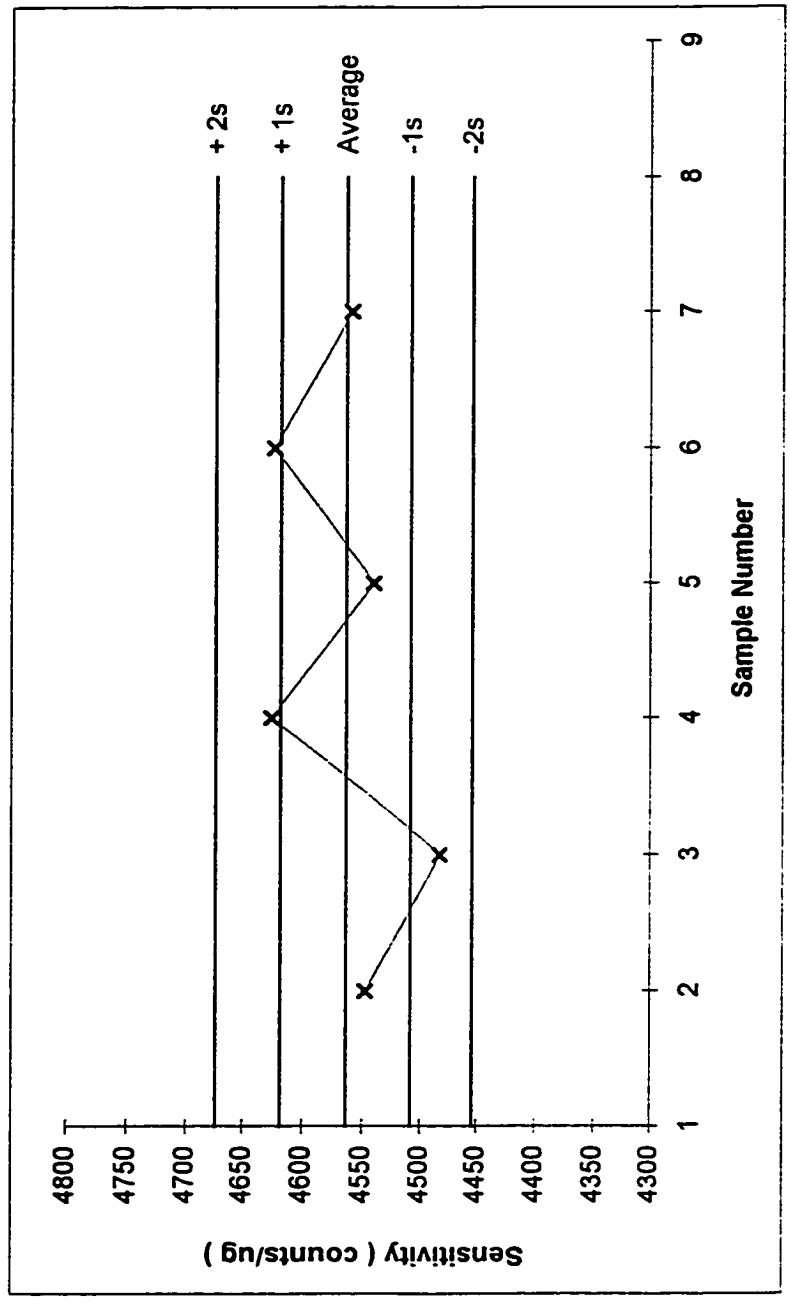

Fig. 3.31. Internal quality control chart for Iodine measurement (average is 4563 +/- 55).

Muscle and Animal Blood contained high levels of Cl and Na. These samples were originally irradiated for 20 min and allowed to decay for 1 min before counting. These conditions gave high activities and dead-time of greater than 10% which could introduce errors unless appropriate corrections are made. The dead-time was reduced to about 5% to 8% employing 10-min irradiations and 1-min decays which were then routinely used for measuring iodine in the above materials.

A reduction in the irradiation time or an increase in the decay time can lower the dead-time. However, the former is better in this case because the nuclides contributing to the background activity have longer half-lives than ^{128}I, and do not decay substantially during the counting time. Thus the dead-time remains almost constant throughout the counting period. For example, for a decay time of 30 min, the dead-time could be only be reduced by 2% from its original value while the sensitivity of ^{128}I would be reduced by more than 50%. Therefore, the sample should be counted as soon as possible after the irradiation. For these reasons, an irradiation time of 10 min and a decay time of 1 min were selected for materials with high background activity.

Even then, the dead time was close to 8% for some materials such as NIST Whole Egg Powder, Non-Fat Milk Powder, and IAEA Horse Kidney and Animal Blood. In these cases, an average dead-time correction treatment was done using the following equation [3]:

$$\frac{C'}{C} = \frac{[1-\exp(-\lambda CT)]\times LT}{[1-\exp(-\lambda LT)]\times CT} \qquad [3.25]$$

Where: C' = observed counts, C = true counts, CT = clock time, LT = live time. If the sample and standards differ considerably in their dead-times, it can introduce systematic errors due to different pulse losses. The above correction method was also used for the comparator standards, where applicable.

The SRMs and RMs used in this work cover a wide range of iodine concentrations as shown in Table 3.27. Precision of the EINAA-anticoincidence method was checked by triplicate analysis. It was found that the RSD was about ±5% above 200 ppb, increasing to ±10% at 20 ppb and then to >±30% at about 5 ppb iodine level. The results are summarized in Table 3.27 along with the certified values and current literature data. The analytical uncertainty reported with each value is $\pm 1\sigma$.

Among the 17 RMs analyzed here, only 6 have certified iodine values. The results obtained in this work for four of these materials are in good agreement with the certified values. Values for the other two, namely NIST Whole Egg Powder and Non-Fat Milk Powder, agree better with the literature values than with the certified values. The iodine levels of NIST Hard Wheat Flour, Durum Wheat Flour, Corn Bran, Wheat Gluten, Spinach, Whole Egg Powder, and Non-Fat Milk Powder were earlier measured by a PNAA method [132], and generally agree well with the values obtained in this work. Three of these materials were also analyzed by RNAA [133]. The certified iodine content of NIST Pine Needles agrees with the

Table 3.27. Concentration of iodine measured in reference materials by EINAA and anticoincidence gamma-ray spectrometry.

Reference materials	This work, ppb	Certified, (info.), ppb	Literature values, ppb [Ref]
Hard Wheat Flour (NIST RM 8437)	3.0 ± 1.5	----	4.2 ± 0.3 [132]
Durum Wheat Flour (NIST RM 8436)	5.7 ± 1.7	6 ± 4	5.9 ± 2.1 [132]
Corn Starch (NIST RM 8432)	6.0 ± 1.4	----	
Rice Flour (NIST SRM 1568a)	15 ± 4	(9)	
Animal Muscle (IAEA RM H-4)	15.4 ± 9	14.3 ± 1.7	17 ± 2 [132]
Soft Wheat Flour (NIST RM 8438)	18 ± 2	----	
Corn Bran (NIST RM 8433)	28 ± 3	26 ± 6	26.5 ± 2 [132] 26 ± 1.4 [127]
Wheat Gluten (NIST RM 8418)	61 ± 7	60 ± 13	62 ± 4 [132] 59 ± 3 [127]
Animal Blood (IAEA RM A-13)	82 ± 9	----	
Horse Kidney (IAEA RM H-8)	142 ± 7.4	----	
Pine Needles (NIST SRM 1575)	168 ± 13	----	140 ± 20 [126] 145 [128]
Bovine Liver (NIST SRM 1577b)	180 ± 8	(180)	187 ± 12 [132]
Peach Leaves (NIST SRM 1547)	300 ± 14	(300)	
Spinach (NIST SRM 1570)	775 ± 21	----	1160 ± 40 [132]
Spinach (NIST SRM 1570a)	1265 ± 75	----	
Whole Egg Powder (NIST RM 8415)	1820 ± 40	1970 ± 460	1875 ± 94 [132] 2040 ± 20 [127]
Non-Fat Milk Powder (NIST SRM 1549)	3110 ± 30	3380 ± 20	3150 ± 75 [132]

values obtained here by EINAA but without Compton suppression. There are no data available for the other materials. A comparison of the measured *vs.* literature and/or certified values reveals that the EINAA method in conjunction with anticoincidence counting can produce reliable values.

The PERF of the 442.9-keV peak of ^{128}I is 0.92 ± 0.04 using the anticoincidence counting mode, as given in Table 3.16. This means that background suppression should provide a lower detection limit. In order to illustrate this point, three NIST SRMs were selected. One of them (Non-Fat Milk Powder) had a high iodine level and a high background, the second SRM (Bovine Liver) had a low iodine content but a high background, and the third SRM (Rice Flour) had both low iodine level and low background. These three materials were analyzed for iodine using both conventional and anticoincidence counting modes. The partial gamma-ray spectra of Bovine Liver is shown in Fig. 3.32. It is evident that EINAA coupled to anticoincidence counting gave the best peak shape and lowest background activity.

Various limits of detection, as defined by Currie [134], were calculated using the following equations:

$$L_C=\mu_1(2\times\mu_B)^{\frac{1}{2}} \qquad [3.26]$$

$$L_D=\mu_1{}^2+2L_c \qquad [3.27]$$

$$L_Q=50[1+(1+0.08\times\mu_B)]^{\frac{1}{2}} \qquad [3.28]$$

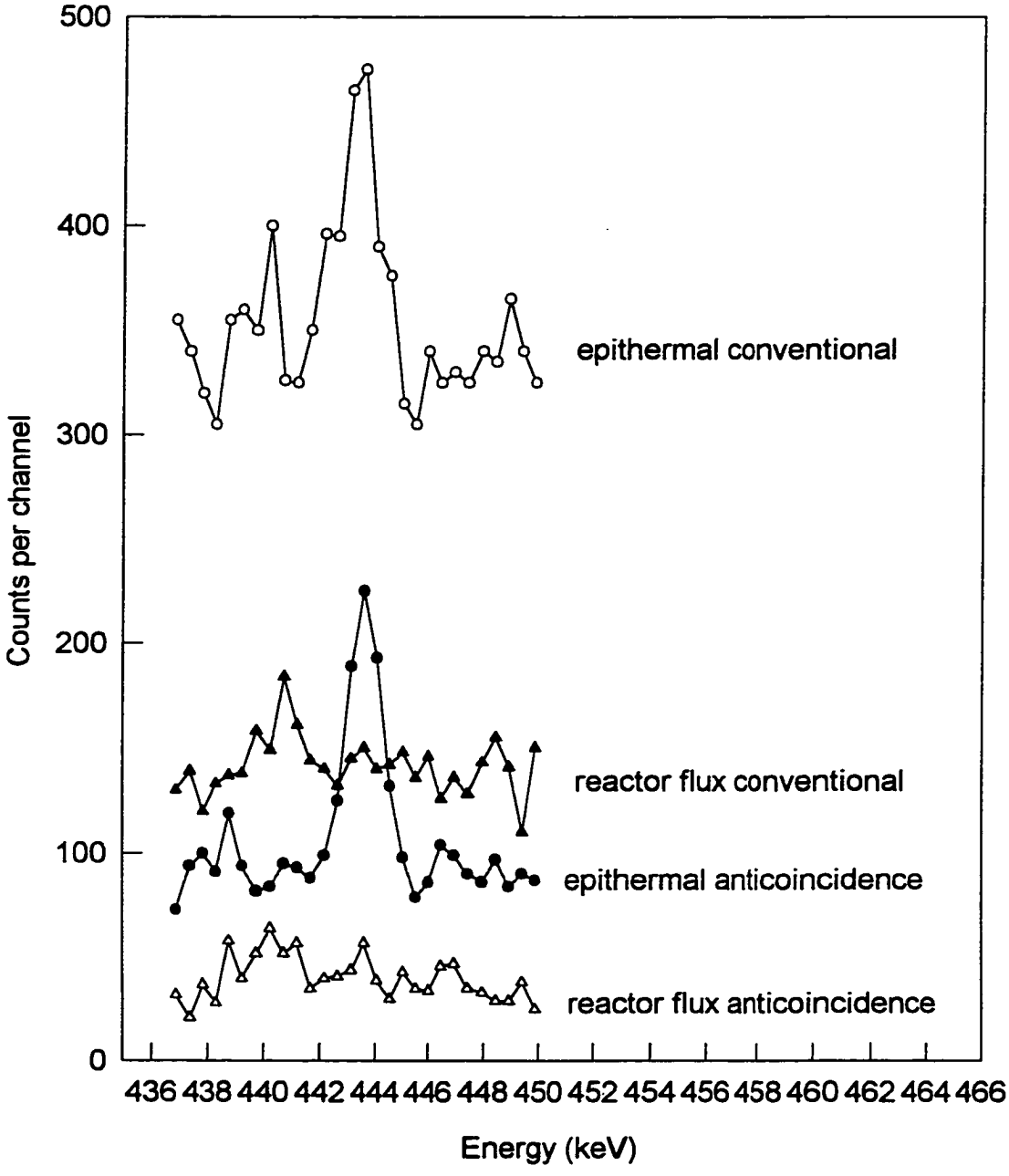

Fig. 3.32. Gamma-ray spectra near 442.9 keV peak of ^{128}I in Bovine Liver (NIST SRM 1577b) by epithermal and reactor flux neutrons in conjunction with conventional and anticoincidence spectrometry.

These limits are: (i) L_c - the critical level of detection and represents the average minimum significant counts; (ii) L_D - the qualitative detection limit (*i.e.* minimum detectable concentration) and it is used to assess the *a priori* detectability; and (iii) L_Q - the quantitative determination limit which means that a measurement can be done at a desired RSD, *e.g.* 10%. μ_B is the background under the peaks. At 95% confidence level, μ_1 equals to 1.645.

The values of L_c, L_D, and L_Q for iodine in the three SRMs are given in Table 3.28. It is evident that the detection limits for iodine in all cases have been lowered by anticoincidence counting. Although Non-Fat Milk Powder had high background activities due to ^{38}Cl, ^{56}Mn and ^{24}Na, its iodine content of about 3100 ppb (Table 3.27) was greater than L_Q by both conventional and anticoincidence spectrometry. The iodine content of about 180 ppb in Bovine Liver (Table 3.27) was greater than the L_Q of 170 ppb by anticoincidence counting. The 442.9-keV peak of ^{128}I in Rice Flour was undetectable using the conventional system but became detectable in the anticoincidence system as the L_c was lowered (Table 3.28).

Table 3.28. Comparison of detection limits (ppb) for iodine in three SRMs using Conventional and Anticoincidence counting systems.

Detection limits	Counting mode	Non-Fat Milk Powder (NIST SRM 1549)	Bovine Liver (NIST SRM 1577b)	Rice Flour (NIST SRM 1568a)
L_c	conv.	1.1×10^2	6.8×10^1	3.5×10^1
	anti.	6.7×10^1	3.0×10^1	1.0×10^1
L_D	conv.	2.1×10^2	1.4×10^2	7.2×10^1
	anti.	1.3×10^2	6.2×10^1	2.1×10^1
L_Q	conv.	6.7×10^2	4.4×10^2	2.4×10^2
	anti.	4.3×10^2	1.7×10^2	8.2×10^1

3.5 Anticoincidence Counting of Long-lived Nuclides

3.5.1 Analytical Potential of Long-lived Nuclides

The anticoincidence counting technique has been applied to long-lived nuclides in INAA. Its application to radioanalytical chemistry problems has been discussed by Cooper [135]. A survey of 85 nuclides with half-lives greater than 2.5 min and produced by neutron activation has been done by the same author who showed that approximately 65% of them had improved sensitivities by anticoincidence counting [135], but no details of PERF of each nuclide and gamma-ray were given.

The nuclear data [107-109] for long-lived nuclides of interest in this thesis are given in Table 3.29. Standards of these elements were irradiated at the DUSR facility at a flux of 5×10^{11} n cm^{-2} s^{-1} for 7 h, allowed to decay for 27 h, and then counted for 20 min using both anticoincidence and conventional gamma-ray spectrometry. The average of three measurements of sensitivities and PERF of these nuclides are presented in Table 3.30.

The full-energy peaks of nuclides such as ^{140}La and ^{82}Br were reduced significantly in anticoincidence counting, because they emit several coincident gamma-rays in cascade. In general, the anticoincidence technique will not improve their measurements, because the detection limit depends on the first power of the peak efficiency and on the inverse square root of background under the peak. Therefore, if the peak efficiency is reduced by 10, the background

Table 3.29. Nuclear data for long-lived nuclides studied by anticoincidence spectrometry.

Elements	Isotope (% abund.)	Cross section, b	Nuclides	Half-life	γ-ray energy keV(% pop.)
As	^{75}As (100)	4.3 ± 1	^{76}As	1.08 d	559.1 (45)
					657.0 (6.2)
					1216.2 (3.42)
Au	^{197}Au (100)	98.8 ± 0.3	^{198}Au	2.70 d	411.8 (95.6)
Br	^{81}Br (49.3)	2.69 ± 0.09	^{82}Br	35.3 h	554.3 (70.8)
					776.5 (83.5)
Ce	^{140}Ce (88.5)	0.57 ± 0.04	^{141}Ce	32.5 d	145.4 (48.2)
Cr	^{50}Cr (4.35)	15.9 ± 0.2	^{51}Cr	27.7 d	320.1 (10.1)
Co	^{59}Co (100)	17 ± 2	^{60}Co	5.27 a	1173.5 (99.9)
					1332.5 (100)
Fe	^{58}Fe (0.31)	1.15 ± 0.02	^{59}Fe	44.5 d	1099.3 (56.5)
					1291.6 (43.2)
Hg	^{196}Hg (0.15)	3080 ± 200	^{197}Hg	64.1 h	191.4 (0.63)
	^{202}Hg (29.7)	4.9 ± 0.1	^{203}Hg	46.6 d	279.2 (33.5)
K	^{41}K (6.7)	1.46 ± 0.03	^{42}K	12.4 h	1524.7 (18.1)
La	^{139}La (99.9)	9.0 ± 0.3	^{140}La	40.2 h	328.8 (20)
					487.0 (45)
					1596.2 (95)
Nd	^{146}Nd (17.2)	1.3 ± 0.1	^{147}Nd	11.0 d	91.1 (20)
					319.4 (1.95)
					531.0 (13.1)
Rb	^{85}Rb (72.2)	0.46 ± 0.02	^{86}Rb	18.6 d	1076.8 (8.64)

Table 3.29 (*continued*)

Elements	Isotope (% abund.)	Cross section, b	Nuclides	Half-life	γ-ray energy keV(% pop.)
Sb	^{121}Sb (57.3)	6.2 ± 0.2	^{122}Sb	2.72 d	564.1 (69)
					692.8 (3.8)
					1140.5 (0.7)
Sc	^{45}Sc (100)	16.9 ± 1	^{46}Sc	83.8 d	889.3 (100)
					1120.5 (100)
Ta	^{181}Ta (100)	21.0 ± 0.7	^{182}Ta	114.4 d	67.7 (41.0)
					100.1 (14.1)
					1121.3 (34.9)
					1221.4 (27.0)
Tb	^{159}Tb (100)	25.5 ± 1.1	^{160}Tb	72.3 d	298.6 (25.5)
					879.3 (30.0)
					966.2 (25.2)
W	^{186}W (28.6)	37.8 ± 1.5	^{187}W	23.7 h	134.2 (8.9)
					479.5 (21.2)
					685.7 (27.6)
Yb	^{174}Yb (31.8)	19 ± 6	^{175}Yb	4.19 d	282.5 (3.0)
					396.3 (3.4)
Zn	^{68}Zn (18.6)	0.072±0.004	^{69m}Zn	13.8 h	438.6 (94.8)
	^{64}Zn (48.9)	0.78 ± 0.02	^{65}Zn	244.3 d	1115.5 (50.6)

Table 3.30. Sensitivities and peak efficiency reduction factors for long-lived nuclides using anticoincidence spectrometry (t_i = 7 h, t_d = 27 h, t_c = 20 min).

Nuclide	γ-ray energy keV (% pop.)	Sensitivity counts/μg ± 1σ	Peak efficiency reduction factor ± 1σ
^{76}As	559.1 (45)	(2.82 ± 0.06) × 10^4	0.83 ± 0.02
	657.0 (6.2)	880 ± 30	0.24 ± 0.03
	1216.2 (3.42)	(1.15 ± 0.07) × 10^3	0.91 ± 0.04
^{198}Au	411.8 (95.6)	(3.56 ± 0.05) × 10^6	0.99 ± 0.03
^{82}Br	554.3 (70.8)	730 ± 16	0.04 ± 0.01
	776.5 (83.5)	520 ± 24	0.04 ± 0.02
^{141}Ce	145.4 (48.2)	340 ± 19	1.01 ± 0.01
^{51}Cr	320.1 (10.1)	146 ± 9	0.99 ± 0.04
^{60}Co	1173.5 (99.9)	103 ± 6	0.27 ± 0.01
	1332.5 (100)	84 ± 6	0.25 ± 0.01
^{59}Fe	1099.3 (56.5)	1.34 ± 0.07	0.94 ± 0.02
	1291.6 (43.2)	1.08 ± 0.05	0.97 ± 0.03
^{197}Hg	191.4 (0.63)	62 ± 3	0.34 ± 0.02
^{203}Hg	279.2 (33.5)	343 ± 9	1.01 ± 0.03
^{42}K	1524.7 (18.1)	92 ± 6	1.00 ± 0.04
^{140}La	328.8 (20)	770 ± 13	0.05 ± 0.02
	487.0 (45)	(3.33 ± 0.05) × 10^3	0.14 ± 0.01
	1596.2 (95)	(3.59 ± 0.02) × 10^3	0.21 ± 0.01
^{147}Nd	91.1 (20)	245 ± 18	0.99 ± 0.02
	319.4 (1.95)	2.67 ± 0.07	0.25 ± 0.01
	531.0 (13.1)	36.7 ± 1.9	0.94 ± 0.06
^{86}Rb	1076.8 (8.64)	39.3 ± 0.6	0.99 ± 0.03

Table 3.30. (*continued*)

Nuclides	γ-ray energy keV (% pop.)	Sensitivity counts/μg ± 1σ	Peak efficiency reduction factor ± 1σ
^{122}Sb	564.1 (69)	(3.04 ± 0.01) × 10^4	0.92 ± 0.02
	692.8 (3.8)	370 ± 11	0.26 ± 0.01
	1140.5 (0.7)	500 ± 16	1.05 ± 0.04
^{46}Sc	889.3 (100)	2330 ± 79	0.26 ± 0.01
	1120.5 (100)	1790 ± 67	0.23 ± 0.01
^{182}Ta	67.7 (41.0)	368 ± 12	1.09 ± 0.03
	100.1 (14.1)	115 ± 9	0.85 ± 0.02
	1121.3 (34.9)	127 ± 11	0.24 ± 0.02
	1221.4 (27.0)	66.7 ± 23	0.18 ± 0.01
^{160}Tb	298.6 (25.5)	651 ± 31	0.20 ± 0.02
	879.3 (30.0)	574 ± 28	0.39 ± 0.01
	966.2 (25.2)	599 ± 16	0.52 ± 0.02
^{187}W	134.2 (8.9)	(6.78 ± 0.04) × 10^3	0.35 ± 0.01
	479.5 (21.2)	(1.54 ± 0.02) × 10^4	0.83 ± 0.03
	685.7 (27.6)	(2.07 ± 0.02) × 10^4	1.01 ± 0.04
^{175}Yb	282.5 (3.0)	(2.47 ± 0.03) × 10^3	0.53 ± 0.02
	396.3 (3.4)	(8.85 ± 0.05) × 10^3	1.04 ± 0.04
^{69m}Zn	438.6 (94.8)	217 ± 11	0.99 ± 0.03
^{65}Zn	1115.5 (50.6)	147 ± 9	0.99 ± 0.03

under the peak must be reduced by more than 100 before any improvement in detection limit can be obtained. However, when the sample activities are contributed mainly by the long-lived nuclides, the advantage of anticoincidence counting is that their Compton background could be reduced by an even greater amount, owing to their coincidence decay scheme.

The single energy peak efficiencies of nuclides such as ^{198}Au, ^{141}Ce, ^{51}Cr, ^{203}Hg, ^{42}K, ^{86}Rb, ^{69m}Zn, and ^{65}Zn did not suffer any reduction, so they can be advantageously detected using an anticoincidence system. It should be noted that the PERF for some of these nuclides depends on the individual peaks, because they are involved in cascading decay to different extents. For example, among the three gamma-rays at 134.2, 479.5 and 685.7 keV peaks of ^{187}W, the peak efficiency of only the 685.7 keV gamma-ray was not reduced. The other two suffered reductions to different extents. Thus, detailed investigations of each gamma-ray of a given nuclide must be done before using anticoincidence spectrometry in conjunction with NAA.

It is also interesting %w note (Table 3.29) that anticoincidence counting could give more reliable measurements of ^{76}As *via* the 559.1 keV peaks by suppressing the strongly interfering peak of 554.3 keV of ^{82}Br. Examinations of the decay schemes of ^{82}Br reveal that their gamma-rays are in cascading decay, and therefore an enhanced suppression of their peaks will occur in anticoincidence spectrometry. The net results are less interference and improved counting statistics for the 559.1 keV peak of ^{76}As. The determination of As by

anticoincidence counting is discussed below in detail (section 3.5.2).

The nuclides such as ^{60}Co and ^{46}Sc, which emit two coincident gamma-rays in cascade, are not likely to have an improved sensitivity because of large reduction in the peak efficiency in anticoincidence counting. However, because of their long half-lives, they can be measured with a relatively low background in a conventional system by increasing the decay and counting times. When applied to samples of much lower activities of ^{60}Co and ^{46}Sc, multidimensional and coincidence in window modes spectrometry will be more beneficial than conventional counting for sensitivity improvement. On the other hand, the 1120.5- keV peak of ^{46}Sc can be substantially suppressed using anticoincidence spectrometry, thereby greatly reducing the extent of interference to the 1115.5 keV peak of ^{65}Zn. The determination of Zn by anticoincidence counting is described below in detail (section 3.5.3).

Among the three peaks of ^{147}Nd (Table 3.30), the 91.1 keV peak is partially cascaded with the 319.4 keV peak; since the cut-off energy of the anticoincidence spectrometer was around 94 keV, no peak reduction was observed for the 91.1-keV peak, and no advantage could be gained for this peak. The 531.0-keV peak of ^{147}Nd does not cascade with other peaks; the PERF is close to 1. Although the 91.1-keV peak has higher sensitivity than the 531.0-keV peak, the Compton background under 91.1-keV peak cannot be reduced using anticoincidence counting. Therefore, both of these factors need to be considered when measuring Nd by anticoincidence spectrometry.

Among the four peaks of ^{182}Ta shown in Table 3.30, the 67.7 keV-peak is cascading 100% with the 1121.3 and 1221.4 keV peaks, and the 100.1-keV peak is partially cascading with the 1121.3 keV peak. Due to the 94-keV cut-off energy of our anticoincidence spectrometer, peaks at 67.7 and 100.1 keV were not suppressed as much as the two high-energy peaks; no background suppression was observed either.

The three peaks of ^{160}Tb have the same order of sensitivity and PERF in the anticoincidence system, but the two middle energy gamma-ray lines of ^{160}Tb are preferred to be used for anticoincidence counting, since the Compton background in the middle-energy region improvement is most apparent (section 3.1.1).

The long-lived nuclide ^{203}Hg shows good PERF by anticoincidence counting compared to its medium-lived nuclide of ^{197}Hg. The 279.2-keV peak of ^{203}Hg is not involved in a cascade. The efficiency of this peak can thus be maintained at 1. Therefore, when measuring Hg by anticoincidence spectrometry, ^{203}Hg should be a better nuclide than ^{197}Hg from the detection limit point of view.

The determinations of Fe and Rb in RMs by anticoincidence gamma-ray spectrometry are described in section 3.5.4.

3.5.2. Determination of Arsenic

Neutron activation analysis is a very sensitive technique for the

determination of As. The 559.1-keV gamma-ray of ^{76}As (half-life = 1.08 d) is most commonly used for As determination. Elemental comparator standards of As were irradiated for 7 h at a neutron flux of 5×10^{11} s^{-1} cm^{-2}, allowed to decay for 24 h, and counted for 8 h. A sensitivity of the order of 10^6 counts/μg of As was obtained; thus nanogram amounts of As in about 0.5 g of sample could be measured. However, in biological materials of complex chemical composition, the major elements such as Br, K, and Na can produce high activities resulting in inferior detection limits of As. At sub-ppm or ppb levels of As commonly found in biological samples, the 559.1-keV peak of ^{76}As (half-life = 25.9 h) is especially interfered with by the 554.3-keV peak of ^{82}Br (35.3 h) and 564.1-keV peak of ^{122}Sb (65.3 h). The modern HPGe detectors usually have good enough resolution for resolving these three peaks. However, when the Br content of the biological sample is high, the tailing of the 554.3-keV peak may mask the 559.1-keV peak of ^{76}As and make its measurement rather difficult, if not impossible. In general, under the experimental conditions described above, an INAA method can only be used to determine As down to a few ppm levels in biological materials.

Due to the longer half-life of ^{82}Br, the interference from the 554.3-keV peak cannot be eliminated by simply extending the decay period. In such cases, chemical separations, either before or after the irradiation, are necessary in order to separate As from the sample activity as well as to achieve the maximum sensitivity and accuracy for the determination of As [136,137]. However, once chemical operations are involved, the procedure can become laborious, time-

consuming, and sometimes more prone to errors and contamination.

The ^{76}As nuclide decays by β-emission and two major gamma-rays, namely 559.1 and 657.0 keV, which are not coincident. The major interference to the 559.1-keV gamma-ray generally comes from the coincident gamma-ray emitter ^{82}Br. Anticoincidence counting technique should be ideal in such a situation. The reduction of the 554.3-keV peak of ^{82}Br will have an effect similar to chemical separation; the detection limit of As can be improved by INAA in conjunction with anticoincidence counting. Some of these points have been discussed in the literature [81]. One of the objectives of the present work is to fully explore the advantages of anticoincidence counting for the determination of As in biological samples.

The concentrations of As in 16 RMs and SRMs were determined by irradiating them at a flux of 5×10^{11} cm^{-2} s^{-1} for 7 h, allowing to decay for about 50 h, and counting for 8 h. The counting geometry, *i.e.* the distance of sample from the detector surface, was adjusted by the level of sample activity so that the dead-time was <5%. This distance was generally 1 cm which was also the optimized position (section 3.1.2) for the best BSR. The As levels along with the certified values as well as the BSR values and detection limits for each material are presented in Table 3.31. Only 6 of the 16 materials analyzed have certified values and another 6 have information values. The measured values generally agree well with the available values where such comparisons can be made. Many of the materials have very high Br levels (Table 3.31), and could not be analyzed by INAA

using conventional gamma-ray spectrometry. It is obvious that BSR varied greatly (from 4 to 27), and depended on the individual material.

Since for some of materials, the 559.1-keV peak of ^{76}As was undetectable in conventional counting mode, the parameters R_{conv} and PA_{conv} of equation 3.15 cannot be calculated. Instead of the AFOM term, the BSR values can be used to describe the improvement of measurement by anticoincidence counting. In the case of As, BSR is defined as the ratio of background counts under the 559.1-keV peak of ^{76}As in conventional spectrum to the background counts in the same region of anticoincidence spectrum.

Under these experimental conditions, the background counts under the 559.1-keV peak of ^{76}As were mainly contributed with by the nuclides ^{82}Br, ^{122}Sb, ^{24}Na, and ^{42}K in these materials. The relationship between BSR and the major elements in the sample was studied through the peak area counts of 554.3-keV peak of ^{82}Br, 564.1-keV peak of ^{122}Sb, 1368.6-keV peak of ^{24}Na, and 1524.7-keV peak of ^{42}K. For each material, the BSR values and the interference peak intensities are summarized in the Table 3.32, and also graphically presented in Fig. 3.33 for easier comparison. The sample numbers in this figure correspond to those listed in Table 3.32; the BSR values for each material is shown on the top of each line. It is obvious from Fig. 3.33 that BSR is mainly dependent on the intensity of the 554.3-keV peak of ^{82}Br.

An positive relationship exists between BSR and the 554.3-keV peak intensities as shown in Fig. 3.34(a). The correlation coefficient for

Table 3.31. Concentrations and detection limits of arsenic as well as background suppression factor for arsenic in reference materials by anticoincidence gamma-ray spectrometry.

Reference material (*IAEA, all others NIST)	This work, ppb	Certified, (information) value, ppb	Bromine, ppb	Background suppression ratio	Det. limit for arsenic ppb
Soft Wheat Flour (RM 8438)	2.1 ± 0.8	----	----	6.7	0.35
Corn Starch (RM 8432)	2.45 ± 0.64	----	----	5	0.75
Non-Fat Milk Powder (SRM 1549)	2.6 ± 1.2	(1.9)	(12000)	13.4	1.9
Hard Wheat Flour (RM 8437)	2.7 ± 1.2	----	----	27	0.75
Corn Bran (RM 8433)	2.7 ± 1.4	2 ± 2	2300 ± 300	15	1.2
Wheat Flour (SRM 1567a)	5.4 ± 1.5	(6)	(6000)	14	0.57
Durum Wheat Flour (RM 8436)	9.0 ± 0.1	(30)	6600 ± 1100	6	0.81
Whole Egg Powder (RM 8415)	11.5 ± 1.8	(10)	----	16	7.3
Animal Blood (RM A-13)*	22 ± 15	----	22000 ± 11000	11	14
Wheat Gluten (RM 8418)	22.6 ± 0.9	(20)	(3600)	15	2.8
Apple Leaves (SRM 1515)	33.7 ± 3	38 ± 7	(1800)	4.5	4.1
Bovine Liver (SRM 1577b)	44.7 ± 12	(50)	(9700)	14.2	3.1
Peach leaves (SRM 1547)	66.8 ± 9.6	60 ± 18	(11000)	6.6	6.1
Spinach (SRM 1570)	177 ± 21	150 ± 50	(54000)	19	21
Rice Flour (SRM 1568a)	241 ± 29	290 ± 30	(8000)	17	0.61
Pine Needle (SRM 1575)	224 ± 16	210 ± 40	(9000)	4.1	3.3

Table 3.32. Background activities and SWA for ^{76}As.

Reference material (*IAEA, all others NIST)	Sample No.	554.3 keV, ^{82}Br, peak area counts x 10^5	564.1 keV, ^{122}Sb, peak area counts x 10^3	1367.8 keV, ^{24}Na, peak area counts x 10^5	1524.5 keV, ^{42}K, peak area counts x 10^4	SWA x 10^3
Corn Bran (RM 8433)	1	2.75	378	17.3	2.15	152
Durum Wheat Flour (RM 8436)	2	3.78	1.83	2.13	37.3	60
Wheat Gluten (RM 8418)	3	1.05	6.09	24.1	0.55	132
Whole Egg Powder (RM 8415)	4	0.92	1.72	35.9	2.52	190
Corn Starch (RM 8432)	5	0.086	4.61	11.9	0.48	61
Apple Leaves (SRM 1515)	6	0.26	4.22	0.39	2.07	6.7
Spinach (SRM 1570)	7	1.78	6.76	17.4	2.69	106
Soft Wheat Flour (RM 8438)	8	0.92	8.36	0.91	15.3	19.2
Hard Wheat Flour (RM 8437)	9	19.5	12.4	3.32	44.5	227
Animal Blood (RM A-13)*	10	0.82	3.60	9.43	0.086	55.7
Non-Fat Milk Powder (SRM 1549)	11	1.36	46.8	21.8	5.38	129
Pine Needle (SRM 1575)	12	1.08	26.5	0.89	7.01	20.1
Rice Flour (SRM 1568a)	13	9.59	4.38	3.13	73.8	134
Bovine Liver (SRM 1577b)	14	1.72	2.64	24.2	8.25	141
Peach leaves (SRM 1547)	15	2.74	59.3	1.60	186	97.1
Wheat Flour (SRM 1567a)	16	8.57	332	2.84	64.2	152

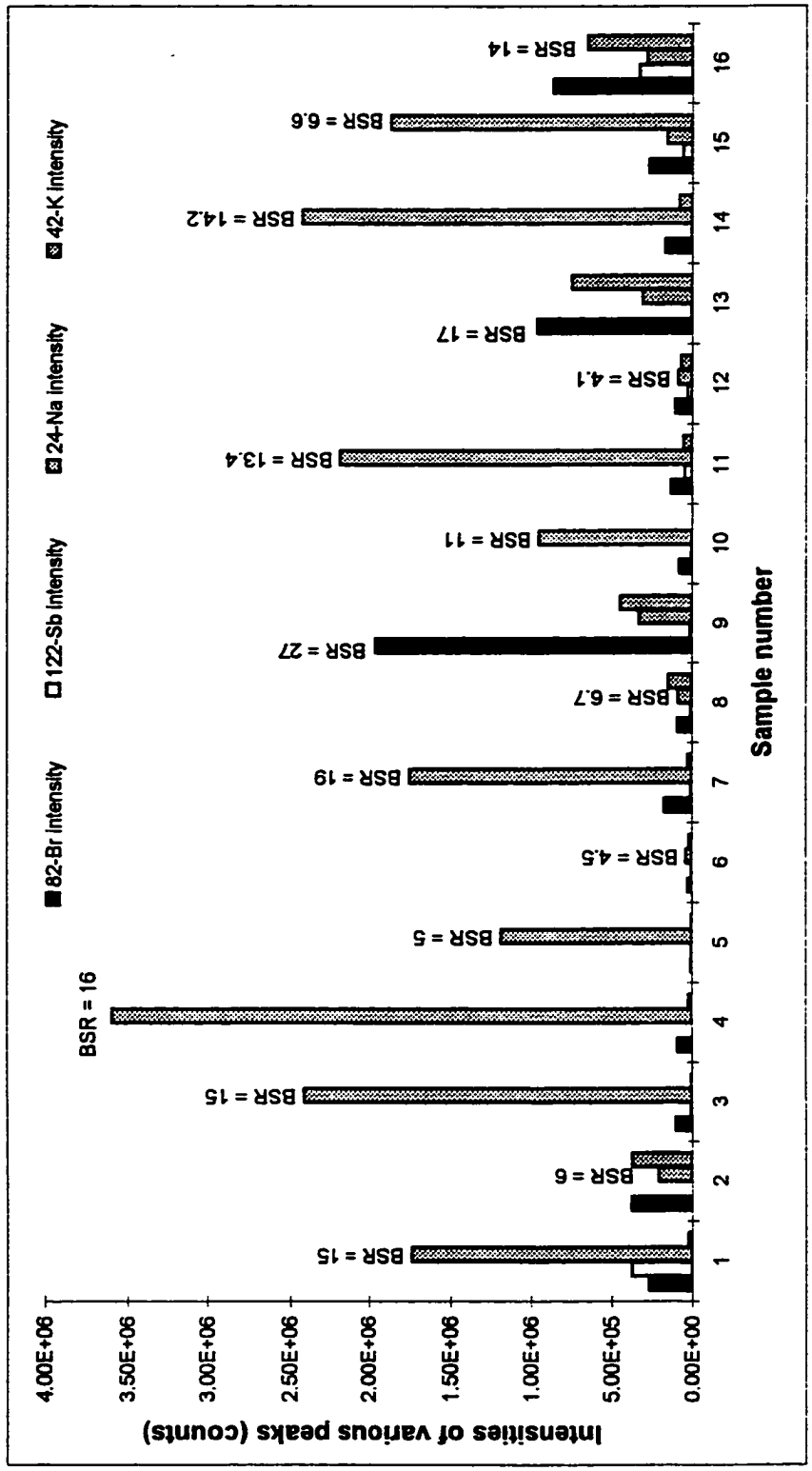

Fig. 3.33. The distribution of peak intensities for nuclides of interest, and background suppression ratios under the 559.1 keV peak of 76-As in 16 reference materials.

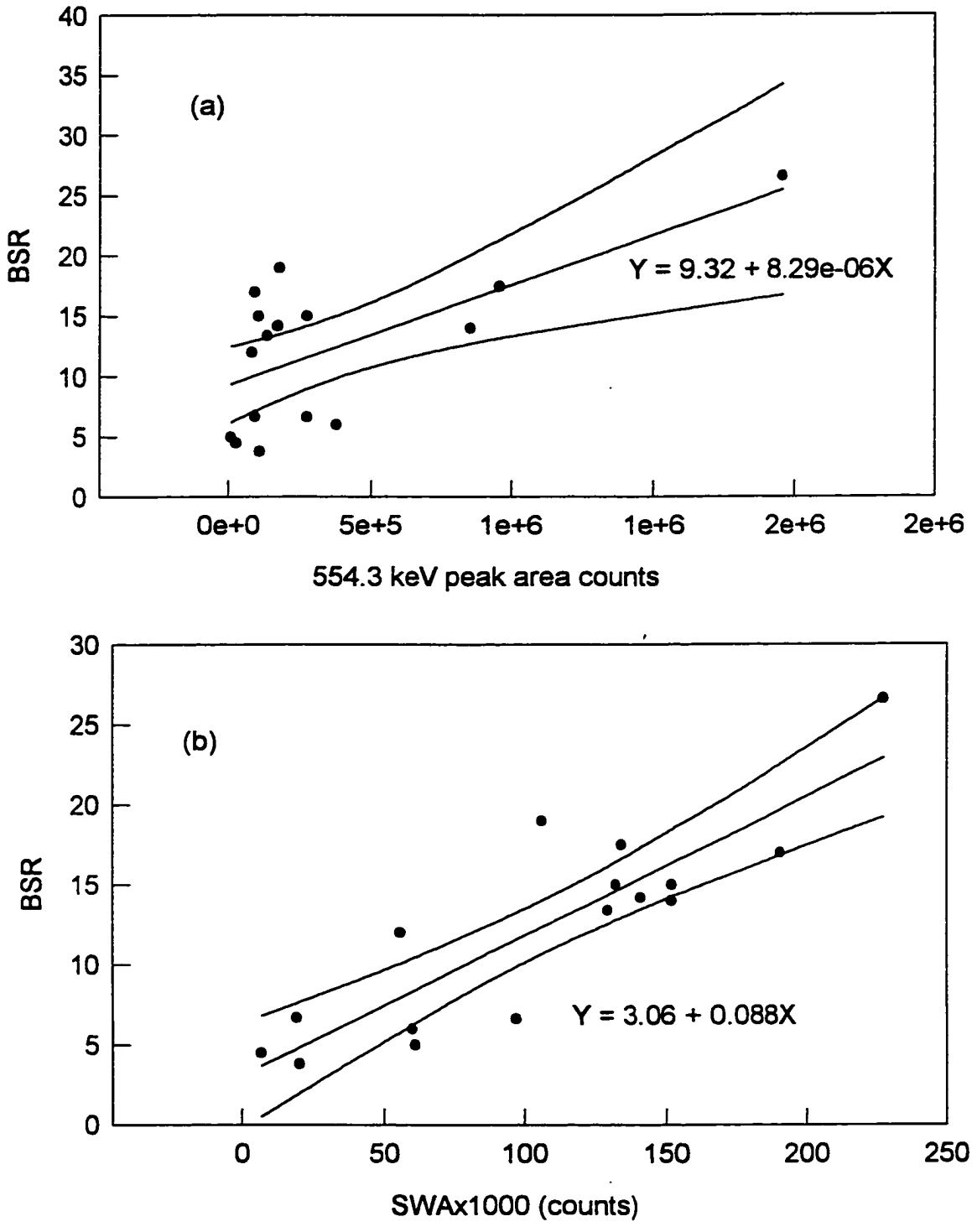

Fig. 3.34. Relationships between (a) background suppression ratios (BSR) and 554.3 keV peak area counts of ^{82}Br, and (b) BSR and sum of weighted activities (SWA).

data is 0.62. However, for several materials with low Br but high K and Na levels, the deviation from linearity is also quite apparent. This deviation suggests that the interferences from ^{122}Sb, ^{24}Na and ^{42}K have to be considered also. A term called sum of weighted activities (SWA) was calculated by the following equation:

$$SWA = P_{554.3} + P_{564.1} + (W_{1368.6} \times P_{1368.6}) + (W_{1524.7} \times P_{1524.7}) \qquad [3.29]$$

where P is peak area, and W is weighting factor for that peak. In order to estimate the values of $W_{1368.1}$ and $W_{1524.7}$, Na and K standard solutions were irradiated at a flux of 5×10^{11} cm^{-2} s^{-1} for 7 h, allowed to decay for about 50 h, and counted for 8 h in the conventional counting mode. A value of 0.5 for $W_{1368.1}$ was obtained by dividing the number of background counts around the 559.1-keV energy region of ^{76}As in the ^{24}Na gamma-ray spectrum by the peak area counts of the 1368.1-keV peak of ^{24}Na. Similarly, a value of 0.3 for $W_{1524.7}$ was obtained for the 1524.7-keV peak of ^{42}K.

The calculated SWA for each material is listed in Table 3.32. The BSR values under the 559-keV photopeak of ^{76}As is plotted as a function of the SWA values in Fig. 3.34(b). Obviously, a better linearity was obtained between the two terms after the inclusion of the contribution from the interfering activities of ^{122}Sb, ^{24}Na, and ^{42}K; a correlation coefficient of 0.89 was obtained.

The application of anticoincidence spectrometry can thus reduce the

554.3-keV peak of ^{82}Br, and can suppress the background under the 559.1-keV peak of ^{76}As. The partial gamma-ray spectra obtained using both conventional and anticoincidence counting modes and covering both photopeaks (540 to 575 keV) of four RMs are shown in Figs. 3.35 through 3.38. Among these materials, NIST Wheat Flour has the highest Br/As ratio of about 1110 (Table 3.31); a well-defined 559.1 keV are presented in Fig. 3.35. As shown in Table 3.31, the 554.3-keV peak intensities in these RMs are all fairly high (*i.e.* over one million counts). It is obvious from these spectra that the 559.1-keV peak of ^{76}As was hardly distinguishable from the background in the conventional counting mode. The background in the anticoincidence spectra was reduced by factors of 19 for Spinach, 6.7 for Soft Wheat Flour, 14 for Wheat Flour and 6.6 for Peach Leaves, as shown in Table 3.31, leading to the detection of the 559.1 keV peak.

The 564.1-keV peak of ^{122}Sb has a PERF of 0.92 (Table 3.30), meaning that there is no reduction in the peak. However, background can be reduced by Compton suppression. The net result is an enhanced 564.1-keV peak which can be used for the determination of low levels of Sb. Unfortunately, the irradiation vials contained detectable amounts of Sb. Reliable Sb results can only be obtained if the irradiated sample is placed in an inactive (fresh) vial prior to counting. No attempts were made in the present work to measure Sb levels in the RMs and SRMs analyzed.

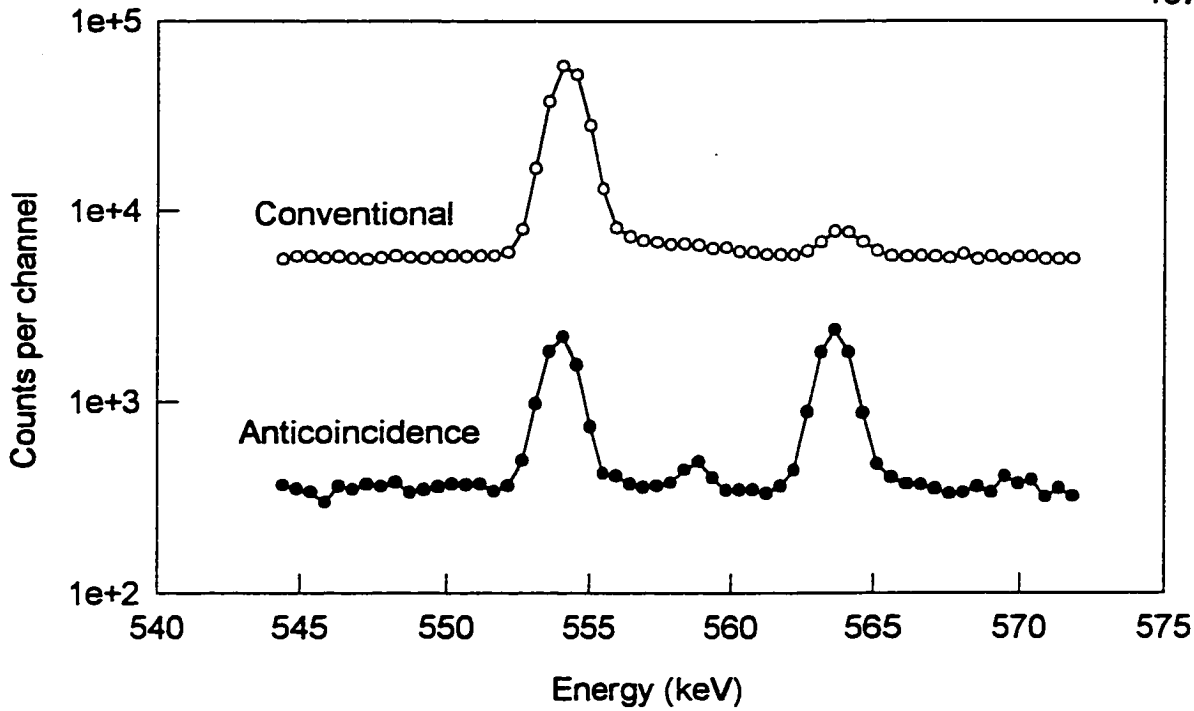

Fig. 3.35. Gamma-ray spectra near the 559.1 keV peak of ^{76}As in Wheat Flour (NIST SRM 1567a) by conventional and anticoincidence spectrometry.

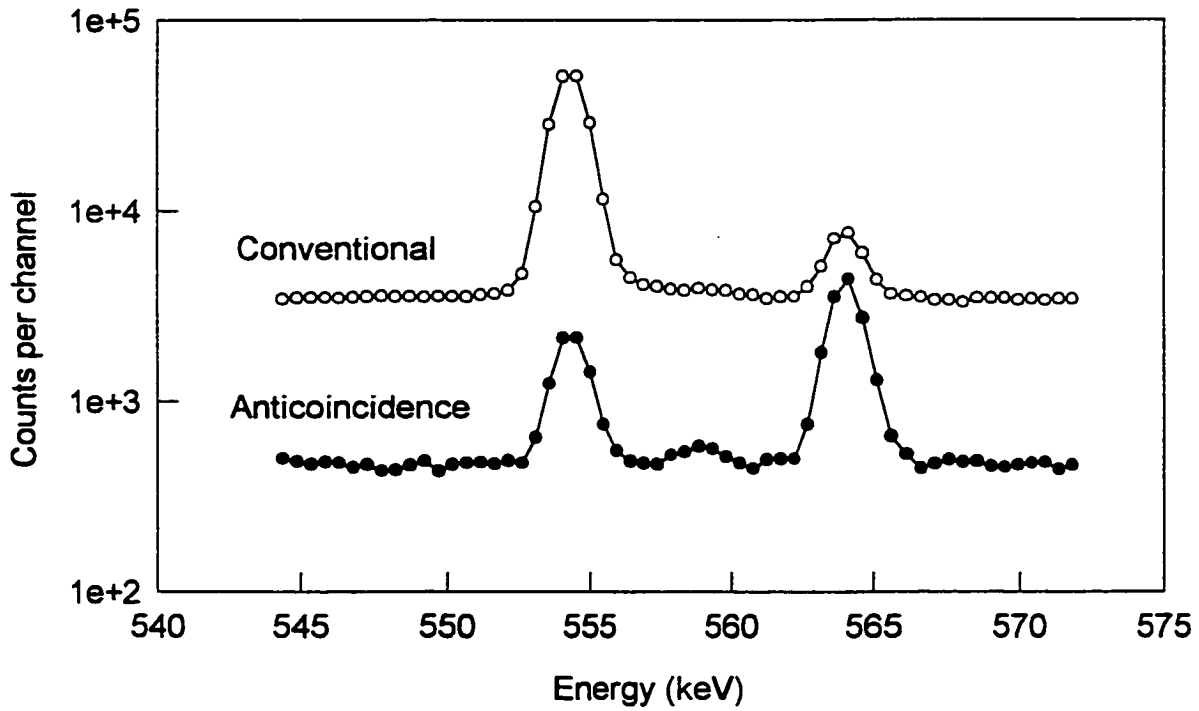

Fig. 3.36. Gamma-ray spectra near the 559.1 keV peak of ^{76}As in Peach Leaves (NIST SRM 1547) by conventional and anticoincidence spectrometry.

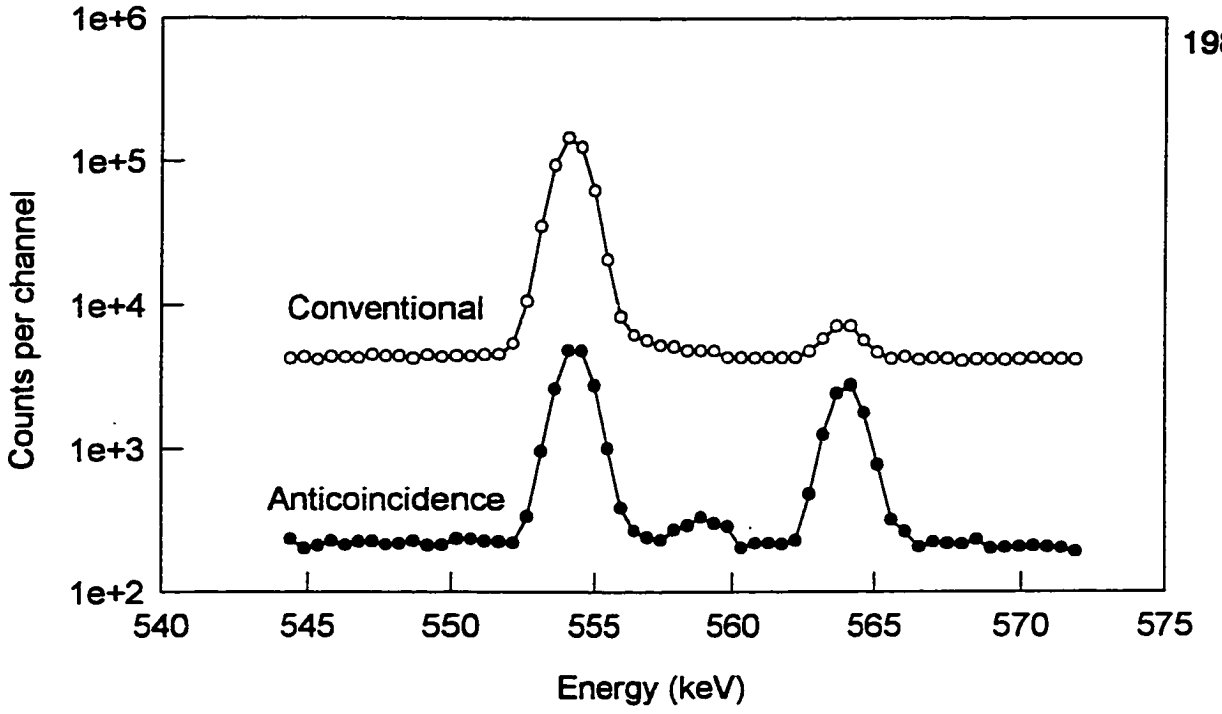

Fig. 3.37. Gamma-ray spectra near the 559.1 keV peak of ^{76}As in Spinach (NIST SRM 1570) by conventional and anticoincidence spectrometry.

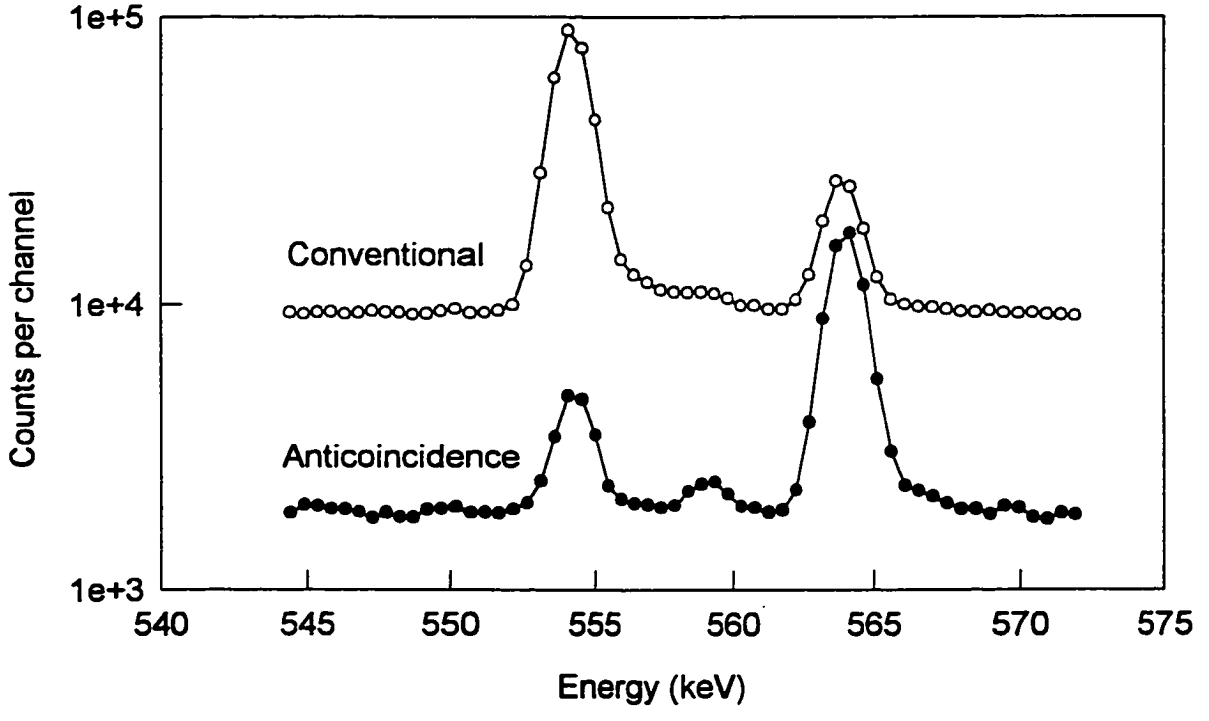

Fig. 3.38. Gamma-ray spectra near the 559.1 keV peak of ^{76}As in Soft Wheat Flour (NIST RM 8438) by conventional and anticoincidence spectrometry.

3.5.3. Determination of Zinc

Instrumental NAA has excellent sensitivity, precision, and accuracy for measuring Zn, and it has been widely used for this purpose [138]. There are two nuclides, namely ^{69m}Zn (half-life = 13.8 h) and ^{65}Zn (244.3 d), which could be used for Zn determination; the corresponding gamma-rays of 438.6 and 1115.5 keV are single gamma-rays, and the PERF values of both are 0.99 ± 0.03 (Table 3.30). Therefore, Zn in biological materials can be advantageously determined by INAA using anticoincidence counting.

If ^{69m}Zn is employed for the determination of Zn, the samples will have to be counted well within a decay time about 60 h due to its shorter half-life among the long-lived nuclides. Due to this relatively short decay time, the Bremsstrahlung radiation from ^{32}P and Compton scattered gamma-rays mostly from ^{82}Br, ^{24}Na, and ^{42}K will increase the background counts under the 438.6-keV peak of ^{69m}Zn and worsen the net peak area statistical accuracy. In order to illustrate these points, 16 RMs were analyzed for Zn by INAA in conjunction with anticoincidence counting. The materials were irradiated at a flux of 5×10^{11} cm^{-2} s^{-1} for 7 h, and counted for 8 h. The decay time of less than 100 h was employed for assaying Zn through the 438.6-keV peak of ^{69m}Zn, and of more than 250 h for the 1115.5-keV peak of ^{65}Zn. Under these experimental conditions the sensitivities of Zn in standard solutions were 540 counts/μg for ^{69m}Zn and 363 counts/μg for ^{65}Zn. The concentrations of Zn determined using both nuclides ^{69m}Zn and ^{65}Zn in the RMs

are presented in Table 3.33 along with their peak counting statistics (PA_{anti}).

The PA_{anti} values obtained through the 1115.5-keV peak of ^{65}Zn were generally less than 5%; the precision of measured values ranged from 1% to 5% RSD with a few exceptions, notably Corn Starch, due to the low level of Zn (*i.e.* <1 ppm). On the other hand, when the 438.6-keV peak of ^{69m}Zn was used, the PA_{anti} values were greater than 10% for most of the materials except NIST RM Durum Wheat Flour and Hard Wheat Flour, and SRM Pine Needles, Rice Flour and Wheat Flour. The RSD of Zn concentrations determined by ^{69m}Zn are fairly low. The agreements between the Zn levels measured using both nuclides and that between the measured and certified values are generally good as shown in Table 3.33. These results suggest that in case of low counting statistics the 438.6-keV peak of ^{69m}Zn could be used instead of the 1115.5-keV peak of the long-lived nuclide ^{65}Zn for Zn determinations. However, when the background under the 438.6-keV peak is high and its counting statistics are poor, this peak cannot be used for Zn determination with high precision.

The 1115.5-keV photopeak of ^{65}Zn could have spectral interference from the 1112.0-keV peak of ^{152}Eu (half-life = 13 a), 1115.5-keV of ^{65}Ni (2.52 h), 1120.5-keV peak of ^{46}Sc (83.8 d), and 1121.2-keV of ^{182}Ta (115 d). Considering the short half-life of ^{65}Ni, no interference is expected. The levels of Eu, Sc, and Ta are low enough in the RMs analyzed in this work so that the interferences were not observed.

Table 3.33. Concentrations of zinc (ppm) determined by 438.6 keV peak of ^{69m}Zn and 1115.5 keV peak of ^{65}Zn, and their net peak area statistical accuracy by anticoincidence spectrometry.

Reference materials (*IAEA, all others NIST)	438.6 keV, Content ± RSD (%)	PA_{anti} (%) 438.6 keV	1115.5 keV, Content ± RSD (%)	PA_{anti} (%) 1115.5 keV	Certified, [literature] value
Corn Starch (RM 8432)	0.50 ± 80	95.1	0.28 ± 14	32.8	0.22 ± 0.05
Soft Wheat Flour (RM 8438)	3.75 ± 77	4.90	4.82 ± 1.6	3.82	5.8 ± 1.3
Hard Wheat Flour (RM 8437)	9.33 ± 6.9	3.36	8.67 ± 11	2.45	10.6 ± 1.4
Wheat Flour (SRM 1567a)	10.5 ± 10	3.90	10.0 ± 4	2.25	11.6 ± 0.4
Apple Leaves (SRM 1515)	11.9 ± 37	22.3	11.6 ± 4.5	5.89	12.5 ± 0.3
Animal Blood (RM A-13)*	18.4 ± 63	69.2	10.8 ± 8.3	5.89	13 ± 1
Corn Bran (RM 8433)	15.1 ± 20	11.0	16.9 ± 4.1	2.07	18.6 ± 2.2
Peach leaves (SRM 1547)	16.3 ± 13	17.7	17.2 ± 1.9	5.80	17.9 ± 0.4
Rice Flour (SRM 1568a)	17.3 ± 2.3	1.69	17.6 ± 3	1.64	19.4 ± 0.5
Durum Wheat Flour (RM 8436)	20.7 ± 6.8	1.90	19.6 ± 4.1	1.69	22.2 ± 1.7
Non-Fat Milk Powder (SRM 1549)	39.7 ± 5.3	36.3	44.7 ± 2.3	1.89	46.1 ± 2.2
Spinach (SRM 1570)	ND	NA	48.2 ± 3.9	2.76	50 ± 2
Wheat Gluten (RM 8418)	54.6 ± 3.8	11.0	48.6 ± 1.4	1.03	53.8 ± 3.7
Pine Needles (SRM 1575)	65.2 ± 4.7	3.72	60.1 ± 1.3	2.06	[67 ± 9]
Whole Egg Powder (RM 8415)	79.2 ± 19	15.8	69.2 ± 3.0	1.90	67.5 ± 7.6
Bovine Liver (SRM 1577b)	ND	NA	127 ± 1.7	0.90	127 ± 17

ND: not detected; NA: not available.

The advantages of anticoincidence counting have been evaluated using the AFOM term developed in this work for short- and medium-lived nuclides, and described earlier. In these cases, the intensity of a full-energy peak of a nuclide of interest decreases more rapidly compared to that of the background activities during the counting period. In the case of long-lived nuclides, the peak intensity is almost constant and the background activities are generally low and almost constant during the counting period. It will be of interest to investigate the relationship between AFOM terms and sample activity for long-lived nuclides.

For the long-lived nuclide ^{65}Zn, the samples were allowed to decay for more than 250 h before the counting was carried out. Although the biological RMs used in this work are of diverse origin, most of the interfering activities have decayed by the time the sample is counted. The ^{32}P Bremsstrahlung radiation then becomes the major activity which contributes mostly to the low-energy portion of spectrum. Therefore, the gamma-ray spectrum near the region of 1115.5 keV of ^{65}Zn is mainly dominated by natural background. A low total count rate of 40 to 250 counts per s (cps), corresponding to a dead time of 1% to 2%, was generally obtained.

In order to obtain the above range of count rates, 16 RMs were analyzed by both conventional and anticoincidence counting techniques. The values for R_{conv}, R_{anti}, R_{PA}, and AFOM for the 1115.5-keV peak of ^{65}Zn at various count rates were calculated, and the results are presented in Table 3.34. The number of cps in the anticoincidence mode is lower than that in the conventional

mode, as expected.

The plot of R_{PA} against R_{conv} values are shown in Fig. 3.39. At low R_{conv} values such as 0.43 for Hard Wheat Flour, a R_{PA} value of 1.90 can be achieved; but for high R_{conv} like 6.40 for Bovine Liver, a R_{PA} value of only 1.08 can be obtained. It could be concluded that the improvement in net peak area statistical accuracy is more pronounced at low R_{conv} compared to that at high R_{conv}.

The AFOM term depends on R_{PA} and peak-to-background ratio improvement as shown in equation 3.15. In Fig. 3.40, the AFOM values are plotted as a function of sample cps in the conventional counting mode; a correlation appears to exist between the AFOM term and total sample cps.

It can be concluded from the above discussions that for long-lived nuclides the higher the count rate the better is the improvement in anticoincidence spectrometry.

3.5.4. Determination of Iron

The ^{59}Fe nuclide (half-life = 44.5 d) has been used for Fe determination by various forms of NAA. It decays by β-emission and then by two major gamma-rays, namely 1099.3 keV and 1291.6 keV, which are not coincident with each other. The 1099.3-keV peak is partially cascaded with the 192.3-keV

Table 3.34. The effectiveness of anticoincidence counting on the long-lived nuclide ^{65}Zn varied with sample activity.

Reference material (*IAEA, all others NIST)	R_{conv}	R_{anti}	R_{PA}	AFOM terms	Counting rate (cps) anti.	conv.
Apple Leaves (SRM 1515)	1.47	3.44	1.45	3.30	32	75
Non-Fat Milk Powder (SRM 1549)	2.81	7.08	1.13	2.41	62	91
Wheat Flour (SRM 1567a)	1.68	6.22	1.28	3.66	39	78
Soft Wheat Flour (RM 8438)	1.74	4.82	1.23	2.76	24	48
Rice Flour (SRM 1568a)	1.91	8.55	1.29	4.49	45	95
Spinach (SRM 1570)	0.90	3.67	1.38	3.72	28	68
Pine Needle (SRM 1575)	1.72	6.43	1.30	3.83	16	43
Peach Leaves (SRM 1547)	1.45	4.33	1.27	2.96	18	52
Bovine Liver (SRM 1577b)	6.40	30.3	1.08	4.49	52	152
Whole Egg Powder (RM 8415)	2.10	7.09	1.22	3.30	48	78
Wheat Gluten (RM 8418)	3.40	15.6	1.20	4.70	58	104
Corn Bran (RM 8433)	1.63	7.23	1.33	4.50	13	43
Durum Wheat Flour (RM 8436)	1.75	7.32	1.29	4.14	57	109
Hard Wheat Flour (RM 8437)	0.43	5.13	1.90	10.6	47	248
Animal Blood (RM A-13)*	0.63	1.54	1.20	1.94	18	40

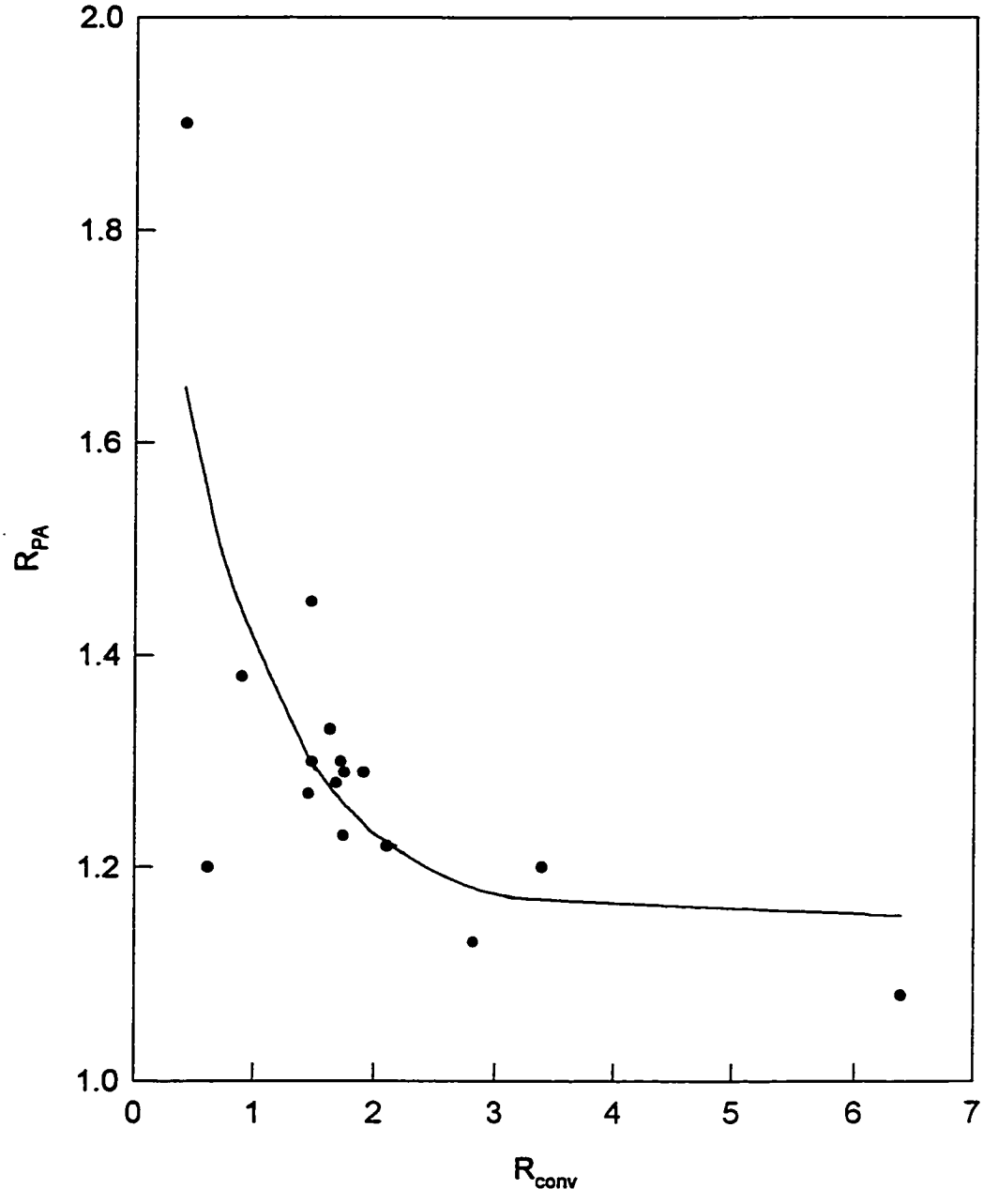

Fig. 3.39. The variation of the net peak area statistical accuracy improvement factor (R_{PA}) with the peak-to-background ratio in conventional counting (R_{conv}) for ^{65}Zn.

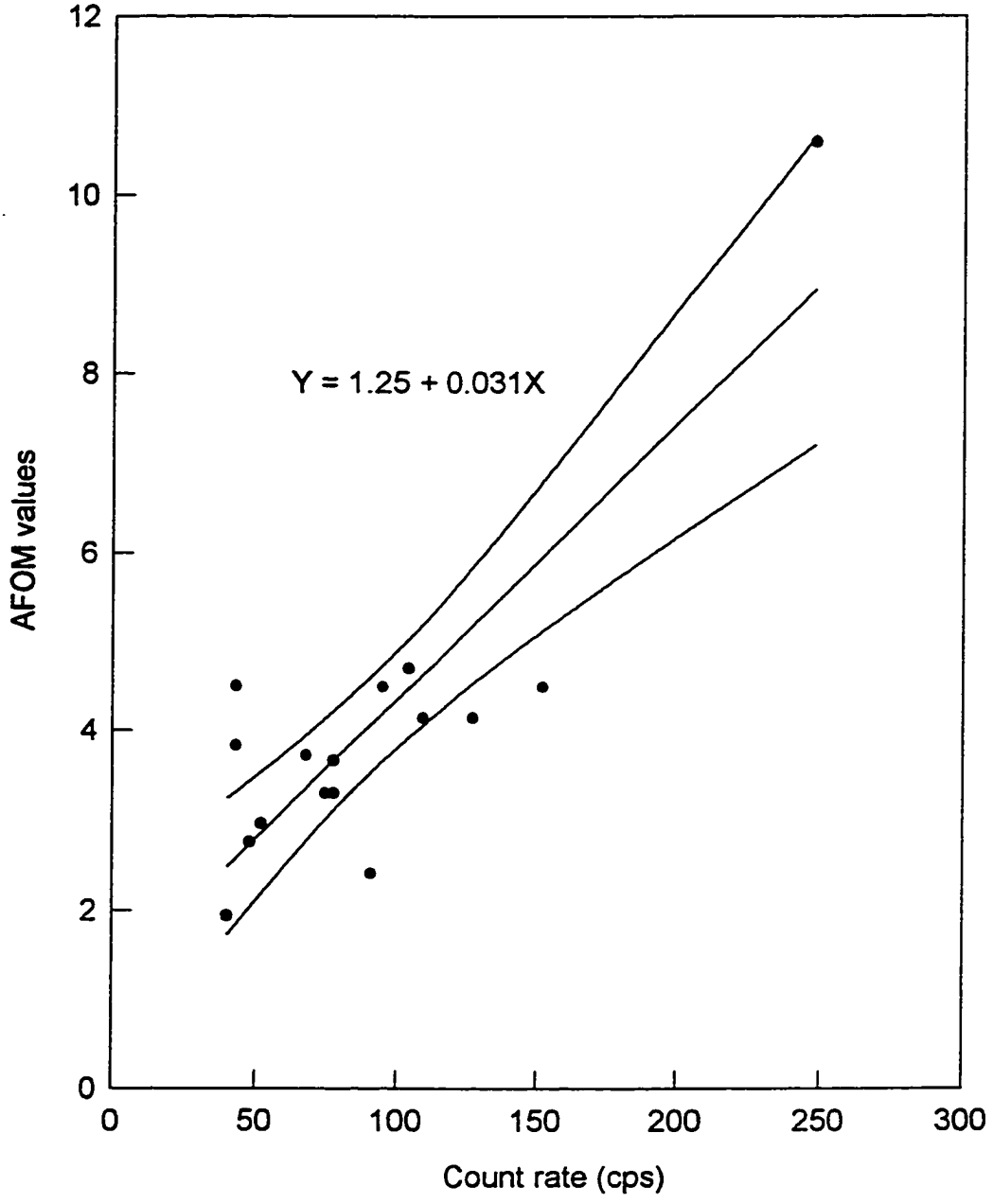

Fig. 3.40. The variation of AFOM factor with the sample count rate in the conventional counting mode for ^{65}Zn.

peak. The use of anticoincidence counting slightly reduces its peak efficiency to 0.94 as shown in Table 3.30. The PERF of the 1291.6 keV peak is 0.97. Therefore, anticoincidence counting for the determination of Fe using either of the peaks should be beneficial. The 1099.3 keV peak of ^{59}Fe is virtually free from interference, and was used in this work. The 1291.6 keV peak could be interfered with the 1293.6-keV peak of ^{41}Ar which can always be detected in the counting room which is adjacent to the reactor.

In order to explore the extent of improvement that can be achieved by anticoincidence counting, diverse types of biological RMs and SRMs were analyzed for Fe by INAA in conjunction with anticoincidence spectrometry. These materials were irradiated at a flux of 5×10^{11} cm^{-2} s^{-1} for 7 h, allowed to decay for more than 250 h, and counted for 8 h. The sensitivity for Fe in standard solutions under these conditions was 24 counts/μg. Sixteen RMs and SRMs were analyzed in triplicate using anticoincidence spectrometry, and their Fe concentrations are presented in Table 3.35. The Fe concentrations of these materials varied by 3 orders of magnitude. The agreement between the measured and certified or information values is generally very good. The detection limits ranged from 0.86 to 8.4 ppm.

After a decay of more than 250 h, the total sample activity was very low, as pointed out in section 3.5.3 for Zn. In the conventional counting mode, the count rates varied from 40 to 250 cps. The background activity is mainly due to two components: natural radioactivity and Bremsstrahlung radiation from ^{32}P.

Table 3.35. Concentrations of iron in reference materials by anticoincidence gamma-ray spectrometry.

Reference material (*IAEA, all others NIST)	This work (ppm)	Certified (information) values (ppm)	Detection limit (ppm)
Non-Fat Milk Powder (SRM 1549)	3.50 ± 0.32	1.78 ± 0.10	2.7
Corn Starch (RM 8432)	4.52 ± 0.35	(5)	0.96
Rice Flour (SRM 1568a)	8.23 ± 1.28	7.4 ± 0.9	0.86
Wheat Flour (SRM 1567a)	17.8 ± 0.8	14.1 ± 0.5	0.87
Corn Bran (RM 8433)	17.8 ± 2.3	14.8 ± 1.8	1.3
Hard Wheat Flour (RM 8437)	29.8 ± 3.1	----	0.97
Soft Wheat Flour (RM 8438)	29.9 ± 1.3	29 ± 10	1.1
Durum Wheat Flour (RM 8436)	42.0 ± 2.1	41.5 ± 4.0	1.2
Wheat Gluten (RM 8418)	54.8 ± 0.4	54.3 ± 6.8	1.3
Apple Leaves (SRM 1515)	80.4 ± 1.3	(83)	4.9
Whole Egg Powder (RM 8415)	120 ± 10	112 ± 16	5.1
Pine Needles (SRM 1575)	191 ± 4	200 ± 10	6.4
Bovine Liver (SRM 1577b)	208 ± 12	(184)	2.9
Peach leaves (SRM 1547)	218 ± 9	218 ± 13	5.7
Spinach (SRM 1570)	512 ± 17	550 ± 20	8.4
Animal Blood (RM A-13)*	2113 ± 34	2400 ± 144	6.3

Decay products of U, Th, and K which are present in and around the detector assembly constitute the natural radioactivity. The applicability of anticoincidence counting in such cases was investigated. The gamma-ray spectra of two materials, namely SRM Rice Flour and RM Hard Wheat Flour, and a blank (*i.e.* no sample on the detector) were recorded using both conventional and anticoincidence spectrometry. The gamma-ray spectra between 100 and 1900 keV were arbitrarily divided into several portions and the background counts per channel were calculated. The average background counts per channel in the anticoincidence counting mode was plotted against the gamma-ray energy; the curves for Rice Flour and the blank are presented in Fig. 3.41. It is clear that anticoincidence counting can suppress the background of Rice Flour down to the natural background levels at energies higher than 400 keV. It has been pointed out earlier that the Bremsstrahlung radiation from ^{32}P present in the low-energy portion cannot be efficiently suppressed by anticoincidence counting.

In order to study the efficiency of anticoincidence counting, BSR values were calculated and plotted as a function of gamma-ray energy as shown in Fig. 3.42. The BSR of Rice Flour (count rate of 95 cps) were higher than those of blanks (around 30 cps); the BSR increased with increasing sample count rate. The SRM Hard Wheat Flour had a count rate of 248 cps, which is about 2.5 times higher than that of Rice Flour; its BSR ranged from 5 to 23 compared to 5-10 for Rice Flour. It is obvious that the higher the sample activity, the higher is the BSR. Furthermore, a BSR of 3 to 5 could be obtained using anticoincidence counting

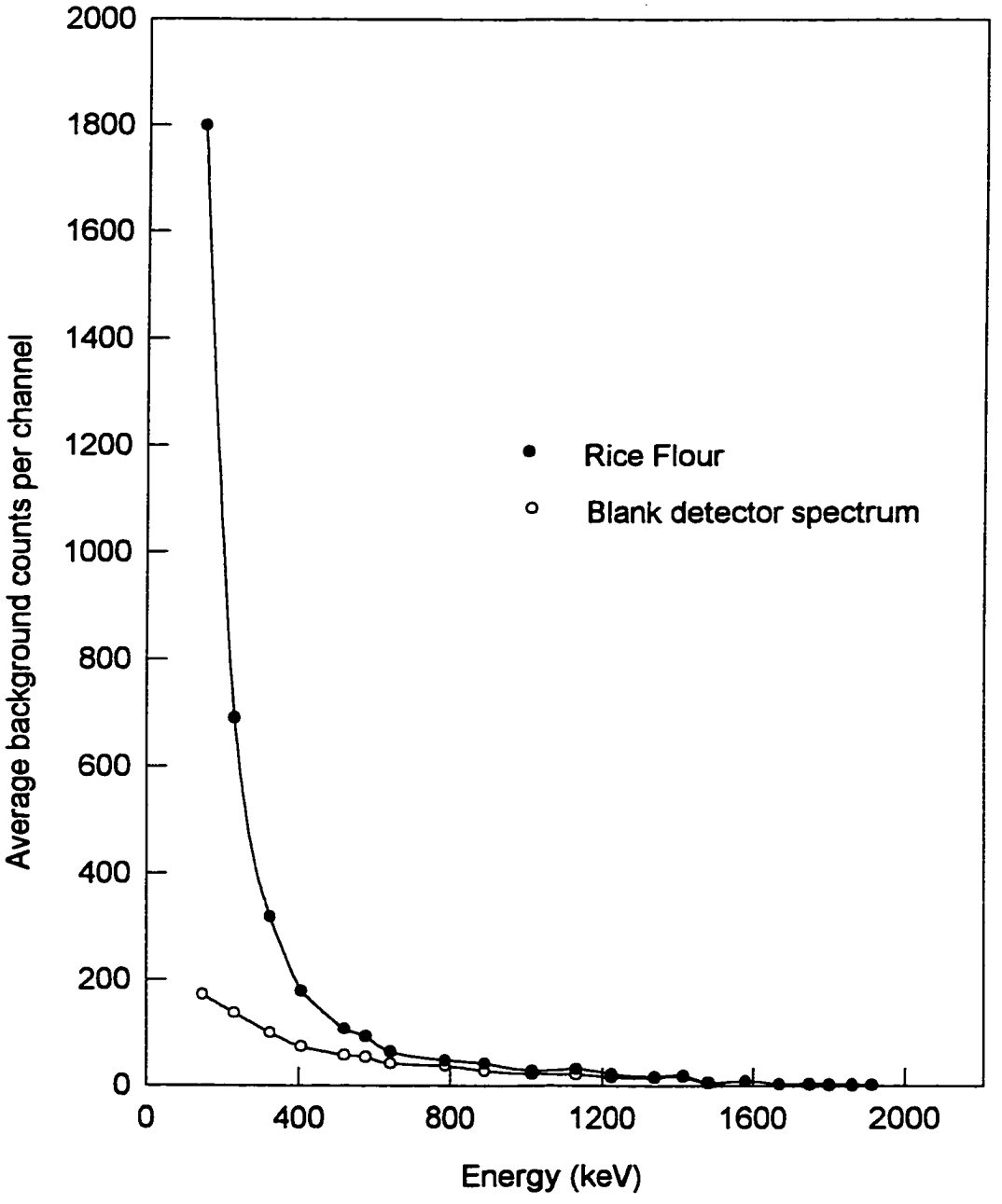

Fig. 3.41. Distribution of background counts in various gamma-ray energy regions of Blank and Rice Flour (NIST SRM 1568a) spectra by by anticoincidence counting.

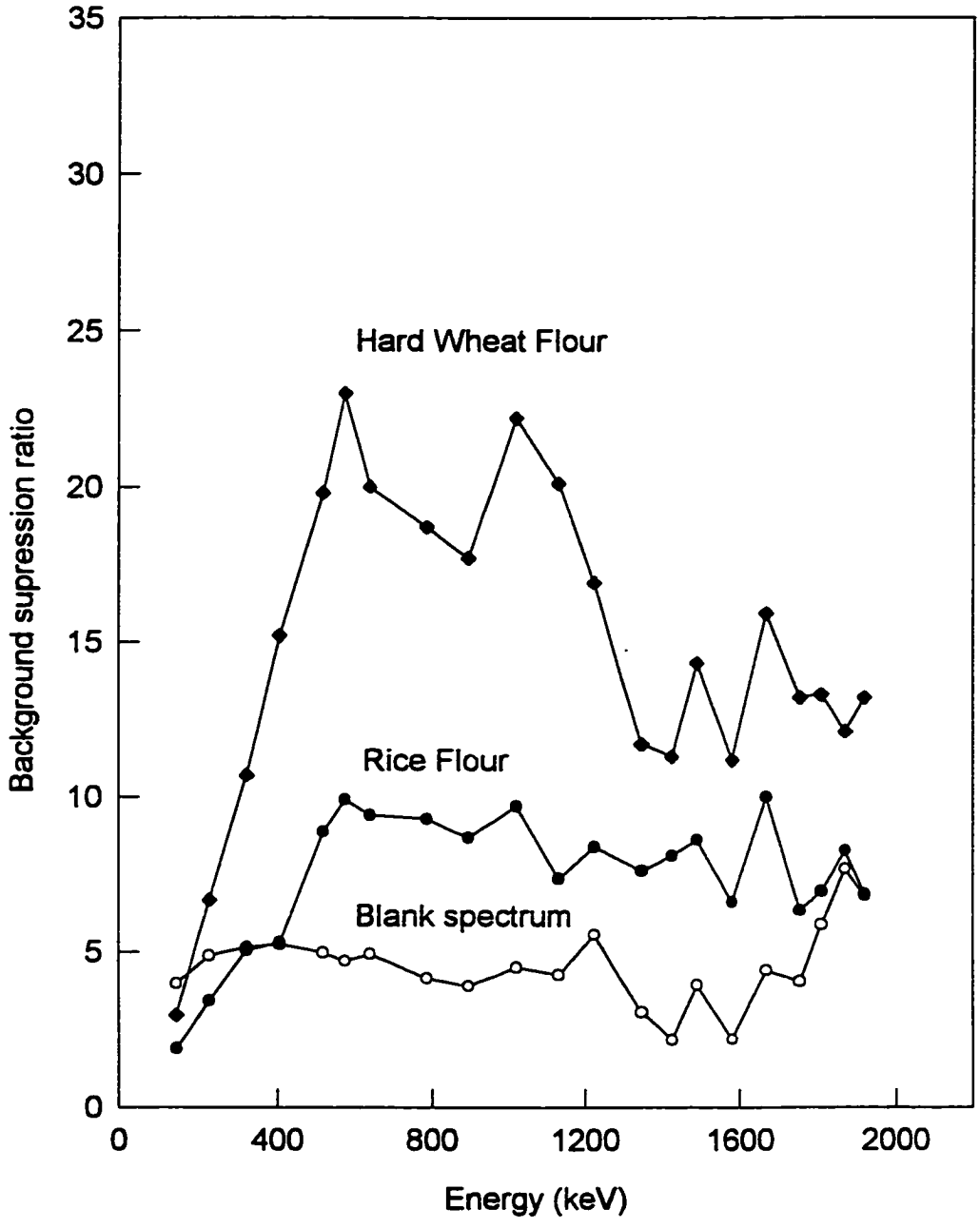

Fig. 3.42. Background suppression ratios for three gamma-ray spectra, of Hard Wheat Flour (NIST RM 8437), Rice Flour (NIST SRM 1568a) and a blank, as a function of energy by anticoincidence counting.

at gamma-ray energies above 400 keV even if the sample activity is at the natural background level.

The advantage of anticoincidence counting with respect to the sample activity was studied using AFOM terms and sample count rates. The values of R_{conv}, R_{anti}, R_{PA}, and AFOM factor of each material were calculated and presented in Table 3.36. The net peak area statistical accuracy (R_{PA}) in the anticoincidence counting mode improved by 1.08 to 3.15 times. The AFOM values ranged from 3.38 to 16.5; these were plotted against sample count rate in the conventional counting mode in Fig. 3.43. The AFOM term appears to be correlated with sample activity at high count rates, indicating that better anticoincidence efficiency is achieved at higher sample activities.

One of the reasons for the deviation from linearity at low count rates could be that the AFOM values are more seriously affected by the conditions of the sample itself (*i.e.* R_{conv}) when the sample activity is close to the natural background level, which was 30 cps in this experiment. For example, the AFOM values for Corn Bran and Rice Flour, which have lower R_{conv} values, have large deviations. This explanation can also be applied to the difference in AFOM values between Fe and Zn. A comparison of AFOM values given in Tables 3.34 and 3.36 shows that because of the lower R_{conv} values of the 1099.3-keV peak of ^{59}Fe for most of the materials, the R_{PA} and AFOM values of Fe are higher than those of the 1115.5-keV peak of ^{65}Zn.

Table 3.36. Sample matrix activity and peak parameters for the 1099.3-keV peak of ^{59}Fe in various reference materials using anticoincidence and conventional spectrometry.

Reference material (*IAEA, all others NIST)	R_{conv}	R_{anti}	R_{PA}	AFOM terms	Count rate (cps) anti.	conv.
Apple Leaves (SRM 1515)	0.23	1.13	1.67	3.92	32	75
Non-Fat Milk Powder (SRM 1549)	0.17	0.31	2.49	6.58	62	91
Wheat Flour (SRM 1567a)	0.18	1.30	2.61	10.3	39	78
Soft Wheat Flour (RM 8438)	0.25	1.70	2.05	6.91	24	48
Rice Flour (SRM 1568a)	0.13	0.32	1.84	3.69	45	95
Spinach (SRM 1570)	0.67	3.72	1.52	4.95	28	68
Pine Needle (SRM 1575)	0.44	1.72	1.49	3.38	16	43
Peach Leaves (SRM 1547)	0.34	2.13	1.86	6.11	18	52
Bovine Liver (SRM 1577b)	0.52	2.13	1.91	9.61	52	152
Whole Egg Powder (RM 8415)	0.23	1.65	2.26	8.35	48	78
Wheat Gluten (RM 8418)	0.20	1.76	2.33	9.28	58	104
Corn Bran (RM 8433)	0.13	1.01	2.75	10.7	13	43
Durum Wheat Flour (RM 8436)	0.22	2.54	2.33	11.1	57	109
Hard Wheat Flour (RM 8437)	0.08	1.46	3.15	16.5	47	248
Animal Blood (RM A-13)*	4.57	20.3	1.08	3.96	18	40

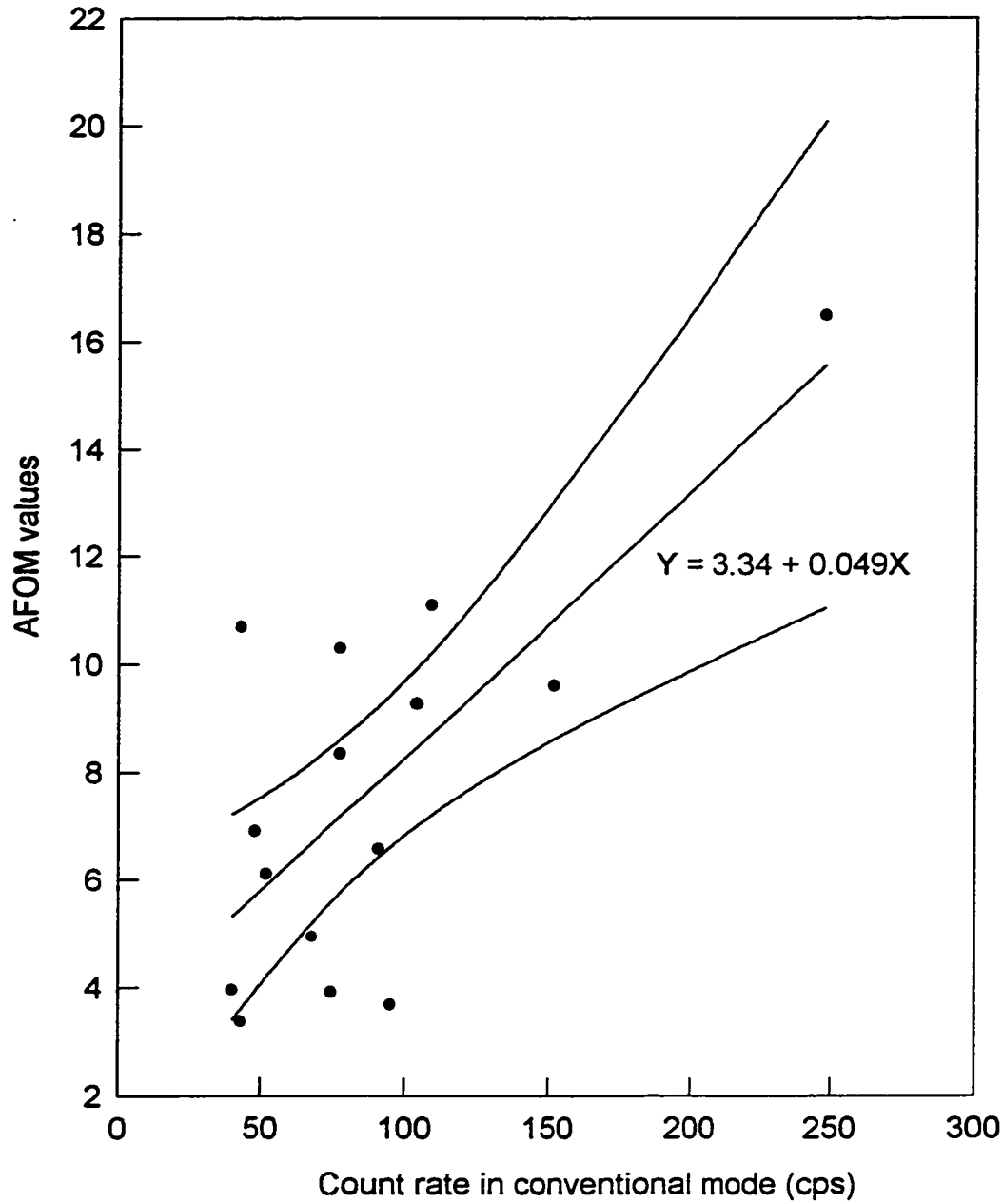

Fig. 3.43. Variation of the AFOM values for ^{59}Fe with the sample count rate in conventional counting mode.

3.5.5. Determination of Rubidium

Rubidium was also determined simultaneously with other long-lived nuclides. The 1076.8-keV peak of ^{86}Rb (half-life = 18.6 d) is not cascaded with other gamma-rays and has a PERF factor of 0.99 (Table 3.30), and is virtually free from interference. The sensitivity for Rb using this gamma-ray is 945 counts/μg. The same 16 biological RMs and SRMs were analyzed for Rb, and the average of 3 determinations of Rb is presented in Table 3.37 along with the detection limits. The certified and information values provided by NIST and IAEA are also reported in this table. The agreement between the measured and certified values is good wherever such comparisons can be made.

The advantages of anticoincidence counting for the 1076.8-keV peak of ^{86}Rb are given by the AFOM values which are listed in Table 3.38 together with R_{conv}, R_{anti}, R_{PA}, and sample count rate. Due to similar R_{conv} values for the 1099.3-keV peak of ^{59}Fe and the 1076.8-keV peak of ^{86}Rb, the AFOM and R_{PA} values of are similar. Like ^{59}Fe, the linear correlation between the AFOM values and sample count rates also exists for ^{86}Rb. It can be concluded that anticoincidence counting can be advantageously used for the determination of Rb at ppb levels because of its high sensitivity.

Table 3.37. Concentrations of rubidium in reference materials by anticoincidence gamma-ray spectrometry.

Reference material (*IAEA, all others NIST)	This work, ppm	Certified, (information) values, ppm	Detection limit, ppm
Corn Starch (RM 8432)	0.08 ± 0.01	----	0.023
Wheat Gluten (RM 8418)	0.42 ± 0.04	(0.4)	0.029
Corn Bran (RM 8433)	0.47 ± 0.02	0.5 ± 0.3	0.033
Wheat Flour (SRM 1567a)	0.65 ± 0.07	0.68 ± 0.03	0.031
Hard Wheat Flour (RM 8437)	0.95 ± 0.05	----	0.027
Soft Wheat Flour (RM 8438)	0.95 ± 0.06	----	0.031
Durum Wheat Flour (RM 8436)	1.66 ± 0.02	2.0 ± 0.4	0.034
Animal Blood (RM A-13)*	2.48 ± 0.22	2.3 ± 0.7	0.16
Whole Egg Powder (RM 8415)	3.53 ± 0.28	----	0.17
Rice Flour (SRM 1568a)	5.79 ± 0.11	6.14 ± 0.09	0.028
Apple Leaves (SRM 1515)	9.87 ± 0.17	10.2 ± 1.3	0.15
Spinach (SRM 1570)	12.5 ± 0.5	12.1 ± 0.2	0.22
Pine Needle (SRM 1575)	12.6 ± 0.6	11.7 ± 0.1	0.16
Non-Fat Milk Powder (SRM 1549)	12.7 ± 0.4	(11)	0.13
Bovine Liver (SRM 1577b)	13.3 ± 0.9	13.7 ± 1.1	0.087
Peach leaves (SRM 1547)	20.2 ± 1.5	(19.7)	0.18

Table 3.38. Sample matrix activity and peak parameters for the 1076.8-keV peak of ^{86}Rb in various reference materials using anticoincidence and conventional spectrometry.

Reference material (*IAEA, all others NIST)	R_{conv}	R_{anti}	R_{PA}	AFOM term	Count rate(cps) anti.	conv.
Apple Leaves (SRM 1515)	0.66	3.69	1.52	4.94	32	75
Non-Fat Milk Powder (SRM 1549)	1.33	5.30	1.32	3.82	62	91
Wheat Flour (SRM 1567a)	0.18	1.73	2.68	12.3	39	78
Soft Wheat Flour (RM 8439)	0.28	1.11	1.58	3.40	24	48
Rice Flour (SRM 1568a)	1.05	9.86	1.56	9.46	45	95
Spinach (SRM 1570)	0.51	3.73	1.78	7.23	28	68
Pine Needles (SRM 1575)	0.74	4.67	1.67	6.79	16	43
Peach Leaves (SRM 1547)	0.66	4.63	1.75	7.63	18	52
Bovine Liver (SRM 1577b)	1.02	6.04	1.97	10.3	52	152
Whole Egg Powder (RM 8415)	0.31	1.79	1.85	5.61	48	78
Wheat Gluten (RM 8418)	0.13	0.89	2.27	6.98	58	104
Corn Bran (RM 8433)	0.21	1.17	1.72	4.24	13	43
Durum Wheat Flour (RM 8436)	0.31	2.85	2.31	11.2	57	109
Hard Wheat Flour (RM 8437)	0.11	1.78	2.95	15.6	47	248
Animal Blood (RM A-13)*	0.18	0.78	1.88	4.51	18	40

3.6 Determination of Selenium using Anticoincidence Spectrometry

The biological essentiality of Se for animals was first evidenced in 1957. However, it was not until 1973 that an enzyme called glutathione peroxidase was proven to be a selenoenzyme. Low levels of Se intake are reported to cause diseases such as Keshan disease, while about two orders of magnitude higher levels of Se are known to cause toxic effects. There is an increasing interest in understanding the role of Se in human nutrition and metabolism. The most commonly used analytical techniques for Se determination are AAS using either electrothermal atomization (ETAAS), hydride generation (HGAAS) or graphite-furnace (GFAAS), and spectrofluorometry. Neutron activation analysis is comparable to, if not better than, many of these methods.

3.6.1 Determination of Selenium using Long-Lived Nuclide ^{75}Se

Selenium has six stable isotopes which can produce seven nuclides on thermal and epithermal/fast neutron activation. The nuclear data [107-109] for various Se isotopes and their activation products are shown in Table 3.39. The most commonly used Se nuclide in NAA is ^{75}Se which has a relatively long half-life of 119.8 d. The target isotope ^{74}Se has a low abundance of only 0.87% but compensated by a fairly high thermal neutron absorption cross section 51.8 b. The use of the ^{75}Se nuclide requires lengthy irradiations at a high neutron flux, and

Table 3.39. Nuclear data for selenium by NAA.

Isotope (% abund.)	σ_{th} (b)	Nuclide	Half-life	γ-ray, keV (% pop.)
^{74}Se (0.87)	51.8 ± 1.2	^{75}Se	119.8 d	121.1 (17.1)
				136.0 (58.7)
				264.7 (58.5)
				279.5 (24.8)
				400.7 (11.4)
^{76}Se (9.02)	21 ± 1	^{77m}Se	17.4 s	161.9 (52.5)
^{77}Se (7.58)	0.733 ± 0.05*	^{77m}Se	17.4 s	161.9 (52.5)
^{78}Se (23.52)	0.33 ± 0.04	^{79m}Se	3.89 min	97.9 (8.9)
^{80}Se (49.82)	0.08 ± 0.01	^{81m}Se	57.28 min	102.9 (12.7)
^{80}Se (49.82)	0.53 ± 0.04	^{81}Se	18.45 min	275.9 (0.67)
				290.1 (0.55)
				828.4 (0.28)
^{82}Se (9.19)	0.039 ± 0.003	^{83}Se	22.3 min	225.2 (32.7)
				356.7 (70)
				510.2 (43)
				718.2 (15)
				836.8 (13)
^{82}Se (9.19)	0.006 ± 0.0004	^{83m}Se	70 s	356 (20)
				676 (17)
				989 (19)
				1031 (30)
				2054 (13)

* fission spectrum neutron cross section.

long decay and counting periods which can lead to a total experimental time of two to three weeks. Obviously, it is a time-consuming and expensive procedure and may not always be desirable for routine analysis of a large number of samples for Se.

Moreover, most of the intense gamma-rays emitted by ^{75}Se are generally subject to interference caused by overlapping gamma-rays from other nuclides. Some of the more important interferences are listed in Table 3.40. For example, the 121.1-keV gamma-ray of ^{75}Se is interfered with by the more abundant 121.8-keV gamma-ray of ^{152}Eu produced from ^{151}Eu which has a relatively high abundance and a very high cross section. There is also a minor interference from ^{177m}Lu. The most commonly used gamma-rays of 136.0 and 264.7 keV of ^{75}Se are interfered with by 136.3-keV gamma-ray of ^{181}Hf and 264.1-keV gamma-ray of ^{182}Ta. The 279.1-keV gamma-ray of ^{203}Hg causes interference on the 279.5-keV gamma-ray of ^{75}Se. The 400.7-keV gamma-ray of ^{75}Se appears to be free from interference but has a low population. Makarewicz and Zeisler [139] used a well-type Ge detector to enhance the sensitivity of Se determination using the 400.7-keV peak. They noted the potential drawbacks of high input count rate, pile-up losses, and decrease in resolution.

In biological materials, interferences from ^{152}Eu, ^{177m}Lu, ^{181}Hf, and ^{182}Ta are expected to be small due to the very low concentrations of the elements, and thus usually neglected. The 279.5-keV gamma-ray of ^{75}Se is

Table 3.40. Interfering nuclides and gamma-rays for selenium by NAA.

Nuclide of Interest		Interfering Nuclide			
Nuclide (half-life)	γ-ray, keV (% pop.)	γ-ray, keV (% pop.)	Nuclide (half-life)	σ_{th} (b)	Isotope (% abund.)
^{75}Se (119.8 d)	121.1 (17.1)	121.8 (28.4)	^{152}Eu (13.54 a)	5900 ± 200	^{151}Eu (47.8)
		121.6 (5.9)	^{177m}Lu (161.4 d)	7 ± 2	^{176}Lu (2.6)
	136.0 (58.7)	136.3 (5.8)	^{181}Hf (42.4 d)	12.6 ± 0.7	^{180}Hf (35.1)
	264.7 (58.5)	264.1 (3.6)	^{182}Ta (114.4 d)	8200 ± 100	^{181}Ta (99.99)
	279.5 (24.8)	279.1 (33.5)	^{203}Hg (46.6 d)	4.9 ± 0.1	^{202}Hg (29.7)
	400.7 (11.4)	398.5 (1.19)	^{233}Pa (27.0 d)	4.7 ± 0.1	^{232}Th (100)
^{77m}Se (17.4 s)	161.9 (52.5)	162.3 (34)	^{116m2}In (2.18 s)	92 ± 14	^{115}In (95.72)

interfered with by the 279.1-keV gamma-ray of ^{203}Hg, and needs to be corrected for before reliable Se results can be obtained. Moreover, all photopeaks of ^{75}Se are likely to be exposed to background interference from the Bremsstrahlung radiation of ^{32}P; phosphorus is a common element in most biological materials. If this background is too high, then erroneous Se results can be obtained due to the poor counting statistics of the 279.5-keV peak which is generally not used.

Three Se standards were irradiated at a flux of 5×10^{11} n cm^{-2} s^{-1} for 7 h, allowed to decay more than 250 h, and counted for 8 h using both conventional and anticoincidence gamma-ray spectrometry. The sensitivities and PERF of four gamma-rays of ^{75}Se are presented in Table 3.41. The 136.0-keV photopeak of ^{75}Se has the highest sensitivity followed by the 264.7, 279.5, and 400.7 keV peaks using conventional gamma-ray spectrometry (Table 3.41). However, in the anticoincidence counting mode, the intensities of 136.0, 264.7, and 279.5 keV photopeaks are significantly reduced because of their cascading decay. The peak at 136.0-keV with complete cascading undergoes the highest degree of peak efficiency suppression (Table 3.41), peak area being almost 10 times less than that by the conventional system. This suggests little advantage of using anticoincidence spectrometry for measuring Se through the 136.0-keV peak of ^{75}Se. Of the other two partial cascading peaks at 264.7 and 279.5 keV, only the 279.5-keV peak has shown some promise of improvement in sensitivity but it is too weak to be routinely used in NAA of samples of low Se content. The technique of windows coincidence counting [140] will likely improve ^{75}Se sensitivity.

The efficiency of the 400.7-keV sumpeak of ^{75}Se, resulting from the events of (121.1 + 279.5 keV), and of (136.0 + 264.7 keV), is not affected in anticoincidence spectrometry because the sumpeak is generated by the internal coincidence events in the main detector. In addition, this peak is generally interference-free, and falls in the spectral region where the Bremsstrahlung radiation background from ^{32}P is relatively less intense, and the anticoincidence efficiency is high (Fig. 3.4). It has recently been reported [91] that the 400.7-keV peak of ^{75}Se could be interfered with by the 398.5-keV peak of ^{233}Th-^{233}Pa. This interference could be significant in environmental samples containing high amounts of Th. However, considering the very low levels of Th in biological materials [141] as well as extremely poor intensity of 1.19% of the 398.5-keV peak, any such interference in the materials analyzed in the present thesis can be discarded. One of the objectives of this project is to explore the possibility of reliable determination of Se by anticoincidence spectrometry using the 400.7-keV sumpeak of ^{75}Se.

In order to evaluate the net peak area statistical accuracy (PA) of the four peaks of ^{75}Se, five RMs and SRMs were analyzed by INAA using the above irradiation, decay, and counting times, as well as conventional and anticoincidence gamma-ray spectrometry. Equation 3.9 was used to calculate the values for PA, and the results are presented in Table 3.42.

It is evident from Table 3.42 that the best net peak area statistical accuracy using conventional counting (PA_{conv}) for all five RMs is obtained at the 136.0-keV photopeak mainly due to its very high sensitivity (Table 3.41). The

Table 3.41. Peak efficiency reduction factors and sensitivities for selenium using conventional and anticoincidence gamma-ray spectrometry.

Nuclides	γ-ray energy keV(% int.)	Sensitivities (counts/μg ± 1σ) conv.	anti.	PERF ± 1σ
^{75}Se	136.0 (58.7)	7330 ± 245	513 ± 31	0.07 ± 0.01
	264.7 (58.5)	4580 ± 125	596 ± 24	0.13 ± 0.01
	279.5(24.8)	1780 ± 75	624 ± 27	0.35 ± 0.01
	400.7 (11.4)	1500 ± 43	1515 ± 34	1.01 ± 0.04
^{77m}Se*	161.9 (52.5)	2200 ± 110	2245 ± 132	0.98 ± 0.02

* obtained using t_i = 30 s, t_d = 10 s, t_c = 40 s.

264.7-keV photopeak of ^{75}Se is most commonly used for Se determination. It also has a fairly low and comparable PA_{conv} value for all materials except Animal Blood. The PA_{conv} values of all four photopeaks for Wheat Flour and Durum Wheat Flour are low (*viz.* 3.84 to 11.3), followed by Whole Egg Powder and Bovine Liver (*viz.* 16.2 to 28.7). For Animal Blood, the PA_{conv} values of all four peaks are very high and range from 32.6 to 82.6; these high values are mainly due to high background activities (possibly ^{32}P) and relatively low Se levels. These differences in PA_{conv} values are easily detected from the graphs shown in Fig. 3.44.

Table 3.42. Comparison of net peak area statistical accuracy (PA) for various photopeaks of ^{75}Se.

Reference material	PA_{conv}				PA_{anti}
	136.0 keV	264.7 keV	279.5 keV	400.7 keV	400.7 keV
Wheat Flour (NIST SRM 1567a)	3.84	4.67	10.2	9.11	4.87
Durum Wheat Flour (NIST RM 8436)	4.95	5.95	9.95	11.3	3.66
Whole Egg Powder (NIST RM 8415)	16.2	13.9	25.6	25.2	3.89
Bovine Liver (NIST SRM 1577b)	18.3	20.1	28.7	22.6	5.85
Animal Blood (IAEA RM A-8)	32.6	87.1	79.6	82.6	8.75

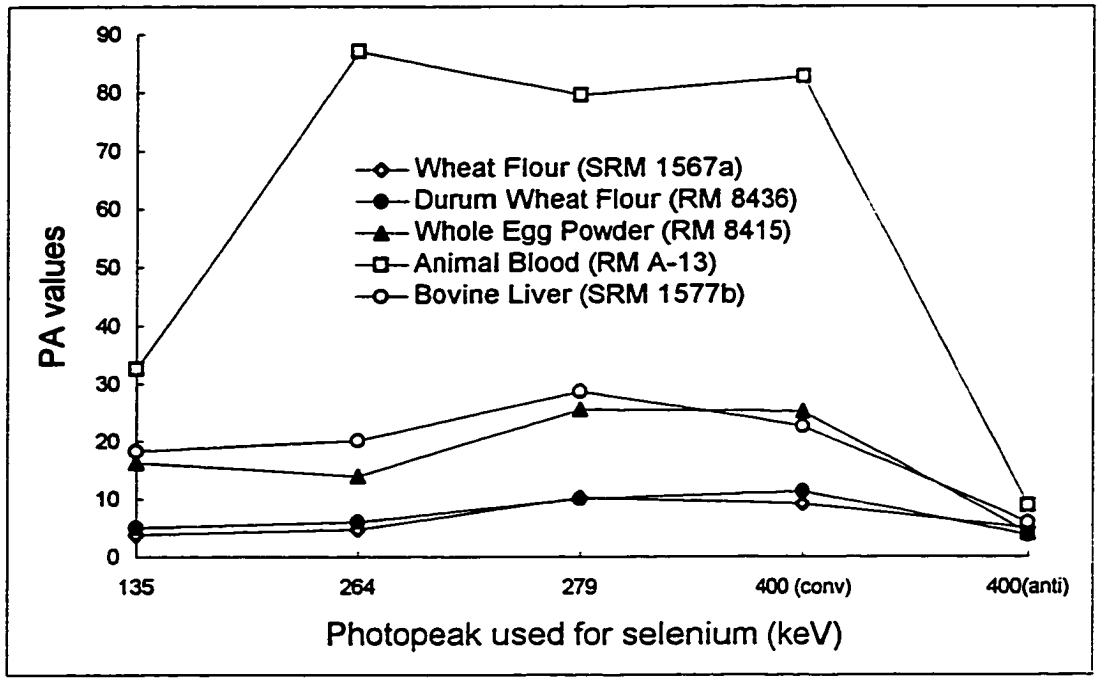

Fig. 3.44. Comparison of net peak area statistical accuracy (PA) for various peaks of 75-Se.

The net peak area statistical accuracy of the 400.7-keV sumpeak using anticoincidence counting (PA_{anti}) is similar to the PA_{conv} values of the 136.0-keV peak for Wheat Flour and Durum Wheat Flour; however, PA_{anti} values of the 400.7-keV peak are lower than the corresponding PA_{conv} values for the same two materials. For the other three RMs in Table 3.42, the PA_{anti} values of the 400.7-keV peak is significantly lower than the PA_{conv} values of both the 136.0-keV and 400.7-keV peaks.

Selenium concentrations in five RMs were measured using four gamma-rays of ^{75}Se by conventional and the 400.7-keV gamma-ray by anticoincidence counting modes. The average of three measurements are shown in Table 3.43. It is evident that in conventional counting mode the RSD values for each material obtained by the 400.7-keV sumpeak ranged from 8.2 to 47% which are poorer than that obtained by the 136.0-keV peak. Although the sensitivities of the 400.7 and 279.5 keV peaks are comparable (Table 3.41), the background activity is lower for the 400.7-keV peak resulting in generally lower RSD values as shown in Table 3.43. The RSD values calculated using the 400.7-keV peak by anticoincidence spectrometry (*viz.* 2.7 to 6.3%) are considerably lower than that by conventional spectrometry (*viz.* 8.2 to 47%). The most pronounced improvement in RSD values can be observed in Animal Blood where an RSD of 77% obtained using the 264.7-keV peak by conventional counting was reduced to 6.3% using the 400.7-keV peak by anticoincidence counting. Selenium concentrations measured using the 400.7-keV by both conventional and

Table 3.43. Selenium concentrations (ppb ± RSD%) determined using various photopeaks of ^{75}Se.

Reference material	Conventional				Anticoincidence		Certified values
	136.0 keV of ^{75}Se	264.7 keV of ^{75}Se	279.5 keV of ^{75}Se	400.7 keV of ^{75}Se	400.7 keV of ^{75}Se	161.9 keV of ^{77m}Se	
Wheat Flour (NIST SRM 1567a)	1100 ± 3	1080 ± 6	1280 ± 15	1160 ± 8	1050 ± 3	1180 ± 2	1100 ± 20
Durum Wheat Flour (NIST RM 8436)	1315 ± 3	1090 ± 4	1470 ± 10	1260 ± 12	1195 ± 5	1235 ± 1	1275 ± 7
Whole Egg Powder (NIST RM 8415)	1105 ± 3	1340 ± 2	1910 ± 25	1478 ± 18	1250 ± 4	1370 ± 2	1390 ± 5
Bovine Liver (NIST SRM 1577b)	670 ± 18	610 ± 25	740 ± 20	738 ± 24	725 ± 5	710 ± 2	730 ± 8
Animal Blood (IAEA RM A-13)	270 ± 22	280 ± 80	300 ± 50	313 ± 47	290 ± 6	205 ± 8	----

anticoincidence counting modes are in good agreement with the certified values as shown in Table 3.43.

Selenium concentrations of Wheat Flour shown in Table 3.43 are graphically presented in Fig. 3.45. The values obtained by various nuclides, photopeaks, and counting modes do not show any detectable bias. All results except one are within $\pm 1\sigma$ of the certified value. Among all the photopeaks of ^{75}Se, the best RSD of 2.7% for Se in Wheat Flour was obtained using the 400.7-keV sumpeak and anticoincidence spectrometry. An equally good RSD of 2.1% can be achieved using the 161.9-keV photopeak of the short-lived nuclide ^{77m}Se. This is discussed in detail in the following section.

3.6.2 Determination of Selenium using Short-Lived Nuclide ^{77m}Se

The short-lived ^{77m}Se (half-life = 17.4 s) nuclide can also be used for Se determinations. It can be produced by thermal neutron capture from ^{76}Se which has a 10 times higher isotopic abundance but 2.5 times lower cross section than ^{74}Se (Table 3.39). Since the half-life of ^{77m}Se is short, saturation activity can be reached in a short time leading to enhanced sensitivity. The 161.9-keV gamma-ray of ^{77m}Se could be interfered with by the 162.3-keV gamma-ray of ^{116m2}In with a half-life of only 2.18 s (Table 3.40). A decay time of 20 s can eliminate this potential interference. It should be noted here that In is rarely detected in biological materials such as foods and diets.

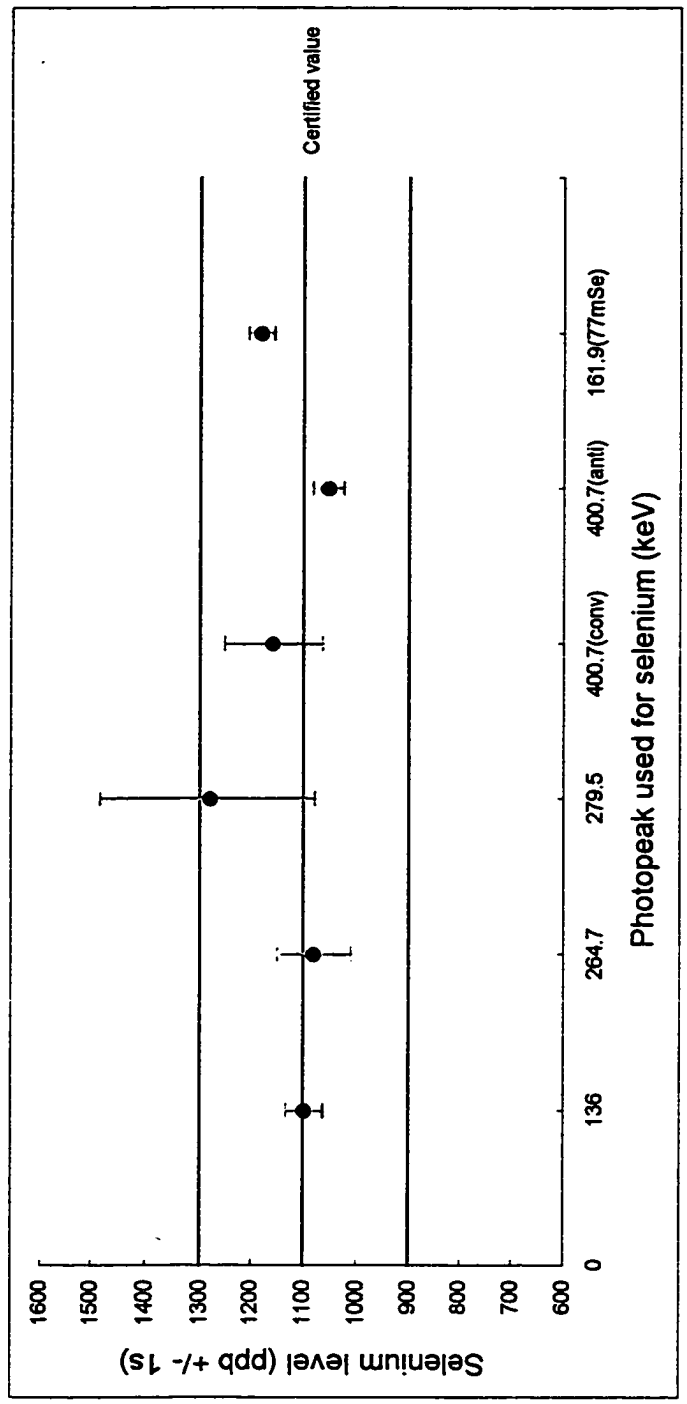

Fig. 3.45. Precision of selenium determination using various nuclides and photopeaks as well as counting modes in Wheat Flour (NIST SRM 1567a).

The use of ^{77m}Se nuclide in routine INAA can considerably reduce the total experimental time and cost. Although the conventional INAA procedure involving an one-shot irradiation-decay-counting scheme can be used, precision and detection limit can be significantly improved by using cyclic INAA (CINAA) and Pseudo-Cyclic INAA (PCINAA). Several INAA, CINAA, and PCINAA methods have earlier been developed in this laboratory for the determination of ppb levels of Se [18,19,142-147] in a variety of matrices.

The 161.9-keV γ-ray of ^{77m}Se is not coincident with other γ-rays, and should be suitable for anticoincident counting. At low count rates (*e.g.* dead time <6%), the PERF of the 161.9-keV peak was measured as 0.98 ± 0.04 (Table 3.11). Therefore, the counts in the peak area will not be reduced by anticoincidence counting while some of the background activities arising from the Compton scattered events can be suppressed. A partial gamma-ray spectrum of NIST Bovine Liver (SRM 1577b) presented in Fig. 3.46 shows that the background can be suppressed by a factor of 3.5. This factor was found to vary between 3 and 5 for the RMs listed in Table 3.48.

All samples and standards were irradiated in the inner pneumatic irradiation sites of the DUSR facility at a thermal flux of 5×10^{11} cm^{-2} s^{-1}. The selection of timing parameters, namely the irradiation time (t_i), decay time (t_d), counting time (t_c), and the number of cycles (n) depended mainly on the sample matrix and the major elements present. A number of RMs and food samples were analyzed using t_i of 30 s, t_d of 10 to 50 s, t_c of 20 to 60 s, and n of up to 5. The

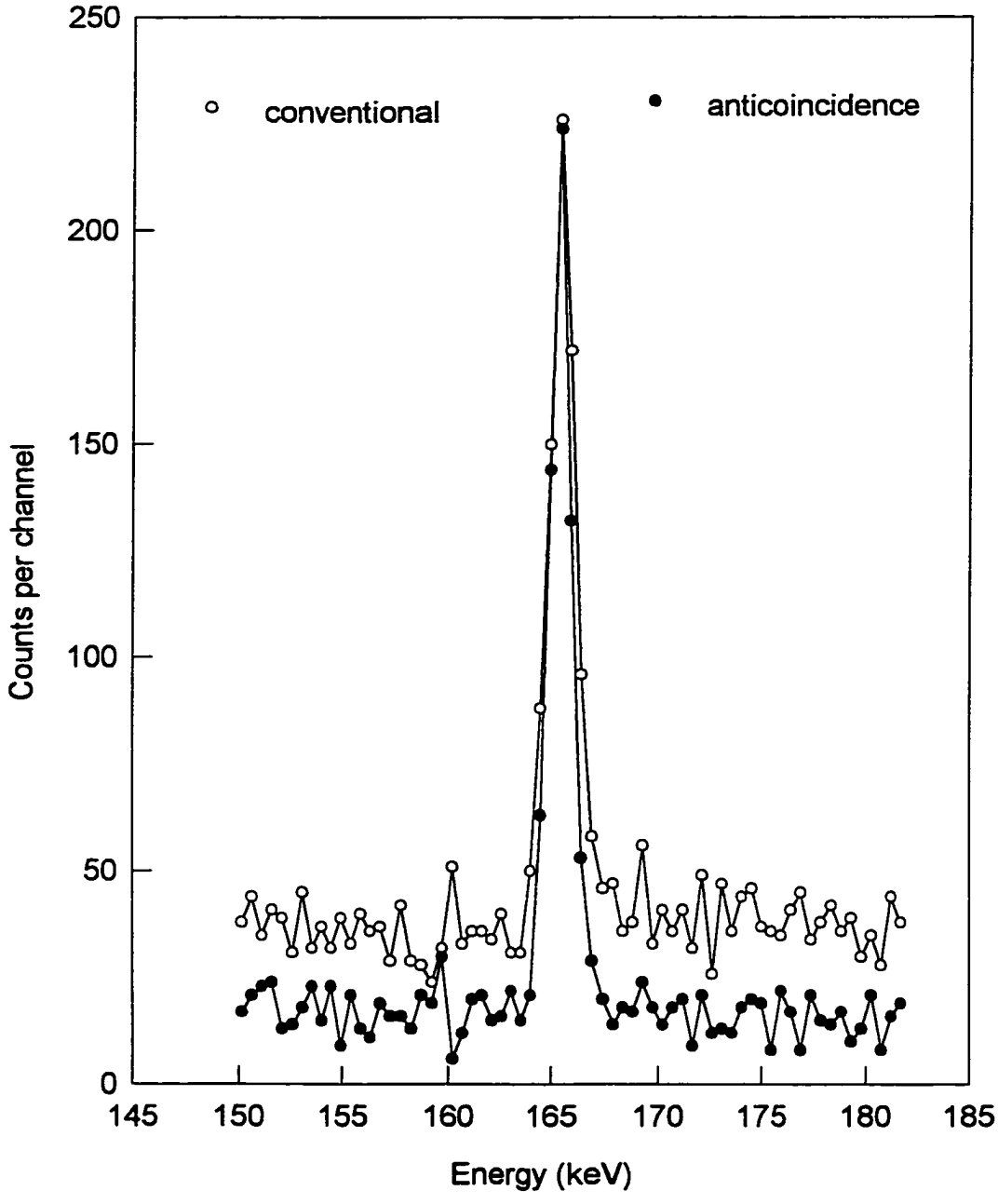

Fig. 3.46. Gamma-ray spectra near the 161.9 keV peak of ^{77m}Se in Bovine Liver (NIST SRM 1577b) using conventional and anticoincidence spectrometry.

161.9-keV gamma-ray of ^{77m}Se was used for assaying Se and it was free from interference under the experimental conditions employed.

3.6.2.1 Selection of Experimental Parameters

Several parameters were first evaluated then optimized for measuring Se levels. The geometry factors, namely the relative position of the NaI(Tl) annulus with respect to the HPGe detector and the distance of the sample from the HPGe detector surface, affecting the anticoincidence counting efficiency were investigated. Experiments were carried out to find the optimum position of the NaI(Tl) annulus with respect to the HPGe detector using a standard source of ^{137}Cs as described in detail in section 3.1.2. The best peak-to-Compton plateau was obtained over a range of 9.5-12.5 cm annulus distance which is position No. 1 (Fig. 2.3). Several samples of IAEA Horse Kidney (RM H-8) were irradiated at the DUSR facility and counted at various distances for this purpose. The source was counted at 0.1 to 4 cm from the surface of the HPGe detector keeping the NaI(Tl) annulus fixed at the position No. "1". The results are graphically presented in Fig. 3.47. It is evident that a linear relationship exists between the RSD and the sample distance. The lowest RSD for the Horse Kidney (H-8) samples was 5.16% at a distance of 0.1 cm from the detector surface, and the sensitivity of the 161.9-keV peak of ^{77m}Se at this position had the highest value of 1789 counts/μg (Table 3.44). The annulus position No. "1", and the sample to HPGe detector distance of

Table 3.44. Effect of counting geometry on standard deviation for selenium in IAEA Horse Kidney (RM H-8).

Sample distance from HPGe detector (cm)	^{77m}Se (162-keV peak) sensitivity (C/μg)	Se content, ppm ± SD N = 6	RSD (%)
0.1	1789 ± 93	4.75 ± 0.25	5.16
1	1112 ± 84	4.99 ± 0.38	7.64
2	959 ± 80	5.11 ± 0.43	8.48
3	652 ± 72	4.97 ± 0.55	11.02
4	387 ± 48	5.46 ± 0.68	12.37

Experimental conditions: t_i = 30 s, t_d = 20 s, t_c = 40 s.

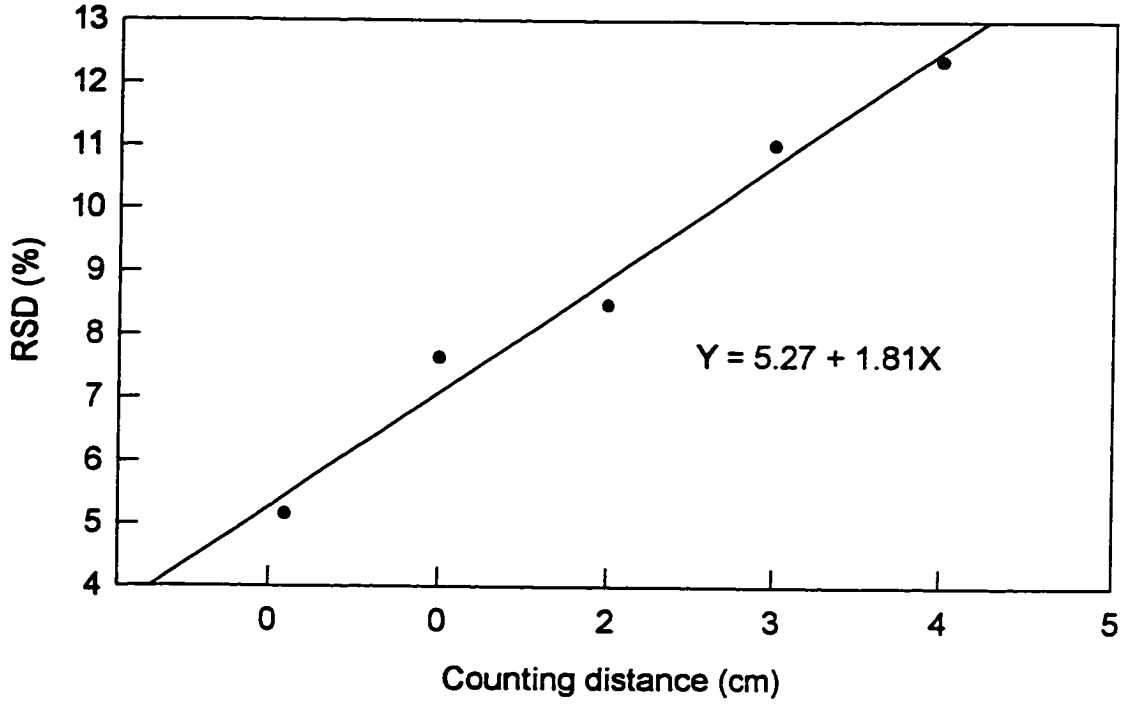

Fig. 3.47. Effect of counting distance on RSD for ^{77m}Se in IAEA Horse Kidney (RM H-8).

0.1 cm were used in subsequent experiments.

The effect of decay time on the RSD for Se was evaluated by analyzing 6 samples of IAEA Horse Kidney. The decay time was varied between 10 and 50 s keeping irradiation and counting times as well as the geometry factors constant. The results are graphically presented in Fig. 3.48. As expected, the RSD of Se levels increased with increasing decay time; the best RSD of 4.09% was obtained for a t_d of 10 s. Thereafter, most analyses were done using a t_d of 10 s. The best sensitivity of about 1800 counts/μg was also obtained at this decay time as shown in Table 3.45.

The effect of counting time on the RSD for Se was also examined using a marine fish sample collected by Health Canada. This fish sample was used because of its higher NaCl content compared to IAEA Horse Kidney. The irradiated samples of fish were counted for 20 to 60 s keeping all other factors constant. The results are graphically presented in Fig. 3.49. The best RSD of 4.68% was obtained at t_c of 40 s. Although the highest sensitivity of about 2000 counts/μg can be obtained at a t_c of 60 s, the RSD increases to 6.01% (Table 3.46). For this reason, almost all samples were analyzed using a t_c of 40 s.

It has been discussed in section 3.3.2 that AFOM terms can be conveniently used for the optimization of number of cycles in PCINAA using anticoincidence counting. In order to evaluate the applicability of AFOM to the determination of Se, Whole Egg Powder (NIST RM 8415) was analyzed using t_i =

Table 3.45. Effect of decay time on standard deviation for selenium in IAEA Horse Kidney (RM H-8).

Decay time (s)	^{77m}Se (162-keV peak) sensitivity (C/μg)	Se content, ppm ± SD N = 6	RSD (%)
10	1801 ± 71	4.93 ± 0.20	4.09
20	1146 ± 58	4.72 ± 0.27	5.75
30	811 ± 45	4.68 ± 0.29	6.20
40	548 ± 26	5.03 ± 0.33	6.55
50	385 ± 24	4.85 ± 0.32	6.63

Experimental conditions: t_i = 30 s, t_c = 40 s.

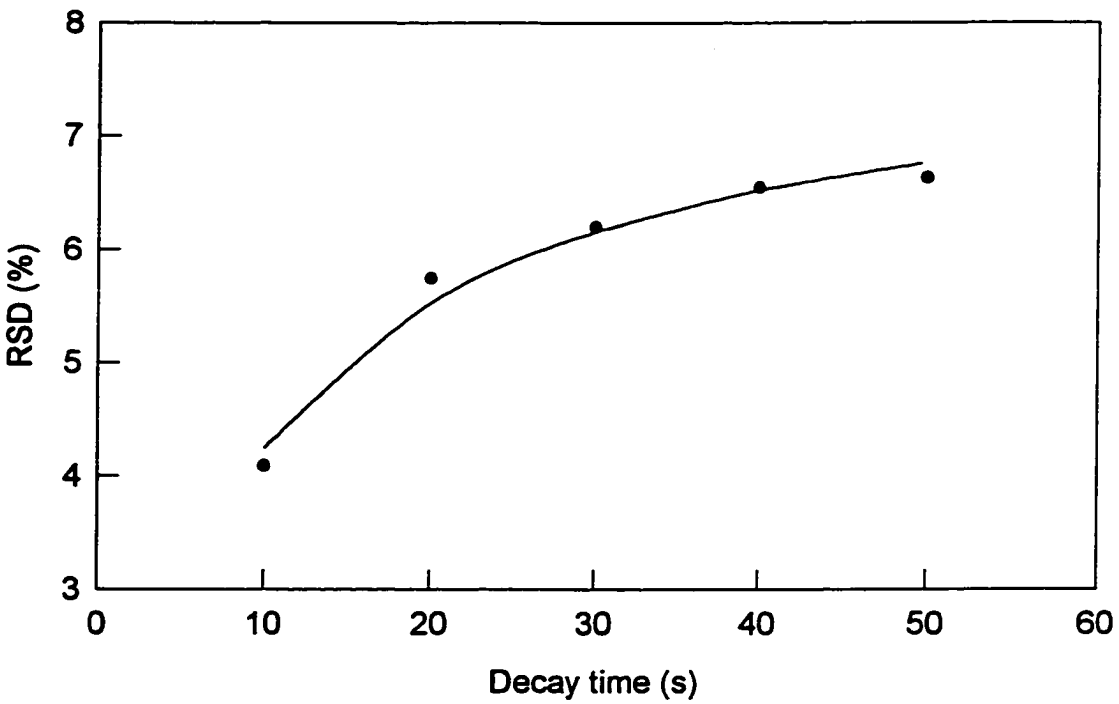

Fig. 3.48. Effect of decay time on RSD for ^{77m}Se in IAEA Horse Kidney.

Table 3.46. Effect of counting time on standard deviation for selenium in a marine fish sample.

Counting time (s)	^{77m}Se (162-keV peak) sensitivity (C/μg)	Se content, ppm ± SD N = 4	RSD (%)
20	1125 ± 61	1.29 ± 0.08	6.13
30	1643 ± 82	1.20 ± 0.07	5.70
40	1801 ± 72	1.21 ± 0.06	4.68
50	1956 ± 96	1.31 ± 0.07	5.06
60	2001 ± 198	1.24 ± 0.07	6.01

Experimental conditions: t_i = 30 s, t_d = 10 s.

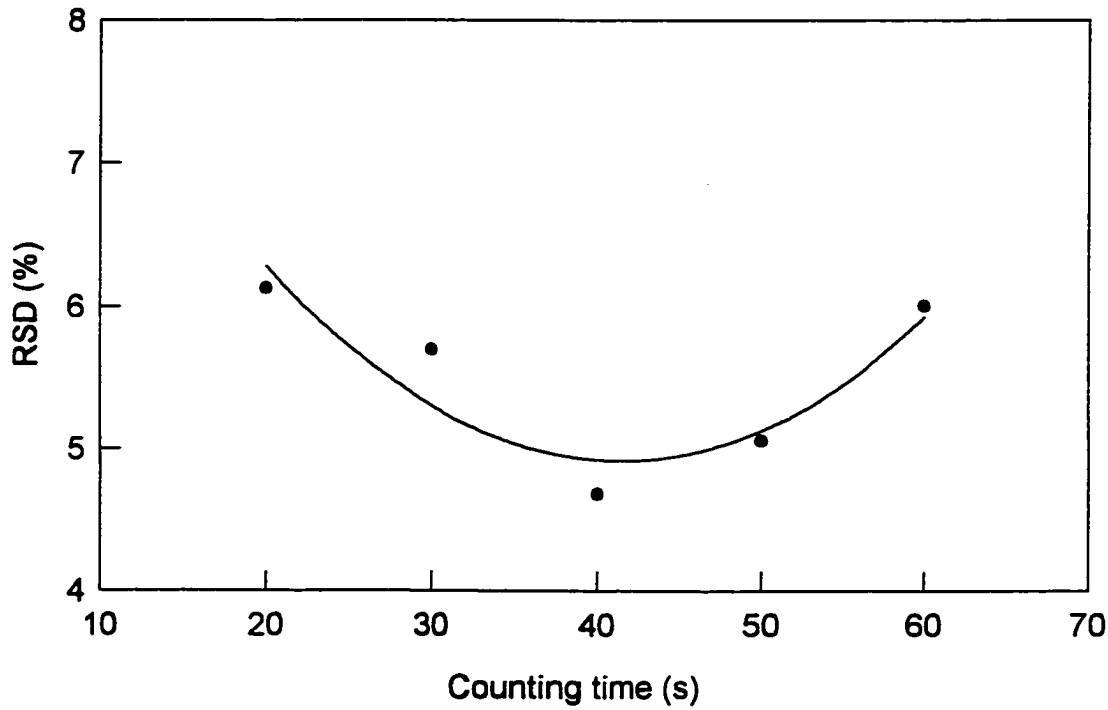

Fig. 3.49. Effect of counting time on RSD for ^{77m}Se in a marine fish sample.

30 s, t_d = 10 s and t_c = 40 s, and counted by both anticoincidence and conventional counting modes. The delay time (t_d,) between two cycles was 24 h. The corresponding detection limits, *i.e.* MDA_{anti} and MDA_{conv}, at each cycle were calculated using equation 3.16; the AFOM terms of each cycle were also calculated according to the method described in section 3.2. The AFOM and MDA values are given in Table 3.47; the variation of MDA and AFOM values with the number of cycles are graphically presented in Fig. 3.50.

For the 161.9-keV peak of ^{77m}Se, both MDA_{anti} and MDA_{conv} decrease with increasing number of cycles, as shown in Table 3.47 and Fig. 3.50. The rate of decrease is greater for MDA_{anti} compared to MDA_{conv}. The rate of improvement in MDA_{anti} appears to slow down beyond the fourth cycle due to the build-up of background activities from nuclides such as ^{38}Cl and ^{56}Mn present in the irradiated samples. As a result, the difference between the MDA_{anti} and MDA_{conv} values becomes smaller with increasing number of cycles. Consequently, the AFOM term starts with a low value in the first cycle then increases with increasing number of cycles, and passes through a maximum at the fourth cycle before starting to decrease. Hence, the optimal number of cycles (n) should be 4.

In summary, the experimental conditions selected for Se analysis using the short-lived nuclide ^{77m}Se were: Irradiation time of 30 s, decay time of 10 s, counting time of 40 s, 4 cycles, NaI(Tl) annulus position of "1", and a sample to HPGe detector distance of 0.1 cm.

Table 3.47. Comparison of detection limits and AFOM factors for ^{77m}Se in Whole Egg Powder (NIST RM 8415) using conventional and anticoincidence counting.

No. of Cycles	MDA_{anti}	MDA_{conv}	AFOM
1	0.052	0.078	2.37
2	0.033	0.062	3.59
3	0.026	0.057	4.73
4	0.025	0.058	5.60
5	0.023	0.050	4.88

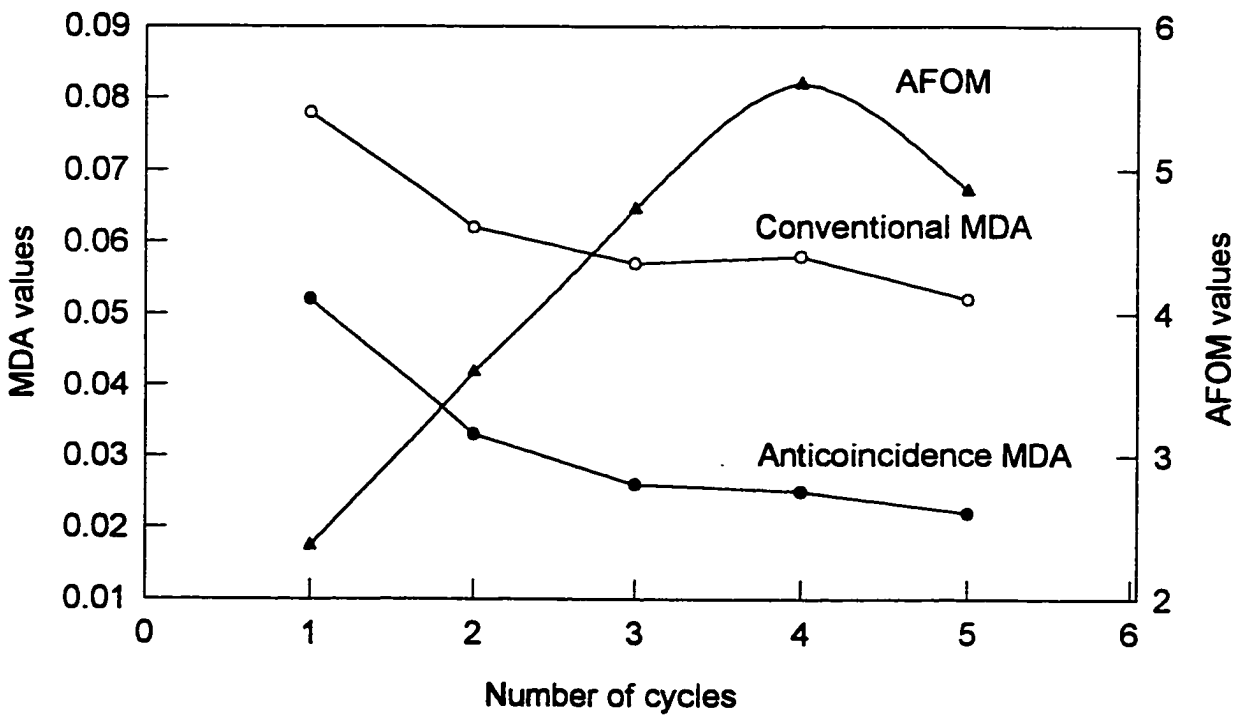

Fig. 3.50. Variation of minimum detectable activity (MDA) and AFOM values with the number of cycles for ^{77m}Se.

3.6.2.2 Quality Assessment

Because of the nutritional significance of Se, a large number of food and diet samples are being analyzed for this element in our and other laboratories. It is important that the Se levels be measured under an extensive quality assurance program. Several publications, such as [148-156], have emphasized the need to maintain a rigorous quality assurance program in an analytical laboratory. Quality assessment and quality control are the two components of quality assurance [153]. Quality assessment is the mechanism employed to verify that the analytical procedure being used is operating within well-defined and acceptable limits. Internal quality assessment deals with the day-to-day precision of measurements of an analyte(s) within a single laboratory, whereas external quality assessment evaluates the accuracy of the results. Both internal and external quality assessments of Se measurements in foods and diets by PCINAA using conventional and anticoincidence gamma-ray spectrometry are described here.

Internal quality assessment was done using a number of steps. The samples and standards were irradiated in an inner site of the Dalhousie University SLOWPOKE-2 Reactor at a total flux of either 5 or 10 x 10^{11} cm^{-2} s^{-1}. The homogeneity, stability, reproducibility and mapping of the neutron flux were carried out in each of the sites [95,96]. The mass of sample, irradiation, decay, counting and transfer times, and number of cycles were optimized for the best AFOM. The 161.9-keV gamma-ray of ^{77m}Se was used for assaying Se and was free from

interference under the experimental conditions employed. Selenium comparator standards were prepared by directly pipetting a known aliquot of ultrapure Se atomic absorption standard solution (Spex Chemicals) by a calibrated Eppendorf pipette onto a sucrose matrix. The Se content of the blank was measured. The comparator standards were of identical geometry and contained approximately similar amounts of Se as the samples. Control charts were constructed. One such chart for 18 analyses is shown in Fig. 3.51. It is clear that most measurements were within $\pm$ 1s, and all were within $\pm$ 2s.

External quality assessment was carried out by various means. The half-life of ^{77m}Se in the real samples was randomly measured. An average value of 17.5 s obtained in this work agrees very well with the literature value of 17.4 s indicating no interference from either ^{116m2}In or the matrix.

A number of RMs and SRMs of biological origin and of a wide range of Se content were analyzed by the PCINAA-anticoincidence method developed in this work. The laboratory means of at least 5 replicate measurements of each of these materials are given in Table 3.48 along with their certified or literature values [157]. These values are also shown as a plot in Fig. 3.52. It is evident that both accuracy and precision of the method are very high. It can be concluded that various simple steps can be incorporated in daily experiments to assure the quality of Se measurements. Many of these steps were employed in the present work and found to be very useful and not too time consuming.

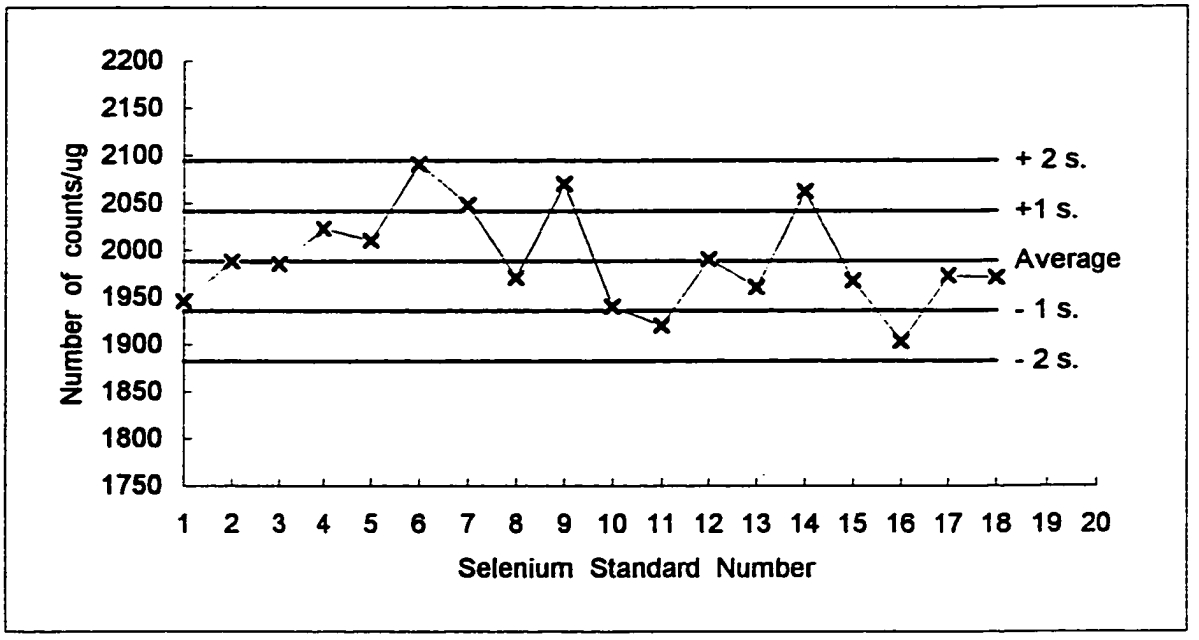

Fig. 3.51. The internal quality assessment chart for selenium using 77m-Se (expressed in terms of standard deviation)

Table 3.48. Concentration of selenium in biological reference materials by PCINAA-anticoincidence gamma-ray spectrometry using short-lived nuclide ^{77m}Se.

Reference material (* IAEA, all others NIST)	This work (ppb)	Certified, [literature] value (ppb)
Corn Starch (RM 8432)	<5	----
Spinach (SRM 1570)	41 ± 9	[40 ± 14]
Corn Bran (RM 8433)	44 ± 4	45 ± 8
Apple Leaves (SRM 1515)	51 ± 7	50 ± 9
Pine Needles (SRM 1575)	59 ± 18	
Soft Wheat Flour (RM 8438)	80 ± 4	76 ± 9
Non-Fat Milk Powder (SRM 1549)	115 ± 9	110 ± 10
Peach leaves (SRM 1547)	145 ± 13	120 ± 9
Animal Blood (RM A-13)*	200 ± 17	240 ± 80
Animal Muscle (RM H-4)*	350 ± 24	280 ± 30
Rice Flour (SRM 1568a)	370 ± 12	380 ± 40
Hard Wheat Flour (RM 8437)	580 ± 38	560 ± 39
Bovine Liver (SRM 1577b)	710 ± 11	730 ± 60
Wheat Flour (SRM 1567a)	1180 ± 25	1100 ± 200
Durum Wheat Flour (RM 8436)	1235 ± 15	1230 ± 90
Whole Egg Powder (RM 8415)	1370 ± 25	1390 ± 170
Wheat Gluten (RM 8418)	2555 ± 14	2580 ± 190
Horse Kidney (RM H-8)*	4720 ± 36	4670 ± 300

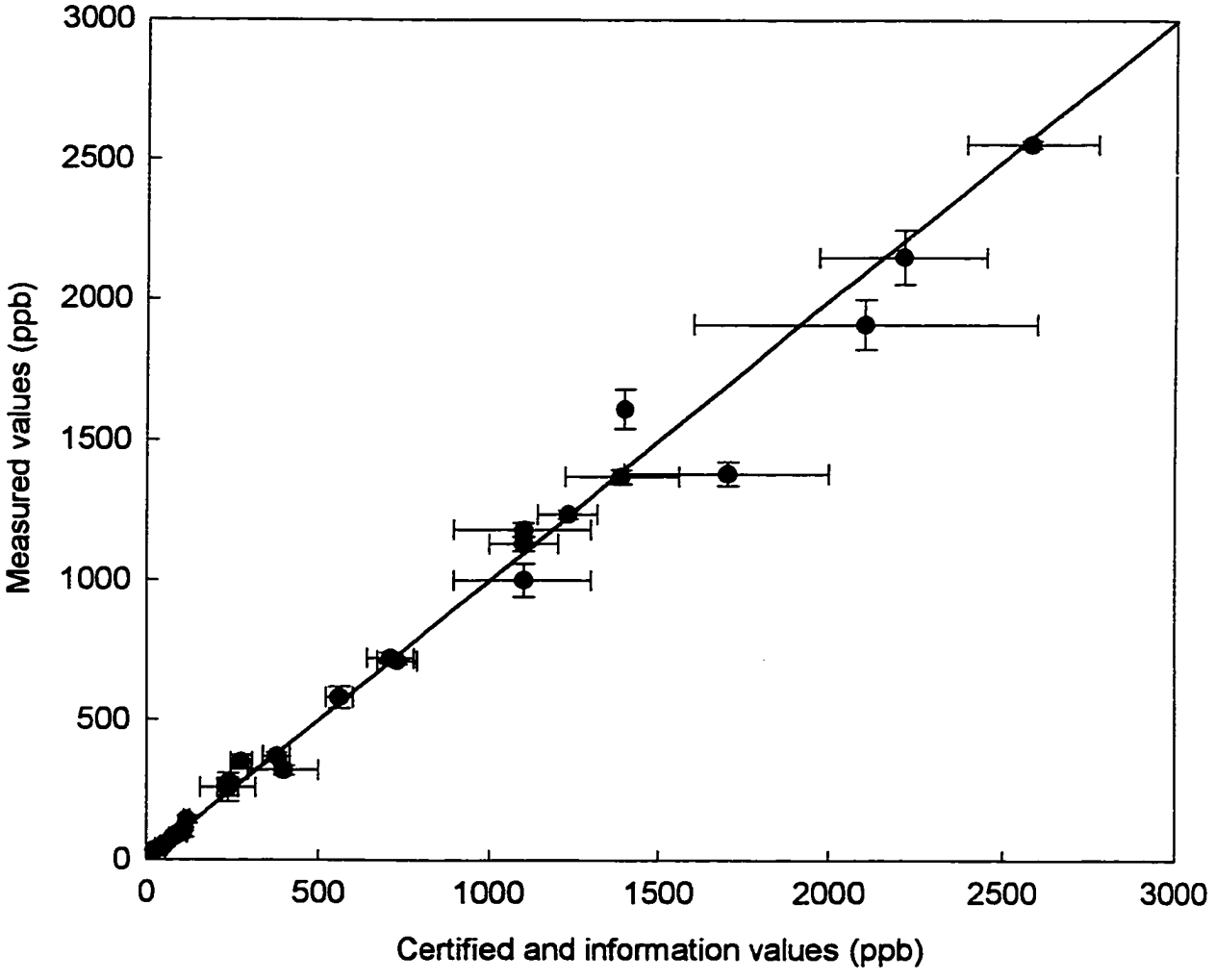

Fig. 3.52. External quality control chart for selenium using the 161.9 keV peak of ^{77m}Se and anticoincidence spectrometry.

This method of Se determination using short-lived nuclide and anticoincidence gamma-ray spectrometry has been applied to 6 food samples collected by Health Canada [158]. The results for replicate measurements are presented in Table 3.49. The RSD was found to vary between 5 and 8.6%. It is also clear from the table that much of this deviation can be accounted for by the counting statistics.

3.6.2.3 Dead Time Correction

Most anticoincidence counting in NAA has been focused on long-lived nuclides of low count rates [75]. When this technique is applied to short-lived nuclides, the count rate may be high. Therefore, it is necessary to carry out a study of the effect of count rate on PERF.

The data set chosen for this study consisted of conventional, anticoincidence, and coincidence γ-ray spectra of Oyster Tissue (SRM-1566). A sample mass range of 40 to 200 mg was used in order to check different dead times and amounts of Se. For anticoincidence spectra, the dead time ranged from 4.47% to 14.37%. The corresponding range of count rates was 445 to 1434 cps. The net peak areas under the 161.9-keV peak of ^{77m}Se in all three types of spectra were calculated. The PERF value was then calculated and plotted against the dead-time of anticoincidence counting, as shown in Fig. 3.53. Since the 161.9-keV peak is not coincident with other γ-rays, its PERF should remain constant with

Table. 3.49. Selenium levels for various foods and their relative standard deviations.

Sample description with HWC code	Se content, ppm ± SD	RSD (%)	Number of measurement	Counting statistics (%)
Beef Steak B01	0.601 ± 0.052	8.58	4	6.82 ± 0.74
Organ Meats, Liver & Kidney B10	2.70 ± 0.09	3.48	4	3.28 ± 0.08
Fish, Marine, Fresh or Frozen D01	1.22 ± 0.07	5.80	4	5.69 ± 0.12
Rice Flour F21	0.465 ± 0.023	4.96	4	5.02 ± 0.29
Mushroom, Canned G12	0.261 ± 0.061	23.4	3	28.8 ± 4.4
Seeds, Shelled J10	0.628 ± 0.053	8.47	3	7.75 ± 0.70

Experimental conditions: t_i = 30 s, t_d = 10 s, t_c =40 s.

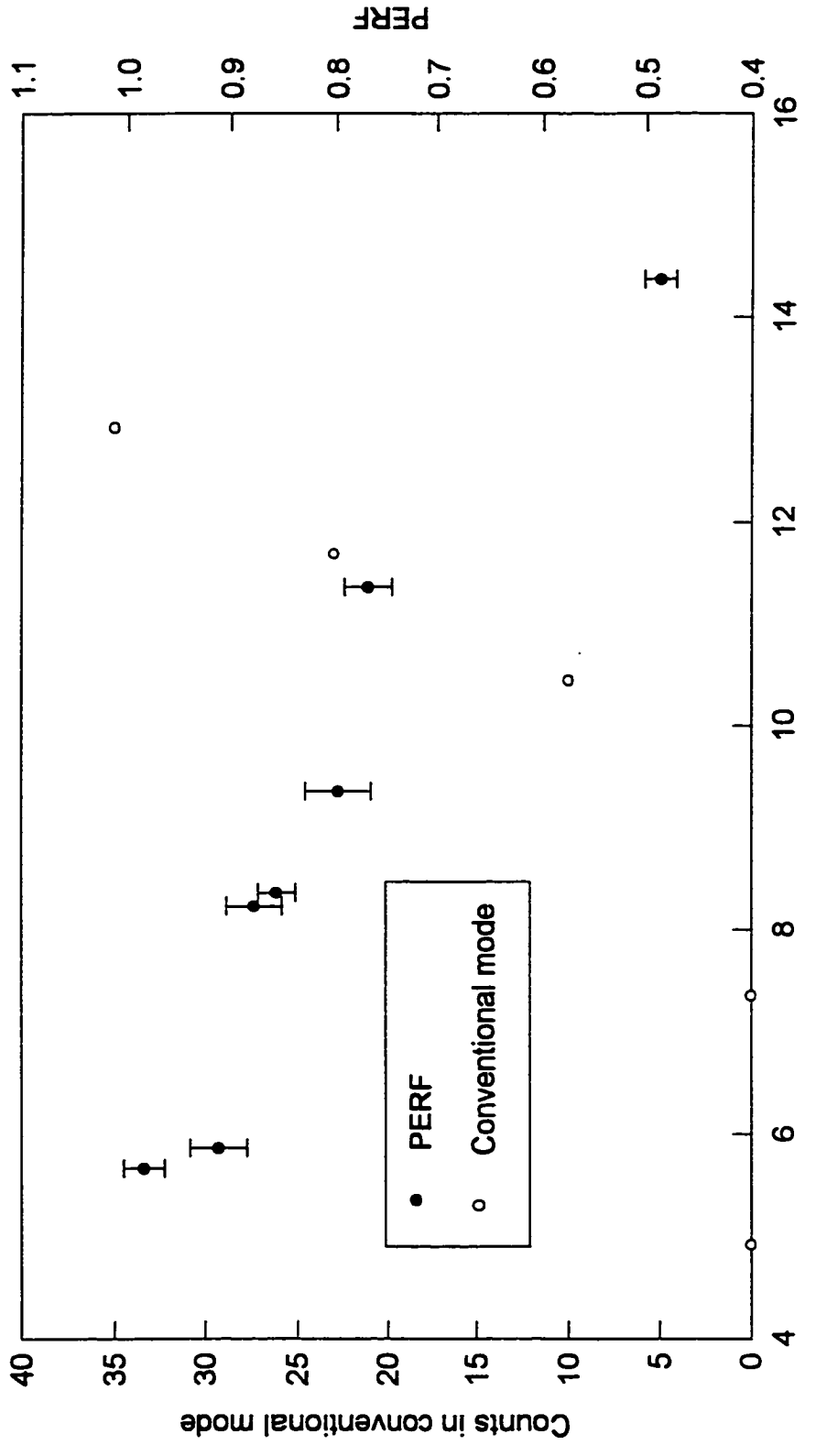

Fig. 3.53. The effect of random coincident events on the 161.9 keV peak of ^{77m}Se.

dead time. However, as shown in Fig. 3.53, the PERF decreased from 0.98 to 0.49 with dead time increasing from 4.47% to 14.37%. The net peak area in the coincidence counting mode is also plotted against the dead time in the same figure (3.53). Theoretically, the peak area of the 161.9-keV gamma-ray in coincidence counting mode should be zero since there are no coincidence events except the accidental events. However, as shown in Fig. 3.53, the curve starts at zero at low dead time and increases with the increasing dead time.

These results suggest that at low count rates accidental coincident loses are insignificant, while at high count rates these events cannot be neglected. Therefore, a calibration plot for quantitative Se determination at varying count rates by anticoincidence spectrometry needs to be constructed. This plot is shown in Fig. 3.54, and was done by analyzing different amounts of Oyster Tissue (NIST SRM 1566). The points on the straight line represent the 161.9-keV peak area counts calculated theoretically using sensitivity and the amount of Se in the sample. On the other hand, the points on the curve are the actual measured 161.9-keV peak area counts. The ratio of these two counts gives the calibration factor at each dead time. This calibration factor was applied to IAEA Horse Kidney and Animal Blood, as well as NIST Whole Egg Powder and Oyster Tissue RMs. Both uncorrected (*i.e.* measured) and corrected values using the correction factor from Fig. 3.54 are given in Table 3.50. It is obvious that higher the dead time, larger is the correction factor. The measured values were also corrected for dead time using equation 3.25, and the values are included in Table 3.50. Although this

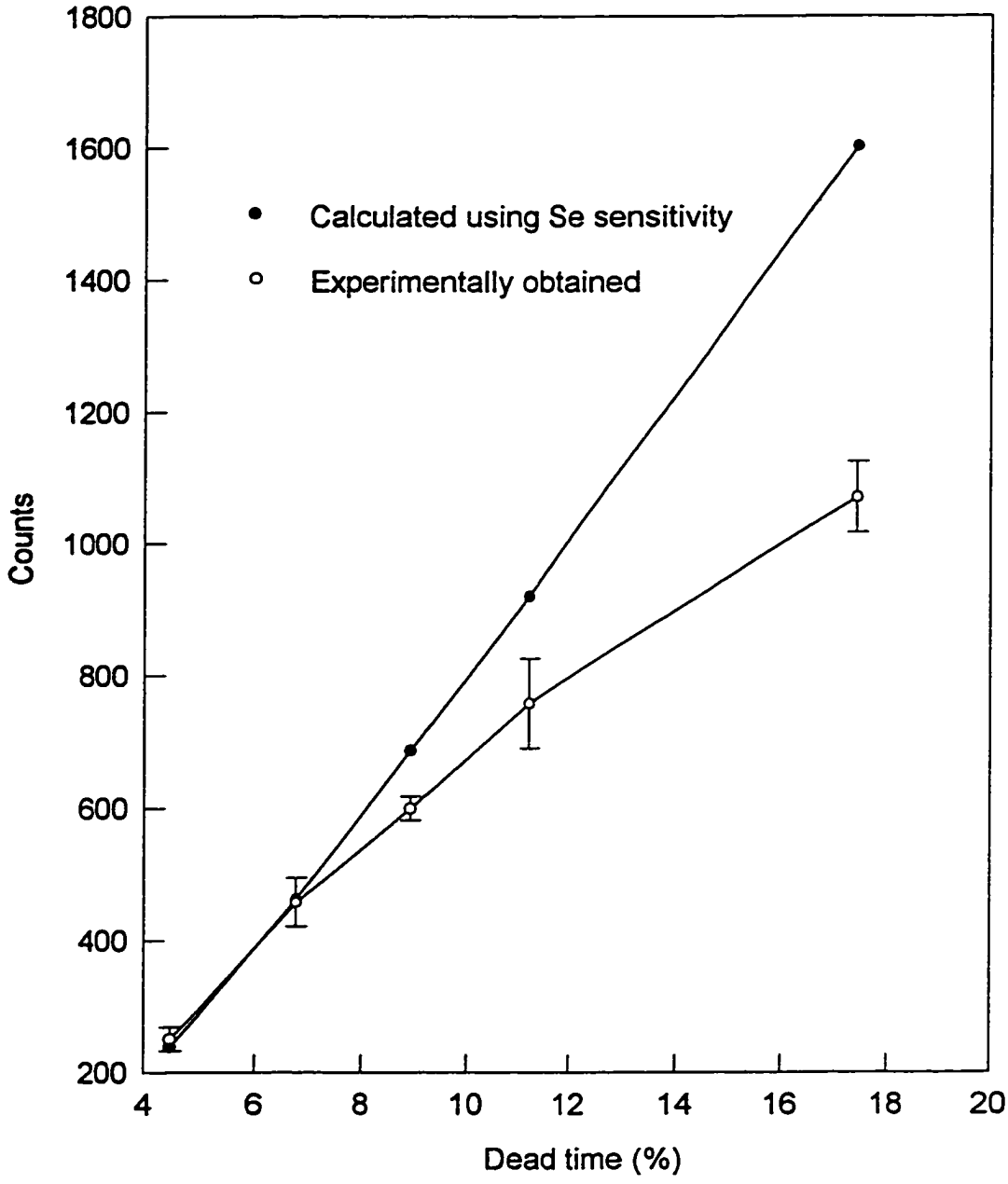

Fig. 3.54. Dead time calibration curve for selenium determination using ^{77m}Se.

Table 3.50. Dead time correction for selenium determination by anticoincidence gamma-ray spectrometry.

Reference materials	Uncorrected values in ppb (% dead time)	Corrected values in ppb (equation 4.23)	Corrected values in ppb (correction factor)	Certified values in ppb
Horse Kidney (IAEA RM H-8)	4000 (8.28%)	4170	4720 (1.18)	4670 ± 300
Animal Blood (IAEA RM A-13)	170 (8.36%)	180	200 (1.20)	240 ± 80
Whole Egg Powder (NIST RM 8415)	1125 (9.36%)	1190	1370 (1.22)	1390 ± 170
Oyster Tissue (NIST SRM 1566)	1725 (11.25%)	1840	2240 (1.3)	2100 ± 500

equation appears to work well in conventional spectrometry and anticoincidence spectrometry with low dead time, it is not that reliable at higher dead times. The best agreement between the certified values and the corrected values are achieved using the calibration curve (Fig. 3.54) as shown in Table 3.50.

A number of RMs were analyzed for Se by both anticoincidence and conventional gamma-ray spectrometry. The detection limits for Se in these materials in both counting modes were calculated and are presented in Table 3.51 along with the dead time. It is evident that the application of anticoincidence spectrometry can improve detection limits by a factor of 2 to 4 and reduce the dead time by a factor about 1.2 to 1.4, depending on the type of material. Consequently, the anticoincidence counting can provide a more reliable measurement of ^{77m}Se through the 161.9-keV peak by minimizing errors that may arise form the higher dead time.

Table 3.51. Comparison of detection limits for selenium in reference materials by anticoincidence and conventional counting modes.

Reference material (*IAEA, all others NIST)	Anticoincidence mode		Conventional mode	
	Dead time (%)	Detection limit (μg)	Dead time (%)	Detection limit (μg)
Corn Starch (SRM 8432)	2.44	2.3×10^{-3}	2.51	4.3×10^{-3}
Soft Wheat Flour (SRM 8438)	2.68	4.7×10^{-3}	3.33	9.2×10^{-3}
Corn Bran (SRM 8433)	2.75	3.5×10^{-3}	2.87	7.4×10^{-3}
Bovine Liver (SRM 1577b)	5.66	9.1×10^{-3}	6.87	1.3×10^{-2}
Peach Leaves (SRM 1547)	5.86	5.2×10^{-3}	7.49	1.1×10^{-2}
Apple Leaves (SRM 1515)	6.76	2.5×10^{-3}	8.11	7.6×10^{-3}
Not-Fat Milk Powder (SRM 1549)	7.54	7.3×10^{-3}	9.67	9.4×10^{-3}
Animal Muscle (RM H-8)*	8.28	1.3×10^{-2}	9.85	1.9×10^{-2}
Animal Blood (RM A-13)*	8.36	8.3×10^{-3}	11.31	1.3×10^{-2}
Whole Egg Powder (SRM 8415)	9.36	7.4×10^{-3}	11.9	1.6×10^{-2}
Pine Needles (SRM 1575)	10.97	3.6×10^{-3}	13.79	1.5×10^{-2}
Spinach (SRM 1570)	14.37	2.9×10^{-3}	17.54	1.3×10^{-2}

4. CONCLUSIONS AND RECOMMENDATIONS

Instrumental neutron activation analysis (INAA) is a well-established analytical technique for the simultaneous determination of multielement concentrations in a variety of sample matrices. One of the problems generally encountered in INAA is the high background activity arising from the scattering of photons, a phenomenon known as the Compton effect. Improved detection limits could be obtained for some elements if the Compton continuum is suppressed. The principal objective of this work was to develop INAA methods in conjunction with anticoincidence gamma-ray spectrometry for improving the detection limits of a number of elements of interest in biological materials.

The anticoincidence gamma-ray spectrometer available at the Dalhousie University SLOWPOKE-2 Reactor (DUSR) facility consists of a high-resolution HPGe detector surrounded by a 10" x 10" NaI(Tl) annulus and a 3" x 3" NaI(Tl) plug. Its performance was evaluated using a ^{137}Cs standard source. The spectrometer has a peak-to-Compton plateau ratio of 582, a peak-to-Compton edge ratio of 410, and a peak-to-total area ratio of 0.17. These values are comparable to other such spectrometers available in a few laboratories around the world.

The background suppression ratio (BSR), *i.e.* the ratio of background counts by conventional gamma-ray spectrometry to that by anticoincidence

spectrometry, were measured for gamma-ray energies between 80 and 2000 keV using a mixed source of ^{152}Eu and ^{154}Eu. The highest values of BSR of about 6 were obtained at 300-1100 keV region where many of the gamma-rays from neutron activation products occur. The value of BSR was about 4 beyond this region.

The geometry factors, namely the distance of the sample from the HPGe detector surface and the relative position of the NaI(Tl) annulus with respect to the HPGe detector, were studied in detail using a home-made attachment for varying the distances. Both cascading and non-cascading standard gamma-ray sources were used in order to obtain the highest anticoincidence counting efficiency of the nuclides of interest.

In the past, much of the studies on INAA employing anticoincidence gamma-ray spectrometry focused either on a few selected elements, long-lived nuclides, or on a specific area of application. In this thesis, a systematic investigation was carried out on the merits and limitations of anticoincidence counting for the nuclides which are most commonly used in NAA. Short-lived nuclides (half-life < 120 s) were studied using both conventional INAA procedure as well as a technique called pseudo-cyclic INAA (PCINAA). The list of short-lived nuclides included: ^{108}Ag, ^{110}Ag, ^{165m}Dy, ^{20}F, ^{75m}Ge, ^{179m}Hf, ^{86m}Rb, ^{46m}Sc, ^{77m}Se, and ^{177m}Yb. Medium-lived nuclides (half-life < 3 h) which are commonly used in NAA, namely ^{28}Al, ^{139}Ba, ^{80}Br, ^{38}Cl, ^{66}Cu, ^{165}Dy, ^{128}I, ^{27}Mg, ^{56}Mn, ^{65}Ni, ^{233}Th, ^{51}Ti, and ^{52}V, were also investigated using anticoincidence counting and conventional INAA. The

long-lived nuclides (half-life > 12.5 h) of interest in the present study were: ^{76}As, ^{198}Au, ^{82}Br, ^{141}Ce, ^{51}Cr, ^{60}Co, ^{59}Fe, ^{197}Hg, ^{203}Hg, ^{42}K, ^{140}La, ^{24}Na, ^{147}Nd, ^{86}Rb, ^{122}Sb, ^{46}Sc, ^{182}Ta, ^{160}Tb, ^{187}W, ^{175}Yb, ^{69m}Zn, and ^{65}Zn.

The benefits of anticoincidence counting are frequently described by the peak efficiency reduction factor (PERF) of the nuclide of interest. Experiments were done in this thesis to calculate the PERF values of major gamma-rays of the above nuclides. The results showed that about 70% of the nuclides studied had no peak efficiency reduction in anticoincidence spectrometry. The improvement for a photopeak with a PERF value between 1 and 0.1 depends on the extent of background suppression and the original peak-to-background ratio. Both of these factors, in turn, depend on the concentrations of the element of interest and of the major or interfering elements in the sample.

An attempt was made in this thesis to define an "analytical figure of merit (AFOM)" term for assessing the practical advantages of anticoincidence counting. This term included parameters such as resolution, peak area, background around the peak, dead time, counting time, and counting statistics which vary with changes in sample matrix activity. The AFOM term was mathematically defined as the minimum detectable activity ratio squared. The effectiveness of the AFOM terms was evaluated by analyzing a number of biological reference materials of diverse types of matrix and varying amounts of major and interfering elements. The variation of AFOM with dead time was investigated. It was concluded that, in most cases, the AFOM terms were very

useful in predicting the advantages of anticoincidence counting.

Several elements were studied in detail. Their concentrations in 16 biological reference materials were determined; precision and accuracy were evaluated using control charts; and detection limits in each of these materials were calculated.

In order to realize the full potential of the anticoincidence system, several recommendations are made in the following paragraphs. One of the major disadvantages of anticoincidence counting is the suppression of full-energy peaks of coincident gamma-ray emitting nuclides. This leads to a reduction of sensitivity when an element is determined through these gamma-rays. This problem can be overcome by adding a windows coincident counting mode into the present system. This renovation can be simply realized by setting a particular energy region on the NaI(Tl) annulus, which is defined by the LLD and ULD through a single channel analyzer. In the windows coincident counting mode, one of the coincident gamma-rays can be selectively measured by adjusting this particular energy region over the NaI(Tl) annulus to its energy region and used as a coincident gating signal for the ADC of HPGe detector measuring only the other coincident gamma-rays. When the system is operated in the window coincidence counting mode, these coincident gamma-rays can be selectively measured with a substantial rejection of background signals. The proposed system can be applied to cases where the nuclides decay with cascade gamma-rays.

Another addition which is suitable for coincident gamma-ray emitting

nuclides can be achieved by coupling a well-type Ge detector with the present NaI(Tl) annulus in the anticoincidence counting mode. It will be possible to better detect and use sumpeaks. This process can be enhanced when a sample is placed in the well-type detector because the rate of summing energy depends principally on the solid angle in a sample to detector geometry configuration. It is interesting to note that the efficiency of the sumpeak in anticoincidence spectrometry is unaffected because of the way it is generated. The measurement quality of a sumpeak will be further improved by the background suppression by incorporating a well-type detector in the present NaI(Tl) annulus.

Because of the complex electronics for gating and timing required in anticoincidence spectrometry, it usually has a higher dead time compared to the conventional spectrometry, even at the same sample activity. The advantage of anticoincidence counting is mainly restricted by the high dead time, in particular when applied to short- and medium-lived nuclides where high count rates are generally encountered. This is because the full-energy peak may suffer from a loss of peak efficiency; the background suppression efficiency of anticoincidence counting may be reduced at high dead times. A better performance by anticoincidence counting, particularly at high count rates, could be achieved by coupling the main detector to the anticoincidence shield by fast coincidence circuitry and by using a faster ADC such as one at 200 MHz.

5. REFERENCES

1. G. Hevesy and H. Levi, Math-fys., "The Action of Neutrons on the Rare Earth Elements", Meddr. 14, No. 5, **1936**, 3.

2. D. DeSoete, R. Gijbels, and J.Hoste, "Neutron Activation Analysis", Wiley-Interscience, New York, **1972**.

3. J.C. Laul, "Neutron Activation Analysis of Geological Materials", Atomic Energy Review, 173, **1979**, 603-648.

4. P. Kruger, "Principles of Activation Analysis", Wiley-Interscience, New York, **1971**.

5. F. Adams and R. Dams, "Applied Gamma-ray Spectrometry", Pergamon Press, Oxford, **1970**.

6. "Nuclear Activation Techniques in the Life Science", Proc. Intern. Symp., IAEA, Vienna, Austria, **1978**.

7. "Nuclear Analytical Methods in the Life Science (NAMLS)", Proc. Intern. conf., (i) NAMSL-I, Eds. R. Zeisler and V.P. Guinn, Humana Press, New Jersey, **1990**; (ii) NAMLS-II, Eds. J. Kucera, I. Obrusnik, and E. Sabbioni, Humana press, New Jersey, **1994**.

8. "Measurement, Detection and Control of Environmental Pollutants", Proc. Intern. Symp., IAEA, Vienna, **1976**.

9. "Methods and Application of Radioanalytical Chemistry (MARC)", Proc. Intern. Conf., (i) MARC-I, **1987**; (ii) MARC-II, **1991**; (iii) MARC-III, **1994**; (iv) MARC-IV, **1997**. Papers published in J. Radioanal. Nucl. Chem.

10. "Nuclear Analytical Chemistry (NAC)", Proc. Intern. Conf., (i) NAC-I, **1985**; (ii) NAC-II, **1992**. Papers published in J. Radioanal. Nucl. Chem.

11. "Modern Trends in Activation Analysis (MTAA)", Proc. Intern. Conf., (i) MTAA-4, **1972**; (ii) MTAA-5, **1976**; (iii) MTAA-6, **1981**; (iv) MTAA-7, **1986**; (v) MTAA-8, **1991**; (vi) MTAA-9, 1995. Papers published in J. Radioanal. Nucl. Chem.

12. "International Conference on Application of Activation Analysis (ICAAA)", Academica Sinica, Beijing, **1990**. Papers published in J. Radioanal. Nucl. Chem.

13. "Harmonization of Health Related Environmental Measurement using Nuclear and Isotopic Techniques", Proc. Intern. Symp., IAEA, **1997** (in press).

14. O.U. Anders, Nucl. Instr. and Meth., 68, **1969**, 205.

15. N.M. Spyrou, K. Ingle, and F. Ozek, Proc. 2nd Intern. Conf. on Nuclear Methods in Environmental Research, J.R. Vogt and W. Meyer, Eds., Univ. of Missouri, Columbia, Mo. **1974**, 151.

16. F. Grass and G.P. Westphal, Nucl. Instr. and Meth., 140, 97, **1977**.

17. A. Chatt, K.N. DeSilva, J. Holzbecher, D.C. Stuart, R.E. Tout, and D.E. Ryan, "Cyclic Neutron Activation Analysis of Biological and Metallurgical Samples", Can. J. Chem., 59, **1981**, 1660.

18. K.N. DeSilva and A. Chatt, "A Method to Improve Precision and Detection Limits for Determining Trace Elements Through Short-Lived Nuclides", J. Trace Microprobe Tech., 1, **1983**, 307.

19. A. Chattopadhyay and K.N. DeSilva, "Pseudo-cyclic Neutron Activation Analysis of Silver, Fluorine, Rubidium, Scandium and Selenium in Biological Materials", Trans. Am. Nucl. Soc., 32, **1979**, 185.

20. R.E. Lapp and H.L. Andrews, "Nuclear Radiation Physics" 4th edn., Englewood Cliffs, New Jersey, **1972**.

21. P.R. Bell, "Scintillation Spectrometer with Improved Response", Science, 120, **1954**, 625-626.

22. J.A. Cooper and R.W. Perkins, "An Anticoincidence-Shielded Dual Ge(Li) Gamma-Ray Spectrometer for Low-Level Environmental Radionuclide Analysis and Gamma-Gamma Coincidence Studies", Nucl. Instr. and Meth., 94, **1971**, 29-38.

23. A.R. Sayres and J.A. Baicker, "The All Germanium Anti-Compton Spectrometer", IEEE Trans. Nucl. Soc., 15, **1968**, 393-396.

24. J.M. Palms, R.E. Wood, and O.H. Puckett, "A Ge(Li) Concentric Duode Spectrometer for Compton Suppression", IEEE Trans. Nucl. Soc., 15, **1968**, 397-406.

25. H. Hick and R. Pepelnik, "Summing Ge(Li)-Compton Spectrometer with High Peak-to-Tail Ratio", Nucl. Instr. and Meth., 68, **1969**, 240-244.

26. V.J. Orphan and N.C. Rasmussen, "A Ge(Li) Spectrometer for Studying Neutron Capture Gamma Rays", Nucl. Instr. and Meth., 48, **1967**, 282-295.

27. R.B. Galloway, "Criteria for Evaluating Background Suppression Techniques in Nuclear Spectroscopy Based on Consideration of Statistical Accuracy", Nucl. Instr. and Meth., 55, **1967**, 29-33.

28. R. Hofstadar and J.A. McIntyre, "Measurement of Gamma-Ray Energies with Two Crystals in Coincidence", Physical Rev., 78, **1950**, 619-620.

29. R.D. Albert, "An Anticoincidence Gamma-Ray Scintillation Spectrometer", Rev. Sci. Instr., 24, **1953**, 1096-1101.

30. K.I. Roulston and S.I.H. Naqvi, "Reduced Compton Effect Scintillation Spectrometer", Rev. Sci. Instr., 27, **1956**, 830-832.

31. R.C. Davis and P.R. Bell, "Response of Total Absorption Spectrometers to Gamma-Rays", IEEE Trans. Nucl. Sci., NS-3, **1956**, 82-86.

32. C.C. Trail, S. Raboy, "Scintillation Spectrometer with an Anticoincidence Annulus of NaI(Tl)", Rev. Sci. Instr., 30, **1959**, 425-429.

33. R.W. Perkins, J.M. Nielson, and R.N. Diebel, "Total Absorption Gamma-Ray Spectrometers Utilizing Anticoincidence Shielding", Rev. Sci. Instr., 31, **1960**, 1344-1349.

34. G. Busuoli, C. Melandri, O. Rimondi, and B. Righini, "A Compton Rejection Gamma-Rays Spectrometer: Utilization of the A.C. Shield as a Well Type Counter", Nucl. Instr. and Meth., 22, **1963**, 324-332.

35. C.O. Bostrom, J.E. Draper, "Anticoincidence Gamma-Ray Spectrometer for Neutron Capture Spectroscopy", Rev. Sci. Instr., 32, **1961**, 1024-1031.

36. A. McG. Beech, J.K. Parry, and D.F. Urquhart, "A Two Crystal Coincidence Gamma Ray Spectrometer Using a Solid State Detector", Nucl. Instr. and Meth., 27, **1964**, 169-171.

37. R.W. Perkins, "An Anticoincidence Shielded-Multidimensional Gamma-Ray Spectrometer", Nucl. Instr. and Meth., 33, **1965**, 71-76.

38. J. Kantele and T. Kohonen, "A Versatile Routing System for Multichannel Analyzers", Nucl. Instr. and Meth., 37, **1965**, 265-267.

39. J. Kantele, O.J. Mastilla, and J. Hattula, "Gamma Spectrometer Systems Employing an Anti-Compton Annulus", Nucl. Instr. and Meth., 39, **1966**, 194-216.

40. A.E. Evans, B. Brown, and J.B. Marion, "Anticoincidence Shielded Gamma-Ray Spectrometer for Nuclear Reaction Studies", Rev. Sci. Instr., 37, **1966**, 991-999.

41. Y. Sever and J. Lippert, "A Compton-Rejection Germanium Spectrometer", Nucl. Instr. and Meth., 33, **1965**, 347-348.

42. J. Kantele and P. Suominen, "A Ge(Li) Gamma Spectrometer Employing an Anti-Compton Mantle of Na(Tl)", Nucl. Instr. and Meth., 41, **1966**, 41-44.

43. N.A. Wogman, D.E. Robertson, and R.W. Perkins, "A Large Detector Anticoincidence Shielded Multidimensional Gamma-Ray Spectrometer", Nucl. Instr. and Meth., 50, **1967**, 1-10.

44. N.A. Wogman, R.W. Perkins, and J.H. Kaye, "An All Sodium Iodide Anticoincidence Shielded Multidimensional Gamma-Ray Spectrometer for Low-Activity Samples", Nucl. Instr. and Meth., 74, **1969**, 197-211.

45. R.L. Auble, D.B. Beery, G. Berzins, L.M. Beyer, R.C. Etherton, W.H. Kelly, and W.C. McHarris, "Coincidence-Anticoincidence Gamma-Ray Spectroscopy with a NaI(Tl) Split Annulus and a Ge(Li) Detector", Nucl. Instr. and Meth., 51, **1967**, 61-71.

46. R.D. Cooper and G.L. Brownell, "A Large Coaxial Ge(Li) Detector with Plastic Anticoincidence Scintillation for Activation Analysis", Nucl. Instr. and Meth., 51, **1967**, 72-76.

47. C.R. Gruhn, J.V. Kane, W.H. Kelly, T. Kuo, and G. Berzins, "A Single Crystal Ge(Li) Compton Spectrometer", Nucl. Instr. and Meth., 54, **1967**, 268-276.

48. W. Michaelis and H. Kupfer, "A High-Resolution Ge(Li) Anti-Compton Spectrometer for Radiative Neutron Capture Spectroscopy", Nucl. Instr. and Meth., 56, **1967**, 181-188.

49. J. Kantele and P. Suominen, "A Simple Summing Compton Ge(Li) Spectrometer", Nucl. Instr. and Meth., 56, **1967**, 351-354.

50. T.K. Alexander, C. Broude, O. Hausser, and J.F. Sharpey-Schafer, "A Pair and Escape-Suppressed Spectrometer Using Ge(Li) and NaI(Tl) Detectors Designed for Accelerator Experiments", Nucl. Instr. and Meth., 65, **1968**, 169-172.

51. D.H. White and R.E. Birkett, "A Ge(Li)-Ge(Li)-NaI(Tl) Coincidence Spectrometer System for (n,γ) Studies", Nucl. Instr. and Meth., 73, **1969**, 260-268.

52. J.A. Cooper and R.W. Perkins, "A Versatile Ge(Li)-NaI(Tl) Coincidence-Anticoincidence Gamma-Ray Spectrometer for Environmental and Biological Problems", Nucl. Instr. and Meth., 99, **1972**, 125-146.

53. S.R. Lewis and N.H. Shafrir, "Low Level Ge(Li) Gamma-Ray Spectrometry in Marine Radioactivity Studies", Nucl. Instr. and Meth., 93, **1971**, 317-332.

54. N.A. Wogman and J.C. Laul, "Natural Contamination in Radionuclide Detection Systems", Pacific Northwest Laboratory, Richland, Washington, **1980**.

55. C. Chung and C.J. Lee, "Environmental Monitoring Using a HPGe-NaI(Tl) Compton Suppression Spectrometer", Nucl. Instr. and Meth. in Phys. Res., A273, **1988**, 436-440.

56. L.J. Yuan, P.S. Weng, and C.C. Chan, "In-Situ Measurement of Low-Level Radioactivities Using the Compton Suppression Technique", Nucl. Tech., 86, **1989**, 30-34.

57. A. Sanchez, M. Moszynski, and J.H. Bjerregard, "Limitation of the Compton Suppression in Ge-BGO Compton Suppression Spectrometers", Nucl. Instr. and Meth. in Phys. Res., A280, **1989**, 73-82.

58. V. Ionescu, J.Kern, C. Nordman, S. Olbrich, and Ch. Rheme, "A Compton Suppression Spectrometer (CSS) for In-Beam Gamma-Ray Spectrometry", Nucl. Instr. and Meth., 163, **1979**, 395-401.

59. R. Beetz, W.L. Posthumus, F.W.N. De Boer, J.L. Maarleved, A. Van Der Schaaf, and J. Konijn, "An In-Beam Ge(Li)-NaI(Tl) Compton Suppression Spectrometer", Nucl. Instr. and Meth., 145, **1977**, 353-357.

60. H.J.M. Aarts, G.A.P. Engelbertink, C.J. Van Der Poel, D.E.C. Scherpenzeel, and H.F.R. Arciszewski, "Improvement of the Performance of a Compton-Suppression Spectrometer by Minimizing the Dead Layer of the Central Ge Detector", Nucl. Instr. and Meth., 172, **1980**, 439-446.

61. H.J.M. Aarts, C.J. Van Der Poel, D.E.C. Scherpenzeel, H.F.R. Arciszewski, and G.A.P. Engelbrtink, "A Compton-Suppression Spectrometer for γ-γ Coincidence Measurements: Large Solid Angle and Excellent Suppression", Nucl. Instr. and Meth., 177, **1980**, 417-425.

62. P. Herges and H.V. Klapdor, "Compton-Suppression Spectrometer for In-Beam Coincidence Measurement and Proposal for a Detector Configuration Consisting of Two Veto Systems with a Large Solid Angle", Nucl. Instr. and Meth., 189, **1981**, 415-422.

63. R.M. Lieder, H. Jager, A. Neskakis, T. Venkova, and C. Michel, "Design of a Bismuth Germanate Anti-Compton Spectrometer and Its Use in Nuclear Spectroscopy", Nucl. Instr. and Meth. in Phys. Res., 220, **1984**, 363-370.

64. P.J. Nolan, D.W. Gifford, and P.J. Twin, "The Performance of a Bismuth Germanate Escape Suppressed Spectrometer", Nucl. Instr. and Meth. in Phys. Res., A236, **1985**, 95-99.

65. A.P. Byrne and G.D. Dracoulis, "Monte Carlo Calculations for Asymmetric NaI(Tl) and BGO Compton Suppression Shields", Nucl. Instr. and Meth. in Phys. Res., A234, **1985**, 281-287.

66. F. Gloystein, F.W. Richter, and U. Watjen, "A Two-Detector Anticoincidence System for Reduction of Compton Scattered High Energy Gamma-Ray Background in PIXE Analysis", Nucl. Instr. and Meth., 181, **1981**, 25-29.

67. R.W. Peelle and R.R. Spencer, "Counting Anticoincidences to Reduce Statistical Uncertainty in the Calibration of a Multiplicity Detector", Nucl. Instr. and Meth., 211, **1983**, 167-170.

68. D.E. Alburger and J.B. Cumming, "Search for the β decay of ^{48}Ca", Phys. Revw. 32, **1985**, 1385-1361.

69. J.B. Cumming and D.E. Alburger, "Search for the decay of ^{180}Ta^{m}" Phys. Rev., 31, **1985**, 1494-1498.

70. N.A. Wogman, H.G. Rieck, J.C. Laul, and K.W. MacMurdo, "High-Sensitivity Isotope Analysis with a ^{252}Cf-^{235}U Fuelled Subcritical Multiplier and Low Background Photon Detector Systems", Nucl. Instr. and Meth., 141, **1977**,

539-547.

71. Y. Murata, S. Hirai, M. Okamoto, and H. Kaihana, "A New System of Gamma-Ray Spectrometry for Activation Analysis", J. Radioanal. Chem., 36, **1977**, 525-535.

72. U. Rosick and P. Bratter, "Improvement of Sensitivity in Neutron Activation Analysis by Means of Anti-Compton Spectrometry with a Central Well-type Ge(Li) Detector", Z. Anal. Chem., 286, **1977**, 336-342.

73. J.C. Laul, E.A. Lepel, W.C. Weimer, and N.A. Wogman, "Precise Trace Rare Earth Analysis by Radiochemical Neutron Activation", J. Radioanal. Chem., 69, **1982**, 181-196.

74. J.C. Laul, E.A. Lepel, and M.R. Smith, "Trace Rare Earth Element Analysis of Briny Groundwaters", J. Radioanal. Nucl. Chem., 123, **1988**, 349-363.

75. H.T. Milard Jr. "Compton Suppression Gamma-counting: The Effect of Count Rate", Nucl. Instr. and Meth, in Phy. Res., 223, **1984**, 416-419.

76. K.W.D. Ledingham, M.G. Kelliher, and S.D. Robertson, "Multielement Photon Activation Analysis of Coal Samples Using a Compton Suppressed Ge(Li) Detector", J. Radioanal. Chem., 74, **1982**, 169-180.

77. R. Zeisler and D.A. Becker, "Determination of Zinc in a Monel Alloy by Compton Suppression Spectrometry", Trans. Am. Nucl. Soc., 55, **1987**, 175-176.

78. H.A. Das and J. Zonderhuis, "Application of Anti-compton Counting in Instrumental Neutron Activation Analysis", J. Radioanal. Nucl. Chem., Art., 114, **1987**, 207-213.

79. H.A. Das, "The Advantage of Anti-Compton Counting in the Measurement of Low-Level Radioactivity by Gamma-Ray Spectrometry", J. Radioanal. Nucl. Chem., Art., 115, **1987**, 159-173.

80. H.A. Das, "The Limits of Decision, Detection, and Determination in Anti-Compton Gamma-ray Spectrometry", J. Radioanal. Nucl. Chem., Art., 99, **1986**, 61-73.

81. S. Landsberger, G. Swift, and J. Neuhoff, "Nondestructive Determination of Arsenic in Urine by Epithermal Neutron Activation Analysis and Compton Suppression", Bio. Trace Elem. Res., 26-27, **1990**, 27-32.

82. S. Landsberger and De Wu, "Determination of Halogens in Bioenvironmental Samples Using Thermal, Epithermal, and Compton Suppression Activation Analysis", Trans. Am. Nucl. Soc., 64, **1991**, 10.

83. S. Landsberger, "The Instrumental Determination of Cadmium in Biological Samples at Nanogram Levels with the Aid of Compton Suppression System and Epithermal Neutron Activation Analysis", J. Radioanal. Nucl. Chem., Art., 161, No.1, **1992**, 5-10.

84. S. Landsberger, S. Larson, and D. Wu, "Determination of Airborne Cadmium in Environmental Tobacco Smoke by Instrumental Neutron Activation Analysis with a Compton Suppression System", Anal. Chem., 65, **1993**, 1506-1509.

85. S. Landsberger and D. Chichester, Personal Communication, **1997**.

86. E. Carlson, "Determination of Cadmium in Biological Certified Reference Materials by Neutron Activation and Compton Suppression", unpublished undergraduate report, Dept. of Nucl. Eng., University of Illinois, **1990**.

87. Y.S. Khrbish and N.M. Spyrou, "Prompt Gamma-Ray Neutron Activation Analysis by the Absolute Method", J. Radioanal. Nucl. Chem., Art., 151, **1991**, 55-61.

88. D. Masse, A. Adam, and J. Laurec, "A Ge-NaI(Tl) Spectrometer with Compton Suppression and Gamma Coincidence Counting. Application to ^{189}Ir and ^{101}Rh Activity Measurements", Nucl. Instr. and Meth. in Phys. Res., A309, **1991**, 227-235.

89. J.B. Cumming, P.P. Parekh, and A.V. Murali, "A Novel Approach to the Determination of Iridium via Ge-Coincidence/ NaI(Tl)-Anticoincidence Gamma-ray Spectrometry", Nucl. Instr. and Meth. in Phys. Res., A265, **1988**, 468-474.

90. A.V. Murali, P.P. Parekh, and J.B. Cumming, "On the Determination of Iridium in Diverse Geological Samples Employing HPGe Coincidence/NaI(Tl)-Anticoincidence Spectrometry", Geochim. Cosmochim. Acta, 54, **1990**, 889-894.

91. X. Lin, Ch. Lierse and W. Wahl, "An Innovative Compton Suppression Spectrometer and its Capability of Evaluation in Multi-element NAA", J. Radioanal. Nucl. Chem., 215, **1997**, 169-178.

92. M.A. Deibel, A. Landsberger, D. Wu, and W.D. Ehmann, "Non-destructive Analysis of Copper in Human Brain Tissue by NAA using Coincidence and Anti-coincidence Techniques", J. Radioanal. Nucl. Chem., 217, **1997**, 153-155.

93. S. Landsberger and S. Peshev, "Compton Suppression NAA: Past, Present and Future", J. Radioanal. Nucl. Chem., 202, Nos 1-2, **1996**, 201-224.

94. E. Mauerhofer, U. Tharun, H.O. Denschlag, R. Schmidt, and J.V. Kratz, "A Compton Suppression Spectrometer for Neutron Activation Analysis", Nucl. Instr. and Meth. Phys. Res., A 371, **1996**, 465-471.

95. D.E. Ryan, D.C. Stuart, and A. Chattopadhyay, "Rapid Multielement Neutron Activation Analysis with a SLOWPOKE Reactor", Anal. Chim. Acta, 100, **1978**, 87-93.

96. J. Holzbecher, A. Chatt, and D.E. Ryan, "SLOWPOKE Epi-Cadmium Neutron Flux in Activation Analysis of Trace Elements", Can. J. Spectros., 30, **1985**, 67-72.

97. P.I. Beazley, "Comparison of Conventional and Anticoincidence Gamma-ray Spectrometry for INAA of Selected Elements", M.Sc. Thesis, Dalhousie University, Halifax, Canada, **1993**.

98. "Low Level Counting Compton Suppression", Harshaw Chemie B.V., de Meern, Holland, **1980**.

99. G.V. Walford and R.M. Keyser, "The Evaluation of System Sensitivity and Capability of a NaI(Tl) Shielded Ge(Li) Detector", Ortec, **1988**.

100. "Anti-Compton Analyzer NC-26R Operating Manual", Harshaw Chmie B.V. de Meern, Halland, **1980**.

101. T.J. Paulus, R.M. Keyser, "Compton Suppression Systems for Environmental Measurements", Inter. Conf. Meth. Appl. Radioanal. Chem. (MARC-II), Kona, Hawaii, **1991**.

102. J.A. Cooper, "Factors Determining the Ultimate Detection Sensitivity of Ge(Li) Gamma-Ray Spectrometers", Nucl. Instr. and Meth., 82, **1970**, 273-277.

103. J.A. Cooper, "Figure-Of-Merit Measurement For Ge(Li) Detectors", Nucl. Instr. and Meth., 94, **1971**, 289-296.

104. M. Rossbach, R. Zeisler, and J.R.W. Woittiez, "The Use of Compton Suppression Spectrometers For Trace Element Studies In Biological Materials", Proc. NAMLS-I, Humana Press, **1990,** 63-73.

105. E. Mauerhofer, "Improvement in the Counting Statistics and in the Limit of Detection with Compton Suppression Spectrometers - A Contribution to Instrumental Neutron Activation Analysis", Appl, Radiat. Isot., 47, **1996**, 649-658.

106. R.E. Tout and A. Chatt, "A Critical Evaluation of Short-Lived and Long-Lived Neutron Activation Products For Trace Element Determinations", Analytica Chimica Acta, 118, **1980**, 341-358.

107. R.L. Heath, "Gamma-Ray Spectrum Catalogs", Idaho National Engineering & Environmental Laboratory, Idaho Falls, ID, USA, β Release, **1997**.

108. "Table of Isotopes", Eds. C.M. Lederer and V.S. Shirley, 7th. Edn., Wiley Interscience, New York, NY, USA, **1978**.

109. G. Erdtmann, "Neutron Activation Tables". Verlag Chemie, Weinheim, **1976**.

110. K.N. DeSilva, "A Correction Method for Coincidence Losses in Neutron Activation Analysis with Short-Lived Nuclides", Ph.D. Thesis, Dalhousie University, Halifax, Canada, **1981**.

111. E. B. Flink, "Trace Elements in Human Health and Disease", Vol. 2, **1976**, 1.

112. J. K. Aikava, "Trace Elements in Human Health and Disease", Vol. 2, **1976**, 47.

113. T. Yamane and E. Goto, "Simultaneous Determination of Calcium and Magnesium by Using a Flow-Injection System with Simultaneous Injection of two Sample Plugs and Masking Agent Plug", Talanta, 38, **1991**, 139-143.

114. G. F. Knoll, "Radiation Detection and Measurement", John Wiley and Sons, New York, **1979**, 738.

115. K. Schwarz, Proc. Intern. Symp. Nuclear Activation Techniques in the Life Science, IAEA, Vienna, **1972**, 3.

116. J.S. Dulka and T.H. Risby, Anal., Chem., 48, 640A, **1976**.

117. R. Dybczynski, H. Maleszewska, and M. Wasek, "An Accurate Method for the Determination of Copper in Biological Materials by Neutron Activation Analysis and Extraction Chromatography", J. Radioanal. Nucl. Chem. Letter, 96, **1986**, 187-200.

118. N.L. Truglio and V.P. Guinn, "Elements Very Rapidly Measurable by INAA in Biological and Environmental Materials", J. Radioanal. Nucl. Chem., Aritcles, 110, **1987**, 41-45.

119. R. Dybczynski, B. Danko, and J. Kaczrowski, "Determination of Copper in Biological Materials by NAA using Short-lived ^{66}Cu", Chemia. Analityczna, 34, **1989**, 103.

120. M.J. Adams, "Chemometrics in Analytical Spectroscopy", The Royal Society of Chemistry, **1995**.

121. Ein*Sight 3.0, by Informetrix, Incorporated, **1991**.

122. L.L. Hopkins and Jr. H.E. Mohr, "The Biological Essentiality of Vanadium", Newer Trace Elements in Nutrition, Wiley, New York, **1971**.

123. M. Yaman and S. Gucer, "Determination of Vanadium in Biological Materials by Flame Atomic Absorption Spectrometry with Activated Carbon Enrichment", Fresenius J. Anal. Chem., 350, **1994**, 504.

124. A.J. Blotcky, F.G. Hamel, A, Stranik, A. Ebrahim, and R.B. Sharma, "Determination of Vanadium in Biological Tissue by Anion Exchange Chromatography and NAA", J. Radioanal. Nucl. Chem., Articles, 131, **1989**, 319-329.

125. A.J. Blotcky, W.C. Duckworth, and A. Ebrahim, "Determination of Vanadium Serum By Pre-irradiation and Post-irradiation Chemistry and Neutron Activation Analysis", J. Radioanal. Nucl. Chem., Aritcles, 134, No. 1, **1989**, 151-160.

126. T. Sato and T. kato, "Estimates of Iodine in Biological Materials by Epithermal Neutron Activation Analysis", J. Radioanal. Chem., 68, **1982**, 175-180.

127. W.B. Stroube and W.C. Cunningham, "Analysis of Foods for Iodine by Epithermal Neutron Activation Analysis", J. Radioanal. Nucl. Chem., 112, **1987**, 34-36.

128. Z.B. Alfassi and N. Lavi, "The Determination of Iodine in Biological Samples by Epithermal Neutron Activation Analysis", J. Radiochem. Radioanal. Letters, 53, **1982**, 173-182.

129. J.J.Fardy and G.D. Mcorist, "Determination of Iodine in Milk Products and Biological Standard Reference Materials by Epithermal NAA", J. Radioanal. Nucl. Chem. Letters, 87, **1984**, 239-246.

130. D.L. Mahesh and Y.G. Deosthale, "A Sensitive Kinetic Assay for the Determination of Iodine in Foodstuffs", Food Chemistry, 43, **1992**, 51-56.

131. R.R. Rao, J. Holzbecher, and A. Chatt, "Epithermal Instrumental Neutron Activation Analysis of Biological Reference Materials for Iodine", Fresenius J. Anal. Chem., 352, **1995**, 53-57.

132. R.R. Rao and A. Chatt, "Microwave Acid Digestion and Preconcentration Neutron Activation Analysis of Biological and Diet Samples for Iodine", Anal. Chem., 63, **1991**, 1298-1302.

133. R.R. Rao and A. Chatt, "Determination of Nanogram Amounts of Iodine in Foods by Radiochemical NAA", Analyst, 118, **1993**, 1247-1250.

134. L.A. Currie, "Limits of Qualitative Detection and Quantitative Determination - Application to Radiochemistry", Anal. Chem., 40, **1968**, 586-593.

135. J.A. Cooper, "Evaluation of Ge(Li) Compton Suppression Spectrometers for Non-Destructive Radiochemical Analysis", J. Radioanal. Nucl. Chem., 6, **1970**, 177-184.

136. A.R. Byrne, "Low-Level Simultaneous Determination of As and Sb in Standard Reference Materials using Radiochemical Neutron Activation Analysis with Isotopic ^{77}As and ^{125}Sb Tracers", Fresenius J. Anal. Chem., 326, **1987**, 733-735.

137. W.M. Mok and C.M. Wai, "Determination of Arsenic and Antimony in Biological Materials by Solvent Extraction and Neutron Activation", Talanta, 35, **1988**, 183-186.

138. S. Landsberger, "Non-Destructive Determination of Zinc in Biological Certified Reference Materials", J. Radioanal. Nucl. Chem., Letters, 127, **1988**, 319-323.

139. M. Makarewicz and R. Zeisler, "Enhanced Sensitivity for the Determination of Selenium by INAA", Proc. Intern. Conf. NAMLS-II, Eds., J. Kucera, I.

Obrusnik, and E. Sabbioni, Humana press, New Jersey, **1994**, 95-104.

140. J.A. Cooper, "Radioanalytical Application of Gamma-Gamma Coincidence Techniques with Lithium-Drifted Ge Detectors", Anal. Chem., 43, **1971**, 838-842.

141. H.S. Dang and A. Chatt, "Preconcentration Neutron Activation Analysis of Uranium and Thorium in Standard Reference Materials", Trans. Am. Nucl. Soc., 53, **1986**, 169-170.

142. L.S. McDowell, P.R. Giffen, and A. Chatt, "Determination of Selenium in Individual Food Items using the Short-Lived Nuclide ^{77m}Se", J. Radioanal. Nucl. Chem., 110, **1987**, 519-529.

143. A. Chatt, "Instrumental and Preconcentration NAA Methods for Selenium in Biological Materials", Trans. Am. Nucl. Soc., 56, **1988**, 152.

144. A. Chatt and J. Holzbecher, "Cyclic and Pseudo-cyclic Neutron Activation Analysis for Trace Elements", Trans. Am. Nucl. Soc., 62, **1990**, 220-222.

145. A. Chatt, R.R. Rao, C.K. Jayawickreme and L.S. McDowell, "Determination of Sampling Constants for Selenium in Biological Reference Materials by Neutron Activation", Fresenius J. Anal. Chem., 338, **1990**, 399-407.

146. R.R. Rao and A. Chatt, "Internal and External Quality Assessment in Cyclic Neutron Activation Analysis for Selenium", Trans. Am. Nucl. Soc., 64, **1991**, 4-5.

147. R.R. Rao, C.K. Jayawickreme, L.S. McDowell, and A. Chatt, "Evaluation of Homogeneity of Selected Reference Materials for Selenium by Cyclic Neutron Activation Analysis" J. Radioanal. Nucl. Chem., 151, **1991**, 167-175.

148. "Guidelines for Data Acquisition and Data Quality Evaluation in Environmental Chemistry", Anal. Chem., 52, **1980**, 2242.

149. "Quality Assurance in Biomedical Neutron Activation Analysis - Report of an Advisory Group of the International Atomic Energy Agency", Anal. Chim. Acta, **165**(1984)1; IAEA-TECDOC-323, Vienna, Austria, **1984**.

150. J.K. Taylor, "Quality Assurance of Chemical Measurements", Lewis Publishers, Chelsea, Michigan, USA, **1987**.

151. K. Heydorn, "Neutron Activation Analysis for Clinical Trace Element Research", Vol. 1 & 2, CRC Press, Boca Raton, FL, USA, **1984**.

152. "Practical Aspects of Operating a Neutron Activation Laboratory", Chapter 9, IAEA-TECDOC-564, Vienna, Austria, **1990**.

153. J.K. Taylor, Anal. Chem., 53, **1981**, 1588A.

154. K. Heydorn and B. Griepink, "Selection of Reference Methods for the Determination of Selenium in Biological Materials", Fresenius J. Anal. Chem., 338, **1990**, 287.

155. F.M. Garfield, "Quality Assurance Principles for Analytical Laboratories", Assoc. Official Anal. Chemists, VA, USA, **1984**.

156. G.T. Wernimont, "Use of Statistics to Develop and Evaluate Analytical Methods", Assoc. Official Anal. Chemists, VA, USA, **1987**.

157. Y. Muramatsu and R.M. Parr, "Survey of Currently Available Reference Materials for use in Connection with the Determination of Trace Elements in Biological and Environmental Materials", IAEA/RL/128, International Atomic Energy Agency, Vienna, Austria, **1985**.

158. R.W. Dabeka, Personal Communication, Health Canada, Ottawa, Canada, **1996**.

IMAGE EVALUATION
TEST TARGET (QA-3)

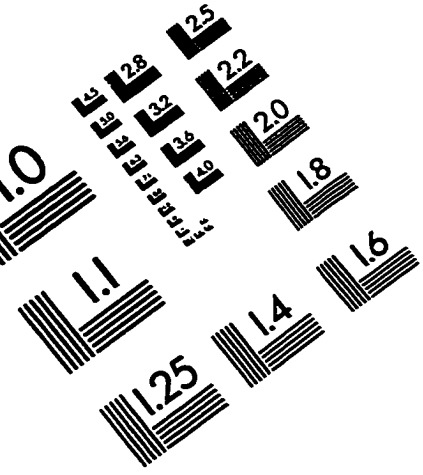

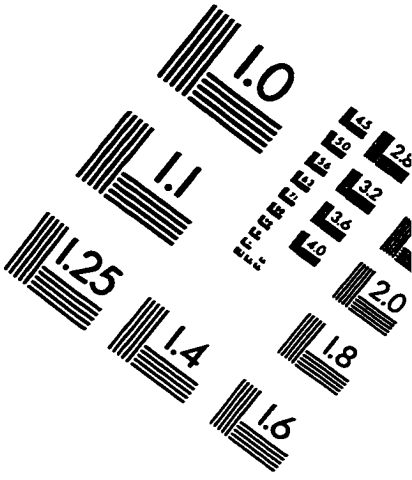

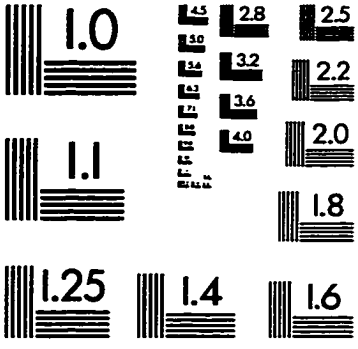

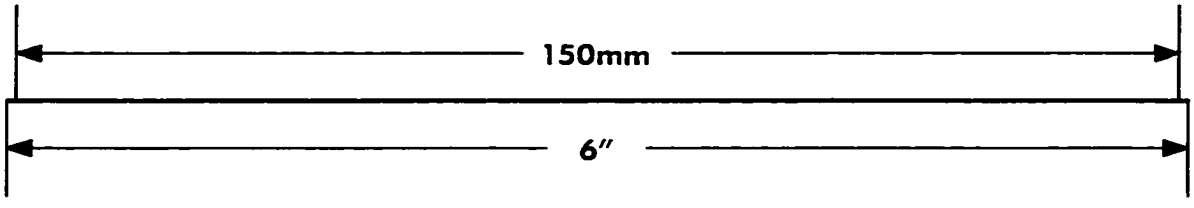

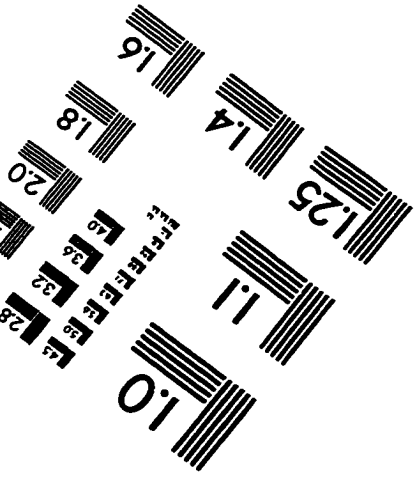

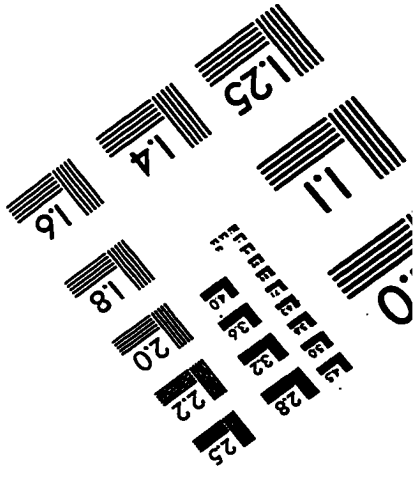

APPLIED IMAGE, Inc
1653 East Main Street
Rochester, NY 14609 USA
Phone: 716/482-0300
Fax: 716/288-5989